UNIVERSITÉ D'ORLÉANS

THÈSE présentée par :

Antonia ZOGKA

soutenue le : **05 décembre 2016**

pour obtenir le grade de : **Docteur de l'Université d'Orléans**
Discipline/ Spécialité : Chimie et Physique de l'Environnement

Atmospheric degradation of a series of methoxy and ethoxy acetates and n-pentyl acetate

THÈSE dirigée par :
  Abdelwahid MELLOUKI   Directeur de recherche au CNRS-Orléans

RAPPORTEURS :
  Alexandre TOMAS   Professeur à l'Ecole des Mines de Douai
  Abdelkhaleq CHAKIR   Maitre de Conférences (HDR) à l'Université de Reims
_____

JURY
  Valery CATOIRE   Professeur à l'Université d'Orléans, Président du jury
  Cécile CŒUR   Maitre de Conférences à l'Université du Littoral
                                                     Côte d'Opale
  Alexandre TOMAS   Professeur à l'Ecole des Mines de Douai
  Abdelkhaleq CHAKIR   Maitre de Conférences (HDR) à l'Université de Reims
  Véronique DAËLE   Chargée de recherche (HDR) au CNRS-Orléans
  Abdelwahid MELLOUKI   Directeur de recherche au CNRS-Orléans

Table of Contents

Abstract

In the context of **DISPATMO** project (forecast study of pollution risks related to the atmospheric dispersal of chemicals), risk studies linked to the fires and the explosions due to chemical storage were conducted. The purpose of this thesis was to perform a thorough kinetic and mechanistic study to determine the gas phase degradation of one of the main component of Tiflex solvent, the 1-methoxy 2-propyl acetate (MPA). Furthermore, the rate coefficients of OH and Cl with a series of alkoxy acetates widely used in painting and coating industries, 2-methoxy-butyl acetate (2MBA), 3-methoxy-butyl acetate (3MBA), methoxy ethyl acetate (MEA), ethoxy ethyl acetate (EEA) and n-pentyl acetate (n-PA), were determined. The experiments were performed employing the pulsed laser photolysis-laser induced fluorescence technique, a low pressure flow tube reactor coupled with a quadrupole mass spectrometer and an atmospheric simulation chamber coupled with a GC-FID, a FTIR and a GC-MS using complementary absolute and relative rate methods. The kinetic data were used to derive the Arrhenius expressions as well as to evaluate the environmental fate of the studied compounds such as their lifetimes and the Photochemical Ozone Creation Potential. Besides, the reaction mechanism was investigated, while the major degradation products and their yields were determined in presence of NO. In addition, the UV-Vis absorption cross sections of MPA, 2MBA and 3MBA were measured in order to evaluate their potential photolysis in the atmosphere. The investigation of the chemical processes and the tropospheric lifetimes of the compounds are used as input data in photochemical atmospheric simulation models and in chemical agent atmospheric dispersion models to evaluate their atmospheric impact.

Keywords: Atmospheric chemistry, Alkoxy acetates, OH radical, Cl atom, rate coefficient, mechanism, lifetime.

Introduction

Atmospheric Chemistry deals with the chemical composition of the natural atmosphere and its reactivity (reactions and interactions), the way gases, liquids, and solids in the atmosphere interact with each other and with the earth's surface. The objective of the Atmospheric Chemistry is to determine the constituents' distribution in the atmosphere and to evaluate the air quality focusing on the nature of the environmental and human impact.

The reactivity of the atmosphere gathers the general interest, as an integral part of Atmospheric Chemistry. It influences and is involved in environmental issues, such as photochemical smog, acid rain, the formation of clouds, and the enhancement of the greenhouse effect.

The development of Photochemistry and Chemical Kinetics has contributed to the understanding of crucial atmospheric (photo)chemical processes and to the prediction of forthcoming chemical changes that take place daily, with the ultimate goal of improving the quality of human's life. In parallel, the technological development has supplied the Chemical Kinetics with the necessary tools to study the processes in real atmospheric conditions.

The large quantity and diversity of organic and inorganic compounds daily emitted in the atmosphere - as a result of anthropogenic and biogenic emissions- undergo a number of physical and (photo)chemical processes leading to their degradation or transformation. As a result, Photochemistry and Chemical Kinetics aims to determine the environmental fate of these compounds and to clarify the physicochemical processes that compounds could participate in the gas, liquid and solid phases. These valuable information are provided through the measurement of kinetic parameters of homogeneous and heterogeneous reactions as well as through the investigation of the reaction mechanism. Specifically, the rate coefficients of gas phase reactions, the uptake coefficients of heterogeneous interactions, the photolysis rates and the absorption cross sections of the species, have been a great deal of interest the past four decades.

The experimental results from the kinetic and mechanistic studies of numerous reactions are implemented in photochemical atmospheric simulation models for air pollution and in chemical agent atmospheric dispersion models. The objective of these models is to simulate the photochemical processes that take place in real atmosphere, to make short or long term predictions and to signify any air quality issue. By this way, we can anticipate and prevent unpleasant situations for the environment and human health. The accuracy of models predictions or the simulation of the physicochemical phenomena is based on the accuracy of the kinetic/mechanistic data provided by Chemical Kinetics. Therefore, these models contribute significantly to the recognition of atmospheric chemistry as one of the most important domains of chemistry, while they make the Chemical Kinetics essential and inseparable with the improvement of the quality of life.

The chemical processes leading to the atmospheric degradation of several OVOCs are the subject of this study. The Thesis is an extension of the activities occurred in DispAtmo project and its main objective is the determination of various gas lifetimes in the troposphere, in existential importance for the environment and humans. The results derived were used as input data in chemical agent atmospheric dispersion models of the project.

Overview of the Thesis

The thesis is divided into seven chapters followed by a conclusion and seven annexes.

The first introductory chapter points out the general framework of this study which is the photo-oxidative pollution and the role of Volatile Organic Compounds (VOCs) in atmospheric chemistry. In particular, emphasis is placed on the oxidative capacity of the troposphere (main oxidants) as well as the sources and effects of the oxygenated VOCs.

The second chapter focuses on the context and the objectives of the work which are part of the DispAtmo project (Etude de la prévention des risques de pollution liés à la DISPersion ATMOsphérique de produits chimiques), a regional project involving public and private partners. The participation and contribution in DispAtmo project as well as the presentation of the selected compounds and the atmospheric reactivity of this family of compounds are the main subjects of this chapter.

Subsequently, four different experimental techniques used during this study are presented in chapter 3. The UV absorption cross sections of a series of OVOCs were determined using an Ultra Violet spectrophotometer, while the kinetic studies were performed using three complementary techniques in a wide field of experimental conditions.

From the fourth chapter, we enter into the heart of the Thesis and the result section. The UltraViolet absorption cross-section of three alkoxy acetates have been measured for the first time and presented in chapter 4. Different experimental conditions - temperature, light source, presence of filter, detection - have been implemented confirming the results obtained.

The kinetic studies of six and five acetates with the hydroxyl radical and the chlorine atom respectively are presented in chapter 5. The experiments have been conducted employing absolute and relative rate methods and three complementary set ups in order to provide accurate kinetic data and study the temperature and pressure dependence.

Regarding, the mechanistic study of the reaction of methoxy-propyl-acetate with the hydroxyl radical and the chlorine atom, in chapter 6, the main degradation products

are detected and quantified. Based on these experimental results, a reaction mechanism is proposed.

Finally, the results are compared with the literature (when available) and theoretical estimations in the last chapter. The reactivity of alkoxy esters is discussed, while the lifetimes and the Photochemical Ozone Creation Potential of the compounds lead to their atmospheric implications.

1. Atmospheric chemistry

1. Atmospheric chemistry

1.A. The atmosphere

The Earth's atmosphere consists of a mixture of several gases and aerosols. The major gases are nitrogen (78.08%), oxygen (20.95%), argon (0.93%), carbon dioxide (0.038%), and water vapor (0.001-5%) which give earth the ability to sustain life. The remaining gases are referred to as trace gases, among which are neon, helium, methane, krypton, hydrogen, nitrous oxide, xenon and ozone.

The Earth's atmosphere is divided into layers that differ in properties such as composition, temperature and pressure. The lowest layer is the troposphere, which includes the boundary layer to a height of 1-2 km and the free troposphere to an altitude of about 10-17 km and contains almost all the water vapor and clouds that are present in the atmosphere. This layer is denser than all its overlying atmospheric layers containing roughly 80% of the atmospheric mass.[1] The stratosphere, extended from 20 to 50 km, includes the ozone layer which absorbs ultraviolet solar radiation (240-320 nm) that would otherwise be harmful to living systems. In addition, ozone layer is responsible for the increase of the temperature with increasing altitude. The mesosphere lies above the stratosphere, extends up to about 90 km and is the layer in which most meteors burn up. The thermosphere extends from 90 km to the base of the exosphere at 650 km and represents the boundary between the Earth's atmosphere and outer space.[2]

The two lowest layers, the troposphere and the stratosphere are the most important layers of the atmosphere. Their interactions with different wavelengths of solar radiation (arriving at each layer) initiate several chemical processes which are widely discussed in this thesis.
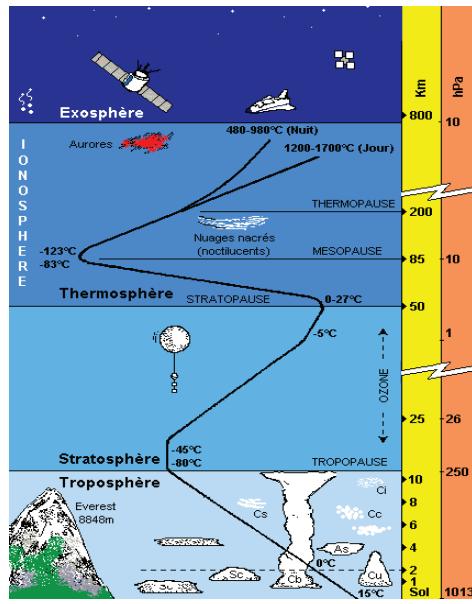
Figure 1.1:Different layers of the atmosphere based on the temperature trend with increasing altitude.[3]

1.B. Solar irradiation and photochemistry

The spectrum of the solar radiation is close to that of a black body with a temperature of about 5777 K.[4] Although the sun produces the gamma and X rays, UV, visible, IR light and microwaves, the spectrum of nearly all solar radiation striking the troposphere and reaching the ground spans at a wavelength larger than 290 nm. Figure 1.2 compares the solar spectrum at the sea level and without atmospheric absorption with the spectrum of an ideal blackbody at 5250 K.

It is remarkable that the solar irradiation is the principal generator of radical species which thereafter initiate reaction chains and exert a substantial influence on the ultimate composition of the atmosphere. The wavelength of interest in tropospheric photochemistry corresponds at 290-800 nm, since infrared has low radiant energy to photodissociate the molecules.

8

1.C. Gas phase tropospheric chemistry

1.C.I Tropospheric oxidants

Thousands of different types of Volatile Organic Compounds (VOCs) are emitted from the Earth's surface from biogenic and anthropogenic sources. A high percentage of these compounds have a stable average concentration in the troposphere, since they are not accumulated but removed from the atmosphere by photolysis or chemical oxidation. The most definitive oxidants of the troposphere are the free radicals OH, HO_2 and NO_3, Cl atoms and O_3. The gas phase reactions of numerous VOCs with these oxidants have been investigated extensively for several decades. The most dominant tropospheric oxidation for many VOCs occurs due to highly reactive OH radicals, although the most abundant of these oxidants is O_3 (table 1.1). However, the reactions of Cl atoms with VOCs may also be an important transformation process in certain regions such as in the Arctic troposphere during springtime, possibly in some coastal regions but also inland areas. The presence of these oxidants, the free radicals OH, HO_2 and NO_3, Cl atoms and O_3, coupled with the presence of VOCs, leads to a number of interrelated reactions.

9

Table 1.1: Typical concentrations and dominant reactions of the oxidants. For OH concentration a 12-h daytime average is given, for Cl concentration a 24-h global average, for NO$_3$ concentration a 12-h night-time average and for O$_3$ a 24-h average.

Oxidant	Average Concentration (molecule cm^{-3})	Reactions
OH	2×10^6 [6]	Dominant reactant in the troposphere. Reacts by H-abstraction and by addition
Cl	10^4 [6] (over marine environments [Cl]max ~10^6 atoms cm^{-3})	Mainly fast H-abstraction. Reacts also by addition
NO$_3$	5×10^8 [7]	Mainly slow H-abstraction. Reacts also by addition. Important for the degradation of unsaturated compounds
HO$_2$	2×10^8 [8]	Reacts easily with aldehydes
O$_3$	7×10^{11} [9]	Reacts slowly but has a relatively high concentration. Important for the degradation of unsaturated compounds

Therefore, the accurate knowledge of the production mechanisms of the oxidants and the production and consumption of ozone help the optimal understanding of tropospheric chemistry. A schematic representation of the most important tropospheric cycles is given in figure 1.3, illustrating the links between emissions, chemical transformation, radical formation and sinks for a range of trace gases.
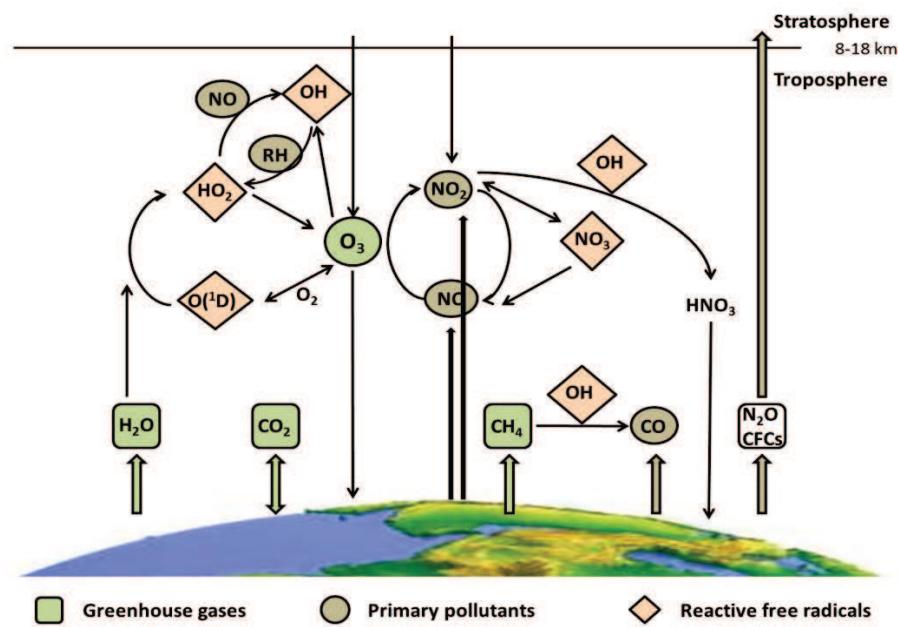
Figure 1.3: Representation of the interconnections in the tropospheric chemistry. Greenhouse gases, pollutants, oxidants, chemical transformations and sinks.

➢ *Hydroxyl radical formation*

The hydroxyl radicals (OH) are the most widespread detergent in the troposphere. They are responsible for the primary degradation of most VOCs, specifying their atmospheric lifetimes (figure 1.4).

The production of OH radicals occurs primarily via photochemical processes, thus their atmospheric activity is stronger during the daytime.
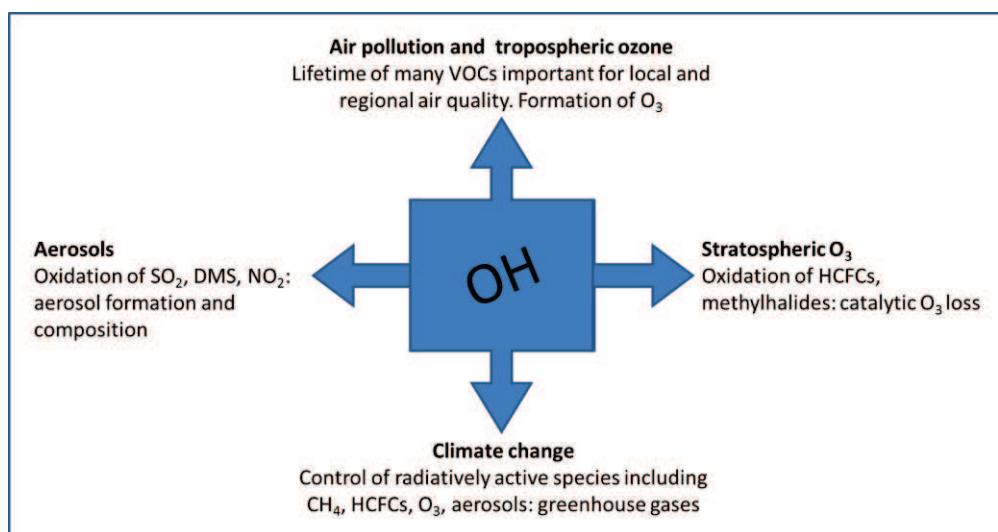
Figure 1.4: Importance of the hydroxyl radical in the atmosphere.

OH is mainly produced by photolysis of ozone to electronically excited atomic oxygen, $O(^1D)$, which then reacts rapidly with abundant water vapor to produce hydroxyl radicals:

$$O_3 + hv\ (\ \lambda \leq 336nm\ ) \rightarrow O(^1D) + O_2 \qquad (R.1.1)$$

$$O(^1D) + H_2O \rightarrow 2OH \qquad (R.1.2)$$
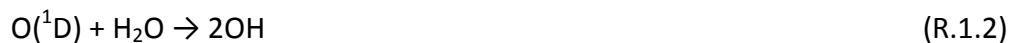
Reaction (R.1.2) is more efficient at lower altitudes, where the concentration of water vapor is high enough. However, the increased total pressure in the region leads to the rapid decay of $O(^1D)$ to $O(^3P)$, through collisions (R.1.3), which acts competitively to the production of hydroxyl radicals:

$$O(^1D) \xrightarrow{\ M\ } O(^3P) \qquad (R.1.3)$$
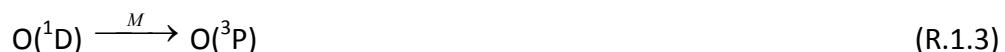
This is the major source of OH, but not the only one, with its contribution varying from 20 to 55% of the total rate of OH production.[8] Furthermore, in areas with strong industrial development, equally important source of hydroxyl radicals is the photolysis of nitrous acid (HONO) and hydrogen peroxide (H_2O_2):

$$HONO + hv\ (\ \lambda < 400\ nm\ ) \rightarrow OH + NO \qquad (R.1.4)$$

$$H_2O_2 + hv\ (\ \lambda < 370\ nm\ ) \rightarrow 2OH \qquad (R.1.5)$$

Specifically, HONO photolysis is by far the major source of OH in the early morning hours and in general it is comparable to that from HCHO:

$$HCHO + hv\ (\lambda < 330\ nm) \rightarrow HCO + H \qquad (R.1.6)$$

$$HCO + O_2 \xrightarrow{\ M\ } HO_2 + CO \qquad (R.1.7)$$

$$H + O_2 \xrightarrow{\ M\ } HO_2 \qquad (R.1.8)$$

$$HO_2 + NO \rightarrow OH + NO_2 \qquad (R.1.9)$$

Note that reaction (R.1.9) becomes really important in polluted regions. Other sources of OH are a) the photolysis of methyl hydro peroxyde (CH$_3$OOH) and b) the reaction of alkenes with ozone.[2]

Regarding OH sinks, CO is the dominant one in most of the troposphere, and CH$_4$ is next in importance. Figure 1.5 presents the OH formation and loss reactions with nitrogen dioxide (NO$_2$), carbon monoxide (CO) and hydrocarbons as well as the recycling of OH from its photochemical siblings HO$_2$ and RO$_2$ through reactions with the common pollutant NO.
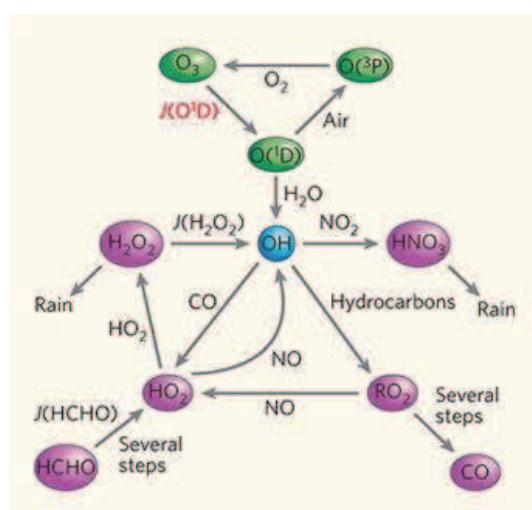
Figure 1.5: The formation and chemistry of atmospheric hydroxyl radicals.[10]

The lifetime of OH is estimated to be less than one second.[11] Because of this short lifetime, atmospheric concentrations of OH are highly variable; they respond rapidly to changes in the sources or sinks.[11] The average OH concentration in the region of the troposphere is 2×10^6 radicals cm^{-3}, while in some areas during the midday hours in the summer is significantly increased (1×10^7 radicals cm^{-3}) due to the photochemical processes.[6,2]

> *Chlorine atom formation*

The chlorine atom (Cl) is very reactive and it can influence the tropospheric chemistry mainly in marine and coastal areas where its concentration is significant. In these areas, wave action generates airborne droplets of seawater from which the

water can evaporate, leaving NaCl particles.[8] Then, chlorine molecule (Cl_2) and $ClNO_2$ are generated via the heterogeneous reaction of NaCl with N_2O_5 and $ClONO_2$:

$$N_2O_5(g) + NaCl(s) \rightarrow ClNO_2(g) + NaNO_3(s) \qquad \text{(R.1.10)}$$
$$ClONO_2(g) + NaCl(s) \rightarrow Cl_2(g) + NaNO_3(s) \qquad \text{(R.1.11)}$$
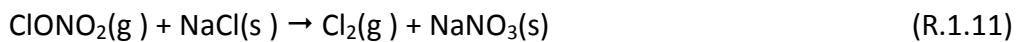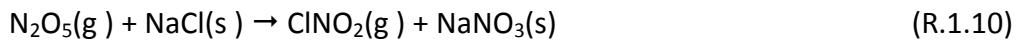
Subsequently, chlorine molecule and $ClNO_2$ can be photolysed to generate chlorine atoms:

$$Cl_2 + hv\ (\leq 400\ nm) \rightarrow 2Cl \qquad \text{(R.1.12)}$$
$$ClNO_2 + hv\ (\sim 843\ nm) \rightarrow Cl + NO_2 \qquad \text{(R.1.13)}$$

However, the rapid hydrolysis of N_2O_5(R.1.14) and $ClONO_2$ (R.1.15) competes the heterogeneous reaction with NaCl (R.1.10) and (R.1.11) inhibiting the formation of Cl.[12]

$$N_2O_5 + H_2O \rightarrow 2HNO_3 \qquad \text{(R.1.14)}$$
$$ClONO_2 + H_2O \rightarrow HOCl + HNO_3 \qquad \text{(R.1.15)}$$

Essentially, Cl atom reacts rapidly with the VOCs contributing to organic oxidations in the marine boundary layer. Spicer et al measure unexpectedly high concentrations of molecular chlorine in coastal air reaching 3.7×10^9 molecules cm^{-3} [13], while the average value of Cl atom concentration is considered to be 10^4 -10^6 atoms cm^{-3} in the marine boundary layer[8].

> ### *Nitrate radical formation*

The nitrate radical (NO_3) is the main night-time oxidant of the troposphere. It has a range of reactivity towards VOCs, such as unsaturated hydrocarbons and a variety of sulphur compounds. Oxidation chemistry by NO_3 leads to the production of secondary pollutants. This is an important difference between night-time NO_3 chemistry and daytime OH chemistry, that NO_3 can initiate, but not catalyze, the

removal of organic compounds.[7] NO$_3$ radical is formed by the reaction of NO$_2$ with O$_3$:

$$NO_2 + O_3 \rightarrow NO_3 + O_2 \qquad\qquad (R.1.16)$$

The time constant for this reaction (R.1.16) is of the order of 15 hours at an ozone concentration of 30 ppbv and T = 290 K. Dinitrogen pentoxide is another source of NO$_3$:

$$N_2O_5 + M \rightarrow NO_3 + NO_2 + M \qquad\qquad (R.1.17)$$

while the two species act in a coupled manner. On the other hand, during the daytime the NO$_3$ radical is rapidly photolysed due to its strong absorption of light in the visible (R.1.18) and (R.1.19), thus its lifetime in the midday is less than 5 sec.[2]

$$NO_3 + hv \ (\lambda < 700 \ nm) \rightarrow NO + O_2 \qquad\qquad (R.1.18)$$
$$NO_3 + hv \ (\lambda < 580 \ nm) \rightarrow NO_2 + O(^3P) \qquad\qquad (R.1.19)$$

The range of NO$_3$ concentrations is between 1.2×10^8 to 1.1×10^{10} radicals cm^{-3},[12] with the maximum values at night-time, and an 12h night-time average of 5×10^8 radicals cm^{-3}.[7]

> ➢ *Hydroperoxy radical formation*

An important compound among the class of oxidants of the atmosphere is hydroperoxy radical (HO$_2$). HO$_2$ has a particular role in the consumption (R.1.23) and (R.1.24) and production (R.1.26) and (R.1.27) of tropospheric ozone and nitrogen oxides (NO$_x$) (R.1.25). Key sources of HO$_2$ are H and HCO radicals derived from a variety of reactions and oxidative cycles. Thus, the photolysis of formaldehyde is the major source of hydroperoxy radicals in the troposphere according to the following reaction scheme:

$$HCHO + hv \ (\lambda < 330 \ nm) \rightarrow H + HCO \qquad\qquad (R.1.20)$$

$$HCO + O_2 \xrightarrow{\quad M \quad} HO_2 + CO \qquad\qquad (R.1.7)$$

$$H + O_2 \xrightarrow{\quad M \quad} HO_2 \qquad\qquad (R.1.8)$$

The photolysis of higher aldehydes, RCHO, also forms HCO and hence HO_2, with lower yields.[8] Equally important source of HO_2 is the oxidation of alkoxy radicals, which are produced by the oxidation of VOCs:

$$RCH_2O + O_2 \rightarrow RCHO + HO_2 \qquad\qquad (R.1.21)$$

In addition, in relatively unpolluted areas (low NO_x), the OH radical reacts with carbon monoxide (or methane) to produce hydrogen atom (R.1.22) and HO_2 (R.1.8)

$$OH + CO \rightarrow H + CO_2 \qquad\qquad (R.1.22)$$

In these areas, HO_2 can then react with ozone leading to further destruction of ozone in a chain sequence involving production of OH:

$$HO_2 + O_3 \rightarrow OH + 2O_2 \qquad\qquad (R.1.23)$$

$$OH + O_3 \rightarrow HO_2 + O_2 \qquad\qquad (R.1.24)$$
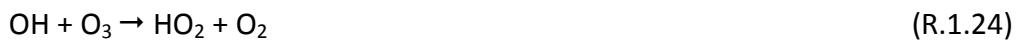
In polluted conditions (high NO_x), HO_2 radicals catalyse the oxidation of NO to NO_2:

$$HO_2 + NO \rightarrow OH + NO_2 \qquad\qquad (R.1.25)$$

The average concentration of HO_2 is about $1\text{-}2 \times 10^8$ radicals cm^{-3}, while in polluted areas are believed to be of the order of 10^9 radicals cm^{-3}.[8]

> ➢ *Ozone formation*

As it was mentioned before, the oxidation of NO (R.1.25) takes place in polluted environment and finally leads to the formation of ozone (O_3) by the two successive reactions:

$$NO_2 + h\nu \ (\lambda < 420 \ nm) \rightarrow NO + O(^3P) \qquad\qquad (R.1.26)$$

$$O(^3P) + O_2 \xrightarrow{\ M\ } O_3 \qquad\qquad (R.1.27)$$

This is coupled with a further inorganic reaction, which regenerates NO_2

$$NO + O_3 \rightarrow NO_2 + O_2 \qquad\qquad (R.1.28)$$

Furthermore, the high concentrated stratospheric ozone provides an additional source of tropospheric ozone, while small concentrations are also formed via the reactions of natural VOC and NO_x.

In the troposphere, ozone concentration range is 4.9×10^{11} to 9.8×10^{11} molecules cm^{-3},[14] and in sub-urban and sub-rural areas it can be $\sim 5 \times 10^{12}$ molecules cm^{-3} or more.[15]

1.C.II Tropospheric ozone

Ozone plays an important role in day and night tropospheric chemistry, since it is sufficiently long-lived compound it can be transported downwind and survives during the night-time hours. It is not only a reaction product, but an intermediate in steady-state concentration between formation and degradation reactions. The cycle of O_3 and NO_2 formation and degradation (R.1.26), (R.1.27) and (R.1.28) appears in figure 1.6 terminated by the reaction of OH with NO_2 to form HNO_3.
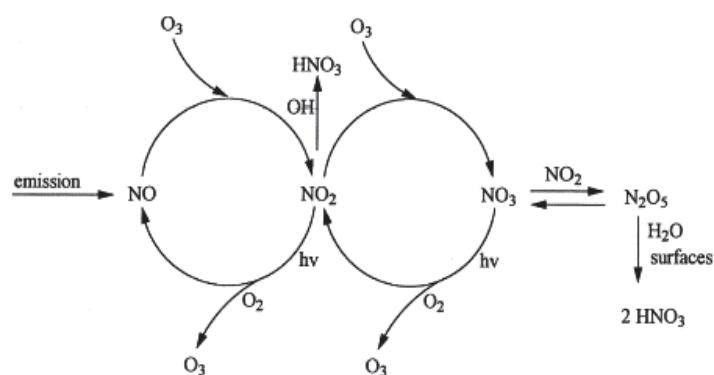
Figure 1.6: The O_3 chemistry is fundamentally linked with the day-time reaction cycles of the nitrogen oxides.[16]

The important role played by the O_3 in the atmospheric chemistry is not only its participation in a host of photochemical processes. Ground-level ozone is an important greenhouse gas, it binds the IR radiation emitted by the Earth's surface and prevents it from escaping from the atmosphere. Subsequently, it enhances the greenhouse effect and contributes to global warming. Besides, in high concentrations is toxic causing harmful effects on human health, vegetation and ecosystems.

> ➤ *Dependence of O_3 production on NO_x and VOCs*

The oxidation of VOCs in the presence of NO_x leads to formation of O_3, which formation occurs by the oxidation of NO to NO_2 by reaction with peroxy radicals:

$RO_2 + NO \rightarrow RO + NO_2$ (R.1.29)

Figure 1.7 presents the reaction cycle:
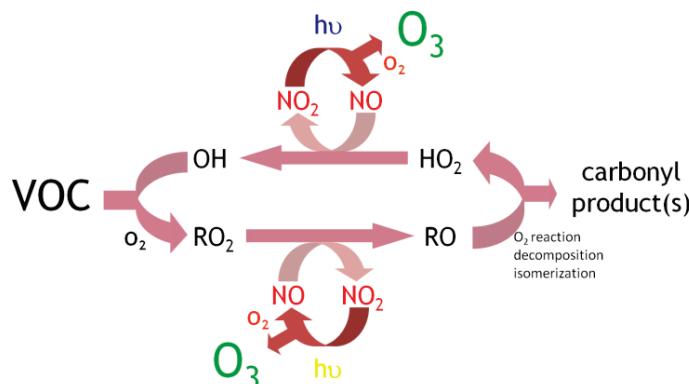
Figure 1.7: The major free-radical propagated cycle, which illustrates the essential "hub" of reactions which form ozone in the atmosphere.[17]

It is evident that the ratio of VOCs and NO_x can alter the efficiency of O_3 production. Higher NO_x emissions can result in less efficient production of O_3. Figure 1.8 (left) presents this ratio where the areas to the left of the bold centermost or ridge line are characteristic of suburban or rural areas; concentrations of VOCs are high in comparison to concentrations of NO_x, thus the O_3 production is limited by NO_x. The areas to the right of the line are representative of urban areas where there is a large amount of NO_x production from combustion in motor vehicles and industrial processes, thus the O_3 production is VOCs-limited. The ridge presents a ratio VOCs/NO_x = 8/1 where there is the maximum production of O_3. Additionally, the

production of ozone can be influenced by environmental conditions such as temperature and humidity. The figure 1.8 (right) displays the required balance for O_3 destruction/production process. At low NO_x conditions the RO_2 radicals are mainly removed through their self-reactions or with reaction with HO_2 according to the following scheme:

$$RO_2 + RO_2 \rightarrow 2RO + O_2 \qquad\qquad (R.1.30)$$
$$\rightarrow R_{-H}OH + RO + O_2 \qquad\qquad (R.1.31)$$
$$RO_2 + HO_2 \rightarrow ROOH + O_2 \qquad\qquad (R.1.32)$$

Subsequently, the HO_2 is converted to OH which will further react with O_3 destroying it. At high NO_x conditions, NO will react with O_3 producing NO_2 and O_2 according to figure 1.6 and tropospheric ozone section.
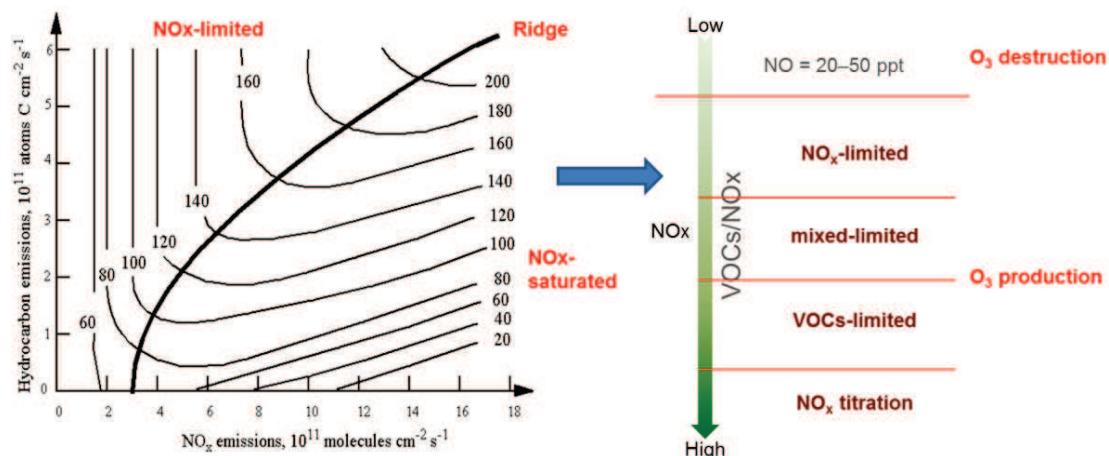
Figure 1.8: O_3 isopleths. Effect of VOCs- NOx ratio in O_3 production.[9]

It should be noted that the efficiency of the photochemical O_3 production, is different for each VOC.

1.D. Volatile Organic Compounds

Trace gases are released into the atmosphere via a variety of biogenic and anthropogenic sources. Of particular importance are Volatile Organic Compounds (VOCs), organic compounds that have boiling point less than or equal to 523 K (1

atm), since they affect the oxidising nature of the atmosphere and some of them are dangerous to human health.

1.D.I. Sources

Biogenic sources of VOCs include emissions from plants, trees, anaerobic processes, volcanoes, marine plankton and natural forest fires. The last decade they constitute the largest percentage of emissions depending on the region. Specifically, in France the biogenic emissions, including emissions of international marine transportation and domestic and international air circulation, reach 51% of the total non-methane VOCs in 2004 and 71% in 2014, respectively.[18] On the other hand organic compounds are released into the atmosphere as a result of numerous human activities such as, transportation, solvents usage, vehicle extractions, industries, coatings, agriculture, combustion processes and oil refining. According to the European Union emission inventory report 1990–2011 [19] and the French inventory report 2016, the anthropogenic emissions of non-methane VOCs in Europe and France have been reduced a lot during the last decade (figure 1.9), while for the years 2011 and 2014 the emissions in France were 734 and 639 kt, respectively. [20,18]
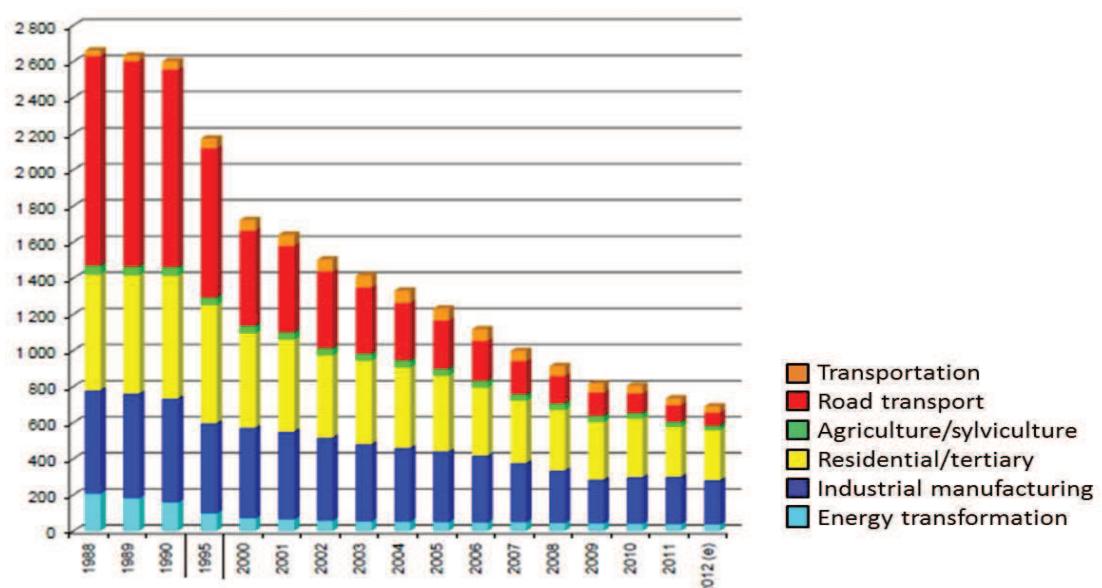
Figure 1.9: Evolution of atmospheric emissions of non-methane VOCs, in kilotons, in France metropolitan due to human activities from 2000 to 2012 according to the national inventory report 2013 of the "Centre Interprofessionnel Technique d'Etudes de la Pollution Atmosphérique" (Citepa).

Figure 1.10 depicts the percentages of the most important sectors of the non-methane VOCs anthropogenic emissions in France. As shown the "use of solvents" sector got the first place with a percentage of 47%. The inconsiderate use of solvents at homes and buildings, such as paints, coatings, adhesives, cleaners, wood combustion and cooking, is the principal source of these emissions.
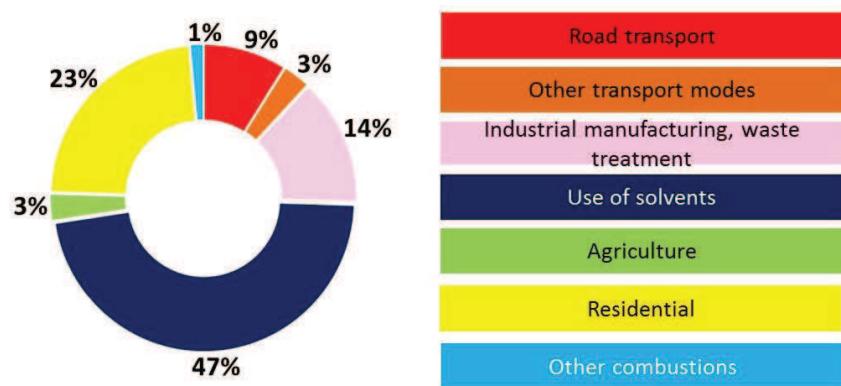
Figure 1.10: Sectors of non-methane VOCs anthropogenic emissions, in 2014, in France metropolitan according to the national inventory report 2016 of the "Centre Interprofessionnel Technique d'Etudes de la *Pollution Atmosphérique*" (Citepa).[18]

1.D.II. Effects of VOCs on human health and the environment

➢ *Direct impact on human*

The ability of organic chemicals to cause health effects varies greatly from those that are highly toxic (benzene and 1,3-butadiene), to those with unknown health effect. As with other pollutants, the extent and nature of the health effect will depend on many factors including level of exposure and length of time exposed. Eye and respiratory tract irritation, headaches, dizziness, visual disorders, and memory impairment are among the immediate symptoms appeared soon after the exposure to organics.[21] Health effects include respiratory, allergic, or immune effects in children are mainly associated with man-made VOCs and other indoor or outdoor air pollutants. The most hazard products including hazard VOCs are: hair sprays, petroleum paints, foam plastic products and carburetor.[22]

➢ *Photochemical smog, ground-level ozone increase, greenhouse effect*

Some compounds, such as styrene and limonene, have an indirect effect on human health depending on their ability to form secondary pollutants and aerosols, thus photochemical smog. The key components of photochemical smog are ozone, organic aerosols, peroxyacyl nitrates (PAN), nitrogen oxides and aldehydes. It can cause sensory irritation symptoms on humans such as shortness of breath, wheezing, coughing, eye and nose irritation.

Furthermore, ground-level O_3 concentration has been climbing over the last decades, as VOCs and NO_x are emitted into the troposphere. It is now a matter of public concern due to its impact in lung function, the respiratory system and the ecosystem including the retardation of plant growth and crop yields.

Additionally, tropospheric ozone is one greenhouse gas (3-7%), among water vapor (36-70%), carbon dioxide (9-26%) and methane (4-9%).[23] These gases increase the radiative forcing enhancing the greenhouse effect and contributing to the global warming.

1.D.III. General oxidation scheme for VOCs

Although the photochemical degradation pathways of each organic compound should be viewed individually, in most cases the reaction mechanism involves formation (at least in part) of an alkyl or substituted alkyl radical (for example, hydroxyalkyl, nitrooxyalkyl or oxoalkylradicals). In general, these alkyl or substituted alkyl radicals react in the troposphere with the key intermediate then being an organic peroxy radical ($RO_2^.$) which is transformed to an alkoxy radical ($RO^.$) in a polluted environment (figure 1.11). Afterwards, RO can rapidly react in three ways, a) reaction with O_2 to form a carbonyl compound b) decomposition by bond fission to form smaller radical and a molecule or c) isomerization by H-migration to form carbon centred radical with an OH group. The relative yields of the 3 reactions depend on the structure of the oxyradical. The species formed in one reaction generation are carbonyls, alcohols, acids, peroxyacyl nitrates and carbon oxides (figure 1.12).
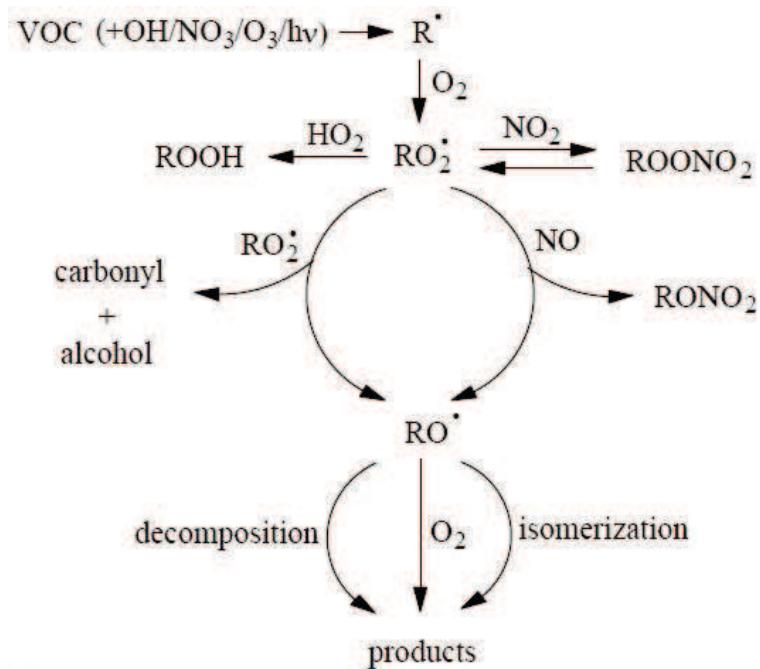
Figure 1.11: General oxidation scheme for VOCs [24]

Figure 1.12 represents the degradation of the given VOC into a set of "first generation products", which are themselves further degraded within the same general framework. This process is continued until the chemistry yields the ultimate carbon-containing product, CO_2.
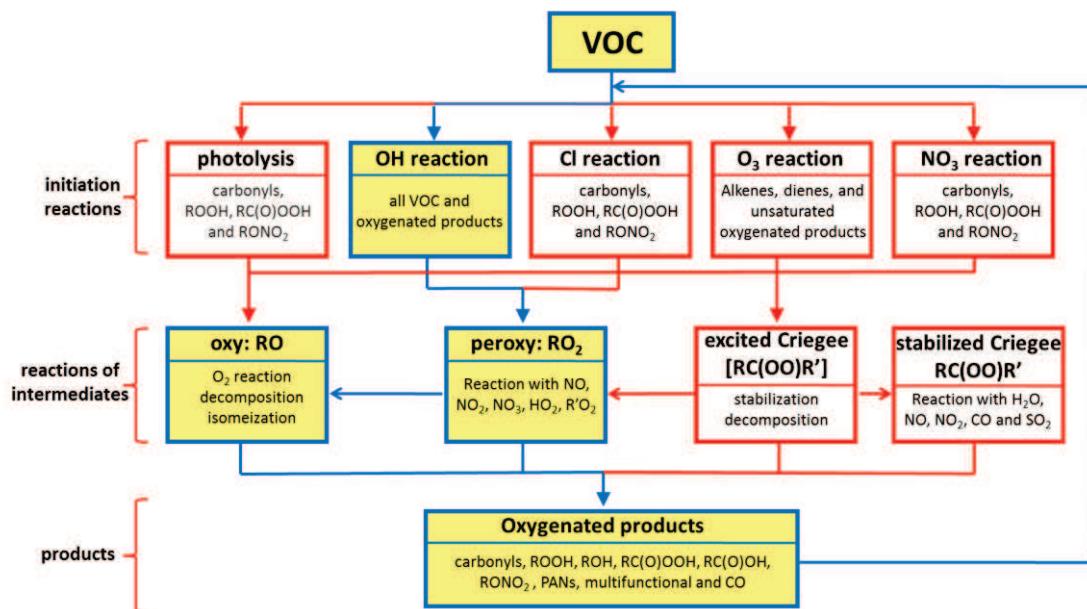
Figure 1.12: General description of a chemical mechanism. The main types of reaction considered and classes of organic intermediate and product which are potentially generated. The dominant pathways are highlighted using bleu/yellow frame.

1.D.IV. Oxygenated VOCs

The oxygenated volatile organic compounds, (OVOCs) often referred to as "oxygenates", make up part of VOCs. They contain carbon, hydrogen and oxygen atoms and optionally other heteroatoms. The most common oxygenates are the alcohols (ROH), ethers (ROR), aldehydes (RCHO), ketones [RC(O)R], esters [RC(O)OR], and acids [RC(O)OH] together with N- and O-atom containing oxygenates and other less abundant classes of oxygen-containing organic compounds.

➤ *Importance of Oxygenates in Atmospheric Chemistry*

All the organic compounds emitted into the atmosphere are converted into oxygenated organic compounds through several oxidation steps. As an example, the oxidation of ethane gives CH_3CHO, C_2H_5OH, and C_2H_5OOH as first generation products and CH_3OH, CH_3OOH, CH_2O, and $HC(O)OH$ as second generation products.[25] Consequently, the impact of OVOCs to the atmosphere is manifold. OVOCs participate in secondary organic aerosol formation, contribute to HO_x chemistry in the upper troposphere, play a role in the transport of pollutants, and are used as proxies for VOC emissions. [25]

➤ *Emissions of Oxygenates in the Troposphere*

These compounds enter the troposphere by several routes such as a) evaporation of oxygenated solvents or fuels used in industry and commercially available; b) emissions from hydrocarbon-fueled mobile or stationary sources from incomplete fuel combustion; c) emissions from biological sources d) evaporation and release from home usage of certain products and e) atmospheric oxidation of all hydrocarbon emissions that enter the atmosphere. It should be noted that since all the VOCs in the atmosphere are eventually rapidly converted into oxygenates, the entire class of VOCs should be considered as existing or potential oxygenates.

Furthermore, a detailed speciation of the top 25 OVOCs emitted in Great Britain for the year 2000 is presented in table 1.2. The order of the compounds is determined by the magnitude of the mass emissions and is not intended to reflect the relative

influence of these compounds on tropospheric chemistry. The total mass emission of all oxygenates is considered to be 312.51 ktonnes yr^{-1}.[25]

Table 1.2: Inventory and speciation of the OVOCs emitted from all anthropogenic sources in Great Britain in 2000. [25]

Species of Oxygenate	Total emissions (ktonnes yr^{-1})
Ethanol	101
Methanol	27.5
Formaldehyde	23.1
Acetone	22.3
2-Butanone	14.5
Butyl acetate	13.0
2-Propanol	11.4
Ethyl acetate	10.4
4-Methyl-2-pentanone	6.55
1-Butanol	6.09
2-Butoxyethanol	5.35
Acetaldehyde	5.06
Methyl acetate	4.82
1-Propanol	3.95
1-Methoxy-2-propanol	3.86
1-Methoxy-2-propyl acetate	**3.01**
Dimethyl ether	2.63
2-(2-Butoxyethoxy)ethanol	2.14
Furfural	1.97
Benzaldehyde	1.86
2-(2-Ethoxyethoxy)ethanol	1.68
Acrolein	1.63
2-Methyl-1-propanol	1.59
1-Propanal	1.56
2-Propyl acetate	1.54

2.   Objective of the study

2. Objective of the study

2.A. DISPATMO project

This study was carried out in the framework of the project DispAtmo (Etude de la prévision des risques de pollution liés à la DISPersion ATMOsphérique de produits chimiques) supported by FEDER (Fonds Européens de Développement des Régions). This chapter includes a presentation of the project, the contribution of the thesis on the project and the thesis objectives.

2.A.I. Presentation of the project

The DispAtmo project represents a framework for crisis management. In particular, it is a platform to aid in the design and management of the Internal Operation Plan (POI) which describes the procedures to be implemented in the event of an incident and maintained until the site is once again made safe. It is important to note that the European Directive Seveso obliges industrial plants to perform risk analyses in order to identify possible accident scenarios, assess their consequences and set up measures of prevention. Its translation into French law via the environmental code requires a POI to be set up and implemented for those sites.

The project was launched in July 2011, and was cooperation between more entities for a common research effort. The partners involved in the project are: Pôle National des Risques Industriels (PNRI-Bourges), Institut Pluridisciplinaire de Recherche en Ingénierie des Systèmes, Mécanique et Energétique (PRISME), Centre National de la Recherche Scientifique, through the Institut de Combustion Aérothermique Réactivité et Environnement (CNRS-ICARE) and private companies such as Nexter Munitions, the Sucrerie de Toury and AB-PROD. The project originally intended to last 36 months ending during 2014.

2.A.II. Objective of the project

The dispersion of chemicals because of an accidental release in the chemical storage area of an industry, attributed to explosions or fires of flammable stored compounds or after a leakage and subsequent evaporation, can pose risks to the environment. The consequences to the environment and the population depend on the nature of the products emitted but especially on their concentrations and toxicity. For the moment, risk studies in these companies take into account the origin of the risk (nature and quantity of hazardous substances) and consider specific danger zones to the risk of fire or explosion, while no environmental criterion is taken into account. Therefore, the objective of this project is to develop and validate numerical prediction tools which can point danger zones for the people and the environment because of a fire or an explosion at the chemical storage area. The goal is to design a risk management plan through a POI, impacting if necessary an intervention plan for the prefecture concerned. By this way the emergency responders have sufficiently accurate and rapid data in order to decide the emergency measures to be taken, such as the evacuation of the surrounding population. Ultimately, this tool will allow to an industry to have its own scenarios related to the combustion and the dispersion of its chemicals.

2.A.III. Modules and tasks of the project

The DispAtmo project is based on four modules. The first of these modules is composed of a digital POI generator and a digital database grouping information from paper-based POIs. This enables the information related to site safety to be updated and also enables the edition of the official document. The second module is based on the QUIC (Quic Urban & Industrial Complex) chemical agent atmospheric dispersion model system. This system enables the simulation of the dispersion of polluting chemical agents resulting from an accidental combustion. The third module, the Cartography module, is based on the use of a Geographical Information System (GIS) namely "Mapwindow GIS". This module supplies a set of functionalities enabling the analysis and representation of the data from QUIC. The final module is

the training simulator composed of a 3D digital world (POI3D) and a specialized MMI (Man Machine Interface). [26] This enables the user to simulate the safety and emergency procedures to be implemented during an incident in a virtual environment.

Furthermore, the project was separated in nine tasks (table 2.1) in order to allocate the activities on each partner according to their skills/expertise and to determine the project's timetable.

Table 2.1: Tasks of the project DISPATMO

1	**Task**	Project coordination
	Partners	PNRI
	Objectives	To coordinate the project to the scientific, technical and administrative and in order to ensure the progress and the implementation of various project tasks.
2	**Task**	Scanning industrial sites and their environment
	Partners	PRISME - MCDS, NEXTER Munitions, Sucrerie de TOURY, ABProd
	Objectives	To scan both industrial sites and their external environment (perimeter of ten kilometers - the distance is refined according to the obtained results of the model), to perform the mapping of pollutants following the evaluation of the dispersion.
3	**Task**	Combustion - Chemical inventory
	Partners	ICARE – CNRS, NEXTER Munitions, Sucrerie de TOURY
	Objectives	To determine the working basis for the chemical risk assessment for some chemicals stored in both industries. • Exhaustive inventory of chemicals stored on each industrial site. • Selection of the chemicals that can be the basis for the study according to their nature, quantities and location on the site.
4	**Task**	Combustion - Characterization of the chemical species
	Partners	ICARE - CNRS, NEXTER Munitions
	Objectives	To determine the combustion products of the four selected chemicals and their lifetimes: Primary products emitted directly from the combustion, and secondary products formed by the reaction of the primary ones.
5	**Task**	Combustion - Environmental impact
	Partners	ICARE - CNRS, NEXTER Munitions
	Objectives	To determine the toxicity of the combustion products of the four selected chemicals. These data were derived from the literature.
6	**Task**	Dispersion
	Partners	ICARE – CNRS, NEXTER Munitions, Sucrerie de TOURY
	Objectives	To achieve a numerical prediction, for the selected species stored and their combustion products, of the dispersion on the site and its external environment (the concentration of the pollutants from

		combustion and the dispersing area), using the emission scenarios (the dispersion origin, the storage location, the way of the molecule release) and the environmental conditions. The results shows if the storage locations are well positioned on the site or they have to be moved.
7	Task	Mapping the dispersion of the cloud on the sites and their environment
	Partners	PRISME - MCDS, NEXTER Munitions, Sucrerie de TOURY
	Objectives	To realize the mapping of pollutants (nature and concentration) around the two industrial sites to assess the chemical impact of an industrial accident on the environment. This mapping facilitates the intervention decisions inside the sites and the public authorities' decisions outside. It forms a POI Dynamic.
8	Task	Simplified tool for decision support
	Partners	PRISME - MCDS, NEXTER Munitions, Sucrerie de TOURY
	Objectives	To obtain, from the software performed, a quick tool and easy to use leading to a dynamic POI. It reacts in real time responding to an incident
9	Task	Synthesis
	Partners	PNRI, PRISME – MCDS, ICARE – CNRS, NEXTER Munitions, Sucrerie de TOURY, ABProd
	Objectives	To synthesize the overall work of the study

2.B. Contribution of the laboratory ICARE and the thesis on the project

The CNRS-ICARE laboratory was involved in tasks 3, 4, 5, 6 and 9 that concern the combustion, the characterization of the chemical species and products and the environmental impact and dispersion.

At first, as described in task 3, the two industries Nexter-Munition and Sucrerie de Toury, provided a detailed report regarding the nature, the location and the quantity of the chemicals stored on their site. Then, two of these species were selected (for each industry) to be the basis for the study. The principal selection criteria were the quantity and the toxicology of the species. Besides those, the chemicals should be flammable hydrocarbons (or mixture of them) in liquid form in order to study the combustion process. The selected chemicals for each industry are presented in table 2.2.

Table 2.2: Selected chemicals to be studied for the two industries

Nexter-Munition	Sucrerie de Toury
Toluene	Ethanol
Tiflex[a]	Butanone

[a] Tiflex solvent is a mixture, its detailed chemical composition is presented in annex I

Thereafter, the laboratory CNRS-ICARE characterized the chemical species as described in task 4. In particular, OH team (Oxydation des Hydrocarbures) determined the primary combustion products of the four selected species and estimated their concentrations. On the other hand, the objective of RA team (Réactivité Atmosphérique) was to define the atmospheric degradation of these chemical species and the one of their primary combustion products as well as to provide accurate kinetic and mechanistic information. To that end the gas phase oxidation of the compounds and their combustion products with the major oxidants of the atmosphere (i.e. $OH/Cl/NO_3/O_3$) and the photolysis rates need to be determined. At this point, it should be noted that for compounds studied extensively in literature (e.g. ethanol, toluene, etc.) no further laboratory measurements were conducted to determine neither the oxidation rate coefficients nor the degradation products, thus the kinetic/mechanistic information were drawn mainly from the literature. In particular, the chemical kinetic database of IUPAC[27] was used to obtain the Arrhenius expressions and the rate coefficients for the reactions of the oxidants with the compounds of interest. Regarding the degradation mechanism and the different oxidation schemes that lead to the second or later generation products formed, useful information were derived using the MCM platform (Master Chemical Mechanism)[17].

Concerning Tiflex solvent, both teams characterized its detailed chemical composition by identifying (OH and RA teams) and quantifying (OH team) the individual hydrocarbons that it consists of (annex I Tiflex composition). Thereafter, literature data were used to provide the kinetics and the oxidation products of the "well studied" Tiflex components. Contra wise, for hydrocarbons for which kinetics and atmospheric degradation mechanism were not studied (i.e. 1-methoxy-2-propyl

acetate), laboratory experiments were conducted by RA team employing the available laboratory techniques.

Subsequently, using the degradation rate coefficients of all the compounds of interest and those of their oxidation products with the main atmospheric oxidants, the estimated lifetime was determined for each hydrocarbon. The calculations were conducted considering a) different ground-level temperature conditions (i.e. 275, 283, 288, 293 K) and b) daytime and night-time conditions (that determined the oxidation process). All these pieces of information were necessary to predict their dispersion to the atmosphere (extended abstract in HARMO-15 Karaca et al.)[28].

In parallel to task 4 and within the framework of task 5, RA team provided the toxicity of the four selected chemicals, as well as the toxicity of the combustion and atmospheric degradation products from the corresponding safety data sheet of the compounds. In particular, the effects on human health and the environment, the Threshold of the First (Seuil des Premiers Effets Létaux - SPEL) and Significant Lethal Effects (Seuil des Effets Létaux Significatifs - SELS) and the Threshold of Reversible (Seuil des Effets Réversibles - SER) and Irreversible Effects (Seuil des Effets Irréversibles - SEI) were obtained from the literature.[29]

The results from the previous tasks were used to feed the dispersion modeling system QUIC, as wished in task 6. The Combustion Turbulent team at ICARE achieved numerical prediction assessing the influence of different parameters such as the real time wind field, building topography and composition-decay characteristics of the initially emitted species with diurnal variation. Considering these parameters at different accuracy levels and taking into account computational time, the dispersion modeling system QUIC obtained concentration contours of the selected species and their combustion products.

2.C. Aim of the thesis

The contribution of the present thesis to DispAtmo project was twofold. On the one hand, a detailed literature survey, as described previously (section2.B), was conducted to provide a) the gas phase degradation rate coefficients of the selected VOCs and those of their products with the oxidants of the atmosphere b) the

detailed oxidation pathways that lead to secondary or later generation products and c) the corresponding compounds toxicity.[28] On the other hand, a thorough kinetic and mechanistic study was carried out to determine the gas phase degradation of one of the main component of Tiflex solvent, the 1-methoxy 2-propyl acetate (MPA). **Nevertheless, the DispAtmo was the initial spark of the dissertation; the objective of the current thesis was to determine the degradation rate coefficients of OH radicals and Cl atoms with a series of acetate compounds that have insufficient or nonexistent literature data and are widely used in painting and coating industry. Besides, the UV absorption cross section coefficients were also determined in order to evaluate the potential photolysis of the chosen acetates. Essentially, the thesis is an extension of the activities occurred in DispAtmo project.** The study were triggered by the wide use of acetates as solvents in chemical industry that leads to the release of significant amounts into the atmosphere, the hazards of the studied compounds, **combined with the insufficient or nonexistent kinetic and mechanistic data in the literature**.

The obtained kinetic data were used to evaluate the environmental fate of the studied compounds. Specifically, the determined rate coefficients were used to estimate a) their lifetimes which reflect their total gas atmospheric degradation and b) their Photochemical Ozone Creation Potential (POCP) which notes the importance of OVOCs contribution to the atmospheric processes, global warming and climate change. Furthermore, the investigation of the mechanism leads to a complete and accurate description of the different degradation pathways, while the determination of the activation energy (for the compounds for which the temperature dependence was studied) indicates the reaction complexity. The kinetic and mechanistic results derived can be used as input data in photochemical atmospheric simulation models or chemical agent atmospheric dispersion models that aim to determine the air quality and distribution of these compounds in the atmosphere.

2.D. Literature survey

The **acetates** represent a class of monofunctional esters with the general formula ROC(O)CH$_3$, where R is an alkyl group. Acetates have found widespread use as

33

solvents. Many esters have pleasant odors and are present in vegetable oils, animal fats, essential oils, fruits, and pheromones and are often added to fragrances and consumer products to provide a pleasant odor.[30] Their emission into the atmosphere, as a result of their extensive use, leads to atmospheric oxidation largely initiated by OH radical attack. The UV absorption by acetates is only important for wavelengths below 240 nm and, hence, photolysis is not a significant tropospheric loss mechanism. Several studies have been performed the last three decades in order to evaluate the atmospheric degradation of the acetates with OH. On the contrary, literature data regarding the Cl or NO_3 oxidation of acetates are limited. Calvert et al.[25] provided recommended values combing data set of the overall studies (table 2.3). **The room temperature (298 K) rate coefficients of the acetates with OH radicals range from 0.35×10^{-12} for the simplest acetate, methyl acetate, to 7.39×10^{-12} cm^3 molecule^{-1} s^{-1} for the one with the longer carbon chain, n-pentyl acetate, while the Cl rate coefficients were at least by one order of magnitude faster.**

Table 2.3: Recommended rate coefficients for the reactions of acetates with OH, Cl and NO_3 at T= 298 K by Calvert et al. combining data set of all the studies performed.[25]

Compound	Formula	k_{OH} (10^{-12}) [a]	k_{Cl} (10^{-11}) [a]	k_{NO3} (10^{-17}) [a]
Methyl Acetate	$CH_3OC(O)CH_3$	0.35±0.07	0.26±0.08	-
Ethyl Acetate	$C_2H_5OC(O)CH_3$	1.67±0.25	1.85±0.37	1.30 [b]
n-Propyl Acetate	$n\text{-}C_3H_7OC(O)CH_3$	3.45±0.86	7.38±1.48	5.00 [b]
iso-Propyl Acetate	$iso\text{-}C_3H_7OC(O)CH_3$	3.79±0.76	2.44±0.61	-
n-Butyl Acetate	$n\text{-}C_4H_9OC(O)CH_3$	5.66±1.10	15.3±3.83	-
iso-Butyl Acetate	$(CH_3)_2CHCH_2OC(O)CH_3$	6.47±0.97	10.5±1.58	-
sec-Butyl Acetate	$C_2H_5(CH_3)CHOC(O)CH_3$	6.10±1.20	9.07±1.81	-
tert-Butyl Acetate	$(CH_3)_3COC(O)CH_3$	0.58±0.14	2.42±0.28[31] 1.58±0.13[32]	-
n-Pentyl Acetate	$n\text{-}C_5H_{11}OC(O)CH_3$	7.39±1.8	-	-

[a] Units of cm^3 molecule^{-1} s^{-1}
[b] Estimated error by a factor of 2

The **alkoxy acetates** is a class of multifunctional oxygenated organic compounds (multifunctional ethers) with the general formula $RO(C_nH_{2n})OC(O)CH_3$, where R is an alkyl group and C_nH_{2n} is an alkyl substituent missing one hydrogen. Alkoxy acetates are increasingly being employed as water-soluble solvents and fuel additives, while another source is the tropospheric degradation of diethers which are also used as solvents and fuel additives.[25] The extensive use of the alkoxy acetates leads to significant emission into the atmosphere. The environmental fate and impact of these compounds has been purely studied in literature. The literature studies are focused on the gas-phase reaction with OH radicals (table 2.4). Particularly, the first literature studies reporting the OH rate coefficient with $CH_3CH_2OCH_2CH_2OC(O)CH_3$ (EEA) were carried out by Hartmann et al. (1987)[33] and Williams et al. (1993)[34]. Thereafter, O'Donnell et al. (2004)[35] have determined the rate coefficients for OH reactions with a series of four alkoxy acetates, $CH_3OCH_2OC(O)CH_3$ (MMA), $CH_3CH_2OCH_2OC(O)CH_3$ (EMA), $CH_3OCH_2CH_2OC(O)CH_3$ (MEA) and EEA (table 2.4) using a combination of relative and absolute techniques. **The room temperature (298 K) rate coefficients of the alkoxy acetates range from 2.74×10^{-12} for the simplest alkoxy acetate, MMA, to 12.3×10^{-12} cm^3 molecule^{-1} s^{-1} for the most complex, EEA.** Furthermore, it has to be noted that rate coefficients for all compounds display negative temperature dependences.

A (10^{-12})	B (K)	k_{OH} (10^{-12})	T (K)	Technique [a]	Reference	Temperature Range (K)
				OH + CH$_3$OCH$_2$OC(O)CH$_3$ (MMA)		
		2.78 ± 0.17	298	RR (n-C$_3$H$_7$OH)	O'Donnell et al.[35]	
1.8 ± 0.4	-(134 ± 75)	3.08 ± 0.07	263	PLP-LIF	O'Donnell et al.[35]	263 – 372
		3.06 ± 0.06	273			
		2.70 ± 0.07	298			
		2.77 ± 0.10	323			
		2.78 ± 0.08	348			
		2.61± 0.10	372			
				OH + CH$_3$CH$_2$OCH$_2$OC(O)CH$_3$ (EMA)		
		6.21 ± 0.28	298	RR (n-C$_3$H$_7$OH)	O'Donnell et al.[35]	
1.9 ± 0.8	-(380 ± 144)	7.79 ± 0.28	263	PLP-LIF	O'Donnell et al.[35]	263 – 372
		8.40 ± 0.37	273			
		6.39 ± 0.43	298			
		5.79 ± 0.22	323			
		5.61 ± 0.16	348			
		5.53 ± 0.30	372			
				OH + CH$_3$OCH$_2$CH$_2$OC(O)CH$_3$ (MEA)		
		8.72 ± 0.76	298	RR (n-C$_3$H$_7$OH)	O'Donnell et al.[35]	
2.9 ± 1.5	-(309 ± 162)	8.95 ± 0.78	273	PLP-LIF	O'Donnell et al.[35]	263 – 372
		7.83 ± 0.31	298			
		7.79 ± 0.29	333			
		6.38 ± 0.30	372			
				OH + CH$_3$CH$_2$OCH$_2$CH$_2$OC(O)CH$_3$ (EEA)		
		13 ± 2	298	PLP-RF	Hartmann et al.[33]	
		11.64 ± 1.44	298	RR (CH$_3$CH=CH$_2$)	Williams et al.[34]	
		13.94 ± 0.64	298	RR (n-C$_4$H$_9$OH)	O'Donnell et al.[35]	
1.4 ± 0.6	-(642 ± 148)	15.53 ± 0.68	273	PLP-LIF	O'Donnell et al.[35]	263 – 372
		12.10 ± 0.29	298			
		9.37 ± 0.61	333			
		8.55 ± 0.43	368			

[a]Abbreviations used for the techniques. RR: relative rate measurements, PLP-LIF: pulse laser photolysis-laser induced fluorescence, PLP-RF: pulse laser photolysis-resonance fluorescence
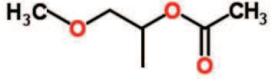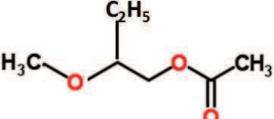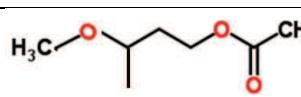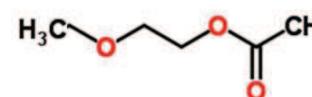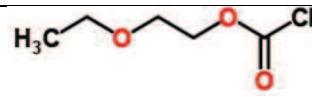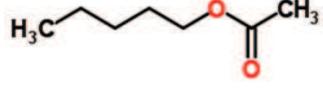
Assuming globally averaged $[OH] \approx 2 \times 10^6$ radicals cm^{-3}, lifetimes for the four alkoxy acetates is quite short, ranging from one-half day (EEA) to 2.1 days (MMA). Product studies on the alkoxy acetates species are limited to only one study of OH-initiated oxidation of EEA by Wells et al. (1996)[36]. The formation of three major products was observed: $CH_3C(O)OCH_2CH_2OCHO$ (37 ± 3%), ethyl formate (33 ± 2%) and $CH_3C(O)OCH_2CH_2OC(O)CH_3$ (4 ± 0.5%) (the oxidation mechanism of EEA by Wells et al. is given in section 6.C).

However, one can note that there is a significant lack of laboratory data regarding the degradation (kinetics and products) of higher molecular weight (> 6 carbons) or multi-branched acetates with OH radicals. Besides, it is also extremely challenging to investigate for the first time the degradation kinetics of this class of compounds with Cl atoms, an important tropospheric oxidant of the troposphere.

2.E. Selection of compounds to be studied

The selected OVOCs for this study were 1-methoxy 2-propyl acetate (MPA), 2-methoxy-butyl acetate (2MBA), 3-methoxy-butyl acetate (3MBA), methoxy ethyl acetate (MEA), ethoxy ethyl acetate (EEA) and n-pentyl acetate (n-PA) (table2.5).

Compound	Molecular formula	Condensed formula	Structural-skeletal formula
1-methoxy-2-propyl acetate (MPA)	$C_6H_{12}O_3$	$CH_3OCH_2CH(CH_3)OC(O)CH_3$	
2-methoxy butyl acetate (2MBA)	$C_7H_{14}O_3$	$CH_3OCH(CH_2CH_3)CH_2OC(O)CH_3$	
3-methoxy butyl acetate (3MBA)	$C_7H_{14}O_3$	$CH_3OCH(CH_3)CH_2CH_2OC(O)CH_3$	
2-methoxy ethyl acetate (MEA)	$C_5H_{10}O_3$	$CH_3OCH_2CH_2OC(O)CH_3$	
2-ethoxy ethyl acetate (EEA)	$C_6H_{12}O_3$	$CH_3CH_2OCH_2CH_2OC(O)CH_3$	
n-pentyl acetate (n-PA)	$C_7H_{14}O_2$	$CH_3CH_2CH_2CH_2CH_2OC(O)CH_3$	

The major atmospheric sources of these compounds are solvent use and chemical industries (table 2.6). The most common use of solvents is in the formulation of industrial coating materials such as paints, inks and adhesives. As described before, evaporation of the solvent and release from home usage after application is an important aspect of its use.

Compound	Total emissions (tons/year)	Sources of emissions
1-methoxy-2-propyl acetate (MPA)	3010[25]	Industrial coatings (metal and plastics, automotive, vehicle refinishing). Industrial uses (solvent). Printing (overprint varnishes, flexible packaging). Wood impregnation (light organic solvent preservative). [25]
2-methoxy butyl acetate (2MBA)	-	-
3-methoxy butyl acetate (3MBA)	8.06[25]	Coating manufacture (paint)[25]. Industrial uses - solvent for cleaning LCD and Semiconductors. Coatings manufacture (paint). Packaging (solvent and additive). Printing (inks).[37]
2-methoxy ethyl acetate (MEA)	382[25]	Industrial uses (solvent). Printing (overprint varnishes, flexible packaging, screen printing). Wood impregnation, (light organic solvent preservative). Industrial adhesives (pressure sensitive tapes). Agrochemical use.[25]
2-ethoxy ethyl acetate (EEA)	693[25]	Industrial uses (solvent). Industrial coatings (metal and plastics). Coatings manufacture (paint). Surface cleaning (textile coating). Industrial coatings (agricultural and construction, marine). Printing (overprint varnishes). [25]
n-pentyl acetate (n-PA)	-	Industrial coatings (additives). Painting (automotive paints, additives, flavoring agent). Industrial uses (solvent, processing aids, petroleum production). Medicine (preparation of penicillin). Cosmetics (personal care, pet care)[38, 39]

Besides, the molecular structure of the selected compounds allowed us to evaluate and clarify the influence of a) the carbon branching b) the chain length and c) the presence of the ether group to the degradation rate coefficients of the acetates with OH and Cl. It is important to note that for most of the studied compounds there are no literature data. Especially, in case of the acetate degradation from Cl atoms, **this is the first experimental kinetic study signifying their atmospheric importance.**

In addition, it should be noted that the ultimate fate of these compounds in the atmosphere is partially related to their physical properties, such as their vapor pressure, boiling point, melting point that are presented in table 2.7. The vapor pressure of a compound is an important data for its usefulness as a solvent and one of the factors that determine whether an oxidation product is expected to appear in the gas or aerosol phase. The lower the vapor pressure of a compound, the greater is the chance that it will reach its saturation concentration in the atmosphere and condense onto existing particles to form secondary organic aerosol. The melting and boiling points indicate if the compound is either liquid or solid at one atmosphere pressure and 293 K.

Table 2.7: Physical properties of the selected compounds derived from chemspider database.[40]

Compound	Melting Point at 760 Torr (K)	Boiling Point at 760 Torr (K)	Vapor Pressure (Torr at 298 K)
MPA	206	418	3.1
2MBA	-	450	1.0
3MBA	193	448	1.2
EEA	208	416	5.4
MEA	211	429	2.9
n-PA	173	423	3.9

3. Experimental techniques

3. Experimental techniques

This chapter includes a comprehensive presentation of the experimental techniques used during the Thesis. The UV absorption cross sections of 1-methoxy 2-propyl acetate (MPA, $CH_3OCH_2CH(CH_3)OC(O)CH_3$), 2-methoxy-butyl acetate (2MBA, $CH_3OCH(C_2H_5)CH_2OC(O)CH_3$), 3-methoxy-butyl acetate (3MBA, $CH_3OCH(CH_3)CH_2CH_2OC(O)CH_3$) were determined using an Ultra Violet spectrophotometer. Kinetic studies for the reactions of OH radicals and Cl atoms with MPA, 2MBA, 3MBA, methoxy ethyl acetate (MEA, $CH_3OCH_2CH_2OC(O)CH_3$), ethoxy ethyl acetate (EEA, $C_2H_5OCH_2CH_2OC(O)CH_3$) and n-pentyl acetate (n-PA, $CH_3CH_2CH_2CH_2CH_2OC(O)CH_3$) were performed using i) a pulsed laser photolysis-laser induced fluorescence technique (PLP-LIF), ii) a low pressure fast flow tube reactor coupled with a quadrupole mass spectrometer (FFT-QMS) and iii) a 200L atmospheric simulation chamber coupled with a gas chromatograph flame ionization detector (ASC-GC/FID). In addition a mechanistic study of MPA oxidation was conducted using the ASC. A brief description of the experimental techniques will be given below while details are presented in previous thesis and publications from the group. From the other hand, a detailed table with all the chemicals used their stated purities and suppliers are given in annex II.

3.A. Ultra Violet absorption cross-section

Ultra Violet spectrophotometry is the quantitative analytical method that measures the reflection or transmission properties of the molecules as a function of the wavelength. It can be used to determine the UV spectra and to measure the absorption cross section of countless compounds. In particular, the UV absorption cross section values can be used to a) estimate the photolysis rates of numerous VOCs, b) determine the concentrations of the compounds in the atmosphere or in the atmospheric simulation chambers using the DOAS method for example and c) verify the absence of the compound photolysis by the PLP-LIF technique.

3.A.I. Apparatus

Ultra Violet - visible (UV-vis) absorption cross section measurements were performed in a double wall Pyrex temperature-controlled absorption cell (100 cm long and 2.5 cm internal diameter) equipped with quartz windows (figure 3.1). Pressure gauges of 0-10 Torr and 0-1000 Torr were used to measure the pressure of the studied compound and the cell pressure respectively. A deuterium (D_2) and a zinc (Zn) lamp were used as UV-Vis light sources. The collimated output of the lamp passed through the absorption cell and was detected by a spectrophotometer (Princeton Instrument, Inc ACTON SP2300i) equipped with a triple grating monochromator. The three different gratings, 1800, 1200 and 600 traits mm^{-1} could be used in the wavelength region of 200-900 nm, with a focal length of 300 nm and 0.2 nm resolution. The spectrophotometer was coupled with a camera Charge Coupled Device ROPER (PIXIS 1024 x 256 pixels) which had a pixel dimension of 26 × 26 μm^2. The experimental set up has been extensively described in thesis[41] and publications[42] from the group.

In the case of Zn lamp the absorption measurements were always performed in presence of an interferential filter centered at 214 nm and the intensity of the UV light was detected either with a diode or with the spectrometer. On the contrary when D_2 lamp was the light source the cross section was determined in the presence or in absence of the interferential filter in order to conduct the measurement at the wavelength of interest. The measurements were conducted under static conditions and the camera was guided by the Winspec software.
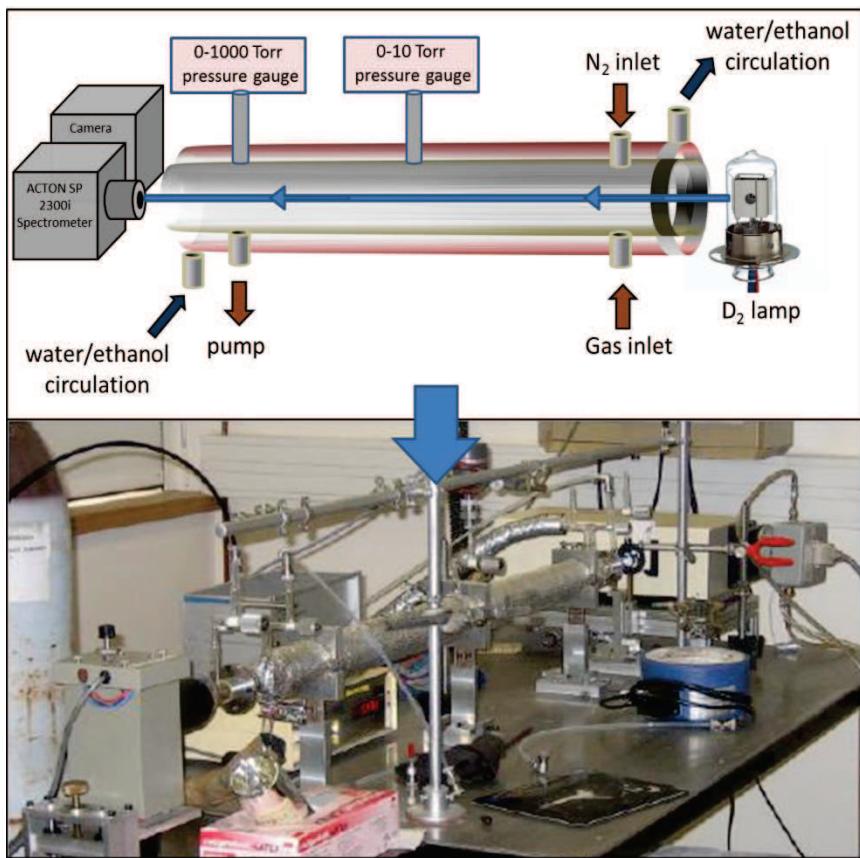
Figure 3.1: Schematic diagram and picture of the UV absorption cross section experimental system.

3.A.II. Procedure

The first step of the experimental procedure was the Camera cooling down to -60 ^{o}C in order to reduce the thermic background of the pixels. Then the grating was set to 1200 traits mm^{-1} within the wavelength region of 200-370 nm and a focus of 60 nm. Before starting the UV absorption cross section measurements, the wavelength scale was calibrated. In particular, emission lines from Zn-lamp (213.8 nm) and Hg Pen ray lamp (253.65, 296.73, 313.15 and 365.02 nm) were used to calibrate the wavelength scale with an accuracy of 0.1 nm. In addition, prior to UV absorption cross section measurements, the cell was repeatedly purged with N_2 - pumped (10^{-2} Torr) to eliminate the presence of absorbing species (i.e. impurities) that could influence the calibration experiment.

Thereafter, the background spectra of the instrument (I_{bkg}) and the reference spectra (I_o) which corresponded to the light intensity without the compound were recorded. Subsequently, several concentrations of the studied compound were introduced in

the cell, the corresponding pressure was measured (pressure gauge 0-10 Torr) and the absorption spectrum (I_{abs}) was recorded (E.3.1). At this point it has to be noted that the absorption experiments were conducted in two different ways a) by increasing progressively the concentration of the compound and b) randomly to avoid the contribution of systematic errors. The concentration range used was not standard but depending on the compound and its vapor pressure. In addition, to ensure that neither condensation of the low vapor pressure of OVOCs on the wall of the absorption cell nor possible photolysis of the OVOC do impact our measurements, I_{abs} was recorded right after pressure stabilization in the reactor (~2 min after OVOC introduction) and after 30 and 45 min of OVOC introduction. The cross section values obtained with the different methods were almost identical (considering the experimental uncertainties).

It has to be noted that all the studied compounds were degassed by repeated freeze-pump-thaw cycles before their use to eliminate the impurities. In addition, the purity of each compound was verified with a GC-MS and showed that the concentration of impurities was beyond the detection limit.

3.A.III. Analysis

The cross section, in cm^2 molecule^{-1}, at wavelength λ was measured using the Beer–Lambert's law:

$$\sigma = -\frac{\ln\left(I_{abs}(\lambda)\big/I_0(\lambda)\right)}{LC} \qquad \text{(E.3.1)}$$

where

I_{abs} : light intensity with the studied compound in the absorption cell

I_0 : light intensity without the studied compound in the absorption cell

L : path length, in cm

C : concentration of the OVOC, in molecule cm^{-3}

The concentration (C) of the studied OVOC, in molecule cm^{-3}, was measured using the following expression derived from the ideal gas law:

$$C = \frac{P_{OVOC}}{k \times T} \qquad\qquad (E.3.2)$$

where,

P_{OVOC} : pressure of the compound in the cell, in the range 0.2-2.1 Torr

k : Boltzmann constant, 1.0356×10^{-19} Torr cm^3 molecule^{-1} K^{-1}

T : temperature of the cell, in the range of 298-335 K

3.B. Pulsed Laser Photolysis - Laser Induced Fluorescence

The Pulsed Laser Photolysis - Laser Induced Fluorescence (PLP-LIF) is an excellent radical generation/detection time resolved method used in the field of chemical kinetics to measure absolute rate coefficients for a large series of reactions involving OH radicals.

In this study the absolute rate coefficients for the OH reaction with a series of methoxy acetates were measured by the PLP-LIF technique. An exciplex laser was used to generate the OH radicals and the laser induced fluorescence was used to detect them.

3.B.I. Production of OH radicals

> *Exciplex laser*

An exciplex laser, often inappropriate called as excimer laser, is a form of ultraviolet laser. This type of laser typically uses a combination of an inert gas (Ar, Kr, or Xe) and a reactive halogen gas (F or Cl). Under the appropriate conditions of electrical stimulation and high pressure, a pseudo-molecule called an excimer, or in the case of noble gas halides an exciplex, is created.*[43] This pseudo-molecule can only exist in an energized state and can give rise to laser light in the ultraviolet range.

Laser action in an excimer molecule occurs not because it has a bound (associative) excited state, but a repulsive (dissociative) ground state. This is because noble gases such as xenon and krypton are highly inert and do not usually form chemical

---

* The term excimer is short for "excited dimer", while exciplex is short for "excited complex".

compounds. However, in an excited state, they can form temporarily bound molecules with themselves (dimers) or with halogens (complexes) such as fluorine and chlorine. The excited compound can give up its excess energy by undergoing spontaneous or stimulated emission, resulting in a strongly repulsive ground state molecule which very quickly (on the order of a picosecond) dissociates back into two unbound atoms. This forms a population inversion.

In particular in these experiments a krypton fluoride laser Coherent Compex Pro 102 was used. The krypton and fluorine gas absorb energy, then the ionized krypton reacts with the ionized fluorine producing krypton fluoride, a temporary complex, in an excited energy state:

$$Kr + e^- \rightarrow Kr^+ + 2e^- \qquad\qquad\qquad (R.3.1)$$

$$F_2 + e^- \rightarrow F^- + F \qquad\qquad\qquad (R.3.2)$$

$$F^- + Kr^+ + He \rightarrow KrF^* + He \qquad\qquad\qquad (R.3.3)$$

The complex can undergo spontaneous or stimulated emission, reducing its energy state to a metastable, but highly repulsive ground state. The ground state complex quickly dissociates into unbound atoms:

$$KrF^* \rightarrow Kr + F + h\nu \qquad\qquad\qquad (R.3.4)$$

The result is an emission of radiation that occurs at 248 nm, corresponding with the energy difference between the ground state and the excited state of the complex. At this wavelength H_2O_2 was photolysed to produce hydroxyl radicals.

$$H_2O_2 + h\nu \ (\lambda=248 \ nm) \rightarrow 2OH \qquad\qquad\qquad (R.3.5)$$

3.B.II. Detection of OH radicals

➢ *Laser Induced Fluorescence spectroscopy*

Laser Induced Fluorescence (LIF) spectroscopy is based on the spontaneous emission of light (fluorescence) of atoms, radicals or molecules, which originally are excited at selected electron quantum levels, absorbing laser (monochromatic) radiation. The transition between the same conditions, single-multiplicity (singlet states, Sx, where x = 0,1,2, …) statements is permissible ($S_1 \rightarrow S_0$) and it is a quick process (10^{-6} - 10^{-9} s). However, it should be noted that the lifetime and the quantum yield of fluorescence are two characteristic parameters of the fluorophore radical or molecule. The fluorescence spectra describe qualitatively and quantitatively the population distribution of the excited and the basic electronic states, and the temperature effect on the molecule distributions in their degrees of freedom. The main advantages of the fluorescence technique are the high resolution and the quantitative measurement of the fluorescence which have made this technique an excellent radical detection method in the field of chemical kinetics.

Quenching can influence the intensity of fluorescence by decreasing the signal. The quenching may be a result of several phenomena, such as chemical reactions of excited states, molecular rearrangement, formation of complexes in the ground state and transfer of energy via collisions. In the experiments of this study quenching is negligible, and in combination with the low background signal, the sensitivity of the technique was increased significantly. However, the presence of even minimal background signal cannot be avoided in LIF spectroscopy, since it originates from the scattered incoming light to the optical ports or inside the reactor. From the other part, an important advantage of the technique of fluorescence is also the homogeneous diffusion of the emitted light (spherical), in all directions in space (the fluorescence is not polarized). The basic disadvantage of the method is the difficulty of the direct and absolute determination of the fluorescent compound concentration from the fluorescence intensity.

It should be noted that for the successful application of the LIF technique several experimental standards should be achieved. The stimulating laser beam and the photomultiplier have to be attached to a suitable arrangement to minimize the light

that arrives in the probe. Thus, the fluorescent signal is not lost in the background even though the laser energy is much larger than that of fluorescence. In addition, the fluorescence has to be monitored at a different wavelength, of that of the laser light. Finally, a suitable interference filter has to be used before the PM in order to detect only the fluorescence signal of interest (without any contributions from other fluorophore components) and to minimize the contribution of the scattered light.

Chemical kinetics experiments require direct, quantitative, sensitive and rapid detection of OH radicals. Critical parameter for the successful application of the technique is the detection limit*; to avoid secondary chemical complications concentrations of OH radicals should be kept quite low. However, the need for kinetic experiments in real-time (time-resolved experiments) and in the time scale of µs - ms, as well as the scattering problems, define detection limit of LIF in ~ 10^9 radicals cm^{-3}. In order to conduct reliable rate coefficient measurements, the detection limit for the measurement of OH radicals, should be at least equal, with their lower concentration. Typical range of OH radical concentration in kinetic experiments is 10^{10}-10^{12} radicals cm^{-3}.

> ### *OH excitation and relaxation*

To excite the fluorophore OH radicals, a dye laser is used. Critical parameter for the detection of OH radicals is the selection and adjustment of the appropriate spectral line of excitation. In those experiments monochromatic irradiation with the wavelength of 282 nm is used to excite the OH radical by exciting simultaneously three overlapping rotational lines ($Q_1$1, $R_2$3 and Q_{21}1) of the band $A^2\Sigma^+$ (v'= 1) ← $X^2\Pi$ (v''= 0) of OH radicals (Figure 3.2).

* Detection limit is the lowest quantity of a substance that can be distinguished from the absence of that substance.
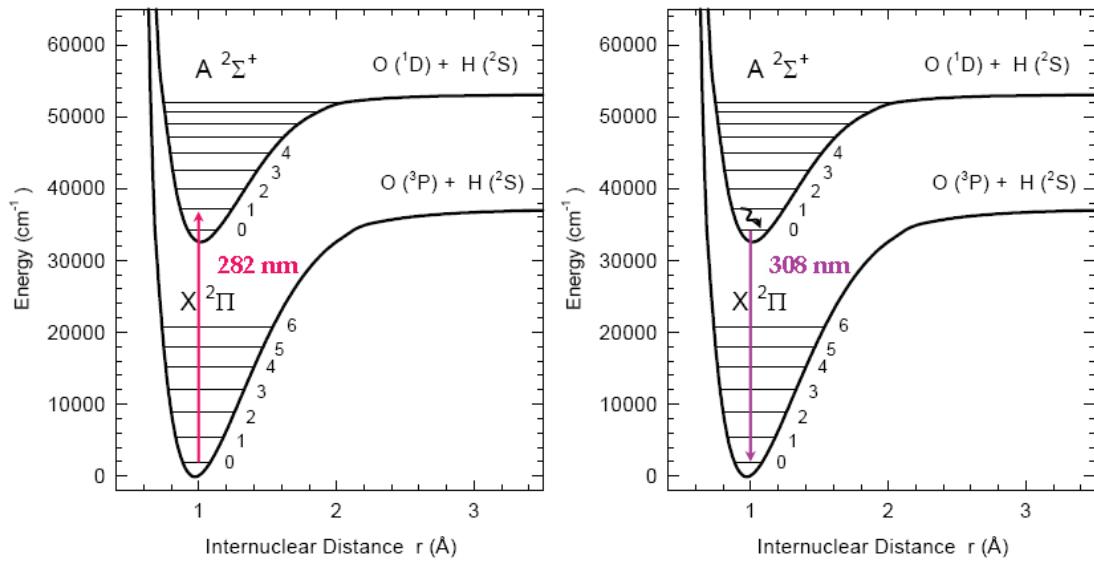
Figure 3.2: Simulated dynamic energy curves of the excitation - thermal relaxation- fluorescence of OH radicals.[2]

The excited OH radicals return to the ground state by fluorescence. The relaxation can bring back the molecules at various vibrational levels of the fundamental electronic state. As a result, the fluorescence can be detected at different wavelengths than that of the initial excitation, reducing the background signal.

$A^2\Sigma^+ (v'=0) \rightarrow X^2\Pi (v''= 1)$ $\qquad$ $\lambda = 343$ nm

$A^2\Sigma^+ (v'=0) \rightarrow X^2\Pi (v''= 0)$ $\qquad$ $\lambda = 308$ nm

$A^2\Sigma^+ (v'=1) \rightarrow X^2\Pi (v''= 1)$ $\qquad$ $\lambda = 314$ nm

$A^2\Sigma^+ (v'=1) \rightarrow X^2\Pi (v''= 0)$ $\qquad$ $\lambda = 282$ nm
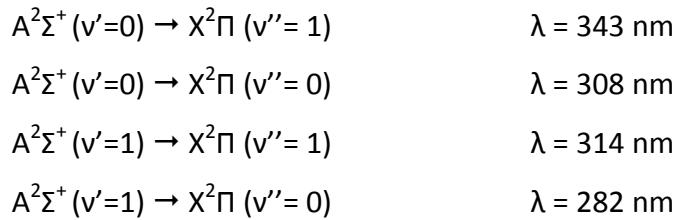
The relaxation time (fluorescence, $\tau \sim 10$ nanosecond) is significantly shorter than that of the reaction (micro-millisecond)[2], ensuring the necessary rapid sampling. Figure 3.3 presents the rotational spectrum of the excitation and relaxation of the OH radicals, between electronic states $X^2\Pi \rightarrow A^2\Sigma$. This spectrum is featured with excellent accuracy and has been studied by many research groups.[2,44]
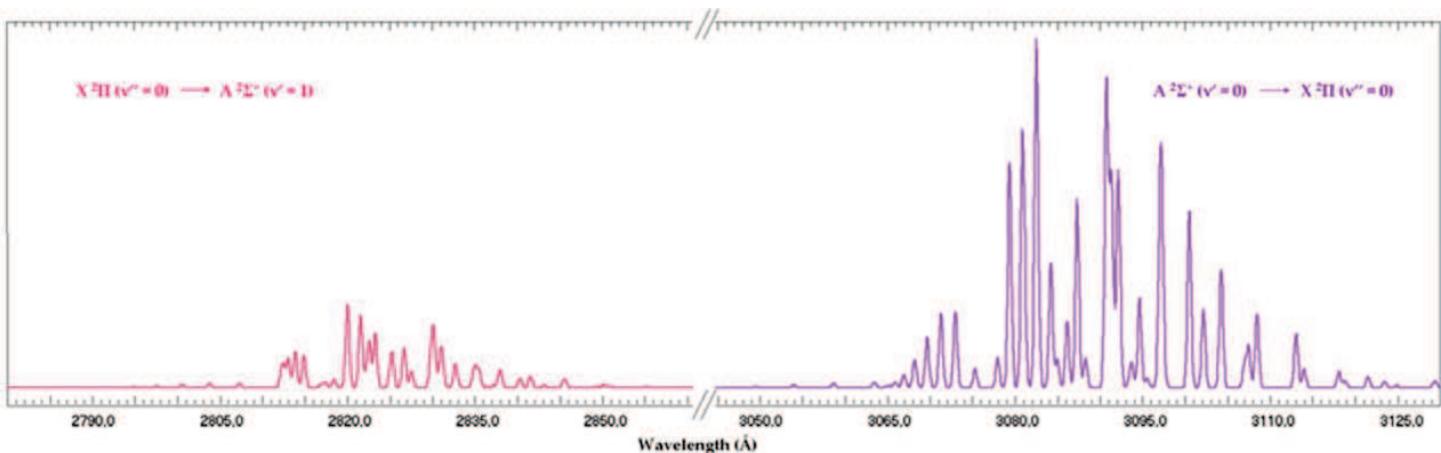
Figure3.3: LIF Excitation – relaxation spectra of OH radicals with a resolution of 0.5 Å and at 2 mbar pressure. [2]

The relaxation of the OH radical takes place via energy transfer processes (collisions with other molecules) in the state $A^2\Sigma^+$ (v'=0) and then fluorescence, OH radical return to the ground state $X^2\Pi$ (v''= 0) as shown in Figure 3.2. The lifetime of the excited state, which coincides with the total lifetime of the fluorescence (the non-radiative internal conversion processes are rapid) is determined to be ~ 0.7 ms.

3.B.III. Apparatus

OH radicals were generated by photolysis of H_2O_2 at 248 nm using a pulsed (10Hz) KrF exciplex laser Coherent Compex Pro 102. The precursor mixture consisted of Kr, F_2, He, Ne at the high pressure of ~ 3300 mbar. The laser beam was driven into the cell by a prism. The energy of the photolysis laser was of the order of 15-25 mJ per pulse in the cell, the pulse hit the cell every 100 ms. The duration of the pulse was 20ns, while the dimensions of the beam were (24x10) mm.

As far as the OH signal measurement is concerned, a Nd:YAG 60 Continuum pumped frequency-doubled dye laser was triggered at a variable time after the photolysis pulse. The dye used was rhodamine 590. This dye gives a pulse at a wavelength, λ = 564 nm. This radiation is passed through a doubling crystal from which a pulse of λ/2 is obtained. The crystal is inserted into the interior of the laser system to allow a permanent adjustment of the wavelength. The final laser pulse obtained is at a wavelength of 282 nm. The beam, with 6mm diameter, was reflected into the cell by

a set of mirrors. The energy of the dye laser in the cell was of the order of 1-2 mJ per pulse, with a pulse width of ~7ns.

The reactor was constructed of Pyrex and had an internal volume of about 200 cm^3. The reaction cell was double-walled in order to regulate the temperature by cooled ethanol-water circulation or heated water circulation. The temperature of the gases in the cell was measured using a chromel-alumel thermocouple which could be moved into the reaction volume. The cell had four ports fitted with quartz windows defining a cross in a horizontal plane. The two of these windows transmitted the UV excitation beam; while the rest two of them transmitted the UV irradiation of the laser induced fluorescence. The two beams intersected at the center of the cell with an angle of 90° maximizing the intersection volume in front of a fifth port. This port had a quartz lens and transmitted the fluorescence of the OH radicals to be detected. The total fluorescence of OH was transmitted through a narrow-band pass filter (~309 nm peak transmission) and imaged onto a photomultiplier (PM), Hamamatsu R292. Both the band pass filter and the PM tube positioned below the reaction vessel and coaxial with the gas flow discriminate against the scattered probe laser light. The output pulse from the PM tube was integrated for a pre-set period by a gated charge integrator. The integrated signal was digitized and sent to the microcomputer for averaging and analysis. A detailed description of the experimental technique has been published in scientific journals[45, 46] and thesis[47].
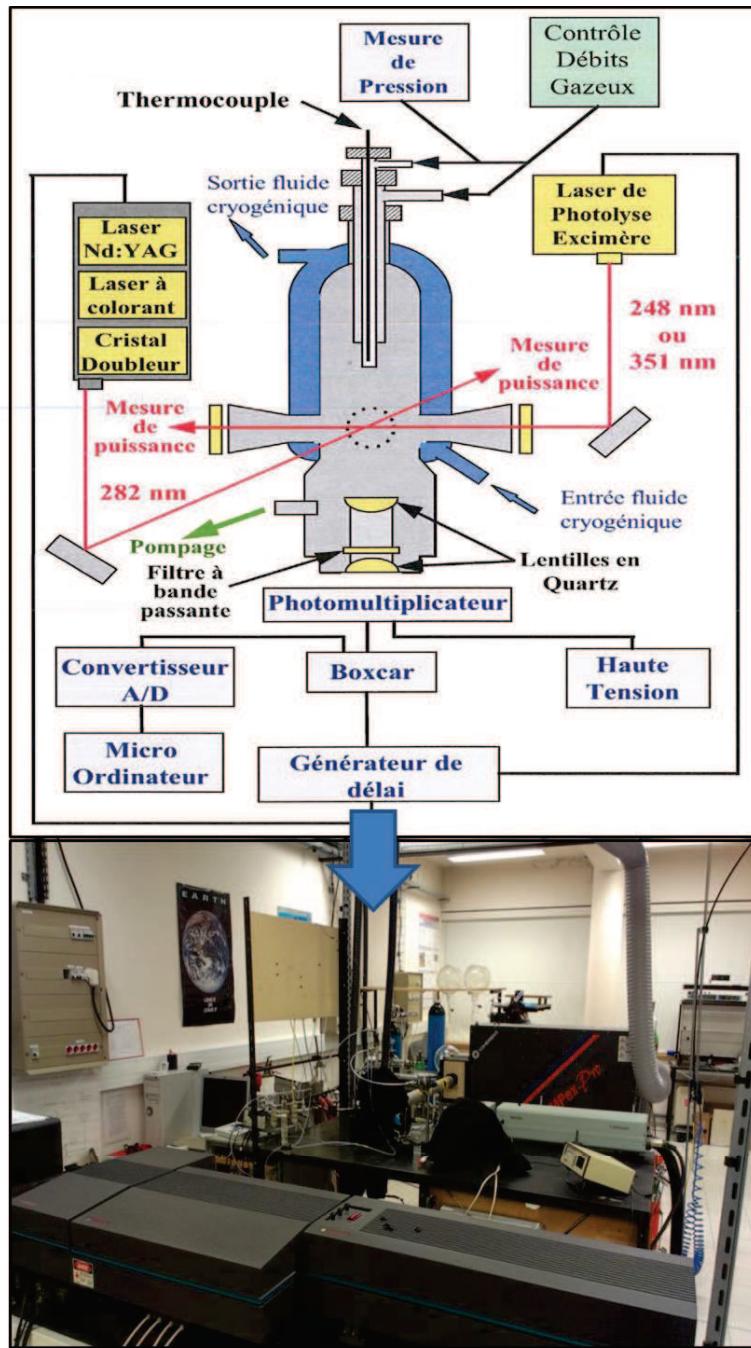
Figure 3.4: Schematic diagram and picture of the PLP-LIF experimental system used in the OH absolute rate measurements.

3.B.IV. Procedure

Hydrogen peroxide (60 wt%) was concentrated by bubbling purified air through the solution for several days prior to use, and constantly during the course of the experiments to remove water. The concentrated H_2O_2 was introduced into the

reaction cell by bubbling a small flow of He (1-2 ml min^{-1}) through a glass H_2O_2 bubbler maintained at room temperature.

A series of experiments were conducted using the UV absorption apparatus in order to check if there is any UV light absorption of the studied compound. The results showed that none of them absorb at the wavelength range of 240-340 nm. Afterwards, all the studied OVOCs were degassed by repeated freeze-pump-thaw cycles and diluted in He in a 10 L glass bulb at a total pressure of about 550-700 Torr, respecting their vapor pressure. The experiments were conducted using different mixtures of the studied compound in He in order to avoid any possible uncertainties in mixture preparation that would affect the OVOCs concentration determination. The OH radical precursor (H_2O_2), the gas mixture of the studied compound, and the He bath gas were flowed vertically (total flow ~360-380 ml min^{-1}) through the cell mutually orthogonal to the photolysis and to the probe laser beams. Their linear velocity had a range between 5 and 20 cm s^{-1}. All the flow rates are measured with mass flow controllers calibrated by measuring the rate of pressure increase in a known volume. The pressure inside the cell was measured with a pressure gauge connected near the entrance of the cell.

OH radicals were generated and monitored at various reaction times. Both the photolysis and the probe laser operate at a repetition rate of 10 Hz. Typically, the fluorescence signal resulting from 200 probe laser shots was measured for 8-20 different delay times and averaged to generate OH concentration-time profiles over at least six lifetimes.

3.B.V. Analysis

The H_2O_2 concentration, in molecule cm^{-3}, introduced in the cell by the bubbler was estimated using the expression:

$$[H_2O_2] = \frac{k'_0 - k_d}{k_{H_2O_2+OH}}$$

(E.3.3)

where,

k'_0 : OH rate coefficient in the absence of the OVOC, in the range of 91-264 s^{-1} in those experimental conditions

k_d : rate coefficient of the OH diffusion, in the range of 30-150 s^{-1} in those experimental conditions

$k_{(H2O2 + OH)}$: rate coefficient of the OH reaction with H_2O_2, ~1.7×10^{-12} cm^3 molecule^{-1} s^{-1} at 298 K[48]

The OH radical concentration, in radical cm^{-3}, produced by the photolysis laser can be estimated by the following expression:

$$[OH] = 5 \times 10^{12} \times \lambda \times f_L \times \sigma \times \phi \times [H_2O_2] \qquad\qquad (E.3.4)$$

where,

λ : photolysis wavelength (λ = 248 nm)

f_L : laser fluence (15 -25 mJ)

σ : absorption cross section of H_2O_2 ($\sigma = 9 \times 10^{-20}$ cm^2 molecule^{-1} at 248 nm[48])

ϕ : OH quantum yield (ϕ = 2)

$[H_2O_2]$ = $(0.23-1.70) \times 10^{14}$ molecule cm^{-3} (estimated by the expression (E.3.3))

In the absence of quenchers of OH fluorescence, with $[H_2O_2]$~ $(0.23-1.70) \times 10^{14}$ molecule cm^{-3} and with a helium pressure of 100 Torr, OH concentration was about $(0.43-7.95) \times 10^{11}$ radical cm^{-3}, corresponding to a signal at least 100 times larger than the background noise. Thus, the OH detection limit for a typical experiment was $(0.52 - 1.76) \times 10^{9}$ radical cm^{-3}.

The energies of the photolysis and probe laser pulses were measured with laser power monitors and were constant over the time period used to record an OH concentration-time-profile. As a result, the signal of OH did not require any correction for laser energy fluctuations.

During the experiment, the concentration of the studied compound was stable and measured using the expression:

$$[\text{OVOC}] = \frac{F_{OVOC}}{F_{tot}} \times P \times \alpha \times \frac{T_{amb}}{T_{cell}} \times 3.24 \times 10^{16} \qquad \text{(E.3.5)}$$

where,

[OVOC] : concentration of the studied compound, in molecule cm^{-3}

F_{OVOC} : flow of the studied compound, in ml min^{-1}

F_{tot} : total flow (He + compound), in ml min^{-1}

P : pressure in the cell, in Torr

α : dilution factor of the compound in the mixture in the bulb

T_{amb} : ambient temperature, in K

T_{cell} : cell temperature, in K

3.24×10^{16} : concentration of 1 Torr of the compound at 298 K

3.C. Fast Flow Tube - Quadrupole Mass Spectrometer

Complementary to the PLP-LIF, the absolute and relative rate coefficient measurements of OH radicals and Cl atoms with the OVOCs of interests were determined using a discharge fast flow tube reactor combined with a modulated molecular beam mass spectrometer.

3.C.I. Apparatus

The experimental set up consisted of three basic parts, a) the gas storage/supply lines, b) the double wall flow tube reactor and c) the differentially pumped stainless steel vacuum chamber where the quadrupole mass spectrometer is hosted (QMG 420). The description of the three basic parts is given below while more details are presented in previous thesis and publications from the group.[49,50] The vacuum lines were made exclusively of glass and consisted of calibrated volume storage flasks (~10 L) where the gas-phase reactants were stored. The supply of the gas-phase species inside the reactor was controlled by low flow metering valves. Furthermore, the flow of the bath gas (Helium, He) was controlled by four flow meters with a maximum flow rate of 500 cm^3 min^{-1}.

The double wall flow tube reactor, 45 cm length and 2.4 cm internal diameter, along with the double movable injector, were made of pyrex glass (figure 3.5). A Julabo 200 thermostatic unit was used to regulate the temperature by circulating liquid ethanol/water through the double walls of the reactor. To eliminate any temperature loss the main body of the reactor was inside a cylindrical stainless steel chamber that was continuously pumped by a rotary vacuum pump (5×10^{-3} Torr). Furthermore, the flow reactor was equipped with 5 inlets for the reagents introduction. Each of them had a particular position. The inlets, the reactor walls and the sliding injector were coated with halocarbon wax in order to minimize the heterogeneous losses. The active species were produced on the side inlet of the external injector (as shown in figure 3.5), flowing known mixtures of their precursor molecules. An Evenson coaxial cavity was placed externally surrounding the inlet of the flow tube. A microwave discharge generator (*EMS Microtron 200, 2.45 GHz*) operated at 60 Watt provides continuously the energy to the cavity, creating a plasma of electrons that ensures the steady production of the active species. To enrich the plasma with electrons that increase the yield of dissociation of the active precursor species, the side inlet was treated with ortho-phosphoric acid. In addition, to reduce the high temperatures achieved from the electron plasma creation, the area around the inlet 3 (figure 3.4) was continuously cooled with compressed air. Furthermore, an additional inlet exists at the end of the reaction zone, 5 cm at the downstream end of the flow tube reactor. Molecular bromide is supplied through that inlet for the chemical conversion of the radical/atoms to stable species that could be easily detected by the mass spectrometer. The pressure inside the cell was measured with a pressure gauge 0-10 Torr.

As the gas mixture exits the reactor the flow passes through a glass skimmer with a pinhole orifice of 0.3 mm diameter, entering the side hypothalamus of the differentially pumped stainless steel chamber (third part of the experimental set up). There, most of the introduced molecules are pumped out by an oil diffusion pump (Balzers, 2000 L s^{-1}) to achieve high vacuum (~8×10^{-6} Torr). The remaining molecules meet the blades of a tuning chopper operated at 35 Hz to create "packages" of molecules with the given frequency. Subsequently, these "packages" of molecules pass through a second skimmer that is used to create the final molecular beam,

entering into the second hypothalamus where the mass spectrometer is hosted. The molecular beam (i.e. molecules with parallel velocity vectors) ensures that the molecules after their exit from the reactor do not interact with each other while the composition of the reaction mixture and the concentrations of its components arrive pure at the mass spectrometer. In the second hypothalamus the vacuum ($\sim 3 \times 10^{-7}$ Torr) is assured by a Balzers TPU 540 turbomolecular pump with pumping efficiency 540 L s^{-1}. At this point it should be noted that the achievement of high vacuum is necessary since it ensured a) the rapid pumping of the reactor, b) the configuration of the reaction mixture in a molecular beam and c) the proper functioning of the mass spectrometer. The "packages" of molecules are ionized in the ion source (Rhenium filaments) of the mass spectrometer that is operated at 35 V. Thereafter the positive ions are focused via electrostatic lenses and the applied electromagnetic field drives the molecules along the rods of the Quadrupole Mass Analyser, (QMA 400). The ions with the "chosen" mass/charge ratio reach the dynodes of a Secondary Electron Multiplier, (SEM), producing an abundance of electrons, i.e. electrical signal. The final signal is collected by an electrometer and is send to the console of the spectrometer. Thereafter, the signal is sent to a Lock-in Amplifier that locks and amplifies only the one that has the frequency of the chopper, i.e. 35Hz. This is necessary since it ensures that the signal detected only comes from the reactor and it is not influenced by randomly moved molecules inside the chamber. Finally, the signal of the chopper is recorded and stored for further analysis.
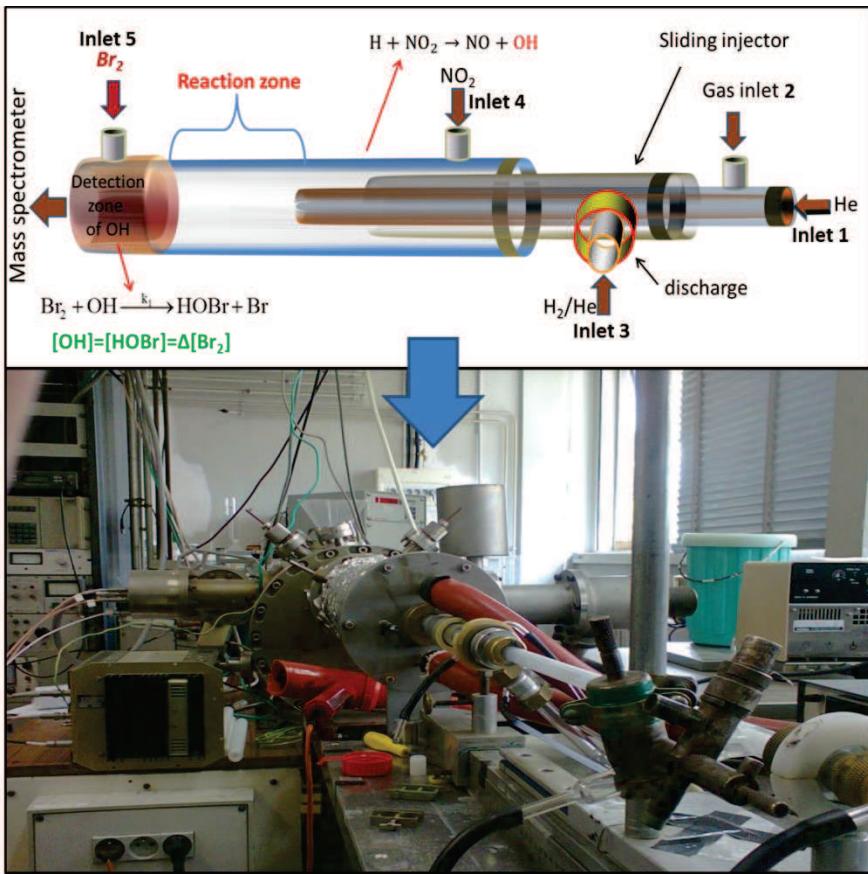
3.C.II. Production of OH radicals and Cl atoms

OH radicals were generated through the fast reaction of hydrogen atoms with NO_2:

$$H + NO_2 \rightarrow OH + NO \qquad k = 4 \times 10^{-11} \exp(-340/T) \text{ cm}^3 \text{ molecule}^{-1} \text{s}^{-1} \qquad (R.3.6)$$

$$k_{298} = 1.47 \times 10^{-10} \text{ cm}^3 \text{ molecule}^{-1} \text{s}^{-1} \text{ [51]}$$
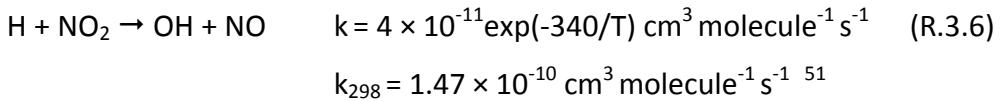
As mentioned above, H atoms were produced on the side arm of the movable injector in a microwave discharge of 10% H_2/He mixtures. Reaction (R.3.6) was carried out in high excess of NO_2 ($[NO_2] = (0.7\text{-}1.0) \times 10^{14}$ molecules cm^{-3}) over H-atoms in order to ensure their rapid and complete consumption.

Regarding Cl atoms, they were formed by the microwave discharge of a 5% Cl_2/He mixture.

$$Cl_2 \rightarrow 2Cl \qquad\qquad\qquad\qquad\qquad\qquad\qquad (R.3.7)$$

3.C.III. Detection of OH radicals and Cl atoms

As far as the absolute rate coefficients measurements is concerned, OH radicals and Cl atoms were detected by mass spectrometry as $HOBr^+$ (m/z = 96/98) and $BrCl^+$ at m/z = 116, respectively. OH and Cl were rapidly converted in $HOBr^+$ and $BrCl^+$ by an excess of Br_2 ([Br_2] = (3.5-5.1) $\times 10^{13}$ molecules cm^{-3} which was introduced at the end of the reaction zone (inlet 5):

$$OH + Br_2 \rightarrow HOBr + Br \quad k_{298} = 4.48 \times 10^{-11} \, cm^3 \, molecule^{-1} \, s^{-1} \, {}^{52} \qquad (R.3.8)$$

$$Cl + Br_2 \rightarrow BrCl + Br \quad k_{298} = 1.46 \times 10^{-10} \, cm^3 \, molecule^{-1} \, s^{-1} \, {}^{50} \qquad (R.3.9)$$
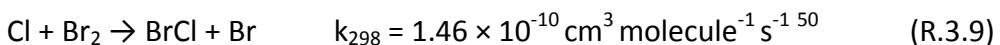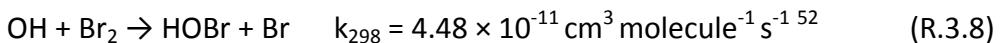
3.C.IV. Procedure

The studied OVOCs compounds and the molecular bromide, prior to their use, were degassed by repeated freeze-pump-thaw cycles. Thereafter the compounds were diluted in helium to prepare known gas phase mixtures, <1% of OVOCs/He and ~10% Br_2/He respectively, at a total pressure of about 700 Torr. In addition, given the high concentrations of NO_2 required for the sufficient scavenging of H atoms, pure NO_2 was used. The gas phase species and the bath gas were mixed before the reactor inlets. The total linear flow velocities in the reactor were in the range of 1231-3430 $cm \, s^{-1}$.

Absolute rate coefficient measurements

Initially, the reactor is supplied with H_2 (inlet 3) and excess concentrations of NO_2 (inlet 4), and Br_2 introduced at the end of the reactor (inlet 5), for the scavenging of the active species. The excess of NO_2 and Br_2 is confirmed upon switching on and off the microwave discharge; no change to the signal of their characteristic mass peaks is observed. For the stable production of OH radicals, the temperature of the discharge should be stabilized (around 15 min). Thereafter, the rate of OH or Cl decay in the absence of the studied compound, k'_0, is measured to determine the heterogeneous loss of the active species on the walls of the reactor. This procedure is repeated before the introduction of the OVOC and after the completion of the

kinetic experiment. The sliding injector was placed in three to five different positions within the length limits of the reaction zone. By this way the reactor volume is changed, thus the reaction time. The monitoring of OH radicals or Cl atoms at various reaction times provides their concentration-time profiles, which is proportional to the intensity recorded. Thereafter, an excess amount of the studied OVOC is introduced (gas inlet 2) and the time profile of the active species is recorded providing the pseudo-first order rate coefficient, k' ($[X]_t = [X]_0 \exp^{-k't}$ where $k' = k_{OVOC} + k'_0$). In a typical experiment, this procedure is repeated for several OVOC concentrations, (at least 6) in a wide range, varying the concentration at least by a factor of 10. The slope of the lineal fit of the k' versus the gas phase concentration of the studied compound provides the bimolecular rate coefficient k_{OVOC} (in cm^3 molecule^{-1} s^{-1}). At the end of the experiment, the OVOC, the Br_2 and the NO_2 are calibrated to obtain all the necessary information regarding the absolute concentrations of the species. In addition, it has to be noted that all the measured values of k' were corrected for axial and radial diffusion of OH and Cl respectively.[53]

Moreover, a series of tests were also performed to verify that Br atom reactions could not affect the concentration of HOBr or BrCl through its formation or consumption reactions, and therefore, they had no impact on the observed kinetics. In addition, it was verified that Br reaction with the studied compounds had a negligible impact on their concentrations under the experimental conditions of the present study. Secondary reactions of the oxidants with primary reaction products was also considered as negligible, taking into account the sufficient excess of the OVOCs concentration over that of OH and Cl. A series of experiments confirmed this assumption by the observation of the independent reaction rate, k', of the initial concentrations of the oxidants.

Relative rate coefficient measurements

In the case of relative rate coefficient measurements the sliding injector position is fixed. The studied OVOC and the reference compound are introduced in the reactor (inlet 1 and 2) and their steady state concentrations are monitored by the mass spectrometer. Subsequently, the discharge was switched on to obtain the first concentration of the active species and the concentration drop of the studied and

reference compounds are detected by the mass spectrometer. Thereafter the concentration of the radical/atoms is varied to achieve higher or lower consumption of the organic compounds. In a typical experiment, at least 6 different concentrations of the OH radicals or Cl are used by regulating the flow of their precursor molecules.

Considering that the detection technique is electron impact mass spectrometry, it is possible that some of the characteristic peaks of the compounds involved to encompass contribution. To this end, prior to the kinetic experiment, sequential test experiments are conducted to examine possible secondary contribution to the mass peaks. Initially the mass spectra of the studied VOC and that of the reference compound are recorded separately. For this test experiment, high concentrations of the organics are used in order to detect minor contributions (<1%) to the mass peaks in which the spectrometer is less sensitive. In the second step, the reaction of the compound of interest with the active species is studied to examine whether the formation of products contribute to the mass peaks of the reference molecule. If not, the same step is repeated for the reaction of the reference with the oxidants. Then, if all these requirements are achieved, the kinetic experiment for the relative rate coefficient determination is performed.

3.C.V. Analysis

To obtain accurate kinetic data as well as to determine the conditions under which the experiment is conducted, it is necessary to accurate by measuring the concentrations of the species involved. The concentration of the compounds, in molecule cm^{-3}, introduced from the bulbs in the reactor is measured using the expression:

$$[X] = \alpha \frac{dn/dt}{Q_t} \qquad \text{(E.3.6)}$$

where,

α : dilution factor of the compound in the mixture in the bulb

dn/dt : molecular flow rate of the mixture

Q_t : total flow of the gases

The compounds were considered as ideal gases, thus the calibration and the measurement of the molecular flow rate of the mixtures in the bulbs was conducted by the drop of bulb pressure in a determined time period using a chronometer and a pressure gauge:

$$\frac{dn}{dt} = \frac{N_A \times V}{RT} \times \frac{dP}{dt}$$
(E.3.7)

N_A : Avogadro constant 6.022×10^{23} mol^{-1}

V : volume of the bulb, 10.28 - 10.53 L

R : constant 0.082 cm^3 L atm K^{-1}

T : temperature of the bulb, in K

dP/dt : pressure drop in the bulb, in atm s^{-1}

This method was used for the calibration of Br_2, NO_2, the reference compounds and the studied OVOCs that had sufficient vapor pressure to prepare a mixture. On the other hand, the absolute calibration of the mass spectrometer for the studied compounds with low vapor pressure was also performed by injecting known liquid amounts inside the flow tube with simultaneous recording of their mass peak intensity. The integrated area of the mass spectrometric signals corresponding to a known total number of molecules injected into the reactor allowed the determination of the calibration factor. Similar (within 10%) results were obtained when each compound was introduced into the reactor from a known mixture with He. The chemical conversions of OH to HOBr and Cl to BrCl is used for the measurement of the absolute concentrations of these species, considering that [OH] = [HOBr] = Δ[Br_2] and [Cl] = [BrCl] = Δ[Br_2]. Thus, [OH] and [Cl] were determined from the consumed fraction of [Br_2]. In turn, the absolute concentrations of Br_2 were measured from the flow rates of known Br_2/He mixtures as discussed previously.

For the absolute rate measurements k' was corrected for axial and radial diffusion of OH and Cl. The diffusion coefficient of OH in He was calculated using the following expression:

$$D_0 = 640 \times (T/298)^{1.85} \text{ Torr cm}^2 \text{ s}^{-1} \quad\quad\quad\quad (E.3.8)$$

and ranged from 636 to 800 Torr cm^2 s^{-1} at P = 1 Torr and T = 297-336 K,[54,55] while the diffusion coefficient of Cl in He, D_{Cl-He}, was calculated from D_{Ar-He}[56] and was 567 cm^2 s^{-1} at P = 1 Torr and T = 298 K. The corrections on k' were generally less than 10%.

3.D. Atmospheric Simulation Chamber

The atmospheric simulation chambers are widely used in chemical kinetics to measure rate coefficients and investigate reaction mechanisms. They are made of Teflon, quartz, Pyrex or stainless steel, FEP coated aluminum, inox and their volume varies to 50 - 300000 L.[57]

3.D.I. Apparatus

The conventional relative-rate method was used to measure the rate coefficients for the reactions of OH radicals and Cl atoms with a series of acetates in a Teflon reaction chamber at 293 $\pm$ 2 K and atmospheric pressure (P=760 Torr of purified air). The experimental setup, described in previous thesis[58] and publications,[59] consisted of a 180 L and later 200 L FEP Teflon bag surrounded by six germicide lamps (Sylvania G30W) and six black lamps (Philips, TL 20W/05) to generate the reactive species by the photolysis of their precursor molecules. They were all hosted in a wooden box with the internal faces covered with aluminum foil to homogenize the radiation of the lamps (figure 3.6). Two electric fans positioned in the box and continuous purified/dry air circulation maintained a constant temperature about 293 $\pm$ 1.5 K during the experiments. The introduction of the reactants and the sampling were performed by two Teflon tubes positioned in the center of the bag. The reactants

were flushed into the chamber by a stream of purified air using a mass flow controller of 0-20 L min^{-1}.

A gas chromatograph system equipped with a DB-1 capillary column and a flame ionization detector (GC-FID, Star 3800 CX, Varian) was used for quantitative analysis of the reactants and products. The column was operated over the temperature range of 403–448 K, and helium was used as carrier gas. Gas samples were automatically collected from the chamber and introduced via a heated sampling loop of 0.25 mL capacity to the gas chromatograph.

In order to perform a thorough mechanistic and product study an Automated Thermal Desorption Gas Chromatography – Mass Spectrometer (GC-MS Clarus 600C coupled with ATD 150 from Perkin Elmer) and a Fourier transform Infrared Spectrometer (FT-IR, Nicolet Magna – IR 550) coupled with a 2 L cell were additionally connected to the chamber for the detection of the chemical species involved. The mechanistic studies were performed in the presence of NO. Chromatographic separation was achieved by using a 30m length Elite 5MS column (0.25µm film thickness) operated at 433 K, using helium as carrier gas. The IR detector was a DTGS KBr and the infrared beam has an absorption path length of 10 m. The infrared spectra were collected within the range of 400-4000 cm^{-1} and correspond to the average of 100 scans recorded with resolution of 1 cm^{-1}.
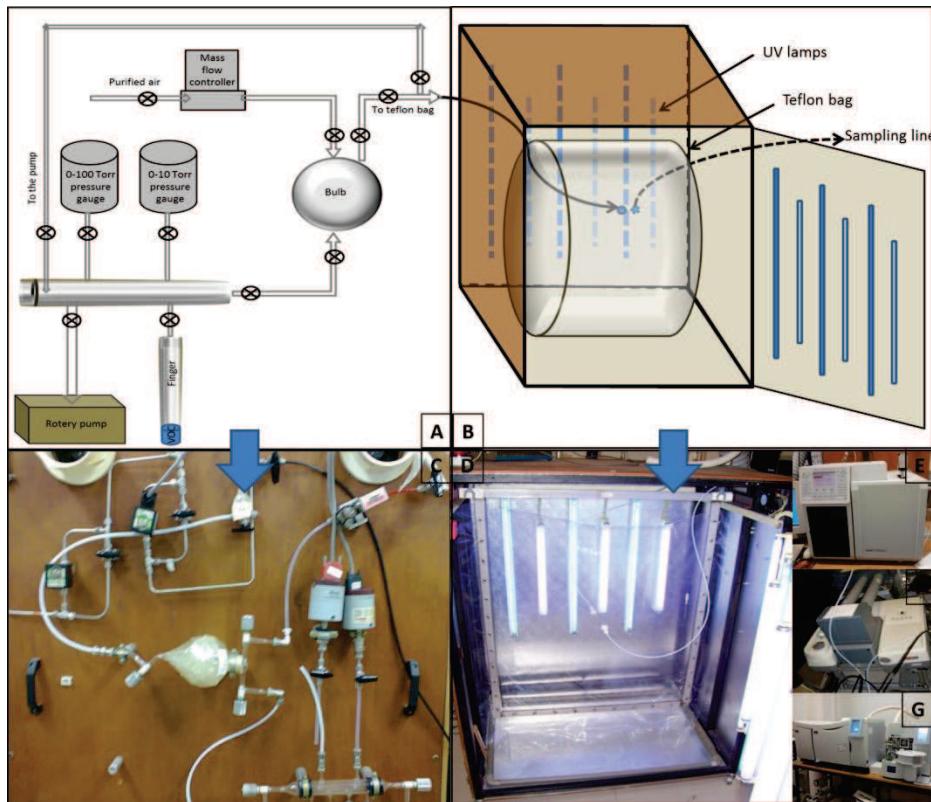
Figure 3.6: Schematic diagrams and pictures of the Atmospheric Simulation Chamber used in the relative rate study. A) Diagram of the introduction system. B) Diagram of the wooden box consisting the 200 L Teflon bag. C) Picture of the introduction system. D) Picture of the wooden box consisting the reaction chamber. E) GC-FID VARIAN CP-3800 (Chromatograph Gas injection valve - Flame ionization Detector). F) Fourier transform Infrared Spectrometer (FT-IR photo, Nicolet Magna – IR 550) coupled with a 2 L cell. G) Automated Thermal Desorption Gas Chromatography – Mass Spectrometer (GC-MS Clarus 600C coupled with ATD 150 from Perkin Elmer).

3.D.II. Procedure

The reactive OH radicals were produced via photolysis of H_2O_2 using 2-6 germicide lamps emitting at 254 nm, while Cl atoms were generated via Cl_2 photolysis using 2-4 black lamps with maximum irradiance at 365 nm.

The studied and reference compounds were degassed by repeated freeze-pump-thaw cycles before their use. For the introduction of all the reactants in the reaction chamber a pressure gauge was used to measure their pressure into a calibrated Pyrex bulb of 579 ml. The measured amounts of the reagents were flushed from the bulb into the reaction-bag by a stream of synthetic/purified air. Some of the studied compounds have low vapor pressure, thus several introductions were carried out. It should be noted that H_2O_2 was introduced into the bag by a Hamilton syringe and a

septum positioned in the introduction line through the stream of pure air. Then the bag was filled with synthetic air to its full capacity at atmospheric pressure and left in the dark for about one hour to ensure the homogeneity of the mixture.*

Before starting the kinetic study the stability of each reactant in the dark and the photostability of each reactant in the absence of radical precursor were checked. In particular, the mixture of the studied and reference compound with and without H_2O_2 and Cl_2 was stable in the dark when it was allowed to stand in the chamber for about 2 hours. The photostability check showed that no photolysis of the reagents occurred when these compounds were irradiated at 254 nm and at 365 nm respectively for about 2 hours. This range of time was selected because once the concentrations of the mixtures were stabilized, the kinetic measurements were carried out for a maximum total time of 2 hours. Moreover, separate irradiations of the oxidant with the reference compound and the oxidant with the studied compound were carried out to investigate the possibility of reaction products with similar retention times to that of the studied compound or the reference compound respectively.

In order to avoid heterogeneous reactions between the reagents on the chamber's wall, the Teflon bag was often renewed and purged several times before each experiment.

3.D.III. Analysis

The concentrations of the studied and reference compounds, as well as Cl_2 concentration were measured using the expression:

$$[OVOC] = \frac{(P_{bulb} \times V_{bulb})}{(P_{bag} \times V_{bag})} \times 10^6 \qquad (E.3.9)$$

where,

[OVOC] : concentration of the studied or reference compound, in ppm

---

*The studied compounds have high molecular weights and low vapor pressure. As a result, it took approximately 30-40 min to homogenize the mixture in the chamber.

P_{bulb} : pressure of the compound in the bulb, in Torr

V_{bulb} : volume of the bulb, 0.579 L

P_{bag} : pressure in the bag (atmospheric), ~760 Torr

V_{bag} : volume of the bag, 180 L or 200 L

Alternatively, the concentration can be calculated by the following expression:

$$[OVOC] = \frac{P_{bulb} \times V_{bulb} \times N_A}{V_{bag} \times R \times T \times 2.46 \times 10^{13}}$$ (E.3.10)

where,

[OVOC] : concentration of the studied or reference compound, in ppm

P_{bulb} : pressure of the compound in the bulb, in Torr

V_{bulb} : volume of the bulb, 0.579 L

N_A : Avogadro constant 6.022 × 10^{23} mol^{-1}

V_{bsg} : volume of the bag, 180 L or 200 L

R: constant 63363.67 cm^3 Torr mole^{-1} K^{-1}

T : temperature of the chamber, in K

2.46 ×10^{13} molecules cm^{-3}: 1 ppm at 298 K in 1 atm

The H_2O_2 concentration, in ppm, introduced by the syringe in the bag was measured using the expression:

$$[H_2O_2] = \frac{V_{H_2O_2} \times d_{H_2O_2} \times purity \times N_A}{M_{H_2O_2} \times V_{bag} \times 2.46 \times 10^{13}}$$ (E.3.11)

V_{H2O2} : volume of H_2O_2 injected, 0.1-0.35 ml

d_{H2O2} : density of H_2O_2 solution, 1.11 g ml^{-1}

purity : purity of H_2O_2 solution, 0.3 and 0.6 (30 and 60% H_2O_2 solution in H_2O was used)

N_A : Avogadro constant 6.022 × 10^{23} mol^{-1}

M_{H2O2} : molecular weight of H_2O_2, 34.01 g mol^{-1}

V_{bag} : volume of the bag, 180 L or 200 L

2.46×10^{13} molecules cm^{-3}: 1 ppm at 298 K in 1 atm

The H_2O_2 concentrations used were in the range 235-523 ppm. On the other side, the concentrations of gas Cl_2 were in the range of 58-152 ppm. The concentrations of the studied and reference compounds were low (comparing to those of H_2O_2 and Cl_2) in the order of 7-34 ppm and 10-95 ppm respectively, to achieve an easily homogenized mixture in the bag and avoid heterogeneous reactions on the bag's wall.

4. Ultra Violet absorption cross-section measurements

4. Ultra Violet absorption cross-section measurements

The UV absorption spectra and the UV absorption cross section measurements of 1-methoxy-2-propyl acetate (MPA), 2-methoxy butyl acetate (2MBA) and 3-methoxy butyl acetate (3MBA) were performed under static conditions in a double wall absorption cell. Deuterium (D_2) and zinc (Zn) lamps were used as UV-Vis light sources. The Emission Lines of a Deuterium and a Zinc lamp are given in annex III. The transmitted light was detected by the spectrometer and in some cases by a photodiode. Furthermore it should be noted that the experiments were conducted in a relative limited concentration range due to the low vapor pressure of the molecules.

The cross section, in cm^2 molecule^{-1}, at wavelength λ was measured based on the Beer-Lambert's law:

$$\sigma = \frac{\ln\left(I_0(\lambda) \big/ I(\lambda)\right)}{LC} \qquad (E.4.1)$$

where

I : light intensity with the studied compound in the absorption cell

I_0 : light intensity without the studied compound in the absorption cell

L : absorption cell path length, 100 cm

C : concentration of the OVOC, in molecule cm^{-3}

4.A. UV absorption cross-section measurements of MPA

The UV absorption cross section of MPA was determined in the wavelength range of 200-370 nm. The absorption experiments were performed at 300±2 and 335±2 K, by varying the gas phase concentration of MPA between (0.58 - 6.76) × 10^{16} molecule cm^{-3}. The obtained cross section spectrum for an average of four different MPA concentrations at 300 K is presented in figure 4.1, where an absorption band center near 215 nm is shown. Above 216 nm we can notice a drastic decrease in the absorption, while at wavelength greater than 260 nm the cross section is below the

detection limit of the spectrometer. Table 4.1 presents the cross section values averaged over 2 nm intervals.
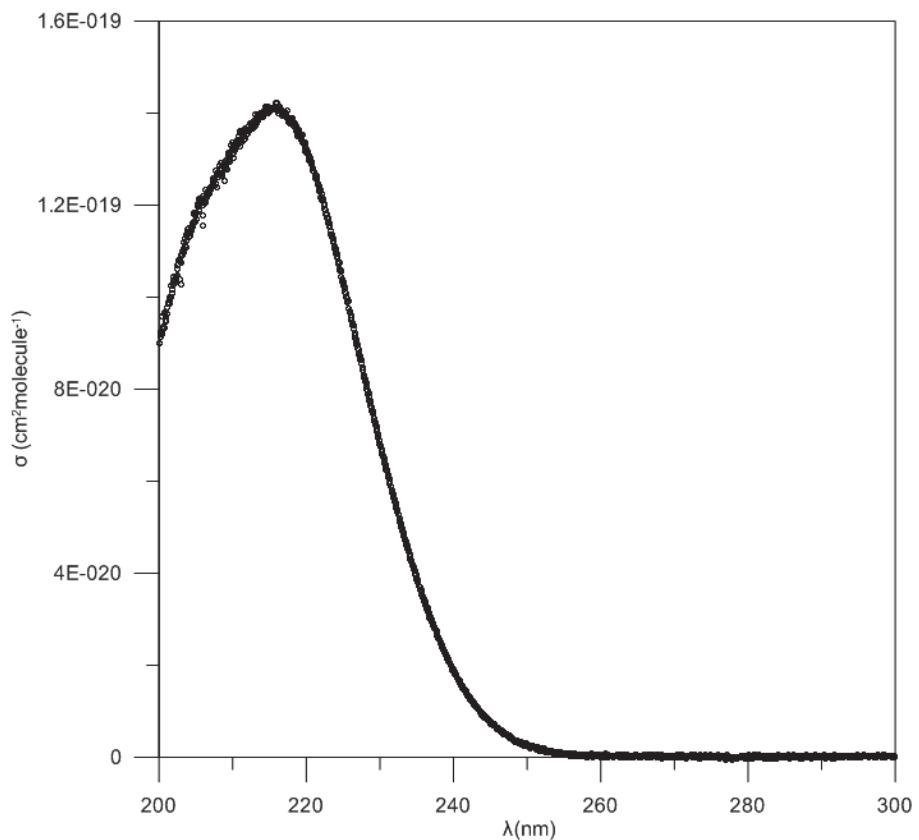

Figure 4.1: UV absorption cross section spectrum of MPA ((2.55 -6.76) × 10^{16} molecule cm^{-3}) using the D$_2$ lamp, between 200 and 300 nm at 300 K.

Table 4.1: MPA absorption cross section at the wavelength range of 200-260 nm using the D_2 lamp at 300 ± 2 K for an average of four different MPA concentrations. Values in bold denotes the maximum absorption cross section of MPA measured between 214-216 nm.

λ [a]	σ [b] (10^{-20})
200	9.33
202	10.25
204	11.35
206	12.08
208	12.62
210	13.18
212	13.59
214	**13.97**
216	**14.08**
218	13.81
220	13.19
222	12.23
224	10.97
226	9.63
228	8.21
230	6.84
232	5.57
234	4.42
236	3.43
238	2.59
240	1.89
242	1.34
244	0.93
246	0.63
248	0.40
250	0.26
252	0.16
254	0.09
256	0.05
258	0.04
260	0.03

[a] Units of nm
[b] Units of $cm^2 molecule^{-1}$

The applicability of Beer-Lambert's law is shown in figure 4.2, where $\ln(I_0/I)$ is plotted as a function of gas phase MPA concentration at 300 and 333 K for the wavelength of 216 nm. According to equation E(4.1), σ is given by the slope of the linear through origin fit. Indeed, the plots of the experimental results have near-zero intercept, pointing to the small uncertainties in concentration measurements. The results showed that σ was temperature independent and the values obtained for the wavelength of 216 nm were $(1.43 \pm 0.14) \times 10^{-19}$ and $(1.46 \pm 0.15) \times 10^{-19}$ for 300 and 335 K*, respectively. In addition, it should be noted that a series of experiments were performed to test possible photolysis and change of MPA cross section by time. The results indicated that MPA photolysis was negligible at this wavelength region, since the cross section was found to be stable when MPA was continuously irradiated for about 1.5 hour.
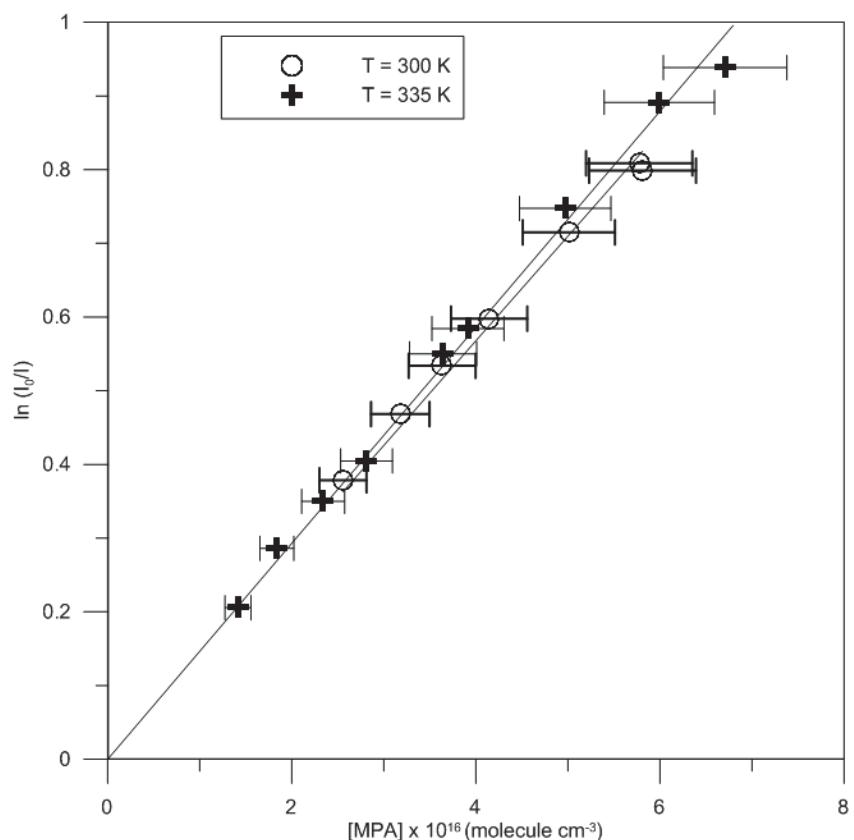

Figure 4.2: UV-absorption cross section of MPA at 216 nm was $(1.43 \pm 0.14) \times 10^{-19}$ and $(1.46 \pm 0.15) \times 10^{-19}$ cm^2 molecule^{-1} using the D$_2$ lamp at 300 and 335 K, respectively. The error quoted on σ values includes the standard deviation (1σ) of the slope and the estimated systematic uncertainties and the error bars for MPA concentrations are 10%.

---

*These values extracted from the through zero plot conclude all the observed points

In addition, several experiments were conducted in presence of a narrow band filter Center Wavelength* at 214 nm either with D_2 lamp or with a zinc (Zn) lamp, to eliminate any interference that could affect the absorption cross section measurements. Figure 4.3 presents the absorption experiments performed with and without the optical filtering, while a summary of the cross section values at 214 nm obtained by the two lamps is shown in table 4.2. The resulting cross section values under all these conditions were in fair agreement within the experimental uncertainties $\sigma = (1.6 \pm 0.2) \times 10^{-19}$ cm^2 molecule^{-1}.
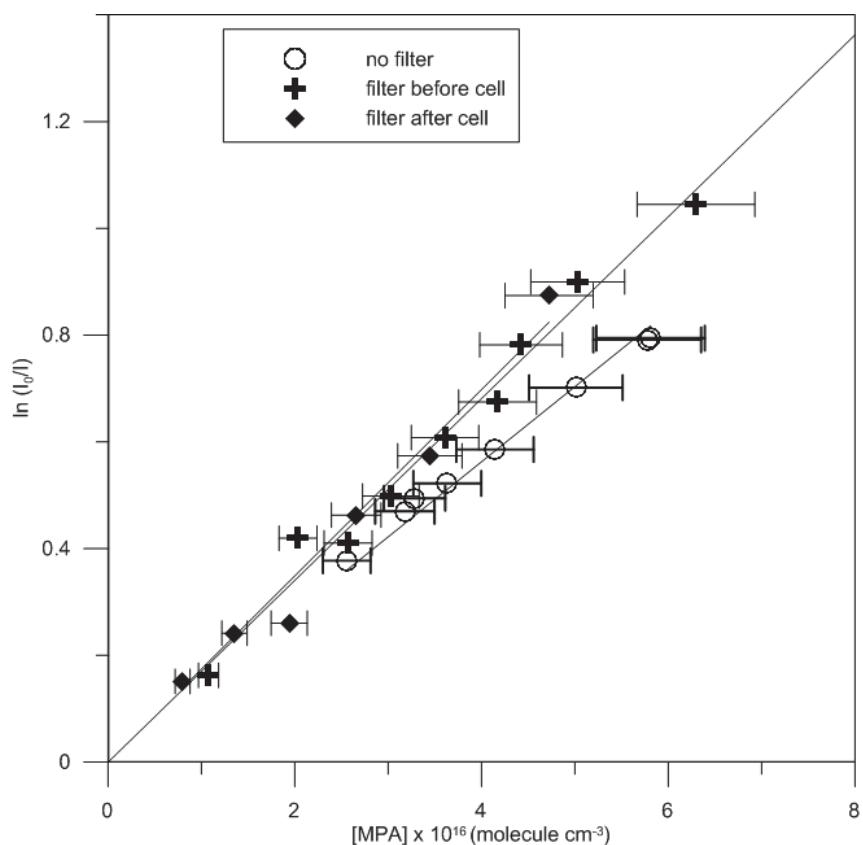
Figure 4.3: UV-absorption cross section of MPA at 214 nm was (1.41 ± 0.14) x 10^{-19}, (1.70 ± 0.17) x 10^{-19} and (1.75 ± 0.19) x 10^{-19} cm^2 molecule^{-1} without and with the filter before and after the cell respectively, using the D_2 lamp at 300 ± 2 K. The error quoted on σ values includes the standard deviation (1σ) of the slope and the estimated systematic uncertainties, while the error bars for MPA concentrations are 10%.

---

* Center Wavelength (CWL) is the midpoint between the wavelengths where transmittance is 50%

Table 4.2: Absorption cross section of MPA at 214 nm, at 300 ± 2 K.

	D$_2$ lamp [a]			Zn lamp	
	No filter	Filter before cell	Filter after cell	Spectrometer	diode
σ [b, c] (10^{-19})	1.41 ± 0.14	1.70 ± 0.17	1.75 ± 0.19	1.80 ± 0.18	1.77 ± 0.18
Average σ (with and without filter)				**1.6 ± 0.2**	

[a] Using the spectrometer

[b] Units of cm^2 molecule^{-1}

[c] The error quoted on σ include the standard deviation (1σ) of the slope and the estimated systematic uncertainties

[d] The error quoted on σ average is the standard deviation of σ values obtained in the presence and the absence of the filter

4.B. UV absorption cross-section measurements of 2MBA

The UV absorption cross section of 2MBA was determined in the wavelength range 205-370 nm. The absorption experiments were performed at 300±2, 318±2 and 335±2 K. The pressure range used was between 0.1 and 1.2 Torr, as a result 2MBA concentration varied between (0.50 – 3.69) × 10^{16} molecule cm^{-3}. The obtained cross section spectrum for an average of three different 2MBA concentrations at 300 K is presented in figure 4.4. An absorption band center near 212-214 nm can be noticed in this figure, while afterwards a drastic decrease in the absorption is shown. Above 260nm the cross section is below the detection limit of the spectrometer. A representation of the cross section values is figured in table 4.3, where the interval between the two absorption measurements is 2 nm.
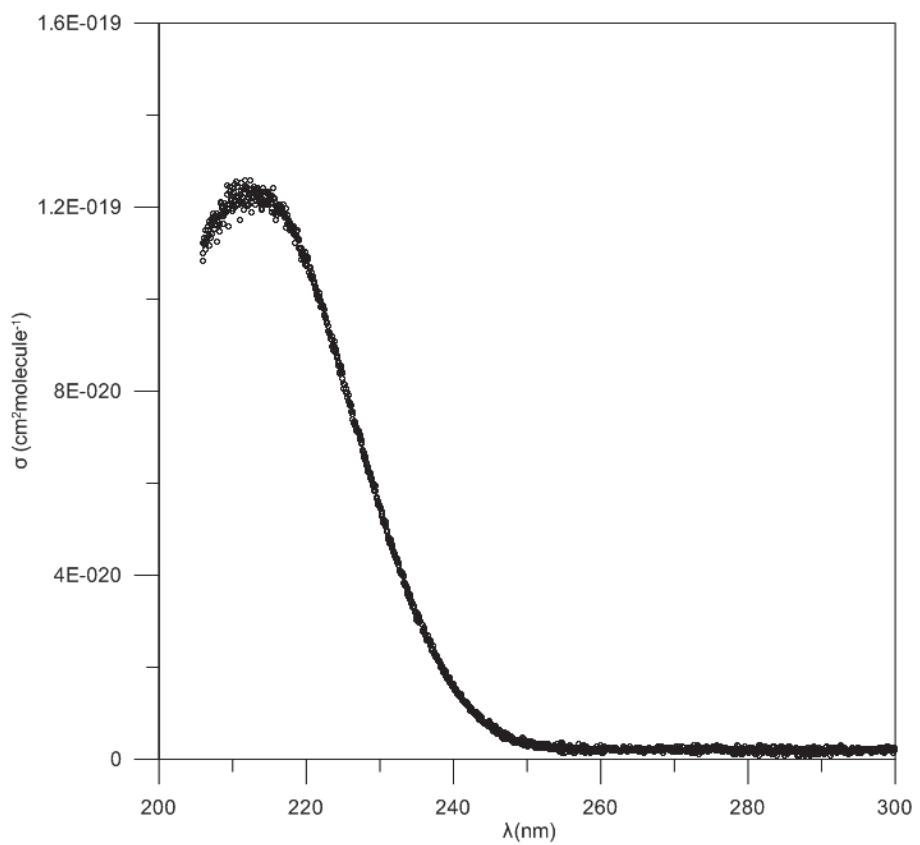
Figure 4.4: UV absorption cross section spectrum of 2MBA ((2.52 - 3.45) × 10^{16} molecule cm^{-3}) using the D$_2$ lamp, between 205 and 300 nm at 300 K.

Table 4.3: 2MBA UV absorption cross section at 300 ± 2 K for an average of three different 2MBA concentrations, at 205-260 nm using the D_2 lamp. The maximum 2MBA absorption cross section at 212-214 nm is pointed out in bold.

λ [a]	σ [b] (10^{-20})
206	11.31
208	11.74
210	12.14
212	**12.26**
214	**12.21**
216	12.01
218	11.56
220	10.80
222	9.89
224	8.83
226	7.67
228	6.57
230	5.47
232	4.46
234	3.57
236	2.79
238	2.13
240	1.57
242	1.15
244	0.85
246	0.61
248	0.44
250	0.35
252	0.29
254	0.25
256	0.22
258	0.21
260	0.21

[a] Units of nm
[b] Units of $cm^2 molecule^{-1}$

As shown in figure 4.5 the light absorbance (i.e. ln (I_0/I)) at 212 nm was found to increase linearly with the 2MBA concentration and to follow the Beer-Lambert law. The results showed that σ was temperature independent for the three temperatures

studied and the values obtained were $(1.25 \pm 0.13) \times 10^{-19}$, $(1.30 \pm 0.13) \times 10^{-19}$ and $(1.30 \pm 0.13) \times 10^{-19}$ for 300, 318 and 335 K, respectively. In addition, the cross section was found to be stable when 2MBA was continuously irradiated for about 1.5 hour, thus there was no photolysis of 2MBA at this wavelength region.
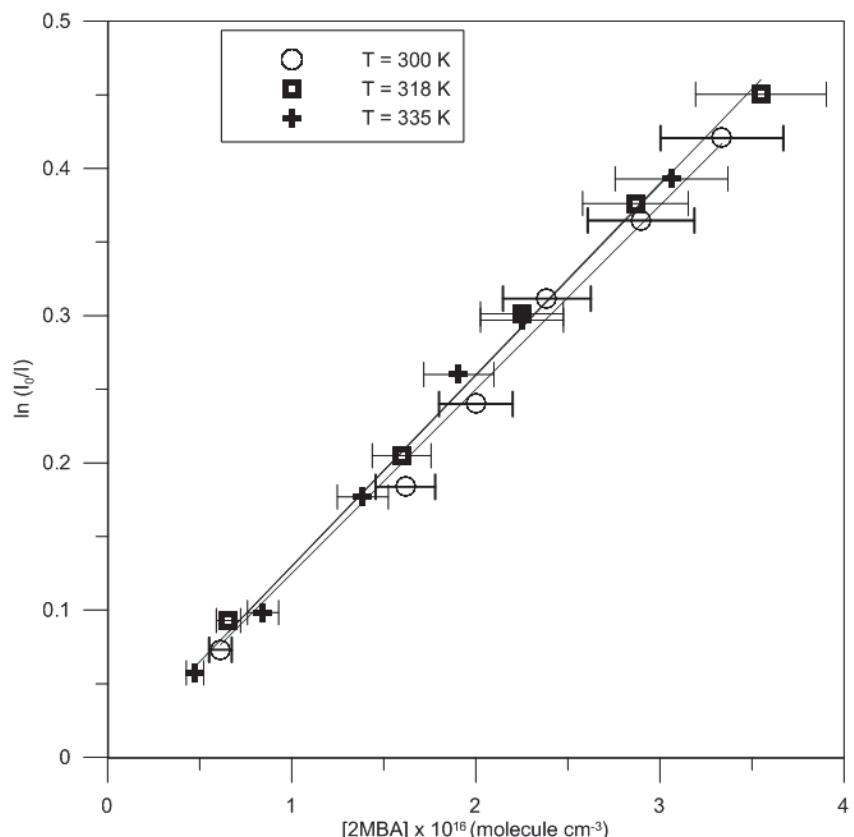

Figure 4.5: UV-absorption cross section of 2MBA at 212 nm was $(1.25 \pm 0.13) \times 10^{-19}$, $(1.30 \pm 0.13) \times 10^{-19}$ and $(1.30 \pm 0.13) \times 10^{-19}$ cm^2 $molecule^{-1}$ using the D_2 lamp at 300, 318 and 335 K, respectively. The error quoted on σ values includes the standard deviation (1σ) of the slope and the estimated systematic uncertainties, while the error bars for 2MBA concentrations are 10%.

Additionally, table 4.4 summarizes the cross section values obtained for the two different light sources and in the absence or presence of the narrow band filter at 214 nm. The resulting cross section values under all these conditions were in fair agreement within the experimental uncertainties: $\sigma = (1.5 \pm 0.2) \times 10^{-19}$ cm^2 $molecule^{-1}$.

Table 4.4: Absorption cross section of 2MBA at 214 nm, at 300 ± 2 K.

	D_2 lamp [b]		Zn lamp	
	No filter	Filter before cell	Spectrometer	diode
σ [a, c] (10^{-19})	1.25 ± 0.13	1.69 ± 0.18	1.60 ± 0.16	1.66 ± 0.17
Average σ [a, d] (with and without filter)			**1.5 ± 0.2**	

[a] Units of $cm^2 molecule^{-1}$

[b] Using the spectrometer

[c] The error quoted on σ include the standard deviation (1σ) of the slope and the estimated systematic uncertainties

[d] The error quoted on σ average is the standard deviation of σ values obtained in the presence and the absence of the filter

4.C. UV absorption cross-section measurements of 3MBA

The UV absorption cross section of 3MBA was determined in the wavelength range 210-370 nm at 300±2 and 335±2 K. The pressure range used was 0.2-1.1 Torr, thus its concentration varied between $(0.68-3.38) \times 10^{16}$ molecule cm^{-3}. The obtained cross section spectrum for an average of six different 3MBA concentrations at 300 K is presented in figure 4.6, where an absorption band center near 212-214 nm is shown. Table 4.5 presents the cross section values averaged over 2nm intervals.
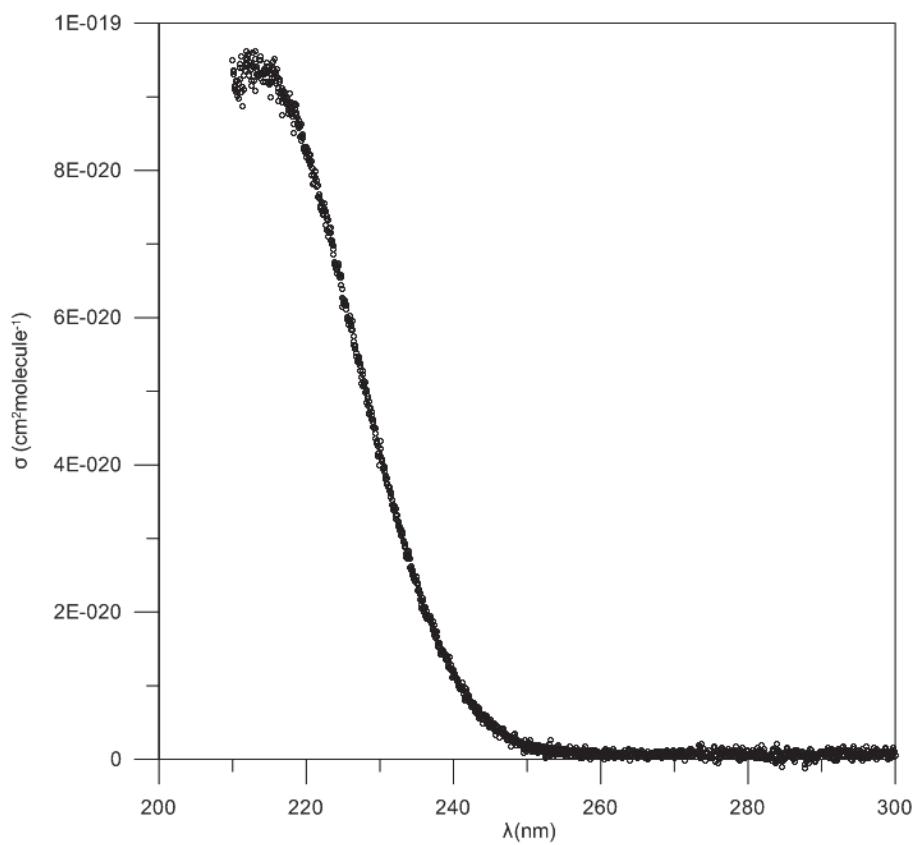
Figure 4.6: UV absorption cross section spectrum of 3MBA ((1.69 -3.38) × 10^{16} molecule cm^{-3}) using the D$_2$ lamp, between 210 and 300 nm at 300 K.

Table 4.5: UV absorption cross section of 3MBA measured at the wavelength range of 210-260 nm using the D_2 lamp at 300 ± 2 K for an average of six different 3MBA concentrations. The maximum absorption cross section of 3MBA in bold was measured between 212-214 nm.

λ [a]	σ [b] (10^{-20})
210	9.19
212	**9.35**
214	**9.34**
216	9.18
218	8.83
220	8.28
222	7.58
224	6.77
226	5.87
228	5.02
230	4.15
232	3.39
234	2.71
236	2.08
238	1.58
240	1.17
242	0.83
244	0.57
246	0.40
248	0.27
250	0.18
252	0.12
254	0.12
256	0.10
258	0.07
260	0.07

[a] Units of nm
[b] Units of cm^2 molecule^{-1}

The UV absorption cross section measurements at 212 nm for 300 and 335 K are presented in figure 4.7. Once again, absorbance and gas phase concentration are linearly correlated and σ was temperature independent for the two temperatures studied. The σ values obtained were (9.36 ± 0.95) x 10^{-20} and (9.45 ± 0.98) x 10^{-20} for 300 and 335 K, respectively. In addition, irradiating a known amount of 3MBA for

about 1.5 hours didn't cause any change to its concentration, pointing that photolysis is negligible within the studied wavelength range.
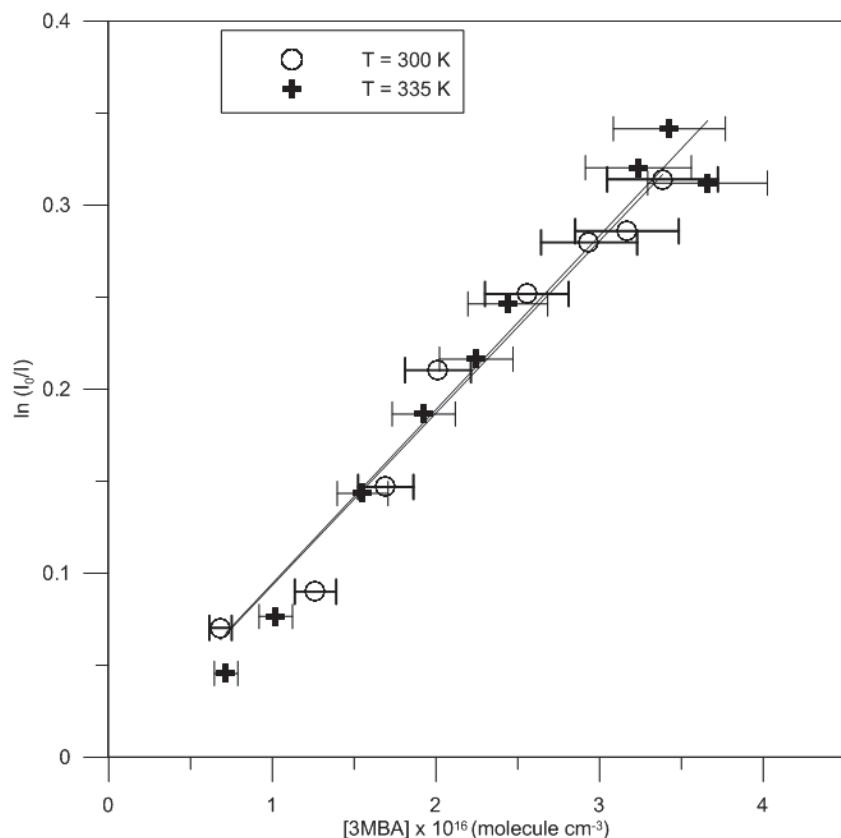

Figure 4.7: Slopes of the through zero linear least-squares analysis according to E(4.1) for UV-absorption cross section measurements of 3MBA using the D_2 lamp at 212 nm at 300 and 335 K. The σ values were (9.36 ± 0.95) x 10^{-20} and (9.45 ± 0.98) x 10^{-20} $cm^2 molecule^{-1}$ at 300 and 335 K, respectively. The error quoted on σ values includes the standard deviation (1σ) of the slope and the estimated systematic uncertainties, while the error bars for 3MBA concentrations are 10%.

Moreover, in table 4.6 the cross section values at 214 nm obtained by the two lamps with and without the narrow band filter are given. The cross section values determined under different experimental conditions were in fair agreement considering the experimental uncertainties and was, σ = (1.2 ± 0.3) x 10^{-19} cm^2 $molecule^{-1}$.

	D_2 lamp [b]		Zn lamp	
	No filter	Filter before cell	Spectrometer	diode
σ [a, c] (10^{-19})	0.94 ± 0.10	1.39 ± 0.16	1.34 ± 0.14	1.38 ± 0.14
Average σ (with and without filter)			**1.2 ± 0.3**	

[a] Units of $cm^2 molecule^{-1}$

[b] Using the spectrometer

[c] The error quoted on σ include the standard deviation (1σ) of the slope and the estimated systematic uncertainties

[d] The error quoted on σ average is the standard deviation of σ values obtained in the presence and the absence of the filter

4.D. Discussion and comparison

The UV radiation energy absorbed by molecules may produce electronic transitions with broad bands. These electronic transitions are accompanied by changes in vibrational and rotational states of the ground and the excited state as well (sub-levels). Figure 4.8 represents the electronic transitions due to the absorbed UV-vis radiation by organic compounds. Most of these transitions from bonding orbitals are of too high frequency to measure easily, thus most of the absorptions observed involve only $\pi \rightarrow \pi^*$, $n \rightarrow \sigma^*$ and $n \rightarrow \pi^*$ transitions.[60]
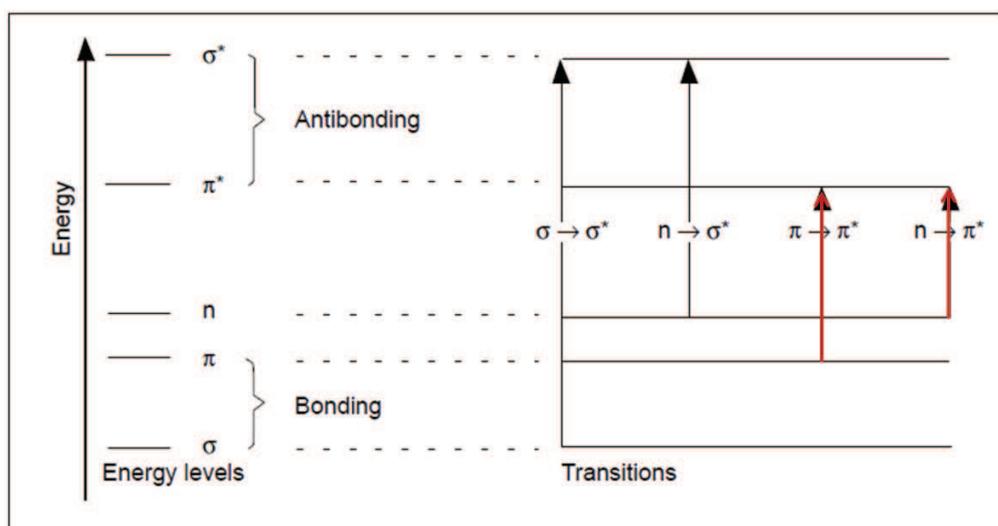

Figure 4.8: Electron transitions in UV visible spectroscopy. The transitions in red ($\pi \rightarrow \pi^*$ and $n \rightarrow \pi^*$) are observed in the range of 200-700 nm.[60]

Saturated carbonyl compounds have three principal UV absorption bands due to the n → σ* transitions which absorbs near 190 nm, the allowed π → π* transitions at 170-200 nm (figure 4.9) and the forbidden with low molar absorptivity n → π* transitions at 270-290 nm (figure 4.9).[61]
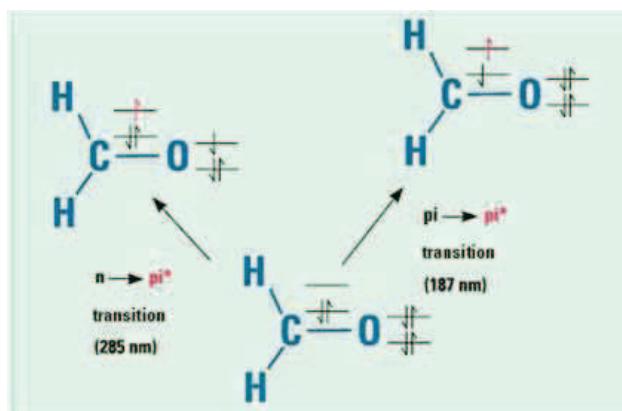
In esters, the substituent OR on the carbonyl group show pronounced hypsochromic effect (blue shift) on the n → π* transitions. The hypsochromic effect is due to inductive effect of the oxygen atom. This oxygen (R-C(O)-O-R') withdraws electrons from carbonyl carbon and makes carbonyl oxygen lone pair of electrons more stabilized due to its involvement in increasing C=O bond order. As a result, the n →π* transition of C=O of the esters is blue shifted to 204-210 nm relative to 270-290 nm in aldehydes and ketones. [63] For instance, compared to acetaldehyde (λ_{max} = 293 nm), the band for ethylacetate is shifted to 207 nm.[61, 64]

The three studied compounds (alkoxy-esters) have a broad band with the maximum absorbance in the wavelength range of 212-216 nm. Therefore, their maximum absorbance is red shifted compared to the base ester band maximum expected to appear between 204-210 nm. The red shifting from the base ester band (λ_{max} = 207 nm) is attributed to the presence of an additional alkoxy functional group in the studied compounds that acts as an auxochrome.[65,] In particular, the R-O-auxochrome provides additional opportunity for charge delocalization and thus provides smaller energy increments for transition to excited states. In the three

methoxy acetates studied, the lone pairs of the alkoxy oxygen can interact with the π electrons of C=O and stabilizes the π^* state, affecting the extend of delocalization, so the position and the intensity of the absorption band as well. Subsequently, a bathochromic shift (red shift) in the UV absorption maximum is observed, which is expected to be around 6 nm. [66]

The average cross section values in the presence or absence of the narrow band filter as well as using different light sources for MPA, 2MBA and 3MBA at 214 nm at 300 K were $(1.6 \pm 0.2) \times 10^{-19}$, $(1.5 \pm 0.2) \times 10^{-19}$ and $(1.2 \pm 0.3) \times 10^{-19}$ cm^2 $molecule^{-1}$ respectively and are presented in table 4.7. For comparison purposes, figure 4.10 displays the UV absorption cross section spectrum of the compounds studied in the absence of filter using the D_2 lamp, at 300 K.
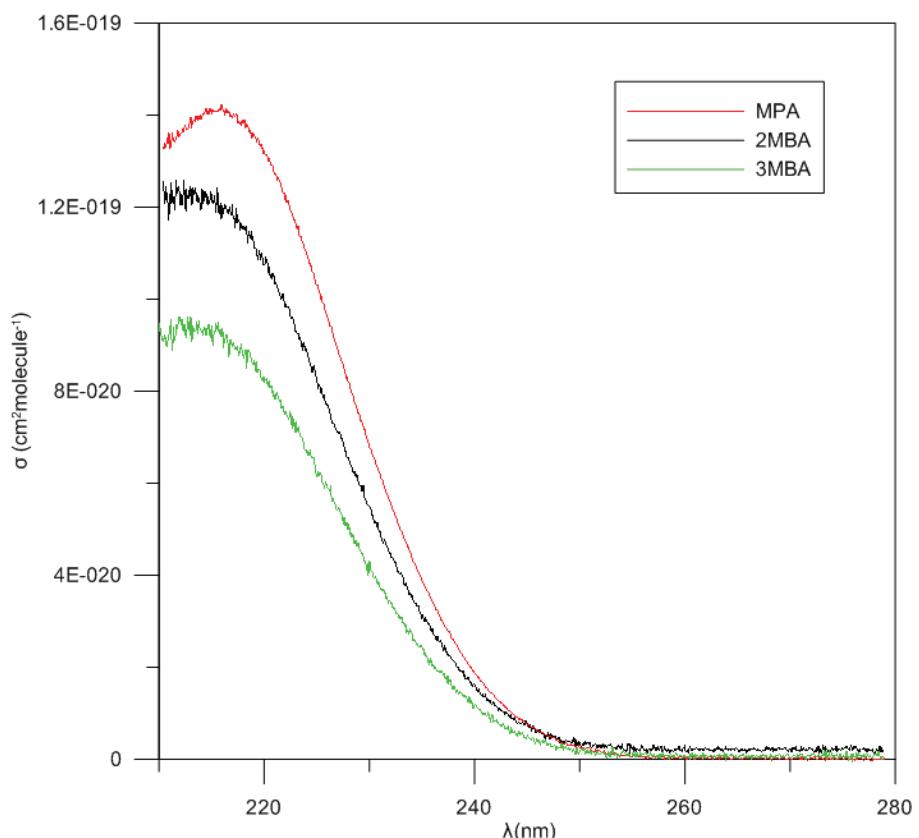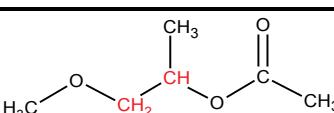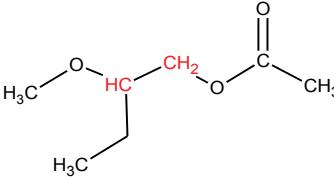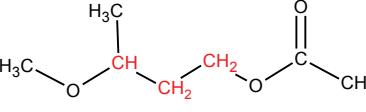

Figure 4.10: UV absorption cross section spectrum of the 3 compounds using the D_2 lamp, between 210 and 280 nm at 300 K.

Comparing MPA and 2MBA with 3MBA, we can note that as the number of carbon atoms increases between the alkoxy and the ester functional group (the distance of the alkoxy oxygen and C=O increases), σ decreases. Specifically, the σ of 3MBA is

lower than that of the two other compounds that have two carbon atoms in the chain between the oxygen atoms instead of three. Furthermore, it has to be noted that comparing MPA with 2MBA we conclude that the increase in the number of carbon atoms (branching) of the alkyl group has a result of sigma bond resonance, due to the stability lower radiation energy is absorbed.

Table 4.7: Average absorption cross section σ of the three studied molecules at 214 nm, at 300 ± 2 K is given in 10^{-19} cm^2 molecule^{-1}. The error quoted for σ is the standard deviation of the average. The carbon atoms in red are those in the chain between the alkoxy and the ester functional group.

Compound	Molecular structure	σ^a (10^{-19})
MPA		1.6 ± 0.2
2MBA		1.5 ± 0.2
3MBA		1.2 ± 0.3

^{a} Units of cm^2 molecule^{-1}

In addition, it is remarkable that the data from the different experimental conditions (i.e. light source, detection method, optical filtering) were in general in good agreement and falls within the combined uncertainties. Nevertheless, we have systematically noticed that optical filtering provided higher cross section values at 214 nm. In general, band-pass filters serve to isolate the molecular transition of interest and reduce light intensity from unwanted lines within the absorption cell. Indeed, the absorption experiments performed with optical filtering caused a decrease of the light intensity by one order of magnitude and the data points collected were more scattered (figure 4.3), which could be a source of the observed discrepancies. On the other hand, no change to the cross section was observed when the optical filter was placed before or after the absorption cell. The former

observation points that the origin of the systematically lower σ values measured without optical filtering is not related to light absorption phenomena in the cell.

5. Kinetic study

5. Kinetic study

This chapter includes a comprehensive presentation of the kinetic results obtained during the Thesis. The first section of the chapter is dedicated to the report of the compounds studied and to the experimental techniques that were employed for the measurements of the gas phase rate coefficients with OH radicals and Cl atoms. In addition, the kinetic expressions/equations that were applied for the absolute and relative rate measurements are presented in two separate subsections. To avoid any repetition during the detailed report of the results, the experimental conditions that need to be accomplished and ensured the correct applicability of the kinetic expressions to the experimental results are also discussed. Thereafter, the rate coefficients for the reactions of each OVOC with OH radicals and Cl atoms are quoted respectively; detailed tables listing the kinetic runs and typical figures are included.

Introduction

The rate coefficients for the reactions of OH radicals and Cl atoms with 1-methoxy 2-propyl acetate (MPA, $CH_3OCH_2CH(CH_3)OC(O)CH_3$), 2-methoxy-butyl acetate (2MBA, $CH_3OCH(C_2H_5)CH_2OC(O)CH_3$), 3-methoxy-butyl acetate (3MBA, $CH_3OCH(CH_3)CH_2CH_2OC(O)CH_3$), methoxy ethyl acetate (MEA, $CH_3OCH_2CH_2OC(O)CH_3$), ethoxy ethyl acetate (EEA, $C_2H_5OCH_2CH_2OC(O)CH_3$) and n-pentyl acetate (n-PA, $CH_3CH_2CH_2CH_2CH_2OC(O)CH_3$) in the gas phase were measured using complementary absolute and relative rate methods. The experiments were conducted using i) a pulsed laser photolysis-laser induced fluorescence technique (PLP-LIF), ii) a low pressure fast flow tube reactor coupled with a quadrupole mass spectrometer (FFT-QMS) and iii) a 200L atmospheric simulation chamber coupled with a gas chromatograph flame ionization detector (ASC-GC/FID). However, the set of the three complementary techniques were not always employed/available for the kinetic measurements of each compounds with the oxidants. PLP-LIF and FFT-QMS techniques availability was limited due to either instrumental reparation or accessibility workload. In addition, in case of 2MBA and 3MBA, due to their low

vapor pressure (< 1 Torr), sticky nature and low sensitivity of the GC-FID, it was not feasible to provide accurate kinetic data employing the ASC. Table 5.1 summarizes the techniques, the methods and temperature range used for each reaction.

Table 5.1: Techniques, methods and temperature range used for the reactions of OH and Cl with the studied acetates.

Compound	Reaction with the oxidant	Technique [a]	Method [b]	Temperature range (K)
MPA [d, e]	OH	PLP-LIF, ASC-GC/FID, FFT-QMS	AR, RR	263 - 372
	Cl	FFT-QMS, ASC- GC/FID	AR, RR	293 - 297
2MBA [c, d, e]	OH	PLP-LIF,FFT-QMS	AR, RR	273 - 372
	Cl	FFT-QMS	RR	297
3MBA [c, d]	OH	PLP-LIF	AR	298 - 363
		FFT-QMS	AR, RR	
MEA [e]	OH	ASC-GC/FID	RR	293
	Cl			
EEA [e]	OH	ASC-GC/FID	RR	293
	Cl			
n-PA [e]	OH	ASC-GC/FID	RR	293
	Cl			

[a] PLP-LIF: pulse laser photolysis-laser induced fluorescence, ASC-GC/FID: atmospheric simulation chamber-gas chromatograph/flame ionization detector, FFT-QMS: fast flow tube-quadrupole mass spectrometer
[b] AR: absolute rate measurements, RR: relative rate measurements
[c] Compounds with low vapor pressure
[d] This is the first study of OH rate coefficients
[e] This is the first study of Cl rate coefficients

> *Absolute method*

The absolute rate coefficient measurements were carried out employing the PLP-LIF and FFT-QMS. Helium (He) was used as carrier gas in both techniques. The total pressure was approximately 100 Torr in the PLP-LIF cell and 1 Torr in the FFT-QMS reactor. The absolute rate coefficient measurements were conducted under pseudo-first-order conditions with the concentration of the methoxy acetates in high excess over that of OH radicals and Cl atoms ([methoxy acetate]$_0$>> [oxidant]$_0$), respectively, following the consumption of the oxidant. The oxidant can be lost via the following processes:

$$X + OVOC \xrightarrow{k_{OVOC}} \text{products} \tag{R.5.1}$$

$$X + \text{impurities} \xrightarrow{k_2} \text{products} \tag{R.5.2}$$

$$X + \text{products} \xrightarrow{k_3} \text{secondary products} \tag{R.5.3}$$

$$X \xrightarrow{k_4} \text{diffusion} \tag{R.5.4}$$

X : OH radicals or Cl atoms. Hence,

$$-d\left(\frac{[oxidant]}{dt}\right) = (k_{OVOC}[OVOC] + k_2[impurities] + k_3[products] + k_4)[oxidant]$$

$$\tag{E.5.1}$$

The stated purity of the methoxy acetates as provided by the supplier exceeded 97%. Nevertheless, prior to their use, the compounds were additionally purified by repeated freeze-pump-thaw cycles to remove the lighter fraction of impurities. Subsequently, known OVOCs/He mixtures were prepared in 10 L glass bulbs and were used to supply the reactors. The purity of each mixture was additionally verified with a GC-MS and showed that the concentration of impurities was beyond the detection limit (solely the peak of methoxy acetates appeared in the GC-MS chromatograph). Therefore, it is safe to state that the impact of reaction R.5.2 to the absolute rate coefficient determination of methoxy acetates is expected to be negligible. Furthermore, since the absolute rate measurements are based on the consumption of the reactive species (i.e. OH and Cl), the accurate determination of the rate coefficient could be influenced by secondary reactions. Nevertheless the high $[OVOC]_0/[X]_0$ ratio used in the experiments implies insignificant contribution of secondary chemistry. The later was also verified by performing experiment varying the concentration of the active species; it was observed that the rate coefficient for reaction of methoxy acetates was independent on the initial concentration of OH/Cl and thus, the impact of reaction (R.5.3) could be considered as negligible. An extra process that can influence the kinetic measurements is the diffusion of the reactive species. Concerning PLP-LIF, under the conditions that experiments were performed,

the diffusion of OH out of the detection zone is insignificant compared to the chemical consumption of OH by the OVOC,($k_4 \ll k_{OVOC}$). However, in case of FT-QMS the axial and radial diffusion corrections can reach 15% of the measured rate coefficient, therefore, they should be applied to obtain the true rate coefficient of the OVOCs (see also 3.C section of experimental chapter). In addition, it is important to note that for the experiments conducted using the PLP-LIF the absorbance of the methoxyacetates at 248nm (used for H_2O_2 decomposition for OH production) was negligible and hence reaction of OH radicals with "electronically excited" OVOCs did not contribute to OH loss (see also UV spectra of the corresponding molecules in chapter 4). The later was also verified by performing kinetic runs varying by a factor of two (15 -30 mJ/pusle) the energy emitted by the excimer laser; the measured rate coefficient was found to be independent on the emitted energy of the laser.

Under these conditions, the expression (E.5.1) is simplified to:

$$-d\left(\frac{[oxidant]}{dt}\right) = (k_{OVOC}[OVOC])[oxidant] \qquad \text{(E.5.2)}$$

where the oxidant concentration-time profiles followed a simple exponential rate law according to:

$$[X]_t = [X]_0 \exp^{-k't} \qquad \text{where } k' = k_{OVOC} + k'_0 \qquad \text{(E.5.3)}$$

in which,

k'_0 : the first-order decay rate of the oxidant in the absence of the OVOC

k_{OVOC} : the rate coefficient for the reaction of the oxidant with the OVOC

The rate coefficients k_{OVOC} is then obtained by plotting the pseudo-first-order rate coefficient versus the OVOC concentrations. Details regarding the calculations of methoxy-acetates concentrations are presented in the experimental chapter, sections 3.B.V and 3.C.V for PLP-LIF and FFT- QMS, respectively. For clarity, in case of FFT-QMS the ion peaks used for the monitoring of the studied compounds and the

precursor molecules for OH/Cl productions are given in table 5.2. In addition the mass spectra of MPA, 2MBA and 3MBA derived from the Automated Thermal Desorption - Gas Chromatography - Mass Spectrometer (ATD-GC-MS) are given in annex IV.

Table 5.2: Ion peaks used for the monitoring of the studied and reference compounds and the precursor molecules.

Compound	Ion/Fragment	Ion peak m/z	Reaction studied	Method[a]
$CH_3OCH_2CH(CH_3)OC(O)CH_3$ MPA	$(CH_3C(O)OCH^+)$ $(CH_3OCH_2^+)$	72 45	MPA+OH/Cl	AR/RR
$CH_3OCH(C_2H_5)CH_2OC(O)CH_3$ 2MBA	$(CH_3OCH(CH_2CH_3)^+)$ and $(CH_2OC(O)CH_3^+)$	73	2MBA+OH/Cl	AR/RR
$CH_3OCH(CH_3)CH_2CH_2OC(O)CH_3$ 3MBA	$(CH_3OCCH_2CH_2^+)$ $(CH_3OCHCH_3^+)$ and $(OC(O)CH_3^+)$	71 59	3MBA+OH	AR/RR
Br_2	(Br_2^+)	160	MPA/2MBA/3MBA+OH	AR/RR
OHBr	$(OHBr^+)$	98	MPA/2MBA/3MBA+OH	AR
BrCl	$(BrCl^+)$	116	MPA/2MBA/3MBA+Cl	AR
NO_2	(NO_2^+)	46	MPA/2MBA/3MBA+OH	AR/RR
NO	(NO^+)	30	MPA+OH	RR
$C_3H_6O_2$ 1,3-dioxolane	$(C_3H_6O_2^+)$	73	MPA/3MBA+OH	RR
C_7H_{16} n-heptane	$(C_7H_{16}^+)$	100	2MBA+Cl	RR
$C_4H_8O_2$ 1,3-dioxane	$(C_4H_7O_2^+)$	87	2MBA+OH	RR

[a] AR: absolute rate measurements, RR: relative rate measurements

➢ *Relative method*

The OH and Cl reaction rate coefficients for all the compounds were determined by using the relative rate method. The principle of this method is to measure in the presence of the oxidant the decay rate of the OVOC in interest relative to that of a reference compound for which the OH or Cl reaction rate coefficient is well known.

$$X + OVOC \xrightarrow{\;k_{OVOC}\;} products \qquad\qquad (R.5.1)$$

$$X + Reference \xrightarrow{\;k_{ref}\;} products \qquad\qquad (R.5.5)$$

where,

 X = OH radicals or Cl atoms

The kinetic measurements in the ASC were conducted under static conditions recording the concentration drop of the VOCs as a function of time. On the other hand, the relative rate measurements in the flow tube reactor were performed under flow conditions where the concentration of the oxidant was predominantly varied between $0.4\text{-}6.0 \times 10^{12}$ radicals cm^{-3}. Besides, several kinetic runs were also carried out varying the concentration of the selected OVOC and the reference compound.

There are three presuppositions that need to be ensured for the accurate measurement of the relative rate coefficient: (i) both the reactant and reference compounds are removed solely via reaction with the oxidant in the gas phase; (ii) both the reactant and reference compound have the same exposure to the oxidant; and (iii) the ratio of the reference and compound rate coefficients is between 0.2 and 5, $(0.2 < k_{OVOC}/k_{ref} < 5)$. In the atmospheric simulation chamber, the first requirement was achieved by minimizing the heterogeneous losses (use Teflon inert material, use new and well cleaned Teflon bag, use low concentrations of the reagents, have low ratio ASC wall surface/ASC volume) and performing experiments using synthetic air as a bath gas. The excess of O_2 enables to scavenge the R-radicals formed (R + O_2 $\rightarrow$ products) otherwise the presence of these radicals would potentially lead to errors in k measurements. Moreover, the mixture of the OVOC and reference compound with and without H_2O_2 or Cl_2 was stable in the dark when it was left in the chamber for about 1.5-2 hours. In addition, photolysis of OVOCs or reference compounds was negligible when these compounds were irradiated at 254 nm or 365 nm for the same timescale. The second requirement was overtaken simply by leaving for sufficient time the reaction mixture to be homogeneously mixed within the reactor. Regarding the third presupposition, the reference compounds were selected with respect to $0.2 < k_{OVOC}/k_{ref} < 5$. In the case of the flow tube the first requirement was ensured through the absolute control of the experimental conditions. R-radicals were scavenged by NO_2 which was introduced in high excess in the reaction system. In addition, the short reaction time (ms range)

and the fast reaction of the OH/Cl with the methoxy acetates ensure the limiting impact of the secondary consumption of the stable species from the formed radicals. To verify that, for each compound the relative rate measurements were crosschecked in the two extreme positions of the sliding injector, i.e. variation of reaction time by factor of 3, and no dependence to the measured values of k was observed. Therefore, the impact of the formed radicals not scavenged by NO_2, is negligible. Furthermore, as previously mentioned the relative rate kinetic measurements were conducted varying either the concentration of the active species (OH, Cl) or the studied/reference compounds, pointing that secondary reactions had negligible impact to the measured k_{OVOC}/k_{ref} ratio.

Moreover, the relative rate measurements were not influenced by heterogeneous reactions on the walls of the reactor for temperatures above 293K. However, at low temperatures heterogeneous complications influenced the kinetic measurements. In particular, due to the low vapor pressure of the methoxy acetates and their sticky nature, the active species (OH, Cl) reacted with the acetates adsorbed on the walls of the reactor influencing the equilibrium $[acetate]_{gas\ phase}/[acetate]_{wall\text{-}adsorbed}$ leading to extremely high rate coefficients measurements. That is why the relative kinetic measurements were limited for temperatures above 293K. The second requirement was achieved due to the fast mixing of the reactant before the reaction zone and was verified by the steady intensity of the mass spectrometric signal (all reactants under steady state conditions).

Therefore, the relative rate coefficient can be obtained by the following expression:

$$\ln\left[\frac{[OVOC]_0}{[OVOC]_t}\right] = \frac{k_{OVOC}}{k_{ref}} \times \ln\left[\frac{[ref]_0}{[ref]_t}\right]$$

(E.5.4)

where,

$[OVOC]_0$: concentration of the studied compound at time t=0

$[OVOC]_t$: concentration of the studied compound at time t

$[ref]_0$: concentration of the reference compound at time t=0

$[ref]_t$: concentration of the reference compound at time t

k_{OVOC} : the rate coefficient of the OVOC reaction with the oxidant

k_{ref} : the rate coefficient of the reference compound reaction with the oxidant

Thus, the plot of $\ln([OVOC]_0/[OVOC]_t)$ versus $\ln([Reference]_0/[Reference]_t)$ exhibits linearity with a slope equal to k_{OVOC}/k_{ref}.

Concerning the experiments conducted in the atmospheric simulation chamber, the relative change in concentration of the alkoxy ester and reference compounds was derived from integration of the chromatogram peaks. The plots of the experimental results according to (E.5.4) have near-zero intercept, verifying the absence of secondary reactions. In addition the initial concentrations of the precursors H_2O_2 and Cl_2 were 148-518 ppm and 58-190 ppm, respectively.

In the case of FFT-QMS the gas phase species were detected by mass spectrometry; table 5.2 summarizes all the ions peaks used for the monitoring of the reference compounds, methoxy acetates, and oxidants for the relative rate measurements. Finally, it is important to note that prior to the kinetic measurements, several tests were conducted to crosscheck whether the reference compound contribute to the chosen peak (chromatographic or spectroscopic) of the compound of interest, and vice versa (see also chapter 3.C.IV, relative rate coefficient measurements). The initial concentrations of NO_2 and OH radicals were: $(7.5\text{-}8.6) \times 10^{13}$ molecules cm^{-3} and $(0.4\text{-}6.0) \times 10^{12}$ radicals cm^{-3}, respectively.

Finally, for clarity, table 5.3 summarizes the rate coefficients of OH radicals and Cl atoms with the compounds that were used as references for the relative rate measurements. They were collected either by the latest IUPAC evaluation[52, 67], and by averaging the existing literature values.

Reaction	k (cm^3 molecule^{-1} s^{-1})	Reference	Quoted error
1,3-dioxolane+OH	$(1.13\pm0.11) \times 10^{-11}$	[68]	10%[a]
1-pentanol+OH	$(1.11\pm0.10) \times 10^{-11}$	[69, 70, 71]	st dev[b]
Br$_2$+OH	$2.0 \times 10^{-11} e^{2.00\ [kJ/mole]/RT}$	[52]	10%[a]
1,3-dioxolane+OH	$6.7 \times 10^{-12} e^{1.28\ [kJ/mole]/RT}$	[68]	10%[a]
1,3-dioxane+OH	$(9.60 \pm 0.45) \times 10^{-12}$	[72, 73]	st dev
1-propanol+OH	$(5.84 \pm 0.58) \times 10^{-12}$	[67]	10%[a]
1-butanol+OH	$(8.55 \pm 0.86) \times 10^{-12}$	[67]	10%[a]
cyclohexane+Cl	$(3.32 \pm 0.41) \times 10^{-10}$	[74, 75]	st dev[b]
1-propanol+Cl	$(1.62 \pm 0.14) \times 10^{-10}$	[67]	st dev[b]
n-pentane+Cl	$(2.71 \pm 0.28) \times 10^{-10}$	[76, 75, 74]	st dev[b]
1-butanol+Cl	$(2.18 \pm 0.17) \times 10^{-10}$	[67]	st dev[b]
n-heptane+Cl	$(3.53 \pm 0.12) \times 10^{-10}$	[75, 76]	st dev[b]

[a] Estimated uncertainty on k
[b] Standard deviation of k values determined in literature

5.A. Reactions with OH radicals

5.A.I. Reaction of OH + CH$_3$OCH$_2$CH(CH$_3$)OC(O)CH$_3$ (MPA)

> *Absolute rate measurements*

PLP-LIF

The OH absolute rate coefficient of MPA was measured in the temperature range of 263-372 K. The experiments were conducted using two or three different mixtures in each temperature varied from 0.3 to 0.6% MPA/He. The reaction was studied under pseudo-first-order conditions with the concentration of MPA in high excess (0.19-4.64) × 10^{14} molecules cm^{-3} over that of OH radicals (4.3-59) × 10^{10} molecules cm^{-3}. The OH concentration-time profiles followed first order exponential decay (E.5.3), as depicted in figure 5.1, where the values of k_0' depended on the rates of reaction of OH with its precursor, H$_2$O$_2$, and diffusion from the detection zone, were typically in the range of 91–242 s^{-1}, while k' values were in the range of 301–8071 s^{-1}.
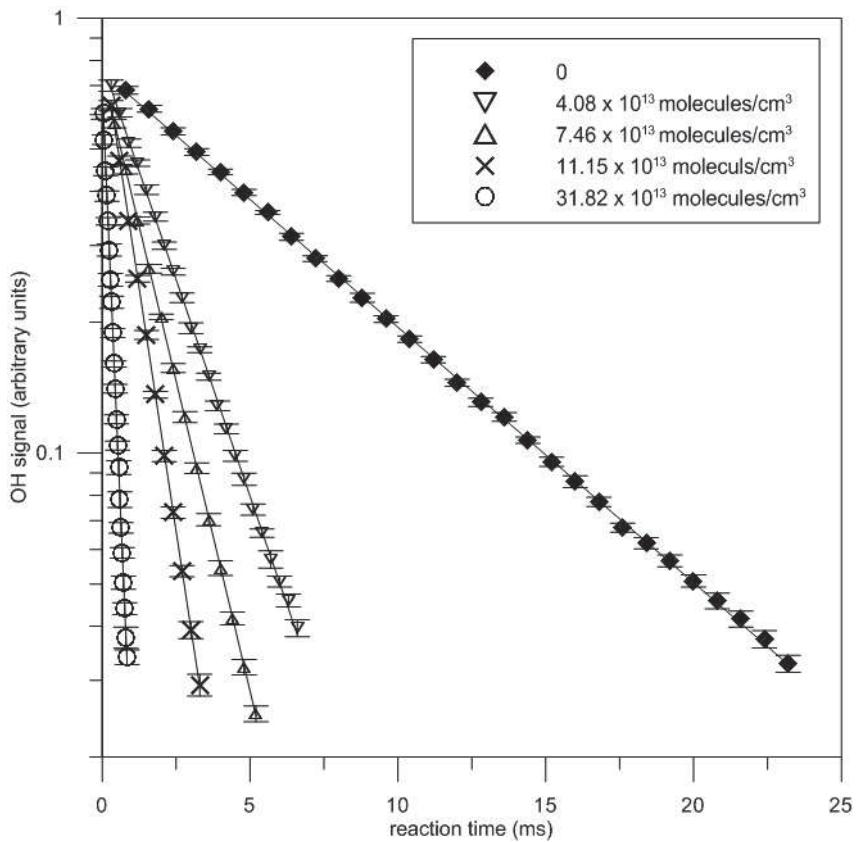
Figure 5.1: First order exponential decay of the OH concentration-time profiles. Reaction of OH radicals with MPA obtained in PLP-LIF at 348 K for different concentrations of MPA. The errors shown for OH signal represent the standard deviation of 20 fluorescence signals.

Figure 5.2 shows an example of typical plots of k' versus MPA concentrations for different temperatures and from which the rate coefficients values were derived. The uncertainty on the MPA concentration measurement was estimated to be 10%, considering the uncertainties in the flow of the reagents, in the MPA mixture preparation and in the temperature and pressure measurements of the cell (more details in annex VII: Uncertainty analysis).

The summary of the experimental conditions and the rate coefficients values obtained are given in table 5.4. It should be noted that for the temperature of 263 K, the concentration range of MPA was limited due to heterogeneous complications. The average of 3 kinetic runs was used and is presented as unique value in table 5.4 and to the Arrhenius plot (figure 5.6). In this way we eliminated any additional uncertainty to the Arrhenius expression determined through an unweighted exponential fit of the experimental results (see temperature and pressure dependence section).

99
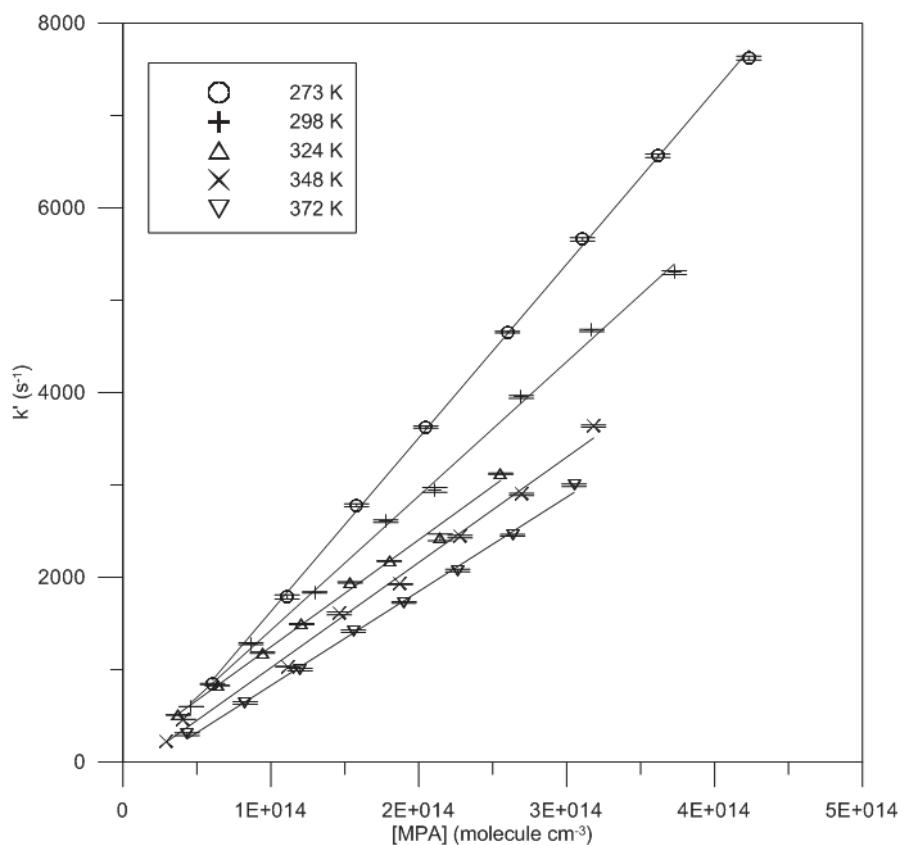
Figure 5.2: Absolute rate data for the reaction of OH radicals with MPA obtained in PLP-LIF at the temperature range of 273-372 K. One run is presented in each temperature. The errors quoted for k' values are the standard deviation (1σ) of the individual exponential and do not include systematic uncertainties.

Table 5.4: Summarized experimental conditions and results obtained from PLP-LIF for the reaction of OH with MPA.

T^a	[MPA] ^{b} (10^{13})	k'_0 (s^{-1})	k' (s^{-1})	($k_{MPA} \pm 1\sigma$)^c (10^{-11})
263	1.86 - 9.12	90 - 190	199 - 1325	1.90 ± 0.14 ^{d}
273	6.28 - 46.39	215 - 227	738 - 8072	1.84 ± 0.05
273	6.06 - 42.32	174 - 209	844 - 7623	1.88 ± 0.02
298	4.62 - 37.28	161 - 181	601 - 5300	1.45 ± 0.03
300	5.50 - 42.55	203 - 249	600 - 5713	1.37 ± 0.03
300	4.46 - 37.28	157 - 183	510 - 5805	1.58 ± 0.06
324	3.10 - 34.41	159 - 174	510 - 3121	1.16 ± 0.04
323	3.75 - 25.54	121 - 165	262 - 3945	1.17 ± 0.07
348	4.08 - 31.82	135 - 148	461 - 3636	1.15 ± 0.04
348	2.93 - 32.82	133 - 161	218 - 3189	0.97 ± 0.04
348	4.17 - 20.00	93 - 125	317 - 1959	1.04 ± 0.03
372	4.34 - 30.50	120 - 128	333 - 3128	1.02 ± 0.02
372	3.89 - 25.09	114 - 118	201 - 2998	1.00 ± 0.02
372	3.01 - 29.53	125 - 133	445 - 2564	1.05 ± 0.01

^{a} Units of K

^{b} Units of molecule cm^{-3}

^{c} Units of cm^3 molecule^{-1} s^{-1}

^{d} The average of 3 kinetic runs was used and is presented as unique value

FFT-QMS

Complementary, the OH absolute rate coefficients of MPA were measured in excess of MPA concentration $(0.1-2.9) \times 10^{13}$ molecules cm^{-3} over that of OH radicals $(0.4-1.3) \times 10^{12}$ molecules cm^{-3}. Experiments were carried out at three temperatures T=297, 303 and 336 K and the rate coefficients were derived following the time profiles of OH concentration (E.5.3). The linear velocity inside the reactor was in the range of 1231 to 1780 cm s^{-1}.

The sensitivity of the mass spectrometer to the parent peak of MPA was substantially lower than the fragments peaks, $I_{parent} < 0.01 \times I_{fragments}$, and thus the concentration of MPA was monitored as a function of the reaction time at the mass peaks $m/z = 72$ ($CH_3CHOC(O)^+$) or $m/z = 45$ ($CH_3OCH_2^+$). Figure 5.3 shows the pseudo–first-order rate coefficients, $k' = k_{MPA} + k'_0$, as a function of the MPA concentration.

k'_0 was measured before and after each experiment and ranged from 10 to 20 s^{-1}, thus it is in good agreement with the corresponding intercept in figure 5.3. The errors shown for k' represent one standard deviation (1σ) of the individual exponential fits and do not include systematic uncertainties. The errors quoted for MPA concentrations are estimated to be nearly 10%, considering the uncertainties in the flow of the reagents into the cell, in the MPA calibration factor and in the temperature and pressure measurements of the reactor (more details in annex VII: Uncertainty analysis). An abnormal increase of the rate coefficient was observed at low temperatures. This phenomenon was attributed to the heterogeneous reaction of OH with surface-adsorbed MPA on the walls of the reactor. For this reason, the absolute measurements of the rate coefficient were carried out at temperatures above 297 K. All the results obtained for the OH rate coefficients and a summary of the experimental conditions are presented in table 5.5.
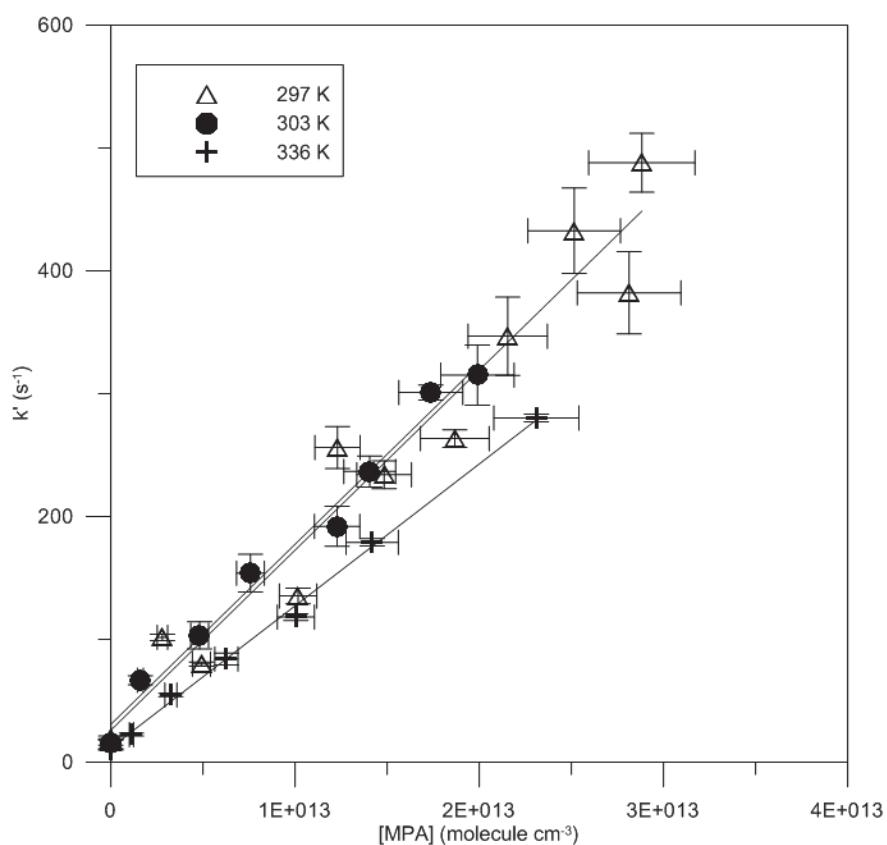

Figure 5.3: Absolute rate data for the reaction of OH radicals with MPA obtained in the FFT-QMS at T = 297, 303, and 336 K. The errors shown for k' represent one standard deviation (1σ) of the individual exponential fits and do not include systematic uncertainties.

Table 5.5: Summarized experimental conditions and results obtained from absolute rate coefficient measurements using FFT-QMS for the reaction of OH with MPA.

T^a	[MPA] ^{b} (10^{13})	k'_0 (s^{-1})	k' (s^{-1})	($k_{MPA} \pm 1\sigma$) ^{c} (10^{-11})
297	0.50 - 2.88	19.4 - 20	80 - 488	1.47 ± 0.13
303	0.16 - 1.99	15.2 - 17.1	67 - 301	1.47 ± 0.07
336	0.11 - 2.31	10.3 - 15.1	22.5 - 280.3	1.16 ± 0.03

^{a} Units of K

^{b} Units of molecule cm^{-3}

^{c} Units of cm^3 molecule^{-1} s^{-1}

> ➢ *Relative rate measurements*

Atmospheric simulation chamber

The rate coefficient for OH reaction with MPA was determined using 1,3-dioxolane, $k_{(OH+1,3-dioxolane)}$= (1.13±0.11) ×10^{-11} [68], and 1-pentanol, $k_{(OH+1-pentanol)}$=(1.11±0.10) × 10^{-11} [69, 70, 71] in cm^3 molecule^{-1} s^{-1} as reference compounds. The initial concentrations of the precursor H_2O_2 into the ASC were in the range of 327 − 485 ppm. For all the reference compounds three different runs were carried out. The plots of the experimental results according to (E.5.4), shown in figures 5.4, have near-zero intercept, verifying the absence of secondary reactions. The experimental conditions, the obtained slopes and rate coefficients for OH reaction are summarized in table 5.6. The errors quoted for k_{MPA}/k_{ref} values in table 5.6 are the standard deviation (1σ) of the slope and do not include systematic uncertainties. The errors quoted for k_{MPA} value in the individual experiments are the errors in k_{MPA}/k_{ref} by taking into account the error of k_{ref}. Errors quoted for the average of the three runs is the standard deviation. Regarding the errors quoted to the final average values of k, the standard deviation of the individual k values was used. A detailed uncertainty analysis is given in annex VII.
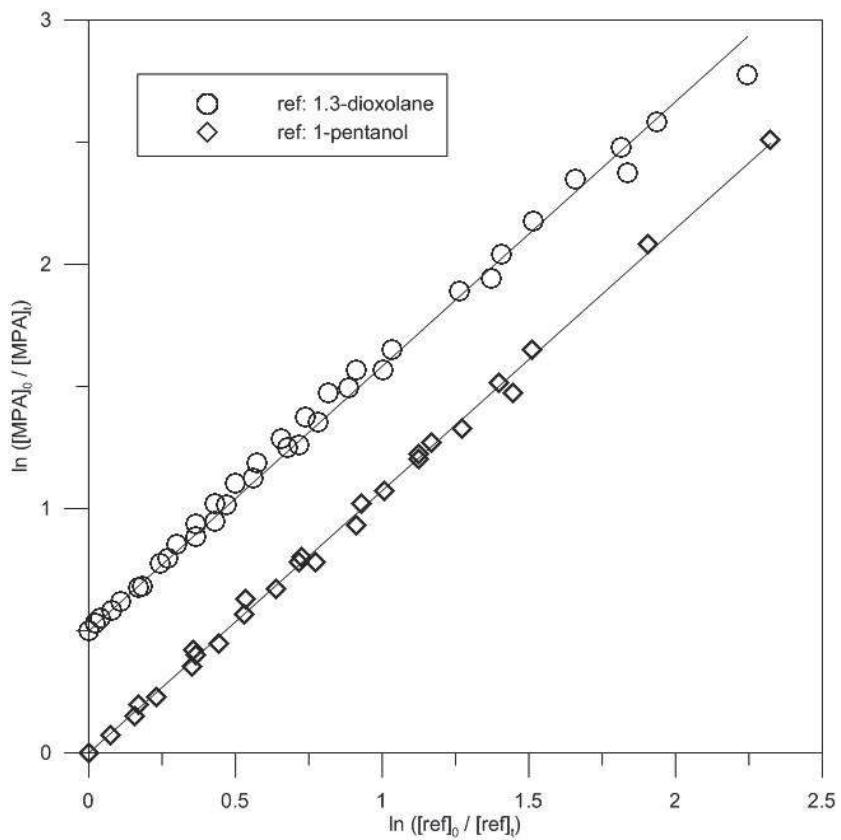
Figure 5.4: Relative rate data for the reaction of OH radicals with MPA obtained in the Atmospheric simulation chamber using 1,3-dioxolane and 1-pentanol as reference compounds. The experimental measurements with 1,3-dioxolane are shifted up on the y axis by + 0.5 ln([MPA]$_0$/ [MPA]$_t$) units for clarity purposes. Three runs are presented in each case.

Table 5.6: Reaction of OH with MPA: Experimental conditions and results obtained in the atmospheric simulation chamber at 293 K.

Ref.	Number of runs	$[ref]_0$ [a]	$[MPA]_0$ [a]	$(k_{MPA}/k_{ref}) \pm 1\sigma$	$(k_{MPA} \pm 1\sigma)$ [b] (10^{-11})
1,3-dioxolane	3	49.74	19.02	1.10 ± 0.004	1.24 ± 0.13
		39.86	21.58	1.19 ± 0.005	1.35 ± 0.14
		35.34	26.43	1.03 ± 0.007	1.16 ± 0.12
				average	**1.25 ±0.09**
1-pentanol	3	15.47	16.66	1.09 ± 0.002	1.21 ± 0.11
		15.68	24.29	1.04 ± 0.007	1.16 ± 0.11
		21.41	33.89	1.10 ± 0.010	1.22 ± 0.12
				average	**1.20 ± 0.04**
	Average				**1.23 ± 0.04**

[a] Units of ppm

[b] Units of cm^3 molecule^{-1} s^{-1}

FFT-QMS

Relative rate measurements of the OH reaction with MPA were also performed in FFT-QMS system, using two reference compounds, Br_2 and 1,3-dioxolane, at 313 and 297 K, respectively. The Arrhenius expressions used for the rate coefficients of the reference reactions were: $k_{(OH+Br_2)} = 2.0 \times 10^{-11} e^{2.00 \ [kJ/mole]/RT}$ [52] and $k_{(OH+1,3-dioxolane)} = 6.7 \times 10^{-12} e^{(1.28\pm0.30)kJ/mole]/RT}$ cm^3 molecule^{-1} s^{-1} [68]. The relative rate coefficients were obtained according to (E.5.4). The experimental data are shown in figure 5.5. A summary of the experimental conditions and the values obtained for the rate coefficients are presented in table 5.7. The errors quoted for k_{MPA}/k_{ref} values in table 5.7 correspond to one standard deviation (1σ) on the determination of the slopes of the straight lines in figure 5.5 and do not include systematic uncertainties. The errors quoted for k_{MPA} include the uncertainty of k_{ref}. Furthermore it is important to stress out that in experiments where Br_2 was used as reference compound, the formed Br atoms had a negligible impact on MPA concentrations and thus did not influence the rate coefficient measurements. The later has also been described in the experimental section (3.C.IV section).
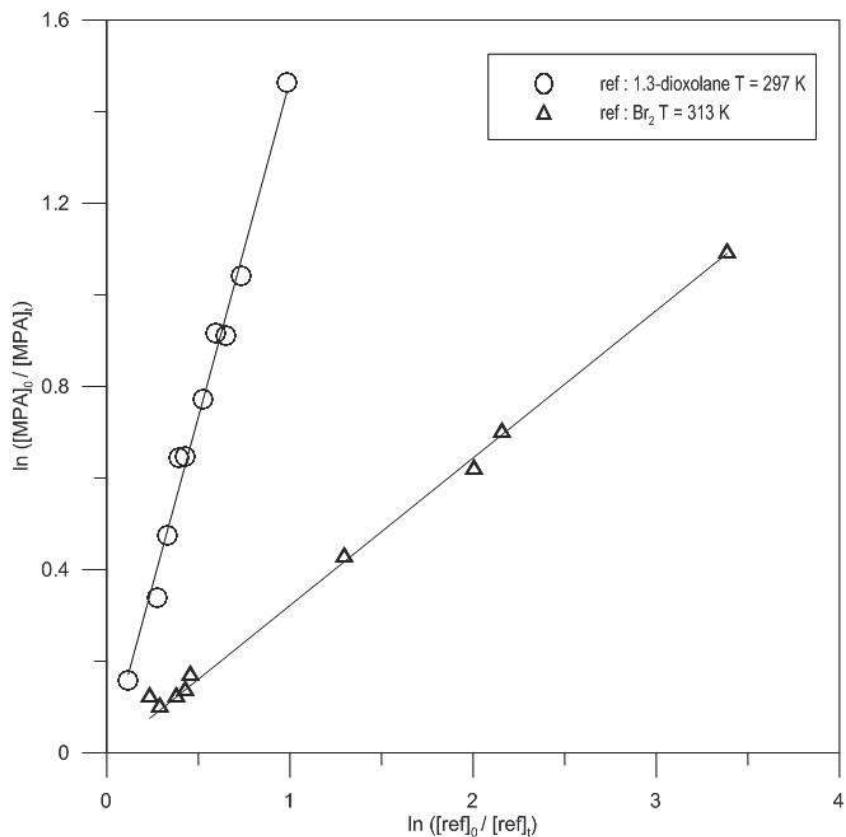
Figure 5.5: Relative rate plots for the reaction of OH with MPA measured in the FFT-QMS system, using 1,3-dioxolane and Br$_2$ as reference compounds at 297 and 313 K, respectively.

Table 5.7: Reaction of OH with MPA: Experimental conditions and results obtained using FFT-QMS. As reference compounds Br$_2$ and 1,3-dioxolane was used at 297 and 313 K, respectively.

T [a]	Ref.	Number of runs	[ref]$_0$[b] (10^{12})	[MPA]$_0$[b] (10^{12})	(k_{MPA}/k_{ref})± 1σ	(k_{MPA}± 1σ)[c] (10^{-11})
297	**1,3-dioxolane**	1	1.9-2.0	1.5-2.5	1.47 ± 0.02	1.65 ± 0.14
313	**Br$_2$**	1	0.5-1.0	2.3	0.32 ± 0.01	1.39 ± 0.16

[a] Units of K

[b] Units of molecule cm^{-3}

[c] Units of cm^3 molecule^{-1} s^{-1}

> ➤ *Temperature and pressure dependence*

The complementary use of PLP-LIF, FFT-QMS and ASC techniques allowed us to determine the absolute and relative rate coefficient of MPA with OH radicals in the temperature range 263 – 372 K and the pressure range 1 -760 Torr. The experimental conditions and measured values of the rate coefficient are listed in table 5.8. The unweighted Arrhenius exponential fit to the *k* is presented in figure 5.6

106

(solid line). The plot shows slight negative temperature dependence and provides the following Arrhenius expression:

$$k_{MPA+OH}(T) = (2.01 \pm 0.02) \times 10^{-12} \exp[(588 \pm 123/T)] \, cm^3 \, molecule^{-1} \, s^{-1}$$

where the quoted uncertainties on E/R and on the preexponential factor (A) are the standard deviation (1σ) and ($A\sigma_{lnA}$), respectively. **The room temperature rate coefficient is k_{298} = 1.44 × 10^{-11} cm^3 $molecule^{-1}$ s^{-1}. The negative activation energy, E = -4.89 kJ mol^{-1}, indicates that the reaction follows a complicated mechanism with probably an adduct formation (discussed in the Arrhenius expression section).** Moreover, comparing the rate coefficients measured with the 3 experimental systems at near room temperature (T=294K) we observed that pressure variation did not have any impact on k (table 5.9). Particularly, the dependence of k on pressure was investigated at T=297±4 K within the pressure range of 1-760 Torr (table 5.9). The results showed no systematic increase of the rate coefficient with pressure; the observed discrepancies between the measurements, could be attributed to experimental uncertainties from the different experimental set ups used and the different methods applied.

Table 5.8: Reaction of OH with MPA: Summarized experimental conditions and results obtained from all the apparatus.

T^a	[MPA] ^{b} (10^{13})	(k ± 1σ)^c (10^{-11})	Technique^d
263	1.86-9.12	1.90 ^{e} ± 0.14	AR, PLP-LIF
273	6.28-46.4	1.84 ± 0.05	AR, PLP-LIF
273	6.06-42.3	1.88 ± 0.02	AR, PLP-LIF
293	47.6-65.6	1.25 ^{f} ± 0.09	RR, ASC-GC/FID
293	41.6-84.7	1.20 ^{g} ± 0.04	RR, ASC-GC/FID
297	0.50-2.88	1.47 ± 0.13	AR, FFT-QMS
297	0.15-0.25	1.65 ^{f} ± 0.14	RR, FFT-QMS
298	4.6-37.3	1.45 ± 0.03	AR, PLP-LIF
300	5.5-42.6	1.37 ± 0.03	AR, PLP-LIF
300	4.46-37.3	1.58 ± 0.06	AR, PLP-LIF
303	0.16-1.99	1.47 ± 0.07	AR, FFT-QMS
313	0.22-0.23	1.39 ^{h} ± 0.16	RR, FFT-QMS
324	3.10-34.4	1.16 ± 0.04	AR, PLP-LIF
323	3.75-25.5	1.17 ± 0.07	AR, PLP-LIF
336	0.11-2.31	1.16 ± 0.03	AR, FFT-QMS
348	4.08-31.8	1.15 ± 0.04	AR, PLP-LIF
348	2.93-32.8	0.97 ± 0.04	AR, PLP-LIF
348	4.17-20.0	1.04 ± 0.03	AR, PLP-LIF
372	4.34-30.5	1.02 ± 0.02	AR, PLP-LIF
372	3.89-25.1	1.00 ± 0.02	AR, PLP-LIF
372	3.01-29.5	1.05 ± 0.01	AR, PLP-LIF

^{a} Units of K

^{b} Units of molecule cm^{-3}

^{c} Units of cm^3 molecule^{-1} s^{-1}

^{d} AR: absolute rate measurements, RR: relative rate measurements, PLP-LIF: pulse laser photolysis-laser induced fluorescence, ASC-GC/FID: atmospheric simulation chamber-gas chromatograph/flame ionization detector, FFT-QMS: fast flow tube-quadrupole mass spectrometer

^{e} The average of 3 kinetic runs was used and is presented as unique value

^{f} Reference compound used: 1,3-dioxolane

^{g} Reference compound used: 1-pentanol

^{h} Reference compound used: Br_2
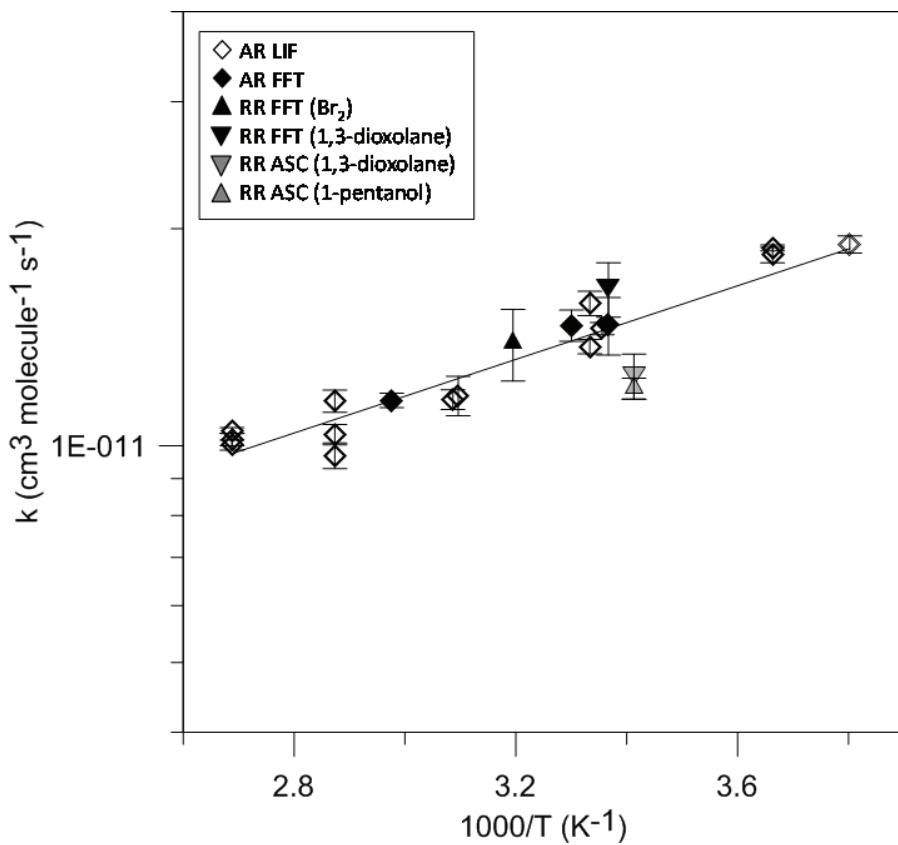
Figure 5.6: Plot of the obtained relative and absolute OH rate coefficients using three complementary techniques on a logarithmic scale as a function of 1000/T (K^{-1}) over the temperature range 263-372 K.

Table 5.9: Reaction of OH with MPA at 297±4 K: Pressure dependence

Number of runs	P[a]	[MPA] [b] (10^{13})	(k ± 1σ)[c] (10^{11})	Technique[d]
1	1	0.50-2.88	1.47 ± 0.13 [e]	AR, FFT-QMS
3	100	4.46-42.55	1.47 ± 0.10 [f]	AR, PLP-LIF
1	1	0.15-0.25	1.65 ± 0.14 [e]	RR, FFT-QMS
6	760	41.65-84.72	1.23 ± 0.04 [g]	RR, ASC-GC/FID

[a] Units of Torr

[b] Units of molecule cm^{-3}

[c] Units of cm^3 molecule^{-1} s^{-1}

[d] AR: absolute rate measurements, RR: relative rate measurements, FFT-QMS: fast flow tube-quadrupole mass spectrometer PLP-LIF: pulse laser photolysis-laser induced fluorescence, ASC-GC/FID: atmospheric simulation chamber-gas chromatograph/flame ionization detector

[e] The error quoted is the standard deviation (1σ) of the slope

[f] The error quoted is the standard deviation of the three runs

[g] The error quoted is the standard deviation of the k values measured using the two reference compounds

109

5.A.II. Reaction of OH + CH$_3$OCH(C$_2$H$_5$)CH$_2$OC(O)CH$_3$ (2MBA)

> ### *Absolute rate measurements*

PLP-LIF

The absolute rate coefficients of 2MBA with OH radicals were measured in the temperature range 273-372 K. The experiments were conducted using two different mixtures of 0.12 and 0.23% 2MBA in He. The reaction was studied under pseudo-first-order conditions with the concentration of 2MBA in high excess (0.94 - 16.88) × 10^{13} molecules cm^{-3} over that of OH radicals (2.23 - 5.58) × 10^{11} molecules cm^{-3}. The values of k$_0$' were typically in the range of 132 - 232 s^{-1}, while k' values were in the range of 217 - 2348 s^{-1}. Figure 5.7 shows an example of typical plots of k' versus 2MBA concentrations for different temperatures and from which the rate coefficients values were derived. The uncertainty on the 2MBA concentration measurement was estimated to be 10%, considering the uncertainties in the flow of the reagents in the cell, in the 2MBA mixture preparation and in the temperature and pressure measurements of the cell. The summary of the experimental conditions and the rate coefficients values obtained are given in table 5.10. It should be noted that for the temperature of 273 K, the concentration range of 2MBA was limited due to heterogeneous complications.
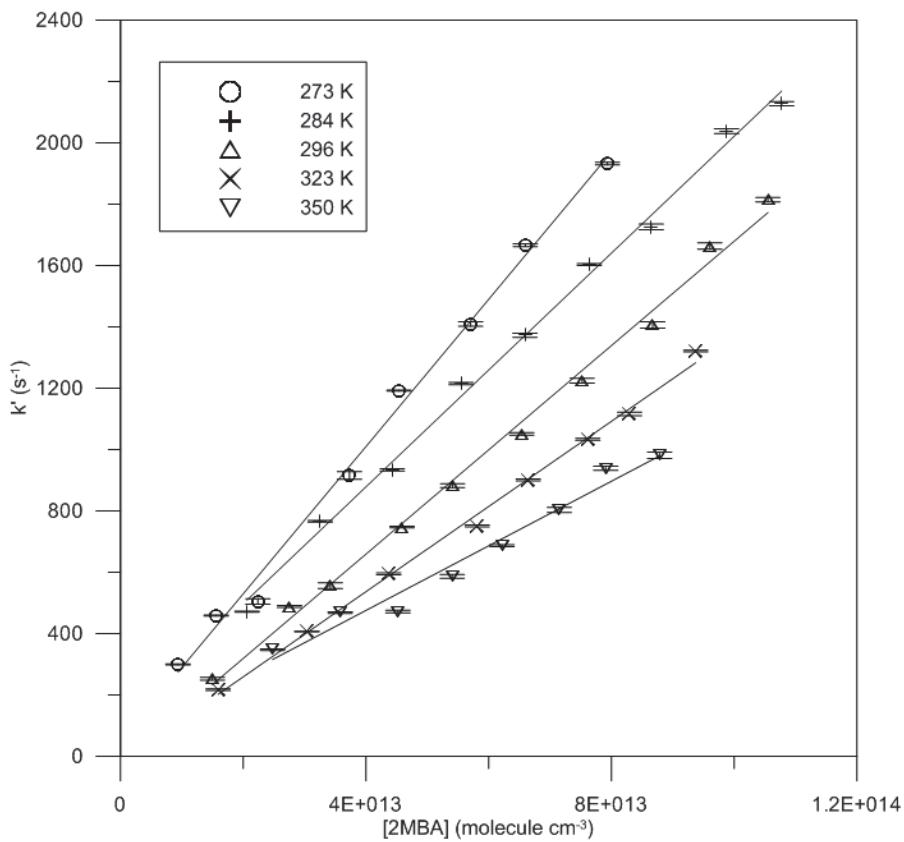
Figure 5.7: Absolute rate data for the reaction of OH radicals with 2MBA obtained in PLP-LIF at the temperature range of 273-350 K. One run is presented in each temperature. The errors quoted for k' values are the standard deviation (1σ) of the individual exponential and do not include systematic uncertainties.

Table 5.10: Summarized experimental conditions and results obtained from PLP-LIF for the reaction of OH with 2MBA.

T^a	[2MBA] ^{b} (10^{13})	k'_0 (s^{-1})	k' (s^{-1})	$(k_{2MBA} \pm 1\sigma)^c$ (10^{11})
273	0.94 – 7.93	188 – 204	504 – 1932	2.38 ± 0.05
284	2.06 – 10.8	195 – 232	471 – 2128	1.91 ± 0.08
296	1.50 - 10.6	161 – 222	253 – 1814	1.70 ± 0.04
299	3.08 – 9.05	212 – 225	650 – 1716	1.78 ± 0.04
323	1.59 - 9.37	147 – 221	217 – 1321	1.39 ± 0.04
325	5.46 - 16.9	177 – 192	688 - 2348	1.48 ± 0.07
350	2.48 - 8.78	157 – 174	472 – 981	1.05 ± 0.07
372	1.63 - 8.23	132 - 168	272 - 961	1.05 ± 0.02

^{a} Units of K

^{b} Units of molecule cm^{-3}

^{c} Units of cm^3 molecule^{-1} s^{-1}

FFT-QMS

The absolute rate coefficient measurements of the OH reaction with 2MBA was carried out under pseudo-first-order conditions in excess of 2MBA (0.05 - 2.15) × 10^{13} molecules cm^{-3} over OH radicals (0.02 - 0.61) × 10^{12} molecules cm^{-3}. Due to the

strong ionization of the molecule in the ion source of the mass spectrometer the parent peak of 2MBA was substantially lower than the fragments peaks, $I_{parent}<0.01\times I_{fragments}$, and thus measured concentrations were monitored as a function of the reaction time at the mass peak 73 ($CH_3OCH(CH_2CH_3)^+$) and ($CH_2OC(O)CH_3^+$). The rate coefficients were derived from the time profiles of OH concentration according to (E.5.3). Experiments were carried out at four temperatures, 303 K, 318 K, 333 K and 350 K. The linear velocity inside the reactor was in the range of 1435 - 1967 cm s^{-1}. Figure 5.8 shows the pseudo–first-order rate coefficients, $k' = k_{2MBA} + k'_0$, as a function of the 2MBA concentration. k'_0 was measured before and after each experiment and ranged from 12.4 to 28.1 s^{-1}, thus it is in good agreement with the corresponding intercept in figure 5.8.

All the results obtained for the OH rate coefficients and a summary of the experimental conditions are presented in table 5.11.
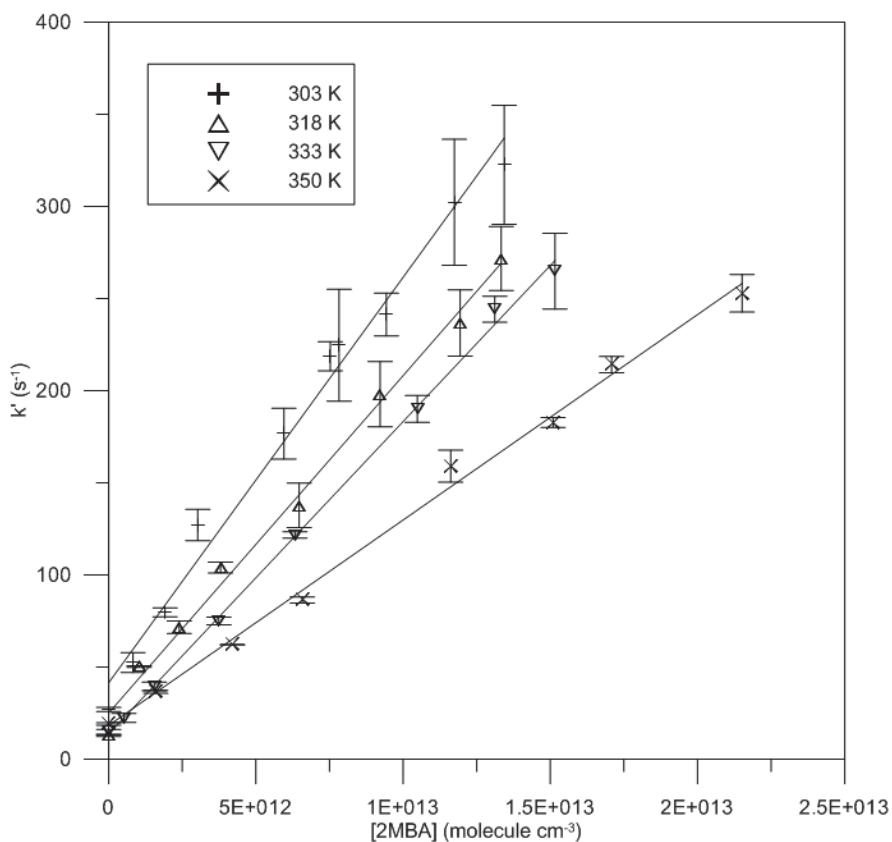

Figure 5.8: Absolute rate data for the reaction of OH radicals with 2MBA obtained in the FFT-QMS at 297, 303, and 336 K. The errors shown for k' represent one standard deviation (1σ) of the individual exponential fits and do not include systematic uncertainties, which could be as high as 15%. The errors quoted for 2MBA concentrations are estimated to be nearly 10%.

Table 5.11: Summarized experimental conditions and results obtained from absolute rate coefficient measurements using FFT-QMS for the reaction of OH with 2MBA.

T^a	[2MBA] ^{b} (10^{13})	k'_0 (s^{-1})	k' (s^{-1})	($k_{2MBA} \pm 1\sigma$)^c (10^{-11})
303	0.08 - 1.34	25.9 – 28.1	52.5 - 322.5	2.20 ± 0.09
318	0.10 - 1.33	12.4 -13.1	50.4 – 271.8	1.83 ± 0.06
333	0.05 – 1.52	14.6 - 15.2	22.4 – 264.9	1.69 ± 0.03
350	0.16 – 2.15	19.0 – 19.4	36.6 – 252.9	1.11 ± 0.03

^{a} Units of K

^{b} Units of molecule cm^{-3}

^{c} Units of cm^3 molecule^{-1} s^{-1}

> ➤ *Relative rate measurements*

FFT-QMS

Relative rate measurements of the OH reaction with 2MBA were also performed in FFT-QMS system at 298, 308, 328 and 348 K, using two reference compounds, 1,3-dioxane and Br_2. The rate coefficient of the OH reaction with 1,3-dioxane was $k_{(OH+1,3-dioxane)}$ = (9.60 ± 0.45) × 10^{-12} cm^3 molecule^{-1} s^{-1} [72, 73], while the Arrhenius expression used for the rate coefficients of the Br_2 reference reaction was: $k_{(OH+Br2)}$ = 2.0 × 10^{-11} e $^{2.00}$ [kJ/mole]/RT [52]. The slopes of the straight lines in figures 5.9 and 5.10 correspond to k_{2MBA}/k_{ref} ratios. A summary of the experimental conditions and the values obtained for the rate coefficients are presented in table 5.12 (errors quoted described previously at the section 5.A.I MPA+OH). As mentioned before, no impact of 2MBA reaction with Br on 2MBA concentration was observed.
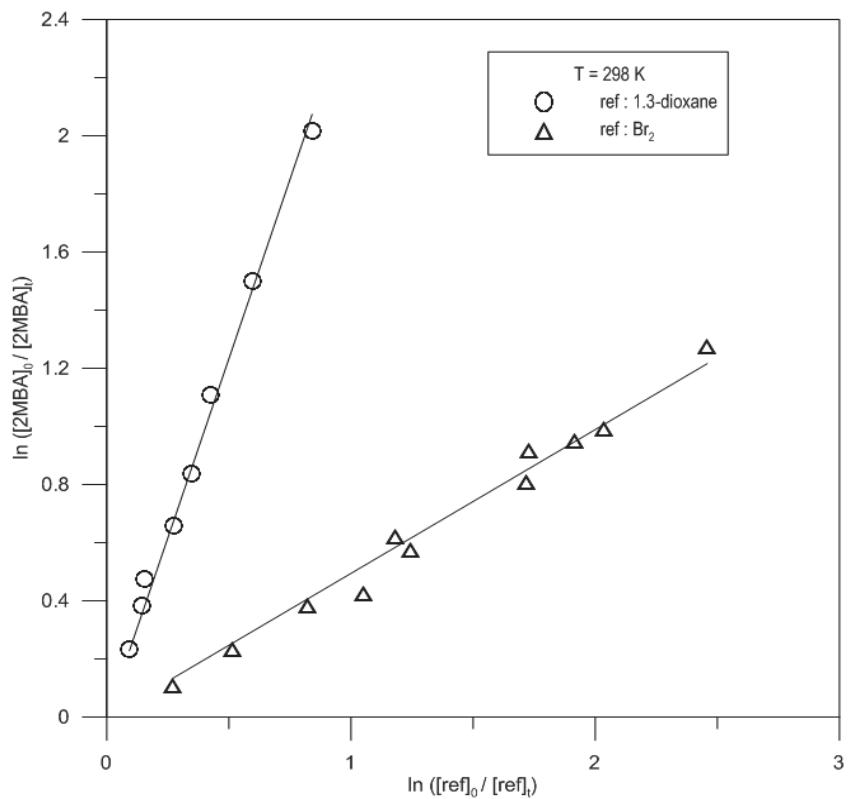
Figure 5.9: Relative rate plots for the reaction of OH with 2MBA measured in the FFT-QMS system, using 1,3-dioxane and Br$_2$ as reference compounds at 298 K.
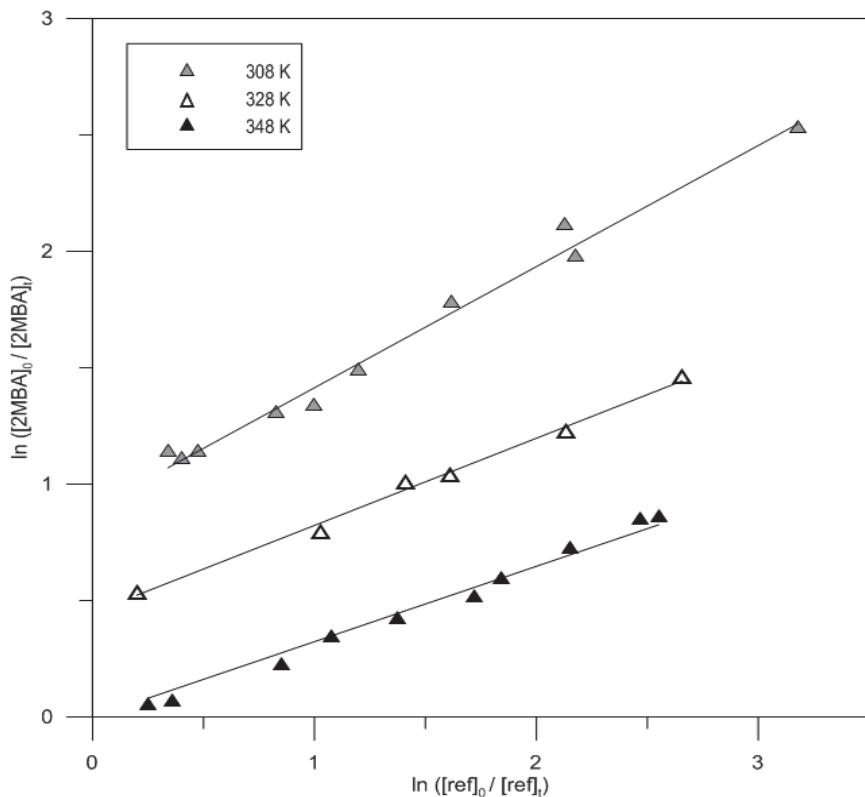

Figure 5.10: Relative rate plots for the reaction of OH with 2MBA measured in the FFT-QMS system, using Br$_2$ as reference compounds at 308, 328 and 348 K. The experimental measurements at 308 K are shifted up on the y axis by + 1), while the measurements at 328 K are shifted up on the y axis by + 0.5) units for clarity purposes.

114

Table 5.12: Reaction of OH with 2MBA: Experimental conditions and results obtained using FFT-QMS. As reference compounds 1,3-dioxane and Br₂ were used.

T [a]	Ref.	[ref]$_0$[b] (10^{11})	[2MBA]$_0$[b] (10^{11})	$k_{2MBA}/k_{ref} \pm 1\sigma$	($k_{2MBA} \pm 1\sigma$)[c] (10^{-11})
298	**1,3-dioxane**	2.94 - 4.14	3.50 -3.86	2.47 ± 0.04	2.37 ± 0.15
298	**Br₂**	3.29 - 5.14	3.28 - 7.56	0.49 ± 0.01	2.22 ± 0.26
308	**Br₂**	3.65 - 4.35	2.19 - 8.17	0.47 ± 0.02	2.03 ± 0.27
328	**Br₂**	2.59 - 4.92	2.47 - 2.69	0.35 ± 0.01	1.45 ± 0.18
348	**Br₂**	4.33 - 7.04	0.23 – 0.58	0.32 ± 0.01	1.29 ± 0.16

[a] Units of K
[b] Units of molecule cm^{-3}
[c] Units of cm^3 molecule^{-1} s^{-1}

> ➢ *Temperature and pressure dependence*

The complementary use of PLP-LIF and FFT-QMS allowed us to determine the absolute and relative rate coefficient of 2MBA with OH radicals in the temperature range 273 – 372 K and the pressure range 1 -100 Torr. The experimental conditions and measured values of the rate coefficient are listed in table 5.13. The unweighted Arrhenius exponential fit to the *k* is presented in figure 5.11 (solid line). The plot shows slight negative temperature dependence and provides the following Arrhenius expression:

$$k_{2MBA+OH}(T) = (9.97 \pm 0.03) \times 10^{-13} \exp[(882 \pm 248/T)] \text{ cm}^3 \text{ molecule}^{-1} \text{ s}^{-1}$$

where the quoted uncertainties on E/R and on the preexponential factor (A) are the standard deviation (1σ) and (Aσ$_{lnA}$), respectively. **The room temperature rate coefficient is k_{298} = 1.92 × 10^{-11} cm^3 molecule^{-1} s^{-1}. The negative activation energy, E = -7.33 kJ mol^{-1},** indicates that the reaction follows a complicated mechanism with probably an adduct formation. Moreover, comparing the absolute and relative rate coefficients measured with the two experimental systems at near room temperature (T=298 K) we observed that pressure variation (1 and 100 Torr) did not have any impact on k (table 5.14).

T^a	$[2MBA]^b$ (10^{13})	$(k \pm 1\sigma)^c$ (10^{-11})	Technique^d
273	0.94 – 7.93	2.38 ± 0.08	AR, PLP-LIF
284	2.06 - 9.87	1.91 ± 0.05	AR, PLP-LIF
296	1.50 - 10.55	1.70 ± 0.04	AR, PLP-LIF
298	0.035 - 0.039	$2.37^f \pm 0.15$	RR, FFT-QMS
298	0.033 - 0.076	$2.22^e \pm 0.26$	RR, FFT-QMS
299	3.08 - 8.02	1.78 ± 0.04	AR, PLP-LIF
303	0.08 - 1.34	2.20 ± 0.09	AR, FFT-QMS
308	0.022 -0.082	$2.03^e \pm 0.27$	RR, FFT-QMS
318	0.10 - 1.33	1.83 ± 0.06	AR, FFT-QMS
323	1.59 - 9.37	1.39 ± 0.04	AR, PLP-LIF
325	5.46 - 16.88	1.48 ± 0.07	AR, PLP-LIF
328	0.025 - 0.027	$1.45^e \pm 0.18$	RR, FFT-QMS
333	0.05 - 1.52	1.69 ± 0.03	AR, FFT-QMS
348	0.002 - 0.006	$1.29^e \pm 0.16$	RR, FFT-QMS
350	0.16 - 2.15	1.11 ± 0.03	AR, FFT-QMS
350	4.52 - 8.78	1.05 ± 0.07	AR, PLP-LIF
372	1.63 - 8.23	1.05 ± 0.02	AR, PLP-LIF

[a] Units of K

[b] Units of molecule cm^{-3}

[c] Units of cm^3 molecule^{-1} s^{-1}

[d] AR: absolute rate measurements, RR: relative rate measurements, PLP-LIF: pulse laser photolysis-laser induced fluorescence, FFT-QMS: fast flow tube-quadrupole mass spectrometer

[e] Reference compound used: Br_2

[f] Reference compound used: 1,3-dioxane
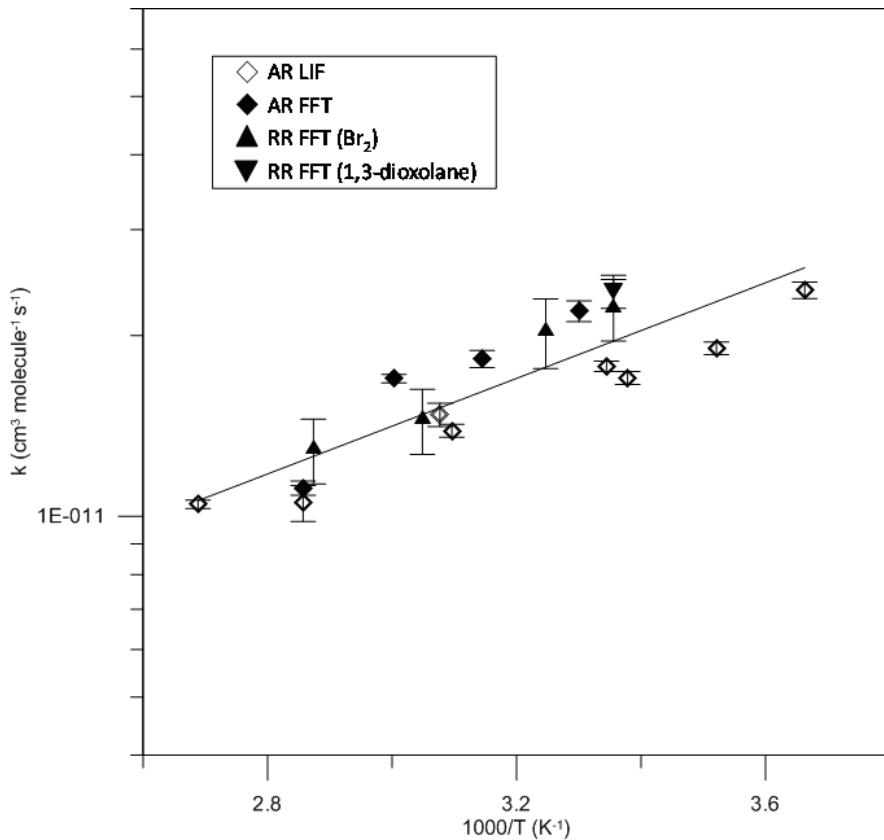
Figure 5.11: Plot of the obtained relative and absolute OH rate coefficients of 2MBA using two complementary techniques, on a logarithmic scale, as a function of 1000/T (K^{-1}), over the temperature range 273-372 K.

Table 5.14: Reaction of OH with 2MBA at 300±4 K: Pressure dependence

Number of runs	P[a]	[2MBA] [b] (10^{13})	(k ± 1σ)[c] (10^{-11})	Technique[d]
1	1	0.08 - 1.34	2.20 ± 0.09 [e]	AR, FFT-QMS
2	100	1.50 - 10.55	1.74 ± 0.06 [f]	AR, PLP-LIF
2	1	0.033 - 0.076	2.29 ± 0.11 [g]	RR, FFT-QMS

[a] Units of Torr

[b] Units of molecule cm^{-3}

[c] Units of cm^3 molecule^{-1} s^{-1}

[d] AR: absolute rate measurements, RR: relative rate measurements, FFT-QMS: fast flow tube-quadrupole mass spectrometer PLP-LIF: pulse laser photolysis-laser induced fluorescence, ASC-GC/FID: atmospheric simulation chamber-gas chromatograph/flame ionization detector

[e] The error quoted is the standard deviation (1σ) of the slope

[f] The error quoted is the standard deviation of the two runs

[g] The error quoted is the standard deviation of the k values measured using the two reference compounds

5.A.III. Reaction of OH + CH$_3$OCH(CH$_3$)CH$_2$CH$_2$OC(O)CH$_3$ (3MBA)

> ### *Absolute rate measurements*

PLP-LIF

The absolute rate coefficients were measured in the temperature range 298-363 K. The experiments were conducted using two different mixtures varied from 0.12 and 0.23% 3MBA/He. The reaction was studied under pseudo-first-order conditions with the concentration of 3MBA in high excess (2.25 – 14.9) × 10^{13} molecules cm^{-3} over that of OH radicals (4.8 – 9.9) × 10^{11} molecules cm^{-3}. The OH concentration-time profiles followed the exponential decay described in (E.5.3). The values of k$_0$' were typically in the range of 194 - 328 s^{-1}, while k' values were in the range of 391 - 2919 s^{-1}. Figure 5.12 shows an example of typical plots of k' versus 3MBA concentrations for different temperatures and from which the rate coefficients values were derived. The uncertainty on the 3MBA concentration measurement was estimated to be 10%, considering the uncertainties in the flow of the reagents in the cell, in the 3MBA mixture preparation and in the temperature and pressure measurements of the cell. The summary of the experimental conditions and the rate coefficients values obtained are given in table 5.15.
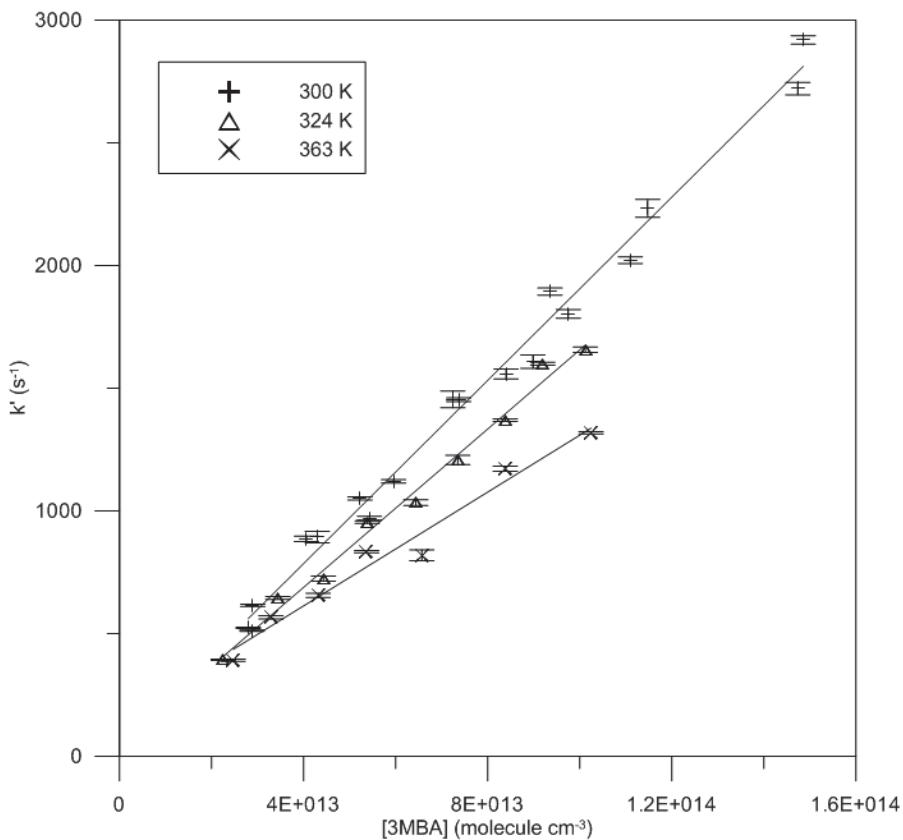
Figure 5.12: Absolute rate data for the reaction of OH radicals with 3MBA obtained in PLP-LIF at 298, 324 and 363 K. Two runs are presented for 298 K, while one run is presented for 324 and 363 K. The errors quoted for k' values are the standard deviation (1σ) of the individual exponential and do not include systematic uncertainties.

Table 5.15: Summarized experimental conditions and results obtained from PLP-LIF for the reaction of OH with 3MBA.

T^a	$[3MBA]^b (10^{13})$	$k'_0 (s^{-1})$	$k' (s^{-1})$	$(k_{3MBA} \pm 1\sigma)^c (10^{-11})$
298	2.80 – 14.7	235 - 247	523 – 2721	1.79 ± 0.05
298	2.90 - 9.35	299 - 328	615 - 1894	1.97 ± 0.06
301	2.88 – 14.9	194 – 235	512 - 2919	1.96 ± 0.07
324	2.25 – 10.1	208 - 222	394 - 1657	1.61 ± 0.06
363	2.47 – 10.2	237 - 264	391 - 1319	1.20 ± 0.07

[a] Units of K
[b] Units of molecule cm^{-3}
[c] Units of cm^3 molecule^{-1} s^{-1}

FFT-QMS

The absolute rate coefficient measurements of the OH reaction with 3MBA was carried out under pseudo-first-order conditions in excess of 3MBA (0.12 − 1.85) × 10^{13} molecules cm^{-3} over OH radicals (0.05-0.77) × 10^{12} molecules cm^{-3}. Experiments were carried out at two temperatures T= 318 and 343 K. The linear velocity inside

the reactor was in the range of 1434 - 1821 cm s^{-1}. The concentration of 3MBA was also monitored as a function of the reaction time. Figure 5.13 shows the pseudo–first-order rate coefficients, $k' = k_{3MBA} + k'_0$, as a function of the 3MBA concentration. k'_0 was measured before and after each experiment and ranged from 16 to 21.6 s^{-1}, thus it is in good agreement with the corresponding intercept in figure 5.13. All the results obtained for the OH rate coefficients and a summary of the experimental conditions are presented in table 5.16.

An abnormal increase of the OH rate coefficient was observed at low temperatures. This phenomenon was attributed to the heterogeneous interaction of OH with surface-adsorbed 3MBA, since 3MBA is a sticky molecule. For this reason, the absolute measurements of the rate coefficient were carried out at temperatures above 297 K. All the results obtained for the OH rate coefficients and a summary of the experimental conditions are presented in table 5.16.
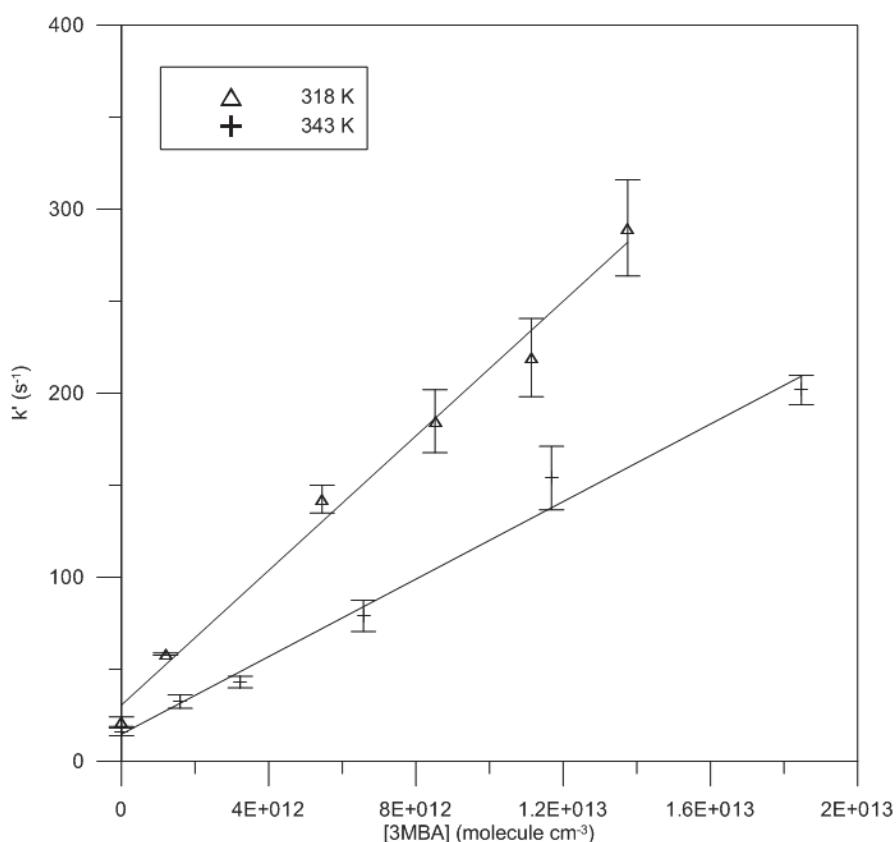

Figure 5.13: Absolute rate data for the reaction of OH radicals with 3MBA obtained in the FFT-QMS at 318 and 343 K. The errors shown for k' represent one standard deviation (1σ) of the individual exponential fits and do not include systematic uncertainties, which could be as high as 15%. The errors quoted for 3MBA concentrations are estimated to be nearly 10%.

Table 5.16: Summarized experimental conditions and results obtained from absolute rate coefficient measurements using FFT-QMS for the reaction of OH with 3MBA.

T^a	[3MBA] [b] (10^{13})	k'_0 (s^{-1})	k' (s^{-1})	($k_{3MBA} \pm 1\sigma$)[c] (10^{-11})
318	0.12 – 1.38	21.6	58.22 – 289. 8	1.83 ± 0.10
343	0.16 – 1.85	16	32.5 – 201.8	1.05 ± 0.06

[a] Units of K

[b] Units of molecule cm^{-3}

[c] Units of cm^3 molecule^{-1} s^{-1}

➢ *Relative rate measurements*

FFT-QMS

Relative rate measurements of the OH reaction with 3MBA were also performed in FFT-QMS system at 298, 308, 328 and 348 K, using Br_2 and 1,3-dioxolane as reference compounds. The rate coefficient of the reaction of OH with 1,3-dioxolane was 6.7 × 10^{-12} e $^{(1.28\pm0.30)kJ/mole]/RT}$ cm^3 molecule^{-1} s^{-1} [68], while the Arrhenius expression used for the rate coefficients of the Br_2 reference reactions was: 2.0 × 10^{-11} e $^{2.00\ [kJ/mole]/RT}$ [52]. The slopes of the straight lines in figure 5.14 correspond to k_{3MBA}/k_{ref} ratio. A summary of the experimental conditions and the values obtained for the rate coefficients are presented in table 5.17 (errors quoted described previously at the section 5.A.I MPA+OH). As mentioned before, no impact of 3MBA reaction with Br on 3MBA concentration was observed.
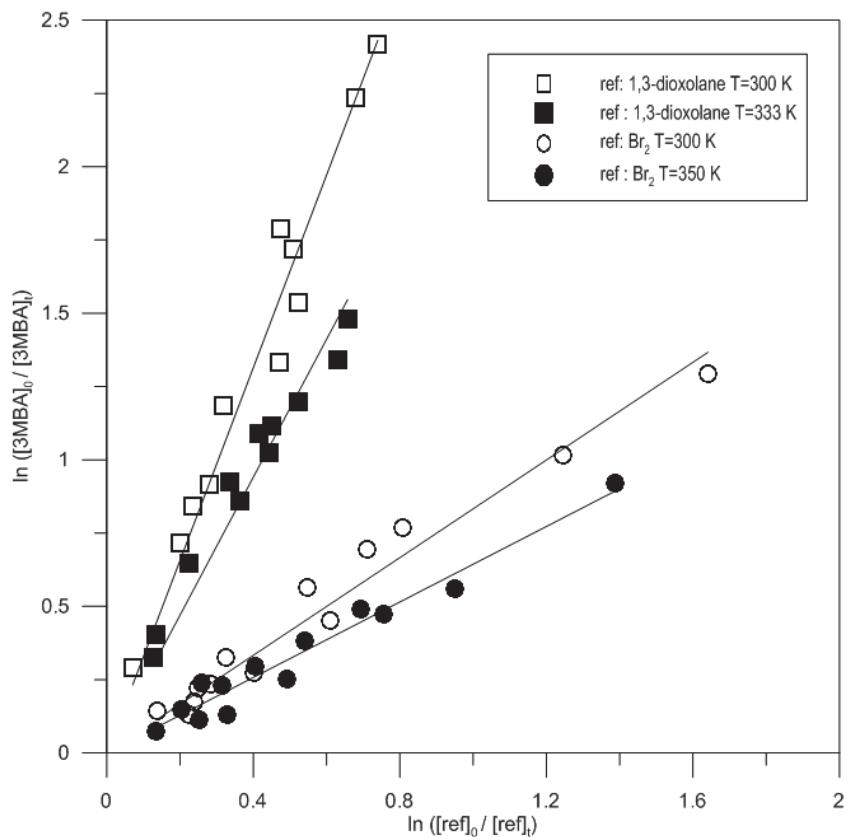
Figure 5.14: Relative rate plots for the reaction of OH with 3MBA measured in the FFT-QMS system, using Br$_2$ at 308 and 350 K and 1,3-dioxolane at 300 and 333 K as reference compounds.

Table 5.17: Reaction of OH with 3MBA: Experimental conditions and results obtained using FFT-QMS. As reference compounds 1,3-dioxolane and Br$_2$ were used.

T [a]	Ref.	Number of runs	[ref]$_0$ [b] (10^{11})	[3MBA]$_0$ [b] (10^{11})	(k_{3MBA}/k_{ref})± 1σ	($k_{3MBA} \pm 1\sigma$) [c] (10^{-11})
300	Br$_2$	1	24.8 - 42.8	26.9 - 53.2	0.42 ± 0.01	1.88 ± 0.24
300	1,3-dioxolane	1	9.71 - 76.1	9.72 - 52.3	1.53 ± 0.05	1.72 ± 0.23
333	1,3-dioxolane	1	7.97 - 13.9	7.81 – 17.1	1.19 ± 0.04	1.26 ± 0.16
350	Br$_2$	1	4.77 - 14.2	13.9 - 26.6	0.30 ± 0.01	1.20 ± 0.15

[a] Units of K
[b] Units of molecule cm^{-3}
[c] Units of cm^3 molecule^{-1} s^{-1}

➢ *Temperature and pressure dependence*

The complementary use of PLP-LIF and FFT-QMS allowed us to determine the absolute and relative rate coefficient of 3MBA with OH radicals in the temperature range 298 - 363 K and the pressure range 1 -100 Torr. The experimental conditions

and measured values of the rate coefficient are listed in table 5.18. The unweighted Arrhenius exponential fit to the k is presented in figure 5.15 (solid line). The plot shows slight negative temperature dependence and provides the following Arrhenius expression:

$$k_{3MBA+OH}(T) = (8.27 \pm 0.03) \times 10^{-13} \exp[(936 \pm 290/T)] \text{ cm}^3 \text{ molecule}^{-1} \text{ s}^{-1}$$

where the quoted uncertainties on E/R and on the preexponential factor (A) are the standard deviation (1σ) and (Aσ$_{lnA}$), respectively. **The room temperature rate coefficient is $k_{298} = 1.91 \times 10^{-11}$ cm^3 molecule^{-1} s^{-1}. The negative activation energy, E = -7.78 kJ mol^{-1}, indicates that the reaction follows a complicated mechanism with probably an adduct formation.**

Moreover, comparing the rate coefficients measured with the 2 experimental systems at near room temperature (T=300 ± 2 K) we observed that they are in excellent agreement (difference <7%) and thus pressure variation did not have any impact on k within the pressure range of 1-100 Torr (table 5.19).

Table 5.18: Reaction of OH with 3MBA: Summarized experimental conditions and results obtained from PLP-LIF and FFT-QMS.

T[a]	[3MBA] [b] (10^{13})	(k ± 1σ)[c] (10^{-11})	Technique[d]
298	2.80 - 14.7	1.79 ± 0.05	AR, PLP-LIF
298	2.90 - 9.35	1.97 ± 0.06	AR, PLP-LIF
300	0.10 - 0.52	1.72 [f] ± 0.23	RR, FFT-QMS
300	0.27 - 0.53	1.88 [e] ± 0.24	RR, FFT-QMS
301	2.88 - 14.9	1.96 ± 0.07	AR, PLP-LIF
318	0.12 - 1.38	1.83 ± 0.10	AR, FFT-QMS
324	2.25 - 10.1	1.61 ± 0.06	AR, PLP-LIF
333	0.08 - 0.17	1.26 [f] ± 0.16	RR, FFT-QMS
343	0.16 - 1.85	1.05 ± 0.06	AR, FFT-QMS
350	0.05 - 0.14	1.20 [e] ± 0.15	RR, FFT-QMS
363	2.47 - 10.2	1.20 ± 0.07	AR, PLP-LIF

[a] Units of K

[b] Units of molecule cm^{-3}

[c] Units of cm^3 molecule^{-1} s^{-1}

[d] AR: absolute rate measurements, RR: relative rate measurements, PLP-LIF: pulse laser photolysis-laser induced fluorescence, FFT-QMS: fast flow tube-quadrupole mass spectrometer

[e] Reference compound used: Br_2

[f] Reference compound used: 1,3-dioxolane
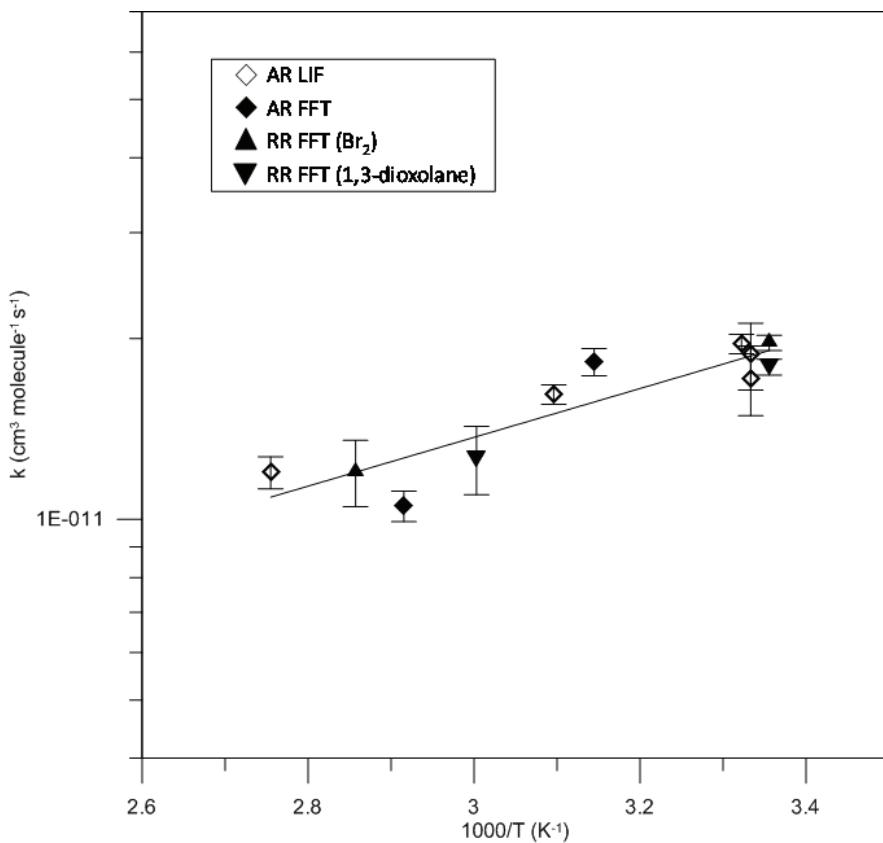
Figure 5.15: Plot of the obtained relative and absolute OH rate coefficients of 3MBA using two complementary techniques on a logarithmic scale as a function of 1000/T (K^{-1}) over the temperature range 298-363 K.

Table 5.19: Reaction of OH with 3MBA at 300±2 K: Pressure dependence

Number of runs	P[a]	[3MBA] [b] (10^{13})	$(k \pm 1\sigma)$ [c] (10^{-11})	Technique[d]
3	100	2.80-14.86	1.91 ± 0.10 [f]	AR, PLP-LIF
2	1	0.10-0.53	1.80 ± 0.12 [g]	RR, FFT-QMS

[a] Units of Torr

[b] Units of molecule cm^{-3}

[c] Units of cm^3 molecule^{-1} s^{-1}

[d] AR: absolute rate measurements, RR: relative rate measurements, FFT-QMS: fast flow tube-quadrupole mass spectrometer PLP-LIF: pulse laser photolysis-laser induced fluorescence, ASC-GC/FID: atmospheric simulation chamber gas chromatograph-flame ionization detector

[e] The error quoted is the standard deviation (1σ) of the slope

[f] The error quoted is the standard deviation of the two runs

[g] The error quoted is the standard deviation of the k values measured using the two reference compounds

124

5.A.IV. Reaction of OH + CH$_3$OCH$_2$CH$_2$OC(O)CH$_3$ (MEA)

> ### *Relative rate measurements*

Atmospheric simulation chamber

The rate coefficient for OH reaction with MEA was determined using 1-propanol and 1-butanol, as reference compounds. The IUPAC (Subcommittee on Gas Kinetic Data Evaluation) preferred rate coefficients were, $k_{(OH+1\text{-propanol})} = (5.84 \pm 0.58) \times 10^{-12}$ cm^3 molecule^{-1} s^{-1} [67] and $k_{(OH+1\text{-butanol})} = (8.55 \pm 0.86) \times 10^{-12}$ cm^3 molecule^{-1} s^{-1} [67] at 293 K, based on the temperature-dependent absolute rate study of Yujing and Mellouki (2001)[77]. The initial concentrations of the precursor H$_2$O$_2$ into the ASC were in the range of 235 - 424 ppm. Figure 5.16 shows the plots of the experimental results, the slopes of the straight lines correspond to k_{MEA}/k_{ref} ratio. The experimental conditions, the obtained slopes and rate coefficients are summarized in table 5.20. The errors quoted for k_{MEA}/k_{ref} values in table 5.20 are the standard deviation (1σ) of the slope and do not include systematic uncertainties. The errors quoted for k_{MEA} value in the individual experiments are the errors in k_{MEA}/k_{ref} by taking into account the error of k_{ref}. Errors quoted as the standard deviation of the average of the two runs. Regarding the errors quoted to the final average values of k, the standard deviation of the individual k values was used.
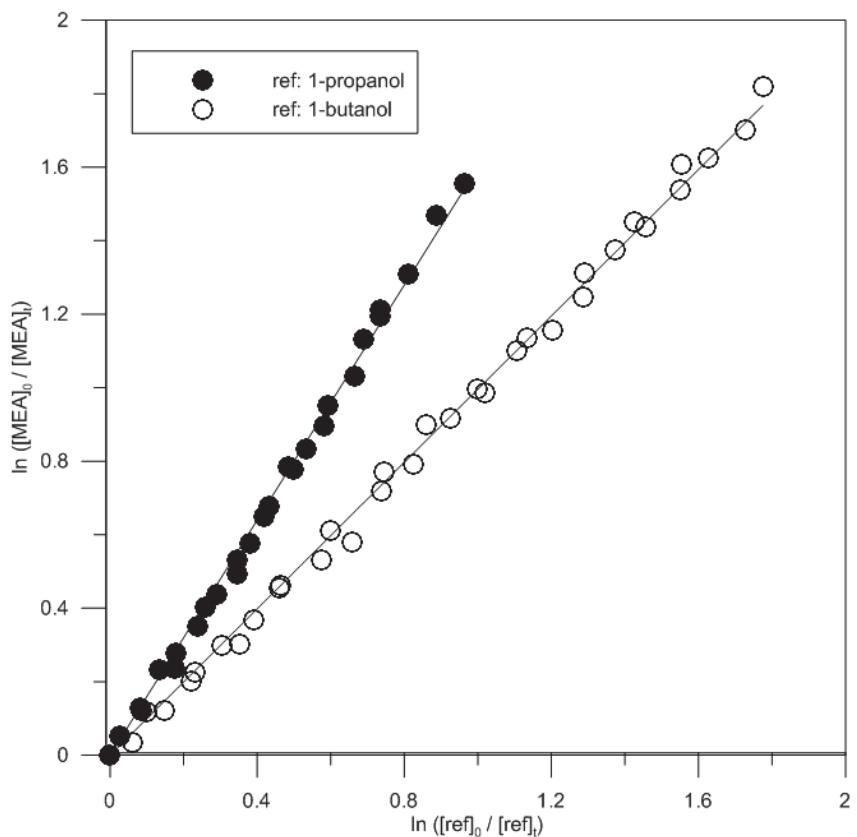
Figure 5.16: Relative rate data for the reaction of OH radicals with MEA obtained in the atmospheric simulation chamber using 1–propanol and 1-butanol as reference compounds. Two runs are presented in each case.

Table 5.20: Reaction of OH with MEA: Experimental conditions and results obtained in the atmospheric simulation chamber at 293 K.

Ref.	Number of runs	$[ref]_0^a$	$[MEA]_0^a$	$k_{MEA}/k_{ref} \pm 1\sigma$	$(k_{MEA} \pm 1\sigma)^b (10^{-12})$
1-propanol	2	63.61	19.43	1.60 ± 0.01	9.35 ± 1.01
		58.05	16.38	1.57 ± 0.02	9.16 ± 1.00
				average	**9.25 ± 0.13**
1-butanol	2	39.02	19.81	0.99 ± 0.006	8.43 ± 0.89
		52.03	22.17	1.02 ± 0.009	8.70 ± 0.93
				average	**8.57 ± 0.19**
		Average			**8.91 ± 0.48**

[a] Units of ppm

[b] Units of $cm^3\,molecule^{-1}\,s^{-1}$

5.A.V. Reaction of OH + CH₃CH₂OCH₂CH₂OC(O)CH₃ (EEA)

> ### *Relative rate measurements*

Atmospheric simulation chamber

The rate coefficient for OH reaction with EEA was determined using 1-propanol, $k_{(OH+1\text{-propanol})}$ = (5.84 ± 0.58) × 10^{-12} cm^3 molecule^{-1} s^{-1} [67], and 1-butanol, $k_{(OH+1\text{-butanol})}$ = (8.55 ± 0.86) × 10^{-12} cm^3 molecule^{-1} s^{-1} [67]. The initial concentrations of the precursor H$_2$O$_2$ into the chamber were in the range of 235 - 518 ppm. The integration of the chromatogram peaks was used to derive the plots (figure 5.17) and the experimental results (table 5.21). The errors quoted in table 5.21 are described in the previous part (MEA + OH).
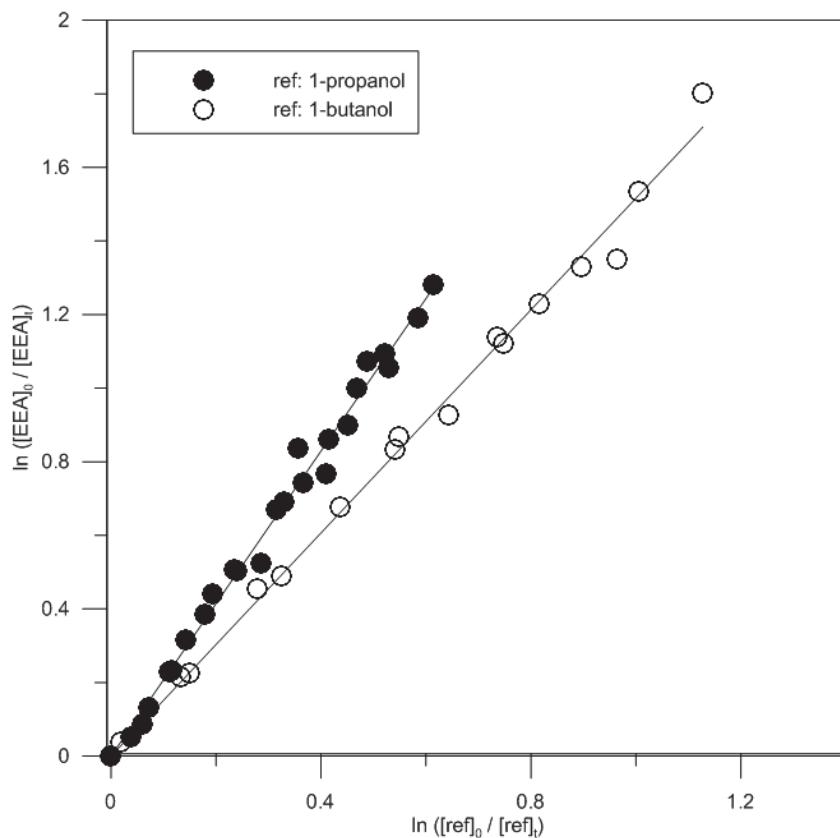

Figure 5.17: Relative rate data for the reaction of OH radicals with EEA obtained in the atmospheric simulation chamber using 1–propanol and 1-butanol as reference compounds. Two runs are presented in each case.

Ref.	Number of runs	$[ref]_0{}^a$	$[EEA]_0{}^a$	$k_{EEA}/k_{ref} \pm 1\sigma$	$(k_{EEA} \pm 1\sigma)^b$ (10^{-11})
1-propanol	2	95.82	7.99	2.13 ± 0.03	1.24 ± 0.14
		63.88	8.76	2.05 ± 0.04	1.19 ± 0.14
				average	**1.22 ± 0.03**
1-butanol	2	36.72	8.19	1.52 ± 0.02	1.29 ± 0.14
		39.74	8.00	1.46 ± 0.03	1.24 ± 0.15
				average	**1.26 ± 0.04**
Average					**1.24 ± 0.03**

^{a} Units of ppm

^{b} Units of cm^3 molecule^{-1} s^{-1}

5.A.VI. Reaction of OH + $CH_3CH_2CH_2CH_2CH_2OC(O)CH_3$ (n-PA)

> *Relative rate measurements*

Atmospheric simulation chamber

The rate coefficient for OH reaction with EEA was determined using 1,3-dioxolane, $k_{(OH+1.3diox)} = (1.13 \pm 0.11) \times 10^{-11}$ cm^3 molecule^{-1} s^{-1} at 293 K [68], and 1-pentanol, $k_{(OH+1-pentanol)} = (1.11 \pm 0.10) \times 10^{-11}$ cm^3 molecule^{-1} s^{-1} [69, 70, 71]. The initial concentrations of the precursor H_2O_2 into the chamber were in the range of 148 - 353 ppm. The experimental data are shown in figure 5.18, while a summary of the experimental conditions and the values obtained for the rate coefficients are presented in table 5.22. The errors quoted (table 5.22) are described previously.
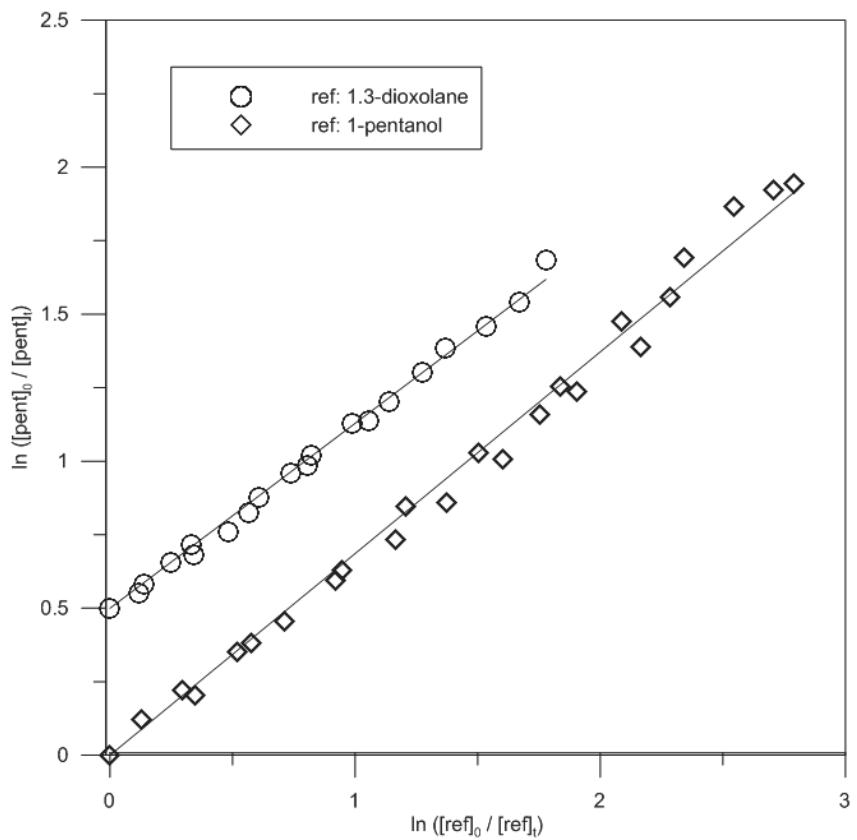
Figure 5.18: Relative rate data for the reaction of OH radicals with n-pentyl acetate obtained in the atmospheric simulation chamber using 1,3-dioxolane and 1-pentanol as reference compounds. The experimental measurements with 1,3-dioxolane are shifted up on the y axis by + 0.5) units for clarity purposes. Two runs are presented in each case.

Table 5.22: Reaction of OH with n-pentyl acetate: Experimental conditions and results obtained in the atmospheric simulation chamber at 293 K.

Ref.	Number of runs	$[ref]_0^a$	$[n\text{-}PA]_0^a$	$k_{pent}/k_{ref} \pm 1\sigma$	$(k_{pent} \pm 1\sigma)^b\ (10^{-12})$
1,3-dioxolane	2	50.74	18.78	0.60 ± 0.007	6.77 ± 0.76
		42.28	17.75	0.63 ± 0.006	7.15 ± 0.78
				average	**6.96 ± 0.27**
1-pentanol	2	10.17	15.85	0.71 ± 0.006	7.85 ± 0.78
		8.64	12.92	0.66 ± 0.009	7.37 ± 0.76
				average	**7.61 ± 0.33**
		Average			**7.29 ± 0.46**

^{a} Units of ppm

^{b} Units of $cm^3\ molecule^{-1}\ s^{-1}$

5.B. Reactions with Cl atoms

5.B.I. Reaction of Cl + $CH_3OCH_2CH(CH_3)OC(O)CH_3$ (MPA)

➢ *Absolute rate measurements*

FFT-QMS

The absolute rate coefficient measurements of the reaction of Cl with MPA were carried out under pseudo–first-order conditions, as described previously, in excess of MPA (0.6-3.9) × 10^{12} molecules cm^{-3} over Cl atoms (0.1-0.8) × 10^{12} atoms cm^{-3}. The rate coefficients were derived from the time profiles of [Cl] according to (E.5.I). Experiments were carried out at 298 K. The linear velocity inside the reactor was in the range of 2395 - 3430 cm s^{-1}. The consumption of MPA was negligible as a result of its sufficient excess. However, in a few kinetic runs, a noticeable consumption of MPA was observed as a result of the use of insufficient excess of MPA over Cl atoms due to limited sensitivity of Cl detection and the high value of k_{MPA}. In these cases, the mean concentration of MPA along the reaction zone was used for the calculations of the rate coefficient.

Figures 5.19 shows the pseudo–first-order rate coefficients, $k' = k_{MPA} + k'_0$, as a function of the MPA concentration. k'_0 was measured before and after each experiment and ranged from 6 to 40 s^{-1}. Its values are somewhat lower than the intercept in figure 5.19, indicating the probable modification of the reactor surface in the presence of MPA. All the measured values of k' were corrected for axial and radial diffusion of Cl.[53] **The value of k_{MPA+Cl} measured at room temperature was (1.95 ± 0.15) × 10^{-10}**, where the quoted error represents one standard deviation on the determination of the slope of the straight line in figure 5.19.
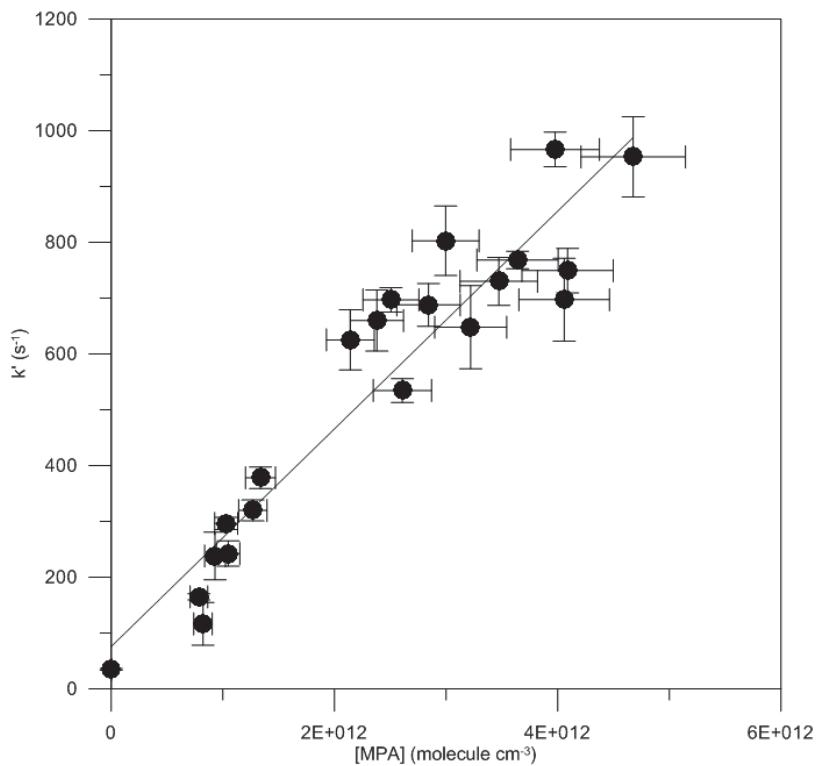
Figure 5.19: Absolute rate data for the reaction of Cl atoms with MPA obtained in the FFT-QMS at 298 K. The errors for k' correspond to one standard deviation (1σ) of the individual exponential fits and do not include systematic uncertainties, which could be as high as 15%. The errors quoted for MPA concentrations are nearly 10 %.

➢ *Relative rate measurements*

Atmospheric simulation chamber

The Teflon reaction chamber was used to measure the relative rate coefficient of Cl reaction with MPA. The relative rate coefficient was obtained by the relation (E.5.4). The rate coefficient for the reaction of Cl atoms with MPA was determined using cyclohexane $k_{(Cl+cyclohexane)}$=(3.32±0.41) × 10^{-10}, [74, 75] 1-propanol $k_{(Cl+1-propanol)}$=(1.62±0.14) × 10^{-10}, [67] and pentane $k_{(Cl+pentane)}$=(2.71±0.28) × 10^{-10}, [76, 75, 74] in cm^3 $molecule^{-1}$ s^{-1} as reference compounds. The initial concentrations of the precursor Cl_2 into the chamber were in the range of 58 - 83 ppm. For pentane solely one run was conducted, while for all others reference compounds three different runs were carried out. The plots of the experimental results according to (E.5.4) are shown in figure 5.20. The experimental conditions, the obtained slopes and rate coefficients for Cl reaction are summarized in table 5.23. The uncertainties quoted for k_{MPA}/k_{ref} values in table 5.23 are the standard deviation (1σ) of the slope and do

not include systematic uncertainties. The errors quoted for k_{MPA} value in the individual experiments are the errors in k_{MPA}/k_{ref} by taking into account the error of k_{ref}. Errors quoted as the standard deviation of the average of the three runs. Regarding the errors quoted to the final average values of k, the standard deviation of the individual k values was used.
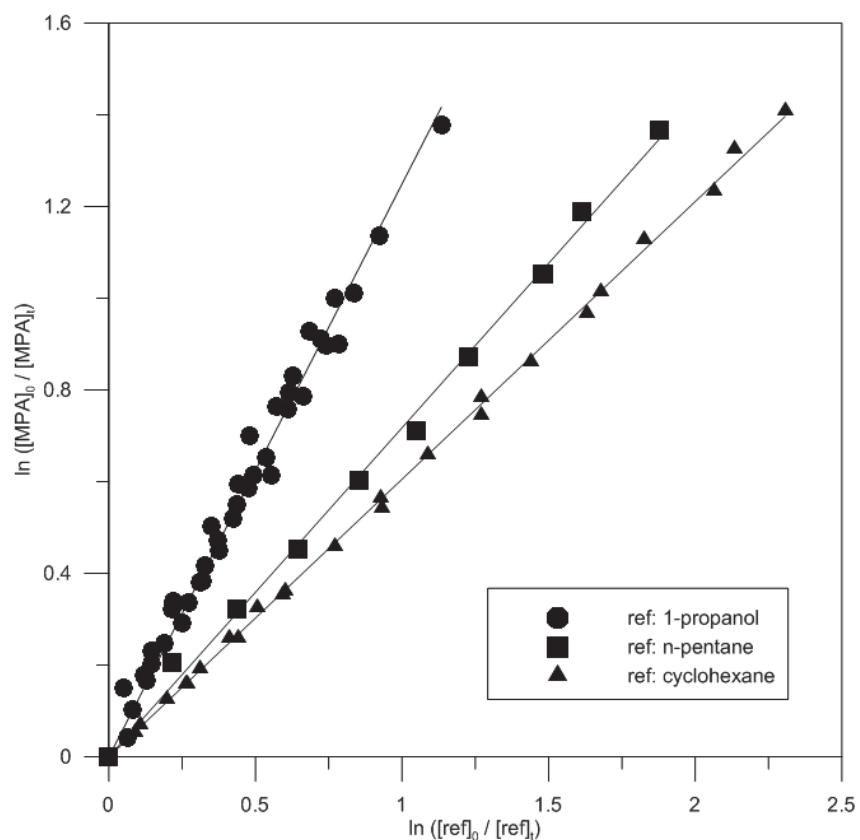

Figure 5.20: Relative rate plots for the Cl reaction with MPA in the atmospheric simulation chamber, using 1-propanol, cyclohexane and n-pentane as reference compounds. Three runs are presented in the case of 1-propanol and cyclohexane, while in the case of n-pentane only one run was contacted.

Ref.	Number of runs	$[ref]_0$[a]	$[MPA]_0$[a]	$k_{MPA}/k_{ref} \pm 1\sigma$	$(k_{MPA} \pm 1\sigma)$[b] (10^{-10})
cyclohexane	3	21.14	17.83	0.63 ± 0.004	2.10 ± 0.27
		17.22	15.87	0.61 ± 0.006	2.01 ± 0.27
		23.59	16.93	0.61 ± 0.003	2.01 ± 0.26
				average	**2.04 ± 0.05**
1-propanol	3	30.02	27.46	1.30 ± 0.025	2.11 ± 0.22
		61.56	26.11	1.19 ± 0.012	1.93 ± 0.19
		44.10	25.03	1.27 ± 0.020	2.06 ± 0.21
				average	**2.03 ± 0.09**
pentane	1	39.61	35.29	0.718 ± 0.006	1.94 ± 0.22
	average				**2.01 ± 0.05**

[a] Units of ppm
[b] Units of $cm^3\,molecule^{-1}\,s^{-1}$

Pressure dependence

The results obtained from the absolute and relative rate coefficient measurements of the Cl reaction with MPA at 295±3 K and at 1 and 760 Torr are listed in table 5.24. The results showed no pressure dependence since the measurements are in very good agreement.

No of experiments	P[a]	$[MPA]$[b] (10^{12})	$(k \pm 1\sigma)$[c] (10^{-10})	Technique[d]
1	1	0.06-0.39	1.95 ± 0.15 [e]	AR, FFT-QMS
7	760	39.68-88.22	2.01 ± 0.05 [f]	RR, ASC-GC/FID
		average	**1.98 ± 0.04** [g]	

[a] Units of Torr

[b] Units of $molecule\,cm^{-3}$

[c] Units of $cm^3\,molecule^{-1}\,s^{-1}$

[d] AR: absolute rate measurements, RR: relative rate measurements, FFT-QMS: fast flow tube-quadrupole mass spectrometer, ASC-GC/FID: atmospheric simulation chamber gas chromatograph-flame ionization detector

[e] The error quoted is the standard deviation (1σ) of the slope

[f] The error quoted is the standard deviation of the k values measured using the three

reference compounds

[g] The error quoted is the standard deviation of the k values measured using the two techniques

5.B.II. Reaction of Cl+ $CH_3OCH(C_2H_5)CH_2OC(O)CH_3$ (2MBA)

➢ *Relative rate measurements*

FFT-QMS

The rate coefficient for Cl reaction with MEA was determined using n-heptane $k_{(Cl+heptane)}$ = (3.53 ± 0.12) × 10^{-10} cm^3 $molecule^{-1}$ s^{-1} [75], [76], as reference compound, at 298 K. The initial concentrations of 2MBA, and n-heptane were in the range of (5.66 - 9.45) × 10^{10}, and (1.03 - 1.43) × 10^{11} molecules cm^{-3}, respectively. The slope of the straight line correspond to k_{2MBA}/k_{ref} ratio presented in figure 5.21 was 0.54 ± 0.01 (error quoted correspond to one standard deviation), while **the value of $k_{2MBA+Cl}$ measured at room temperature was (1.89 ± 0.11) × 10^{-10}**, (errors quoted include the uncertainty of k_{ref}).
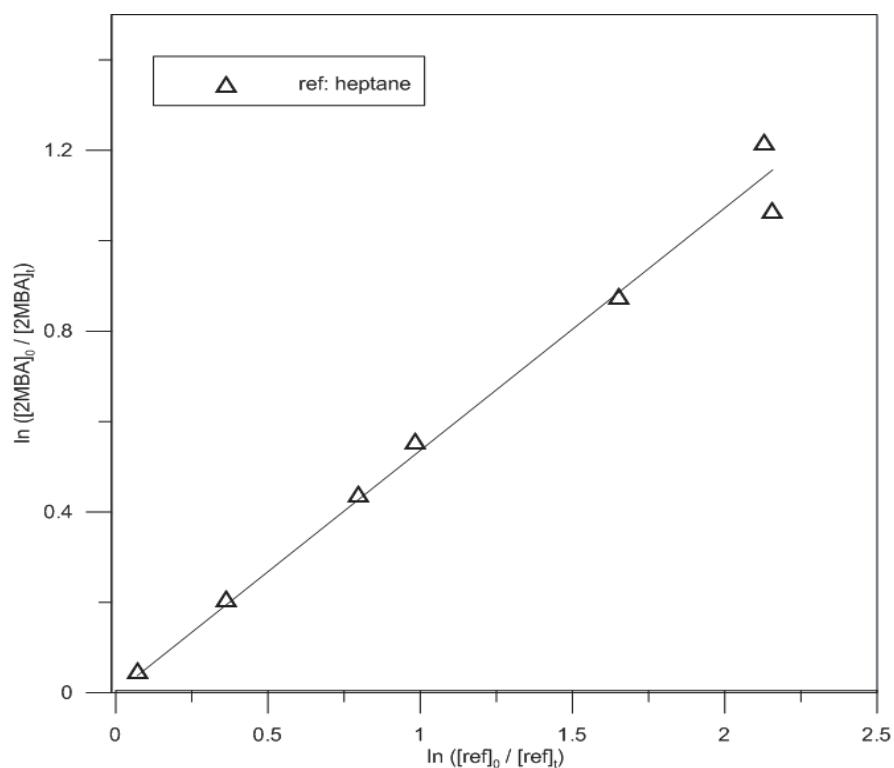

Figure 5.21: Relative rate plot for the Cl reaction with 2MBA in the FFT-QMS, using n-heptane as reference compound.

5.B.III. Reaction of Cl + CH₃OCH₂CH₂OC(O)CH₃ (MEA)

> *Relative rate measurements*

Atmospheric simulation chamber

The rate coefficient for Cl reaction with MEA was determined using cyclohexane, $k_{(Cl+cyclohexane)} = (3.32 \pm 0.41) \times 10^{-10}$ cm^3 molecule^{-1} s^{-1} [74, 75] and heptane $k_{(Cl+heptane)} = (3.53 \pm 0.12) \times 10^{-10}$ cm^3 molecule^{-1} s^{-1} [75, 76], as reference compounds. The initial concentrations of the precursor Cl₂ into the ASC were in the range of 68 - 91 ppm. Figure 5.22 shows the plots of the experimental results, while the experimental conditions and the obtained rate coefficients are summarized in table 5.25 (errors quoted described previously).
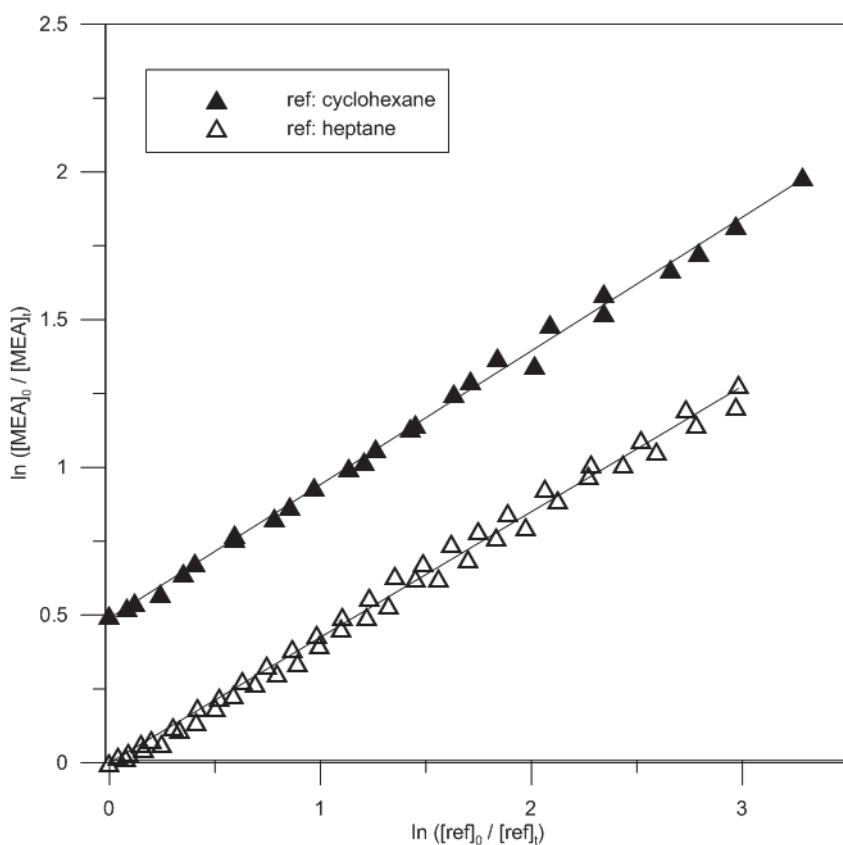

Figure 5.22: Relative rate data for the reaction of Cl atoms with MEA obtained in the atmospheric simulation chamber using cyclohexane and heptane as reference compounds. The experimental measurements with cyclohexane are shifted up on the y axis by + 0.5) units for clarity purposes. Two runs are presented in each case.

Ref.	Number of runs	$[ref]_0^a$	$[MEA]_0^a$	$k_{MEA}/k_{ref} \pm 1\sigma$	$(k_{MEA} \pm 1\sigma)^b$ (10^{-10})
cyclohexane	2	45.6	14.5	0.45 ± 0.004	1.49 ± 0.20
		46.6	13.5	0.45 ± 0.004	1.50 ± 0.20
				average	**1.50 ± 0.01**
heptane	2	52.6	13.0	0.41 ± 0.002	1.45 ± 0.05
		56.7	16.6	0.44 ± 0.002	1.57 ± 0.06
				average	**1.51 ± 0.08**
	Average				**1.50 ± 0.01**

^{a} Units of ppm

^{b} Units of cm^3 molecule^{-1} s^{-1}

5.B.IV. Reaction of Cl + $CH_3CH_2OCH_2CH_2OC(O)CH_3$ (EEA)

> *Relative rate measurements*

Atmospheric simulation chamber

The rate coefficient for Cl reaction with MEA was determined using 1-propanol and 1-butanol as reference compounds. The rate coefficients of the reference compounds used were $k_{(Cl+1-propanol)} = (1.62 \pm 0.14) \times 10^{-10}$ cm^3 molecule^{-1} s^{-1} [67] and $k_{(Cl+1-butanol)} = (2.18 \pm 0.17) \times 10^{-10}$ cm^3 molecule^{-1} s^{-1} [67]. The initial concentrations of the precursor Cl_2 into the chamber were in the range of 88 -190 ppm. Figure 5.23 shows the plots of the experimental results, while the experimental conditions and the obtained rate coefficients are summarized in table 5.26 (errors quoted described previously).
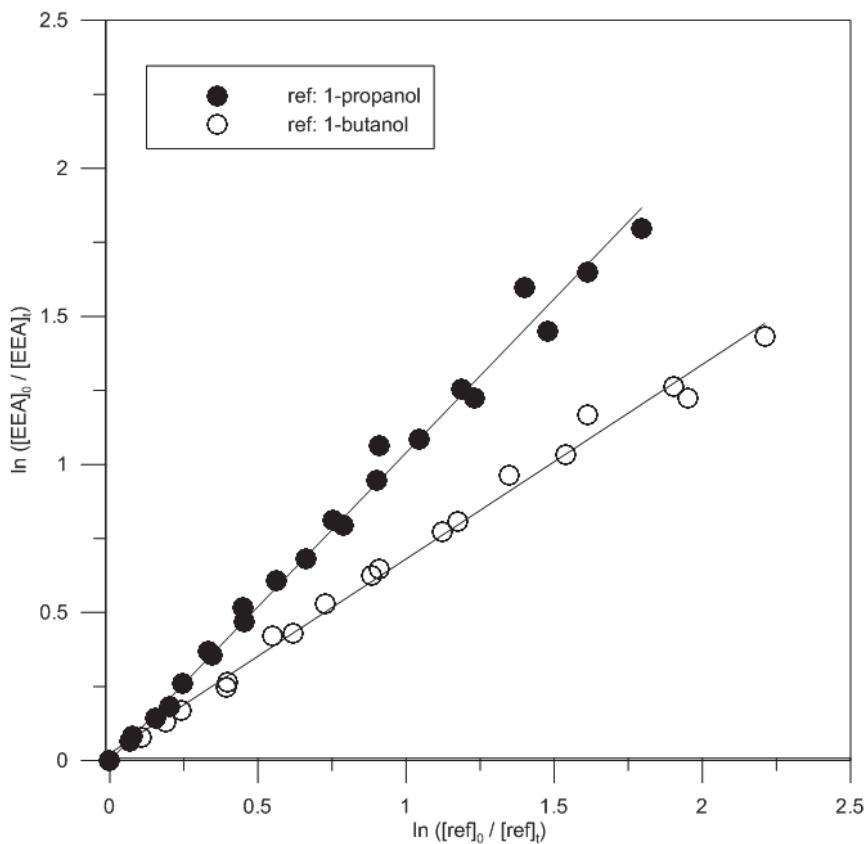
Figure 5.23: Relative rate data for the reaction of Cl atoms with EEA obtained in the atmospheric simulation chamber using 1-propanol and 1-butanol as reference compounds. Two runs are presented in each case.

Table 5.26: Reaction of Cl with EEA: Experimental conditions and results obtained in the atmospheric simulation chamber at 293 K.

Ref.	Number of runs	$[ref]_0^a$	$[EEA]_0^a$	$k_{EEA}/k_{ref} \pm 1\sigma$	$(k_{EEA} \pm 1\sigma)^b$ (10^{-10})
1-propanol	2	55.7	10.3	1.04 ± 0.019	1.68 ± 0.18
		48.5	8.51	1.04 ± 0.015	1.68 ± 0.17
				average	**1.68 ± 0.005**
1-butanol	2	39.3	10.7	0.66 ± 0.011	1.43 ± 0.14
		38.0	11.0	0.70 ± 0.009	1.52 ± 0.14
				average	**1.47 ± 0.06**
		Average			**1.58 ± 0.14**

[a] Units of ppm

[b] Units of $cm^3 \, molecule^{-1} \, s^{-1}$

137

5.B.V. Reaction of Cl + CH$_3$CH$_2$CH$_2$CH$_2$CH$_2$OC(O)CH$_3$ (n-PA)

➢ *Relative rate measurements*

Atmospheric simulation chamber

The rate coefficient for Cl reaction with n-pentyl acetate was determined using n-pentane and 1-butanol as reference compounds. The rate coefficients of the reference compounds used were k $_{(Cl+n-pentane)}$ = (2.71±0.28) × 10^{-10} cm^3 molecule^{-1} s^{-1} [76, 75, 74] and k$_{(Cl+1-butanol)}$ = (2.1±0.17) × 10^{-10} cm^3 molecule^{-1} s^{-1} [67]. The initial concentrations of the precursor Cl$_2$ into the chamber were in the range of 115 - 170 ppm. The experimental data are shown in figure 5.24. A summary of the experimental conditions and the values obtained for the rate coefficients are presented in table 5.27 (errors quoted described previously).
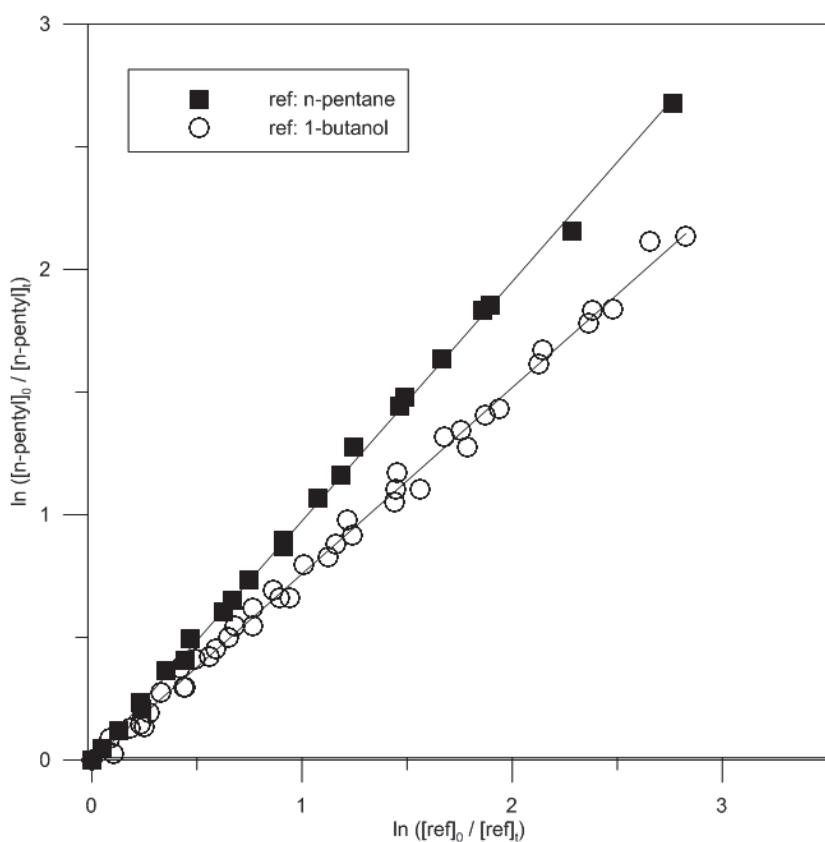

Figure 5.24: Relative rate data for the reaction of Cl atoms with n-pentyl acetate obtained in the atmospheric simulation chamber using n-pentane and 1-butanol as reference compounds. Two runs are presented in each case.

Table 5.27: Reaction of Cl with n-pentyl acetate: Experimental conditions and results obtained in the atmospheric simulation chamber at 293 K.

Ref.	Number of runs	$[\text{ref}]_0^a$	$[\text{n-PA}]_0^a$	$k_{pent}/k_{ref} \pm 1\sigma$	$(k_{pent} \pm 1\sigma)^b$ (10^{-10})
n-pentane	2	29.7	7.40	0.75 ± 0.005	2.04 ± 0.22
		28.7	16.0	0.77 ± 0.005	2.09 ± 0.23
				average	**2.07 ± 0.04**
1-butanol	2	35.5	25.2	0.97 ± 0.006	2.11 ± 0.18
		39.3	25.1	0.99 ± 0.005	2.15 ± 0.18
				average	**2.13 ± 0.03**
Average					**2.10 ± 0.05**

[a] Units of ppm

[b] Units of $cm^3 molecule^{-1} s^{-1}$

6. Mechanistic study and proposed mechanism

6. Mechanistic study and proposed mechanism

The mechanistic investigation and product analysis of the reaction of OH radicals and Cl atoms with MPA were performed using the Atmospheric Simulation Chamber at different initial reactant concentrations. The experiments were conducted at 760 Torr and 293 K in the presence of NO in order to ensure rapid removal of HO_2 and RO_2 and simplify the mechanistic interpretation of the product yields. The initial concentrations of the radicals/atoms precursors, i.e. H_2O_2 and gas Cl_2, were in the range of 270-390 ppm and 53-108 ppm, respectively. On the other side, the concentration of NO was 77-125 ppm, while MPA concentration was in the range of 30-45 ppm. The mechanistic study was carried out for about 1 hour to 3.5 hours. Methyl formate ($HC(O)OCH_3$), acetic acid ($CH_3C(O)OH$), acetic anhydride ($CH_3C(O)OC(O)CH_3$), carbon dioxide (CO_2) and carbon monoxide (CO) were identified as the major products of both OH and Cl reaction with MPA, by using GC-FID, FTIR and GC-MS as detection techniques.

6.A. Reaction of OH + CH₃OCH₂CH(CH₃)OC(O)CH₃ (MPA)

The major products of the OH reaction with MPA were identified by online FTIR spectroscopy and GC-MS analyses. Figure 6.1 displays the IR spectra obtained. The concentrations of MPA and H_2O_2 used for this set of experiment were 31 and 350 ppm, respectively and the consumption of MPA was approximately 94%. Panel (A) of figure 6.1 shows the IR spectrum of MPA and H_2O_2 before the reaction, while panel (B) displays the IR spectrum after 1.5 hours of reaction. The typical reference IR spectra of three identified products, methyl formate, acetic acid and acetic anhydride, are presented in panels (C), (D) and (E) of figure 6.1, respectively. Panel (F) is the IR spectrum after subtraction of reactants and the major identified products (methyl formate, acetic acid and acetic anhydride), where mainly vibrations of CO_2, CO and H_2O can be observed.
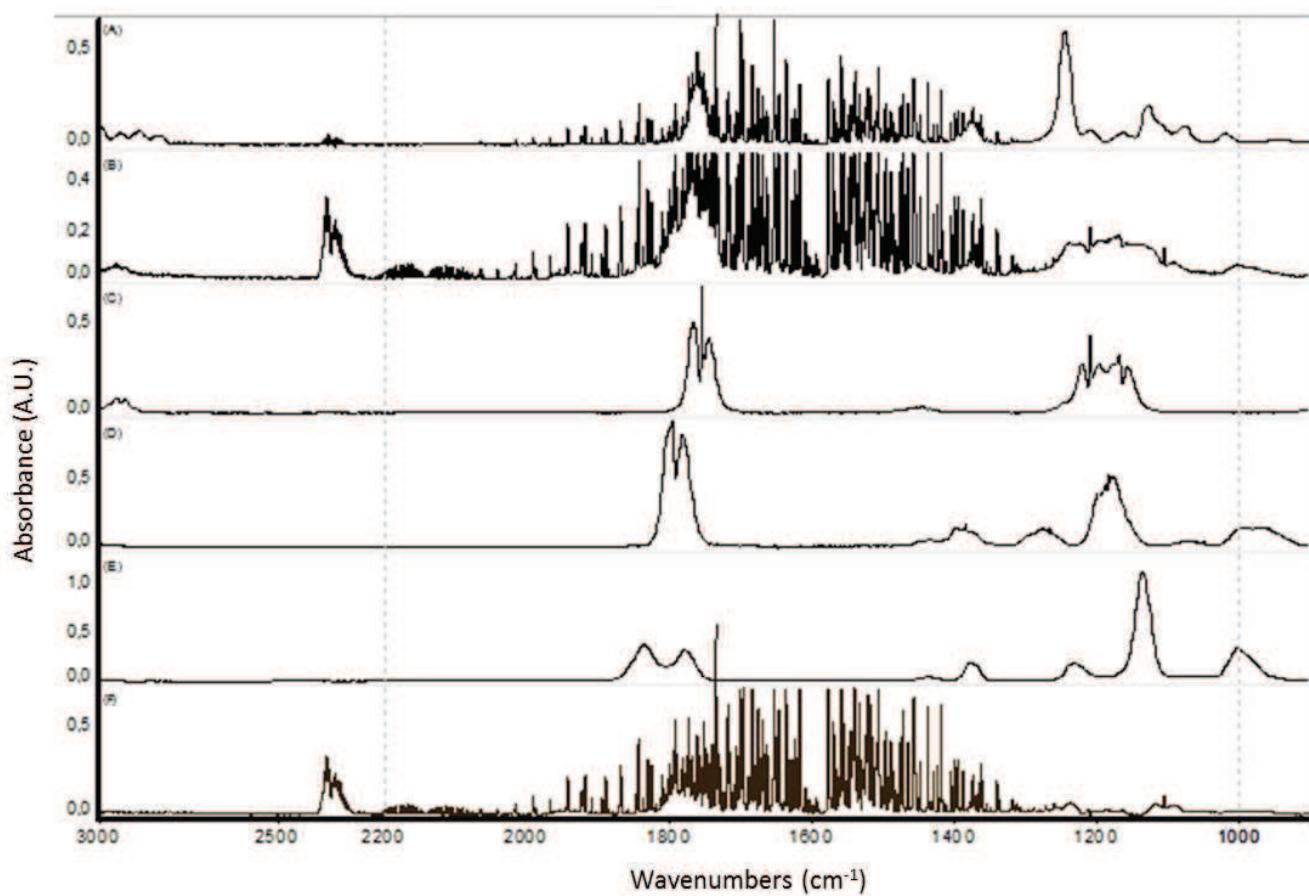
Figure 6.1: Reaction of MPA with OH. IR spectra obtained before (A) and after (B) a 1,5 hours irradiation of a mixture of MPA and H$_2$O$_2$. Panels (C), (D) and (E) present the reference IR spectra of methyl formate, acetic acid and acetic anhydride, respectively. Panel (F) is the IR spectrum after subtraction of reactants and the identified products (methyl formate, acetic acid and acetic anhydride).

Figure 6.2 displays the concentration profiles of MPA and the major products with the reaction time. In this set of experiment the initial concentrations used for MPA and H$_2$O$_2$ were 29 and 270 ppm, respectively.
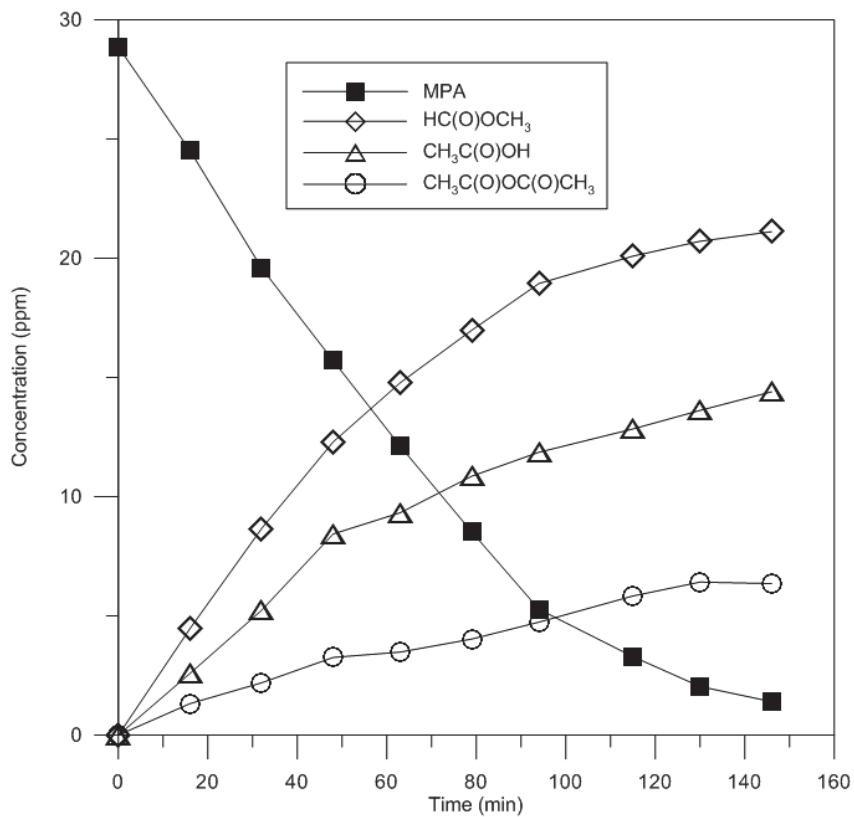
Figure 6.2: Concentration time-profiles of reactant and products for the reaction of MPA with OH in the presence of NO at 760 Torr and 293 K.

The referred reaction products were calibrated using the integration of chromatogram peaks in GC-FID, and their yields, expressed as $\Delta[\text{product}]_t/\Delta[\text{MPA}]_t$, were measured. For the reaction of OH with MPA the product yields were 80 ± 7.3, 50 ± 4.8 and $22 \pm 2.4\%$ for $HC(O)OCH_3$, $CH_3C(O)OH$ and $CH_3C(O)OC(O)CH_3$, respectively (figure 6.3). The error quoted includes: the standard deviation (1σ) of the slope $\Delta[\text{product}]_t$ to $\Delta[\text{MPA}]_t$, the standard deviation (1σ) of the product and MPA calibration factors and the systematic uncertainties. Note that the product yields are referred to the absolute concentrations measured and they are not based on the carbon mass balance. Besides, the structure of the measured products indicates that they could be produced from the same MPA molecule. Nevertheless, a rough estimation of the carbon mass balance considering the yields of the three OVOCs formed is 58%.
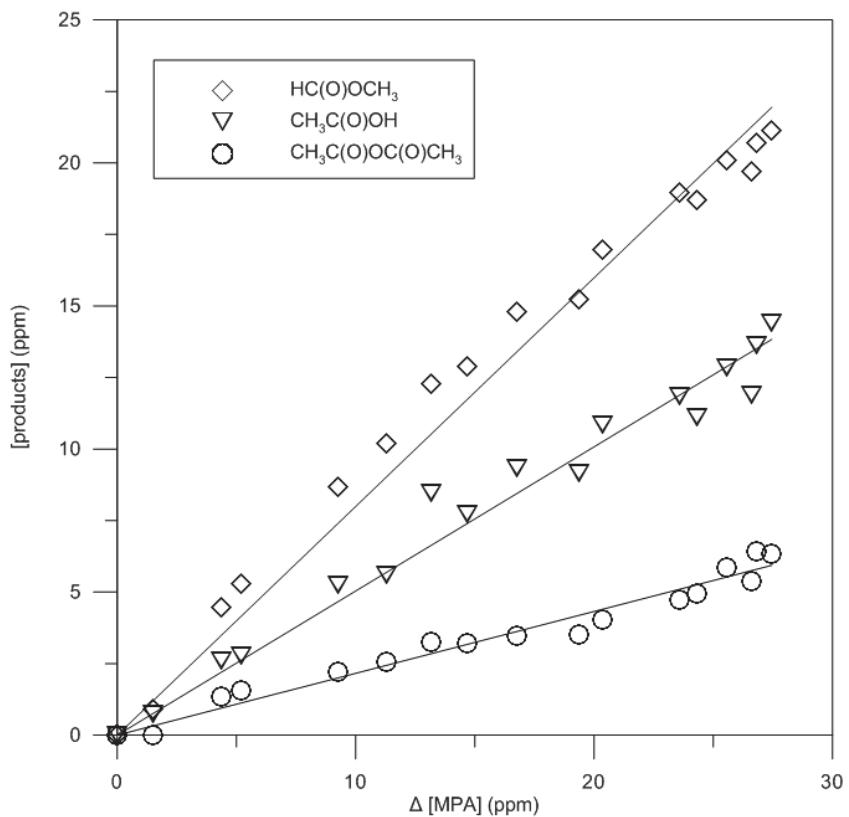
Figure 6.3: Time evolution of MPA and the identified products concentrations for the MPA+OH reaction in the presence of NO. The product yields are calculated from the slope of the fits: methyl formate, acetic acid and acetic anhydride product yields were 80 ± 7.3, 50 ± 4.8 and 22 ± 2.4%, respectively.

CO_2 and CO were also produced during the course of the reaction and identified by FTIR but not quantified. The slopes of the linear least-squares analysis with 97% confidence intervals indicate that products are not lost or produced by any other side/secondary reactions. This was also verified from the "relatively slow" rate coefficients of OH radicals with the products formed compared with that of OH with MPA. Particularly, the values of the OH rate coefficients reported in the literature are: 6.90×10^{-13} [67] and 2.27×10^{-13} [78] cm^3 molecule^{-1} s^{-1} for $CH_3C(O)OH$ and $HC(O)OCH_3$. Regarding acetic anhydride there are not experimental data, thus we estimated its OH rate coefficient employing SAR method (more details in annex V). The estimated value obtained is $k_{\text{acetic anhydride+OH}} = 2.01 \times 10^{-13}$ cm^3 molecule^{-1} s^{-1}. For these reasons, the yields quoted above were not corrected for secondary formation or losses.

6.B. Reaction of Cl + CH$_3$OCH$_2$CH(CH$_3$)OC(O)CH$_3$ (MPA)

The identification of the products formed upon reaction of Cl atoms with MPA was achieved employing online FTIR spectroscopy and GC-MS analyses. The sequential IR spectra recorded are shown in figure 6.4. Particularly, figure 6.4 display the IR spectra of MPA and Cl$_2$ before (A) and after (B) 50min of reaction, as well as the typical reference IR spectra of methyl formate (C), acetic acid (D) acetic anhydride (E), so as the spectrum (F) after subtraction of reactants and products. In this set of experiment MPA and Cl$_2$ concentrations were 35 and 74 ppm, respectively, while MPA consumption at the end of the experiment was ~ 72%.
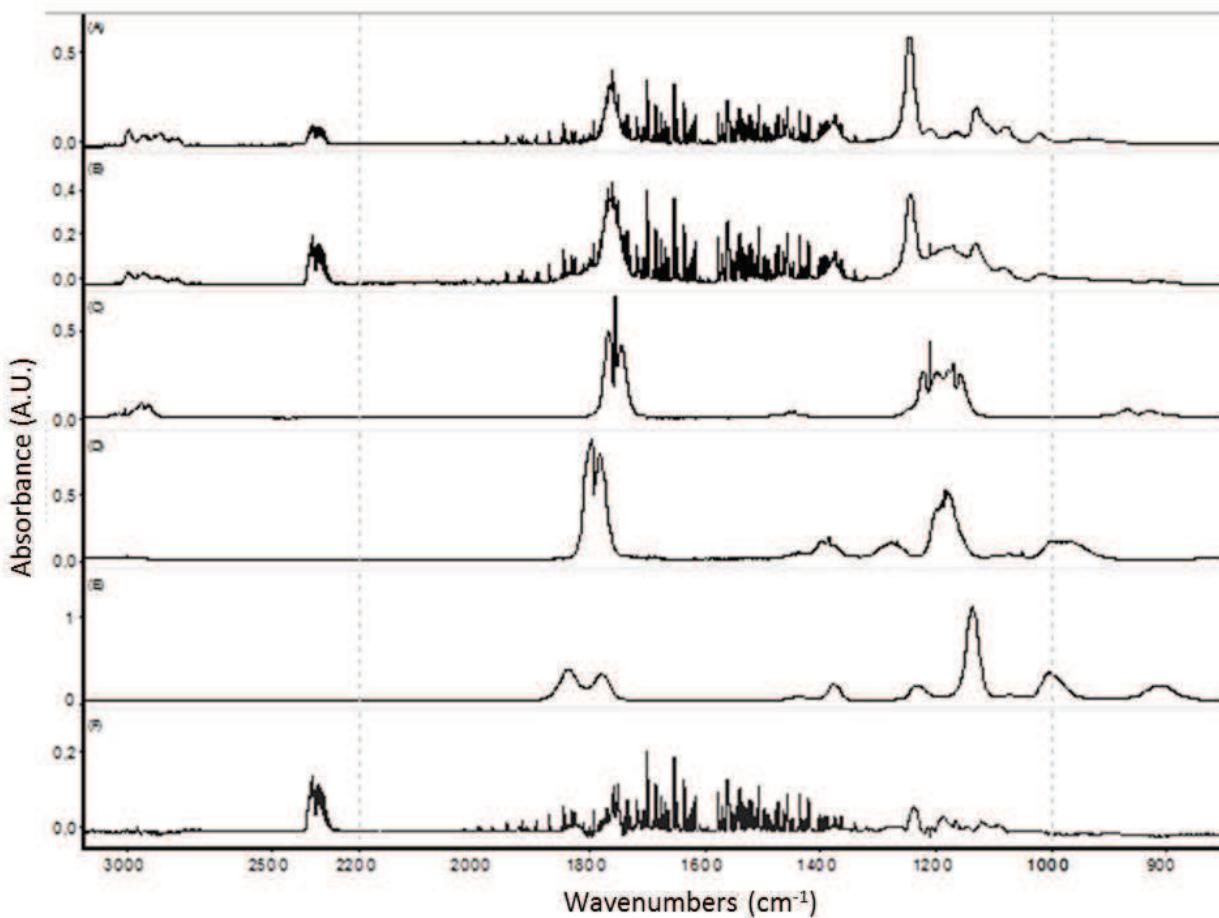
**Figure 6.4: Reaction of MPA with Cl. IR spectra obtained before (A) and after (B) a 50min irradiation of a mixture of MPA and Cl$_2$. Panels (C), (D) and (E) present the reference IR spectra of methyl formate, acetic acid and acetic anhydride, respectively. Panel (F) is the IR spectrum after subtraction of reactants and the identified products (methyl formate, acetic acid and acetic anhydride).**

In addition, figure 6.5 displays the concentration profiles of MPA and the major products as a function of reaction time. The initial concentrations used for MPA and Cl_2 were 30 and 77 ppm, respectively.
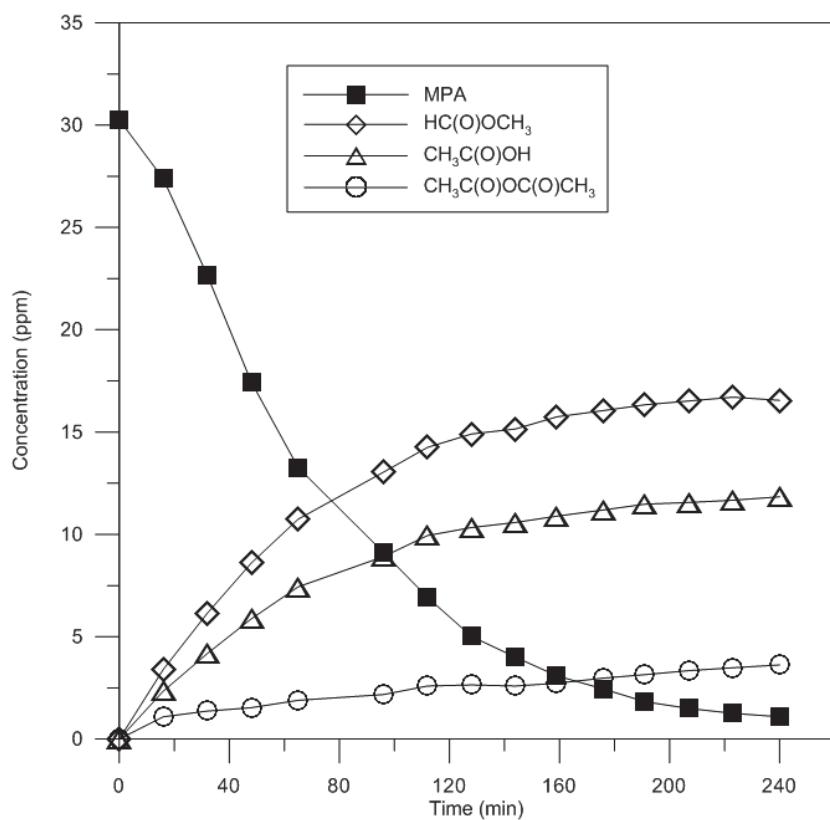

Figure 6.5: Concentration time-profiles of reactants and products for the reaction of MPA with Cl in the presence of NO at 760 Torr and 293 K.

The reaction products were calibrated using the integration of chromatogram peaks in GC-FID, and their yields, expressed as $\Delta[product]_t/\Delta[MPA]_t$, were measured. The recorded yields were slightly lower than those for the OH reaction: 60 ± 5.4, 41 ± 3.8 and $11 \pm 1.2\%$ for ($HC(O)OCH_3$), ($CH_3C(O)OH$) and ($CH_3C(O)OC(O)CH_3$), respectively, as shown in figure 6.6 where three runs are presented in all cases. The error quoted includes: the standard deviation (1σ) of the slope $\Delta[product]_t$ to $\Delta[MPA]_t$, the standard deviation (1σ) of the products and MPA calibration factors and the systematic uncertainties. Besides, the structure of the measured products indicates that they could be produced from the same MPA molecule. Nevertheless, a rough estimation of the carbon mass balance considering the yields of the three OVOCs formed is 41%.
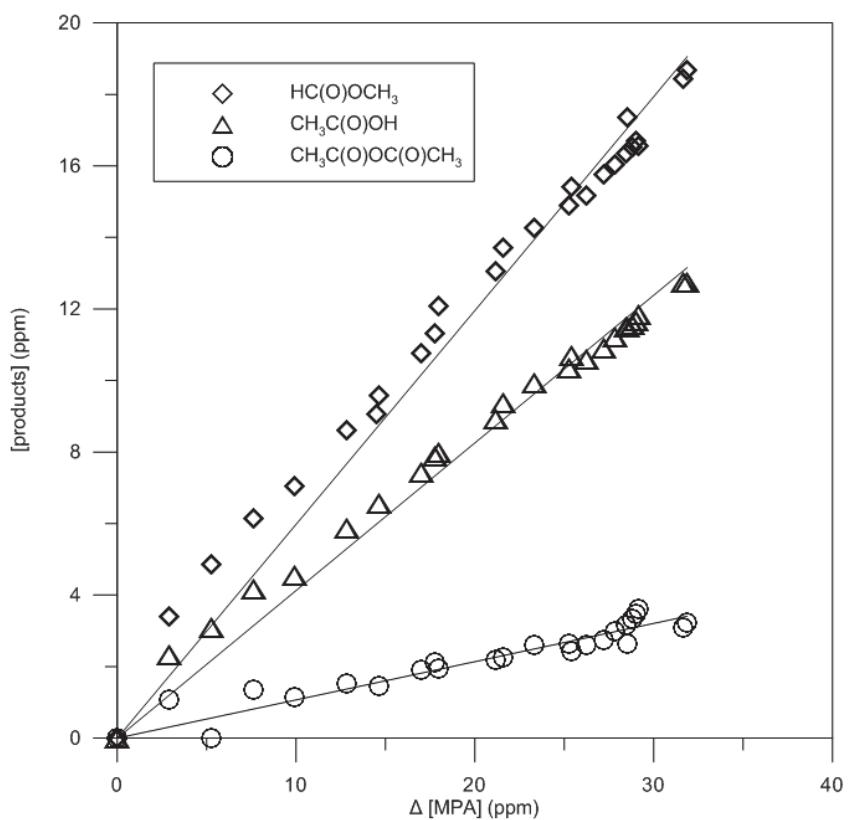
Figure 6.6: Time evolution of MPA and the identified products concentrations for the MPA + Cl reaction in the presence of NO. The product yields are calculated from the slope of the fit: methyl formate, acetic acid and acetic anhydride product yields were 60 ± 5.4, 41 ± 3.8 and 11 ± 1.2% respectively.

CO_2, CO and HCl were also produced and identified by FTIR but not quantified. The slopes of the linear least-squares analysis with 97% confidence intervals indicate that products are not lost or produced by any other side/secondary reactions. This was also verified from the "relatively slow" rate coefficients of Cl atoms with the products formed compared with that of Cl with MPA. Particularly, the values of the Cl rate coefficients reported in the literature are: 2.62×10^{-14} [67, 79] and 1.30×10^{-12} cm^3 molecule^{-1} s^{-1} [80] for $CH_3C(O)OH$ and $HC(O)OCH_3$, respectively. Regarding acetic anhydride there are not experimental data. For these reasons, the yields quoted above were not corrected for secondary formation or losses.

6.C. Proposed mechanism of OH/Cl + MPA

MPA has five C-H sites available for attack from OH and Cl. Based on our experimental observations, reaction rates and observed products, the oxidant abstracts one hydrogen atom principally from the methylene which is bonded with the alkyl group and the proposed mechanistic scheme for the reaction of OH and Cl with MPA is presented in figure 6.7. The presence of NO ensures rapid removal of HO_2 and RO_2 and simplifies the mechanistic interpretation of the product yields providing a more direct conversion of peroxy into alkoxy radicals, thus eliminating the reactions of HO_2 and RO_2 with RO_2. Subsequently, the most possible pathway for the alkoxy radical CH_3-O-(CHO$^{\cdot}$)-CH(CH_3)-O-C(O)-CH_3 formation is decomposition by breaking the C-C bond to form methyl formate and the CH_3-(CH$^{\cdot}$)-O-C(O)-CH_3 radical.

CH_3-O-**CH_2**-CH(CH_3)-O-C(O)-CH_3 + X$^{\cdot}$ → CH_3-O-(CH$^{\cdot}$)-CH(CH_3)-O-C(O)-CH_3 + HX   (R.6.1)

CH_3-O-(CH$^{\cdot}$)-CH(CH_3)-O-C(O)-CH_3 + O_2 + NO → CH_3-O-(CHO$^{\cdot}$)-CH(CH_3)-O-C(O)-CH_3 + NO_2(R.6.2)

CH_3-O-(CHO$^{\cdot}$)-CH(CH_3)-O-C(O)-CH_3 → **CH_3-O-CHO (methyl formate)** + CH_3-(CH$^{\cdot}$)-O-C(O)-CH_3

(R.6.3)

Further decomposition of this radical could follow a similar reaction sequence as shown in reactions:

CH_3-(CH$^{\cdot}$)-O-C(O)-CH_3 + O_2 + NO → CH_3-(CHO$^{\cdot}$)-O-C(O)-CH_3 + NO_2 (R.6.4)

CH_3-(CHO$^{\cdot}$)-O-C(O)-CH_3 + O_2 → **CH_3-C(O)-O-C(O)-CH_3** (acetic anhydride) + HO_2 (R.6.5)

In the presence of water, acetic anhydride would decompose to acetic acid.

CH_3-C(O)-O-C(O)-CH_3 + H_2O → 2 **CH_3-C(O)OH (acetic acid)**   (R.6.6)

The estimation method SAR[81] (detailed in annex V) shows that OH abstracts one hydrogen atom principally from the methylene and methane groups which are bonded to the ether oxygen of the methoxy functional group. H-abstraction from the methylene group (-O-CH_2-) has a high percentage of 84 %, which is in excellent

agreement with the experimental determined yields in our work, 72-80 %. On the other hand, the H-abstraction from methane group (CH_3-O -) has a possibility of 10%.
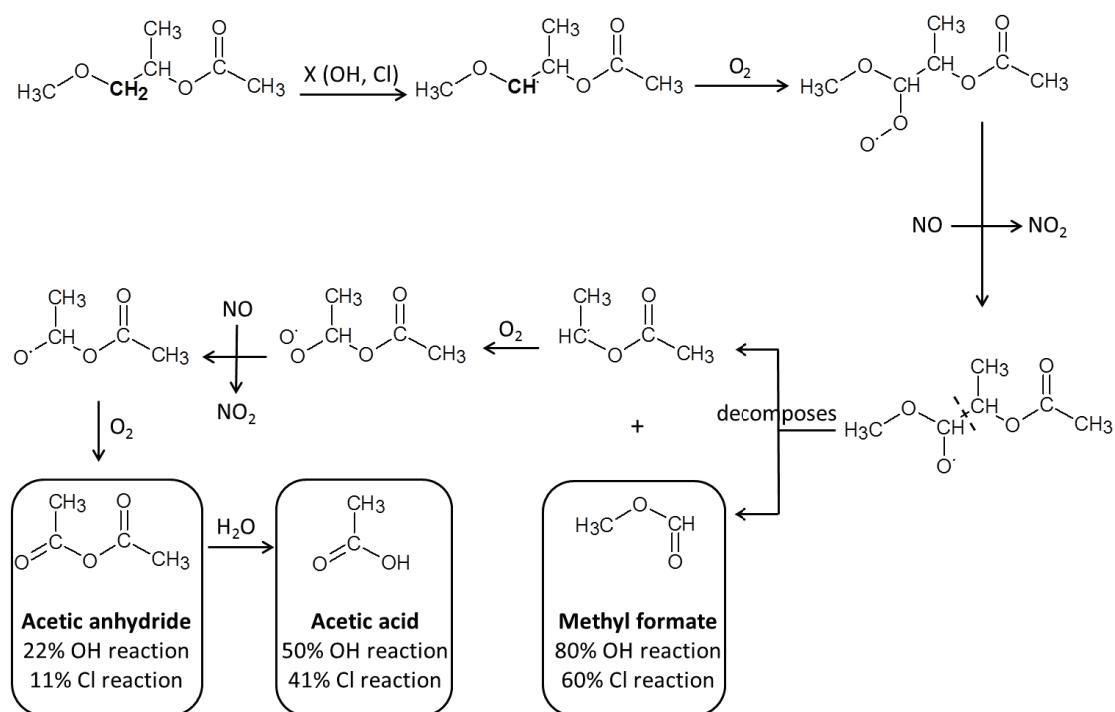

Figure 6.7: Reaction of MPA with oxidant in the presence of NO. Proposed mechanism scheme for H abstraction from methylene of the methoxy functional group.

The former observations and the proposed mechanistic scheme is consistent with the literature reports which suggest that OH radical reacts predominantly with the alkoxy end of an ester rather than the acyl end [36] (and references therein). Several studies [82, 83] have proposed that the initial step for the OH reaction with oxygenated organic compounds does not involve a direct H-atom abstraction pathway but the formation of a complex in which a hydrogen bond exists between the H-atom of the attacking OH radical and the O atom of the ether group. A second hydrogen bond is then formed in the complex between the O atom of the OH radical and an H atom in the hydrocarbon chain, resulting in intramolecular hydrogen atom transfer via a cyclic transition state. To validate that, Density Functional Theory (DFT) calculations were conducted using Gaussian 09 suite to locate a possible pre-reaction complex formed upon the interaction of the OH radical with an H atom at the α-position of the alkyl side of MPA. Indeed, the calculations verify the presence of an intermediate (figure 6.8) on the potential energy surface of the reaction. This complex could be

the explanation of the low negative activation energy for the reaction of OH with MPA.[82] In contrast, this transition state is not possible in Cl atom reactions.[35]
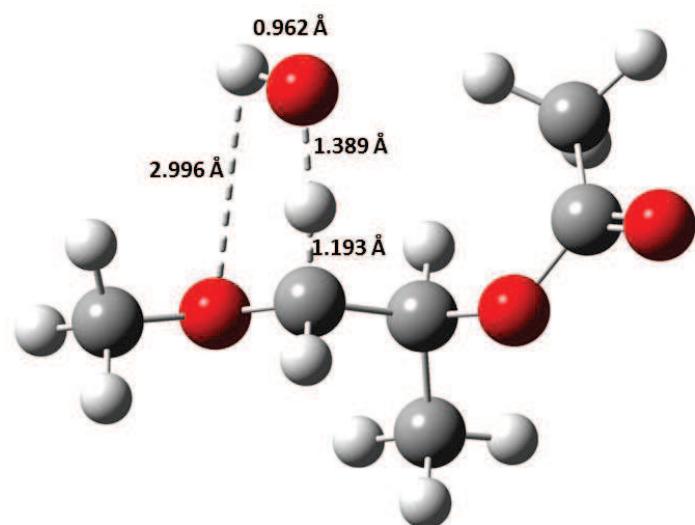

Figure 6.8: Adduct formed upon the interaction of the OH radical with an H atom at the α-position of the alkyl group of MPA. The geometries of OH, MPA and the intermediate involved in the reaction were optimized employing DFT calculations at the BHandHLYP/AUG-cc-pVDZ level of theory.

It has to be noted that Wells et al.[36] have reported a similar mechanistic scheme (figure 6.9) concerning the OH radical initiated oxidation of ethoxy ethyl acetate, EEA (MPA's isomer). The major products detected, ethyl formate (EF) and 1.2 ethanediol acetate formate (EAF), are consistent with H-atom abstraction with approximately the same degree of selectivity, from the two $-CH_2-$ groups next to the oxygen of the ether group. EAF and EF formation yields were determined to be 33% and 37%, respectively.   Ethylene glycol monoacetate ($CH_3C(O)OCH_2CH_2OH$), acetic acid ($CH_3C(O)OH$), acetaldehyde (CH_3CHO), formaldehyde (HCHO) and ethyl 2- (acetyloxy) acetate ($CH_3C(O)OCH_2C(O)OCH_2CH_3$) were also consistently observed products.

$$CH_3C(O)OCH_2CH_2OCH_2CH_3 + OH$$

$$| \ O_2$$

$$CH_3C(O)OCH_2CH(O_2\cdot)OCH_2CH_3 \qquad CH_3C(O)OCH_2CH_2OC(O_2\cdot)HCH_3$$

$$NO \xrightarrow{\quad\quad} NO_2 \qquad\qquad NO \xrightarrow{\quad\quad} NO_2$$

$$CH_3C(O)OCH_2CH(O\cdot)OCH_2CH_3 \quad CH_3C(O)OCH_2CH_2OC(O\cdot)HCH_3$$

decomposes   decomposes O_2

$$CH_3C(O)OCH_2\cdot + HC(O)OCH_2CH_3 \quad CH_3C(O)OCH_2CH_2OC(O)H$$

Ethyl Formate (EF)   Ethanediol Acetate Formate (EAF)

$$CH_3C(O)OCH_2CH_2OC(O)CH_3$$

Ethylene Glycol Diacetate (EGD)
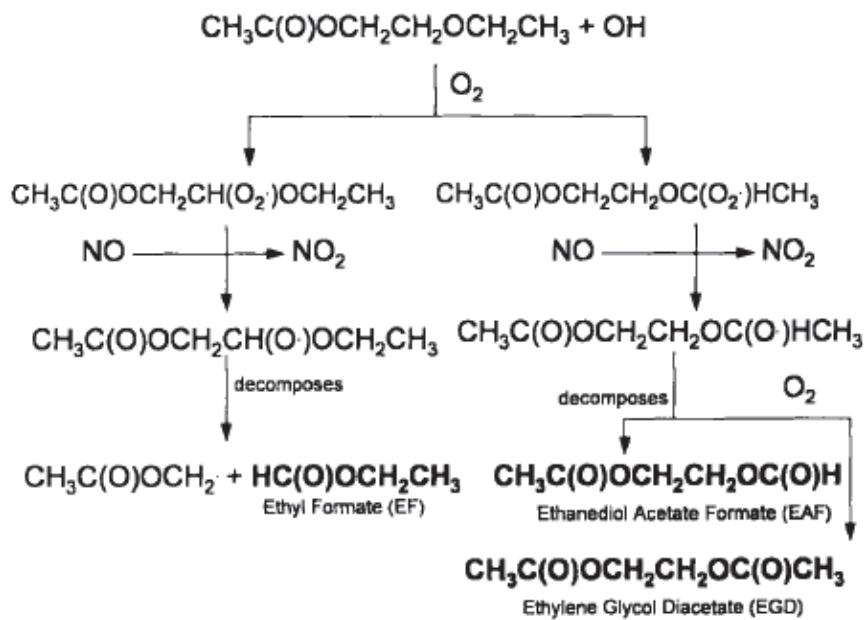
Figure 6.9: Reaction of MPA' isomer, EEA, with OH in the presence of NO. Proposed mechanism scheme for H abstraction from the two methylene sides of the ether functional group.[36]

151

7.Discussion, comparison and atmospheric implications

7. Discussion, comparison and atmospheric implications

7.A. OH reactions

7.A.I. Comparison with other studies and SAR

The reaction rate coefficients of OH radicals with the OVOCs measured in the current study as well as those reported in literature and those calculated with the SAR method are listed in table 7.1. Regarding MPA ($CH_3OCH_2CH(CH_3)OC(O)CH_3$), 2MBA ($CH_3OCH(C_2H_5)CH_2OC(O)CH_3$) and 3MBA ($CH_3OCH(CH_3)CH_2CH_2OC(O)CH_3$), to the best of our knowledge, there are no experimental data to compare our measurements. There is only one theoretical determination for the reaction rate coefficient of the MPA with OH radicals from Meylan et al.[84] and the calculated rate coefficient is in good agreement with our value (within 17%). Besides, the rate coefficients determined for MEA ($CH_3OCH_2CH_2OC(O)CH_3$), EEA ($C_2H_5OCH_2CH_2OC(O)CH_3$) and n-PA ($CH_3CH_2CH_2CH_2CH_2OC(O)CH_3$) are in excellent agreement with those reported in literature. The observed discrepancies between those values obtained and the literature are less than 15% which could be attributed to the different experimental systems used and the different methods applied.

Comparing the experimental values with those estimated with the SAR method (detailed estimation given in annex V), there are significant discrepancies. In particular, for MPA and n-PA the SAR method underestimates the rate coefficients (ca. 20%) while for the other compounds SAR overestimates the OH rate coefficients. Deviation between the measured and estimated rate coefficients for the alkoxy esters may be expected, since the SAR treatment employed only considers α-substituent groups. Essentially, SAR assumes that a substituent group influences the reactivity of only the neighboring groups. It worth's mentioning that problems have previously been encountered in obtaining agreement between calculated and experimentally measured rate coefficients for alkoxy esters[35] and multifunctional ethers[73, 83]. The latter indicates that for this class of compounds, the SAR method needs to be improved in order to provide more accurate predictions.

Table 7.1: Comparison of OH rate coefficients of the OVOCs measured in this study, reported in the literature and calculated using the SAR method.

Compound	k_{OH} (10^{-11}) [a]	Reference
MPA	1.44	This study (298 K)
	1.19	Meylan et al. (theoretical)[84]
	1.14	SAR
2MBA	1.92	This study (298 K)
	2.90	SAR
3MBA	1.91	This study (298 K)
	2.47	SAR
MEA	0.89	This study (293 K)
	0.83	O'Donnell et al.[35]
	1.27	SAR
EEA	1.24	This study (293 K)
	1.3	Hartmann et al.[33]
	1.33	O'Donnell et al.[35]
	1.16	Williams et al.[34]
	1.96	SAR
n-PA	0.73	This study (293K)
	0.74	Boubali et al.[85]
	0.75	Williams et al.[34]
	0.61	SAR

[a] Units of $cm^3 molecule^{-1} s^{-1}$

7.A.II. Comparison of the OH rate coefficients of the studied molecules

The rate coefficients of OH radicals with the OVOCs measured in the framework of the current study are summarized in table 7.2. As expected, the measured $k_{OVOC+OH}$ value depends on the structure of the molecule (conformer structures of the studied compounds are given in annex VI). Comparing the alkoxy acetate compounds, it was observed that the longer is the carbon chain the faster is the corresponding OH rate coefficient. For instance, the k_{OH} increases from MEA to EEA by a factor of 1.4, where the carbon chain in the alkoxy group is increased. When the carbon chain of the alkyl group increases from MEA (un-branched) to MPA (CH_3 branching in β position of the alkyl group) the k_{OH} increases by a factor of 1.62. Nevertheless, this increase should not only be attributed to the presence of the branching, since the rate coefficient

measured for MPA was found to be similar (~14% faster) with that of its isomer, EEA. In addition, when the alkyl group increases by two carbon atoms from MEA to MBA isomers the k_{OH} increases by a factor of 2.15. Attempting to compare the rate coefficients determined for MPA and MBA isomers, where the carbon chain in the alkyl group is increased while the branching is delocalized, an increase by a factor of 1.33 to the MBA k values was observed at 298K. Similar increases of the rate coefficient with the number of carbon atoms are also observed for the OH reactions with aliphatic alkanes[86], ethers[87, 88], esters[78,89] etc. Therefore, the number of carbon atoms and the chain length possess the principal role affecting significantly the rate coefficient value.

EEA
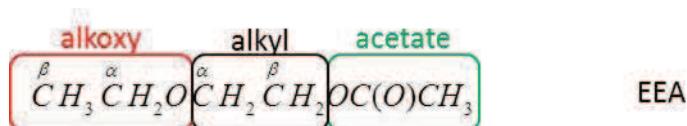
On the contrary, the rate coefficients of the isomers 2MBA and 3MBA were almost identical. The branching for the two compounds is localized at the α-position of the alkyl group. Considering that the principal pathway of H atom elimination is the α-position of the alkyl group (it has been discussed in section 6.C),[36] it seems that the position of the branching is important and not its length.

Finally, the OH rate coefficients measured in the literature for the alkoxy esters[35] are higher than those of the corresponding alkyl esters[90,85]. The reactivity of alkoxy esters is quite affected by the ether functional group which causes a reactivity increase. It has been suggested that this enhancement is due to activation of the H atoms of the neighbor carbons to the ether group, as a result of the initial formation of a hydrogen-bonded adduct followed by formation of a cyclic transition state.[73] In our case the structure of the alkoxy ester EEA is essentially the same as this of the alkyl ester n-PA but contain an O atom instead of a methylene. The results indicate that the presence of the ether group causes a substantial increase to the reaction rate coefficient by a factor of 1.7. Comparing the k_{EEA+OH} with the k of the corresponding monofunctional ester, n-butyl acetate, $CH_3CH_2CH_2CH_2OC(O)CH_3$, $k_{(CH3CH2CH2CH2OC(O)CH3+OH)}$ = 0.57 x 10^{-11} cm^3 $molecule^{-1}$ s^{-1} [30] at 298 K an increase by a factor of 2.2 is observed. Similarly, there is a difference by a factor of 2.4 between the OH rate coefficients values for MPA and the corresponding monofunctional

ester, sec-butyl acetate (CH$_3$CH$_2$CH(CH$_3$)OC(O)CH$_3$, SBA), $k_{(CH3CH2CH(CH3)OC(O)CH3+OH)}$ = 0.61 x 10^{-11} cm^3 molecule^{-1} s^{-1} [30] at 298 K.

Table 7.2: Reaction rate coefficients of OH radicals with the studied OVOCs determined at 295±3 K. The red highlighted part of the formula is the acetate group that is common for all the compounds. The α-position of alkyl group that corresponds to the dominant pathway of H atom elimination of alkoxy acetates is green highlighted.

Compound	Formula	k_{OH} (10^{-11}) [a]
MEA (C$_5$H$_{10}$O$_3$)	CH$_3$OCH$_2$CH$_2$OC(O)CH$_3$	0.89
EEA (C$_6$H$_{12}$O$_3$)	CH$_3$CH$_2$OCH$_2$CH$_2$OC(O)CH$_3$	1.24
MPA (C$_6$H$_{12}$O$_3$)	CH$_3$OCH$_2$CH(CH$_3$)OC(O)CH$_3$	1.44
2MBA (C$_7$H$_{14}$O$_3$)	CH$_3$OCH(CH$_2$CH$_3$)CH$_2$OC(O)CH$_3$	1.92
3MBA (C$_7$H$_{14}$O$_3$)	CH$_3$OCH(CH$_3$)CH$_2$CH$_2$OC(O)CH$_3$	1.91
n-PA (C$_7$H$_{14}$O$_2$)	CH$_3$CH$_2$CH$_2$CH$_2$CH$_2$OC(O)CH$_3$	0.73

[a] Units of cm^3 molecule^{-1} s^{-1}

7.A.III. Arrhenius expressions of MPA and MBA isomers

The temperature dependence of OH radical's reaction with MPA, 2MBA and 3MBA provided useful information regarding the mechanism of OH attack to the corresponding molecule. The Arrhenius expressions of the three molecules obtained were:

$k_{MPA+OH}(T) = (2.01 \pm 0.02) \times 10^{-12} \exp[(588 \pm 123/T)] \, cm^3 \, molecule^{-1} \, s^{-1}$,

$k_{2MBA+OH}(T) = (9.97 \pm 0.03) \times 10^{-13} \exp[(882 \pm 248/T)] \, cm^3 \, molecule^{-1} \, s^{-1}$

$k_{3MBA+OH}(T) = (8.27 \pm 0.03) \times 10^{-13} \exp[(936 \pm 290/T)] \, cm^3 \, molecule^{-1} \, s^{-1}$

and are presented in figure 7.1. One can note that the activation energies (Ea)* determined from the previous Arrhenius expressions are negative pointing to a complicated mechanistic scheme. In particular, the Ea values were, **-4.89 kJ mol^{-1}, -7.33 kJ mol^{-1} and -7.78 kJ mol^{-1} for MPA, 2-MBA and 3-MBA respectively.** This fact is attributed to the formation of weakly bound complexes between the OH radical and the alkoxy esters which either decompose back to reactant or eliminate H_2O. Essentially, a hydrogen-bonded adduct is initially formed involving the OH radical and the oxygen atom of the ether followed by intramolecular H-atom transfer. Similar results with small negative activation energies have been obtained in literature for monofunctional esters[85,90], ethers[46] and alkoxy esters[35]. The observed lower Ea values for 2 and 3-MBA compared to MPA could be attributed to the presence of an additional carbon to MBA isomers (C7 for MBA isomers compared to C6 for MPA) that stabilizes the corresponding adduct formed. Specifically, the distribution of the excess energy to the vibrational modes of the C7 adduct looks to be more efficient than to the C6 leading to lower Ea values and at the same time faster reaction rates.

---

* The activation energy corresponds to the energy required by the system to overcome the saddle point and move to the products.
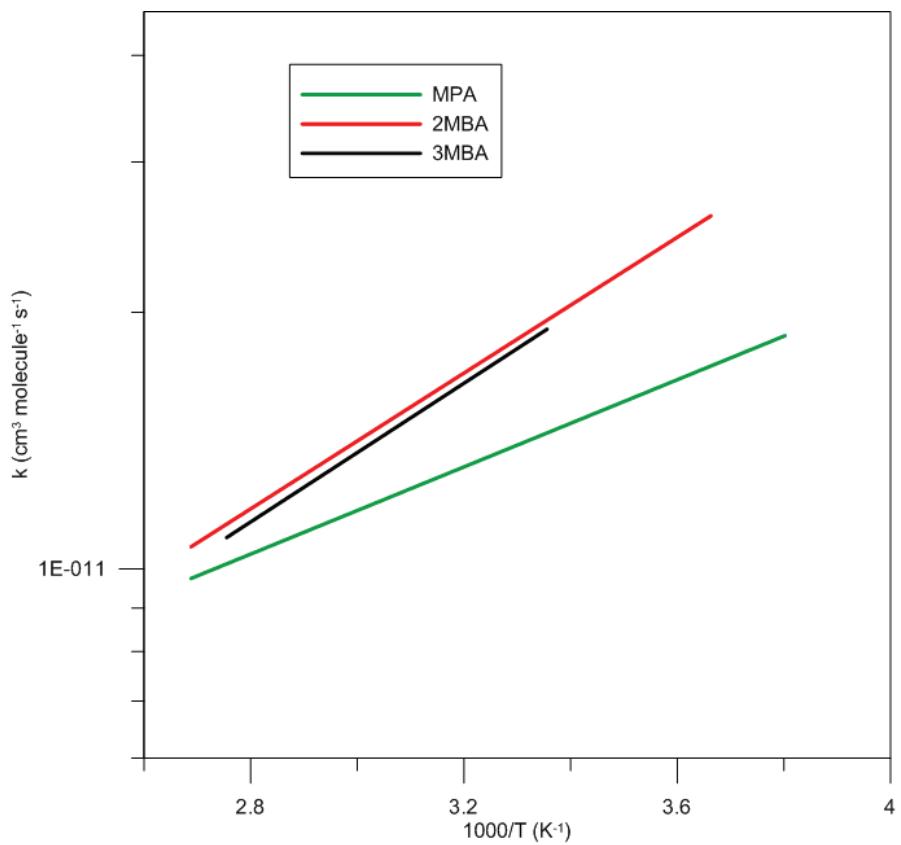
Figure 7.1: Arrhenius plots of MPA, 2MBA and 3MBA.

158

7.B. Cl reactions

7.B.I. Comparison of the Cl rate coefficients of the studied molecules

The rate coefficients of Cl atoms with the OVOCs are presented in table 7.3. To the best of our knowledge there are no literature data to compare our results. The rate coefficients of the studied compounds were extremely fast, in the order of 1.5-2.1 10^{-10} cm^3 molecule^{-1} s^{-1}. Although the k_{cl} values determined were close (within the range of 30%) it was observed that the longer is the carbon chain the faster is the corresponding Cl rate coefficient. The latter could be attributed to the presence of an additional CH$_2$ or CH$_3$ group that provides an extra site of attack for H atom abstraction. On the other hand, the increase of the carbon chain or the presence of a branching could cause stereochemical limitations, hindering Cl to approach the site of attack leading to a decrease to the rate coefficient. These two opposite effects are expected to influence the rate coefficient of the compound studied.

The k_{Cl} increases from MEA to EEA by a factor of 1.05, while from MEA (un-branched) to MPA (CH$_3$ branching in β position of the alkyl group) the k_{Cl} increases by a factor of 1.32. In addition, when the alkyl group increases by two carbon atoms from MEA to 2MBA the k_{Cl} increases by a factor of 1.26. Attempting to compare the rate coefficients determined for MPA and 2MBA, where the carbon chain in the alkyl group is increased while the branching is delocalized, a small unexpected decrease by a factor of 1.05 to the 2MBA k value was observed that could possibly be attributed to hindering effects as discussed previously. It has to be noted that the general trend observed in the literature points to an increase of the Cl rate coefficient with the number of carbon atoms[31] for the Cl reactions with aliphatic alkanes[86] and esters[78, 31] etc. Furthermore, the rate coefficient measured for MPA was found to be faster than that of its isomer, EEA by a factor of 1.25. In addition, the substitution of the ether group in EEA with a methylene group in n-PA caused 25% increase to the corresponding EEA rate coefficient. The former observation also points to the non-selective nature of H atom abstraction from Cl and the impact of the carbon chain length discussed previously.

Comparing the k_{EEA+Cl} with the k of the corresponding monofunctional ester, n-butyl acetate, $CH_3CH_2CH_2CH_2OC(O)CH_3$, $k_{(CH3CH2CH2CH2OC(O)CH3+Cl)} = 1.53 \times 10^{-10}$ cm^3 molecule^{-1} s^{-1} [30] at 298 K, a slight increase is observed. Similarly, attempting to compare the rate coefficients of MPA and sec-butyl acetate (SBA), $k_{(CH3C(O)OCH(CH3)CH2CH3+Cl)} = 9.07 \times 10^{-11}$ cm^3 molecule^{-1} s^{-1} [30] at 298 K, k_{SBA} is lower by a factor of 2.2 than the k_{MPA} measured herein. Therefore, it seems that the presence of the ether group increase the rate coefficient in a similar way as observed in case of OH reaction.

The rate coefficients of Cl atoms were at least by one order of magnitude faster than those of OH radicals. This is a general trend that has also been observed in literature for H atom abstraction mechanisms.[67] The latter has been attributed to the significant "strong desire" of Cl atoms for electron density (electrophilicity) compared to OH radicals that leads to faster rates and non-selective behavior.

Table 7.3: Reaction rate coefficients of Cl atoms with the studied OVOCs determined at 295±3 K. The red highlighted part of the formula is the acetate group that is common for all the compounds. The α-position of alkyl group that corresponds to the dominant pathway of H atom elimination of alkoxy acetates is green highlighted.

Compound	Formula	k_{Cl} (10^{-11}) [a]	k_{OH} (10^{-11}) [a]	k_{Cl}/k_{OH}
MEA ($C_5H_{10}O_3$)	$CH_3OCH_2CH_2OC(O)CH_3$	15.0	0.89	16.85
EEA ($C_6H_{12}O_3$)	$CH_3CH_2OCH_2CH_2OC(O)CH_3$	15.8	1.24	12.74
MPA ($C_6H_{12}O_3$)	$CH_3OCH_2CH(CH_3)OC(O)CH_3$	19.8	1.44	13.75
2MBA ($C_7H_{14}O_3$)	$CH_3OCH(CH_2CH_3)CH_2OC(O)CH_3$	18.9	1.92	10.48
n-PA ($C_7H_{14}O_2$)	$CH_3CH_2CH_2CH_2CH_2OC(O)CH_3$	21.0	0.73	28.87

[a] Units of cm^3 molecule^{-1} s^{-1}

7.C. Atmospheric implications

7.C.I. Lifetimes

The gas phase removal of the studied acetates occurs mainly through their reactions with OH radicals which is the major atmospheric sink for these compounds and Cl atoms, while reactions with O_3 and NO_3 are expected to be negligible. The atmospheric lifetimes, τ_{OH}, τ_{Cl} and τ_{tot}, based on the OH, Cl and total degradation respectively can be estimated from the following expressions:

$$\tau_{OH} = \frac{1}{k_{OH} \times [OH]} \qquad (E.7.1)$$

$$\tau_{Cl} = \frac{1}{k_{Cl} \times [Cl]} \qquad (E.7.2)$$

$$\frac{1}{\tau_{tot}} = \frac{1}{\tau_{OH}} + \frac{1}{\tau_{Cl}} \qquad (E.7.3)$$

where k_{OH} and k_{Cl} are the bimolecular rate coefficients for the corresponding reactions of the OVOC with OH radicals and Cl atoms, [OH] and [Cl] are the average tropospheric gas phase concentration of OH and Cl. In a relative polluted atmosphere [OH] is generally 2×10^6 radicals cm^{-3}, while that of [Cl] is 10^4 atoms cm^{-3} respectively.[6] The calculated lifetimes for the OVOCs studied are shown in table 7.4. The obtained results shows relatively short lifetime for OH, $\tau_{OH} \approx$ 7-19 hours, and substantially longer for Cl, $\tau_{Cl} \approx$ 5-8 days. However, the reactions of Cl atoms with VOCs may also be an important transformation process in coastal areas and where Cl atom concentrations are much higher, $[Cl]_{max} \sim 10^6$ atoms cm^{-3}.

According to the total lifetimes of the studied molecules their degradation will occur mainly in the free troposphere close to their emission source and their long-range transportation will be of little importance. Nevertheless, the long-range transportation can be significant for the degradation products of the acetates. For

instance, the total lifetimes for methyl formate and acetic acid which are the main reaction products of the OH reaction with MPA, 80% and 50% respectively, are 24.8 and 8.4 days respectively. (the k values reported in the literature are: 2.27×10^{-13} [78] and 6.90×10^{-13} [67] cm^3 molecule^{-1} s^{-1} for $HC(O)OCH_3$ and $CH_3C(O)OH$ with OH and 1.30×10^{-12} [80] and 2.62×10^{-14} [67, 79] cm^3 molecule^{-1} s^{-1} with Cl, respectively).

Table 7.4: Estimates lifetimes for the studied compounds.

Compound	$k_{OH} (10^{-11})$ [a]	τ_{OH} [b]	k_{Cl} [a] (10^{-10})	τ_{Cl} [c, d]	τ_{Cl} [b, e]	τ_{tot} [b]
MPA	1.44 [f]	9.65	1.98 [g]	5.85	1.40	**9.02**
2MBA	1.92 [f]	7.23	1.89 [f]	6.12	1.47	**6.89**
3MBA	1.91 [f]	7.27	-	-	-	**7.27**
MEA	0.89 [h]	15.61	1.50 [h]	7.72	1.85	**14.39**
EEA	1.24 [h]	11.20	1.58 [h]	7.33	1.76	**10.53**
n-PA	0.73 [h]	19.03	2.10 [h]	5.51	1.32	**16.63**

[a] Units of cm^3 molecule^{-1} s^{-1}
[b] Units of hours
[c] Units of days
[d] [Cl] = 10^4 atoms cm^{-3}
[e] [Cl] = 10^6 atoms cm^{-3}
[f] At T =298 K
[g] k average of measurements at T= 293 and 298 K
[h] At T = 293 K

7.C.II. Photochemical Ozone Creation Potential

It is well established that ozone is generated in situ from the sunlight-initiated oxidation of VOCs, in the presence of nitrogen oxides (figure 1.7). The estimated photochemical ozone creation potential (POCP) presents a value who can classify VOCs by their ability to form ozone in the tropospheric boundary layer through Europe during 5 days along a given trajectory.[91] The term was introduced for the first time in 1990 by Derwent R.G., while a detailed POCP report was first released in 1996. POCP is derived from chemistry-transport models using a) concentrations of trace gases (measured NO, NO2) b) movement of air masses and c) degradation of VOCs (rates and products). Then, an expected concentration of VOC (120 VOCs studied) inserts in the area and production of O_3 is calculated (model). Subsequently, a method was developed by Derwent et al[92] to estimate POCPs of VOCs in terms of their structures and their reactivity with OH radicals. Therefore, considering the OH gas-phase loss of the studied OVOCs as their main degradation pathway, the impact of the studied compounds oxidation to the ozone formation in the troposphere can be estimated. The estimated POCP (ε^{POCP}) of these compounds were derived using their OH rate coefficients at 298 K measured in this work and the generic equation[91]:

$$\varepsilon^{POCP} = \alpha_1 \times \gamma_S \times \gamma_R{}^{\beta} \times \left(1 - \alpha_2 \times n_C\right) \qquad \text{(E.7.4)}$$

where

α_1, α_2 and β: fitted parameters for the entire class of OVOCs defined on the basis of the compound reactivity with OH

γ_S : structure-based ozone formation index

γ_R : reactivity-based ozone formation index

n_C : the number of carbon atoms of the OVOC

In equation (E.7.4) the simple structure-based ozone formation index, γ_S, normalized to a value of 100 for ethene, is derived by considering the total quantity of ozone formed as a by-product from the complete compound oxidation to CO_2 and H_2O, catalyzed by NO_x and sunlight. This index is given by the expression:

$$\gamma_S = \left(\frac{n_{B_{OVOC}}}{M_{OVOC}} \right) \times \left(\frac{M_{ethene}}{n_{B_{ethene}}} \right) \times 100 \qquad\qquad (E.7.5)$$

which is related to the number of reactive bonds (n_B) in the molecule namely the broken bonds during the complete oxidation of the compound. M_{OVOC} and M_{ethene} are the molecular weights of the compound and ethane respectively in g mol^{-1}.

The OH-reactivity-based ozone formation index, γ_R, normalized to a value of 100 for ethene, provides an indication of how quickly the OVOC forms ozone in the boundary layer. This index is given by the following expression:

$$\gamma_R = \left(\frac{k_{OH_{OVOC}}}{M_{OVOC}} \right) \times \left(\frac{M_{ethene}}{k_{OH_{ethene}}} \right) \times 100 \qquad\qquad (E.7.6)$$

According to Derwent et al[92] for the organic compounds with $k_{OH} > 6.0 \times 10^{-12}$ cm^3 molecule^{-1} s^{-1}, the equation (E.7.4) is converted to:

$$\varepsilon^{POCP} = 0.351 \times \gamma_S \times \gamma_R{}^{0.25} \times (1 - 0.05 \times n_C) \qquad\qquad (E.7.7)$$

The obtained results presented in table 7.5, show relatively significant POCP for the studied compounds ranged between 32.5 and 37.3. It is notable that the ε^{POCP} for methyl formate, and acetic acid, the main reaction product of the OH reaction with MPA, are 5.3 and 10.99 respectively. These low values are partially due to their low OH-reactivity.

Table 7.5: Obtained results from the POCP estimation.

Compound	k_{OH} (10^{-11}) [a]	ε^{POCP}
ethene	0.852 [81]	100.00
MPA	1.44 [b]	36.08
2MBA	1.92 [b]	37.34
3MBA	1.91 [b]	37.29
MEA	0.89 [c]	32.48
EEA	1.24 [c]	34.76
n-PA	0.73 [c]	33.89
methyl formate	0.023 [78]	5.30 [d]
acetic acid	0.069 [67]	10.99 [d]

[a] Units of cm^3 $molecule^{-1}$ s^{-1}

[b] Average rate data from the present study at T = 298 K

[c] At T =293 K

[d] Estimation using (E.7.4) with parameters defined on OH compound reactivity

Summary, conclusions and perspectives

The objective of the current thesis was to investigate the processes controlling the atmospheric degradation of a series of oxygenated volatile organic compounds. The study was part of the scientific objectives of the DispAtmo project and triggered by a) the wide use of acetates as solvent in chemical industries that lead to the release of significant amounts into the atmosphere, b) the possible environmental hazards of the studied compounds, as well as c) the insufficient or nonexistent kinetic and mechanistic data in the literature.

During this thesis a thorough kinetic and mechanistic study was carried out to investigate the gas phase degradation processes of one of the main components of Tiflex solvent, the 1-methoxy 2-propyl acetate (MPA). To the best of our knowledge, this is the first experimental study aiming at understanding the fate and the implication of MPA degradation in the atmosphere. In particular, the rate coefficients for the reactions of OH radicals and Cl atoms with MPA were measured using complementary absolute and relative rate methods. The kinetic study on the OH-reaction was conducted in a wide temperature (263-373) K and pressure (1-760) Torr range employing the pulsed laser photolysis-laser induced fluorescence technique (PLP-LIF), a low pressure fast flow tube reactor coupled with a quadrupole mass spectrometer (FFT-QMS) and an atmospheric simulation chamber (ASC) coupled with a GC-FID. The kinetic data were used to derive the Arrhenius expression: $\mathbf{k_{MPA+OH}(T) = (2.01 \pm 0.02) \times 10^{-12} \exp[(588 \pm 123/T)] \; cm^3 \; molecule^{-1} \; s^{-1}}$. The absolute and relative rate coefficients for the gas phase reaction of Cl with MPA were measured at room temperature, at 1 and 760 Torr, in the flow reactor and the atmospheric chamber, respectively. The obtained rate coefficient was $\mathbf{k_{MPA+Cl} = (1.95 \pm 0.15) \times 10^{-10} \; cm^3 \; molecule^{-1} \; s^{-1}}$.

In order to obtain more insights regarding the degradation mechanism, a detailed product study was conducted and the major degradation products were detected. GC-FID, GC-MS and FT-IR techniques were used to investigate the mechanism of the OH and Cl reaction with MPA and determine the major degradation products in presence of NO. The products formed from **the reaction of MPA with OH and their yields were methyl formate (80±7.3%), acetic acid (50±4.8%) and acetic anhydride (22±2.4%)**

while for Cl-reaction, the obtained yields were 60±5.4, 41±3.8 and 11±1.2%, respectively. The proposed mechanistic scheme shows that H-atom abstraction is predominantly conducted from the methylene group (~80% for OH and 60% for Cl) bonded to the ether oxygen of the methoxy functional group (OCH_2). As far as the OH reaction is concerned a possible pre-reaction complex (adduct) is proposed upon the interaction of the OH radical with an H atom of this methylene.

The derived kinetic and mechanistic results for MPA has already been used as input data in chemical agent atmospheric dispersion model that aims to determine the air quality, the distribution of this compound in the atmosphere and the effects on human health and environment.

Furthermore, the degradation of 2-methoxy-butyl acetate (2MBA) and its isomer 3-methoxy-butyl acetate (3MBA) was studied for the first time. The rate coefficients of OH with 2MBA and 3MBA were measured employing complementary the PLP-LIF and the FFT-QMS (absolute and relative rate methods). The experiments were conducted in a wide temperature range at 1 and 100 Torr. The obtained Arrhenius expressions were: $k_{2MBA+OH}$(T) = (9.97 ± 0.03) × 10^{-13} exp[(882 ± 248/T)] cm^3 molecule^{-1} s^{-1} and $k_{3MBA+OH}$(T) = (8.27 ± 0.03) × 10^{-13} exp[(936 ± 290/T)] cm^3 molecule^{-1} s^{-1}. The relative rate coefficient for the Cl reaction with 2MBA was measured at room temperature using the FFT-QMS. The obtained rate coefficient was $k_{2MBA+Cl}$ = (1.89 ± 0.11) × 10^{-10} cm^3 molecule^{-1} s^{-1}.

Experiments have been also performed in the ASC in order to determine the relative rate coefficient of the OH and Cl reaction with methoxy ethyl acetate (MEA), ethoxy ethyl acetate (EEA) and n-pentyl acetate (n-PA) at room temperature. The experimental results for the OH reaction were: k_{MEA+OH} = (8.91 ± 0.48) × 10^{-11} cm^3 molecule^{-1} s^{-1}, k_{EEA+OH} = (1.24 ± 0.03) × 10^{-11} cm^3 molecule^{-1} s^{-1}, $k_{n-PA+OH}$ = (7.29 ± 0.46) × 10^{-11} cm^3 molecule^{-1} s^{-1}, while for the reaction with Cl were k_{MEA+Cl} = (1.50 ± 0.01) × 10^{-10} cm^3 molecule^{-1} s^{-1}, k_{EEA+CL} = (1.58 ± 0.14) × 10^{-10} cm^3 molecule^{-1} s^{-1}, $k_{n-PA+OH}$ = (2.10 ± 0.05) × 10^{-10} cm^3 molecule^{-1} s^{-1}, respectively. The OH rate coefficients determined are in excellent agreement with those reported in literature, while for the Cl reactions there are no experimental data to compare our measurements with. Comparing the rate coefficients of Cl atoms with those of OH radicals the k_{Cl} were at least by one

order of magnitude higher than those of OH. This fact is mainly attributed to the Cl electrophilicity as well as its non-selective behavior.

In addition, the OH rate coefficients for the sum of compounds were calculated with the SAR method in order to compare the experimental and the calculated rate coefficients. There are significant discrepancies between k_{exp} and k_{cal} since the SAR treatment considers only α-substituent groups. Regarding the observed reactivity trends the rate coefficient increases with the number of carbon atoms, while the presence of an ether group influence significantly the reactivity of the molecule.

The experimental kinetic data obtained were used to estimate the atmospheric lifetime of the compounds which reflect their total gas atmospheric degradation and their Photochemical Ozone Creation Potential (POCP) which notes their contribution to the atmospheric processes. The obtained results show relatively short total lifetime for all the studied compounds, $\boldsymbol{\tau_{tot} \approx}$ **7-17 hours**, consequently their degradation will occur mainly in the troposphere close to their emission sources and their long-range transportation will be of little importance. Furthermore, the estimated POCP (ε^{POCP}) of these compounds show relatively significant capacity to form ozone and the **POCP ranged between 32.5 and 37.3**.

Besides the kinetic and the mechanistic investigation, the UV absorption cross section spectrum of MPA, 2MBA and 3MBA were determined in the wavelength range 210-370 nm at 300±2 and 335±2 K. The cross section values determined under different experimental conditions at 215±1nm at 300±2 K were: $\boldsymbol{\sigma_{MPA}}$ **= (1.6 ± 0.2) x 10^{-19} cm^2 molecule^{-1}, σ_{2MBA} = (1.5 ± 0.2) x 10^{-19} cm^2 molecule^{-1}** and $\boldsymbol{\sigma_{3MBA}}$ **= (1.1 ± 0.3) x 10^{-19} cm^2 molecule^{-1}**, for the three molecules respectively. Therefore, the study has shown no photolysis of MPA, 2MBA or 3MBA under atmospheric conditions.

To conclude, within the framework of the current thesis and DispAtmo project, a thorough investigation of crucial chemical processes has been carried out to determine the tropospheric lifetimes of a series of OVOCs that are massively produced due to human activities. The kinetic and mechanistic results derived can be used as input data in photochemical atmospheric simulation models or chemical agent atmospheric dispersion models that aim to determine the distribution of these compounds in the atmosphere, the air quality, the contribution to global warming and climate change as well as the environmental and human impact.

In order to complete this work, the UV absorption cross section measurements as well as the mechanistic study could be realized for the reaction of OH and Cl with MEA, EEA and n-PA. In parallel with the lifetime, the photolysis investigation and the identification of the oxidation products could complementary define the atmospheric impact of these compounds. Furthermore, the temperature dependence investigation of the OH reaction with these three acetates could determine the impact in different regions and altitudes.

As far as the estimation of OH reaction rate coefficients using SAR is concerned, the optimization of the substituent factors for this class of compounds could improve the SAR method and provide more accurate predictions in agreement with the experimental data. In order to improve the substituent factors, the experimental OH rate coefficients for a larger number of alkoxy acetates need to be determined.

References

1.   Parker, S. P., *McGraw-Hill Concise Encyclopedia of Science & Technology*. McGraw-Hill: 1984.

2.   Papadimitriou, V. A kinetic study of the reaction of OH radicals and Cl atoms with a series of fluorinated alkools in the gas phase and the mechanistic investigation of their tropospheric degradation. University of Crete, Crete, Greece, 2005.

3.   L'atmosphère. http://murakami.free.fr/SpaceInvaders/Atmosphere.html

4.   NASA Sun: Facts & Figures.
http://solarsystem.nasa.gov/planets/profile.cfm?Object=Sun&Display=Facts

5.   wikipedia
https://upload.wikimedia.org/wikipedia/commons/thumb/e/e7/Solar_spectrum_en.svg/2000px-Solar_spectrum_en.svg.png

6.   Hein, R.; Crutzen, P. J.; Heimann, M., An Inverse Modeling Approach to Investigate the Global Atmospheric Methane Cycle. *Global Biogeochem. Cycles* 1997, *11*, (1), 43-76.

7.   Hewitt, C. N.; Jackson, A. V., *Atmospheric Science for Environmental Scientists*. Wiley: 2009.

8.   Finlayson-Pitts, B. J.; Pitts Jr, J. N., Preface. In *Chemistry of the Upper and Lower Atmosphere*, Finlayson-Pitts, B. J.; Pitts, J. N., Eds. Academic Press: San Diego, 2000.

9.   Kanakidou M., M. N., Kouvarakis G., *Special issue for Environmental Chemistry*. University of Crete: Heraklion Greece, 2004.

10.   Wennberg, P. O., Atmospheric chemistry: Radicals follow the Sun. *Nature* 2006, *442*, (7099), 145-146.

11.   Jacob, D., *Introduction to Atmospheric Chemistry*. Princeton University Press: 1999.

12.   Solomon, S.; Garcia, R. R.; Rowland, F. S.; Wuebbles, D. J., On the depletion of Antarctic ozone. *Nature* 1986, *321*, (6072), 755-758.

13.   Spicer, C. W.; Chapman, E. G.; Finlayson-Pitts, B. J.; Plastridge, R. A.; Hubbe, J. M.; Fast, J. D.; Berkowitz, C. M., Unexpectedly high concentrations of molecular chlorine in coastal air. *Nature* 1998, *394*, (6691), 353-356.

14.   Liu, S. C.; Trainer, M.; Fehsenfeld, F. C.; Parrish, D. D.; Williams, E. J.; Fahey, D. W.; Hübler, G.; Murphy, P. C., Ozone production in the rural troposphere and the implications for regional and global ozone distributions. *Journal of Geophysical Research: Atmospheres* 1987, *92*, (D4), 4191-4207.

15.   Wang, T.; Xue, L.; Brimblecombe, P.; Lam, Y. F.; Li, L.; Zhang, L., Ozone pollution in China: A review of concentrations, meteorological influences, chemical precursors, and effects. *Science of The Total Environment* 2017, *575*, 1582-1596.

16.   Atkinson, R., Atmospheric chemistry of VOCs and NOx. *Atmospheric Environment* 2000, *34*, (12–14), 2063-2101.

17.   Leeds-University; MCM Website. http://mcm.leeds.ac.uk/MCM/project.htt

18.   CITEPA; *Inventaire des émissions de polluants atmosphériques et de gaz à effet de serre en France séries sectorielles et analyses étendues*; Centre Interprofessionnel Technique d'Etudes de la Pollution Atmosphérique: FRANCE, 2016.

19.   Agency, E. E. *European Union emission inventory report 1990–2011 under the UNECE Convention on Long-range Transboundary Air Pollution (LRTAP)*; 10/2013; European Environment Agency: Denmark, 2013.

20.   Atmosphérique, C. I. T. d. E. d. l. P. *Inventaire des émissions de polluants atmosphériques et de gaz à effet de serre en France séries sectorielles et analyses étendues*; CITEPA 1057; Centre Interprofessionnel Technique d'Etudes de la Pollution Atmosphérique: FRANCE, 2013.

21.   *Environmental Protection Agency. An Introduction to Indoor Air Quality: Volatile Organic Compounds (VOCs)*; 2012.

22.	Ismail, O. M. S.; Hameed, R. S. A., Environmental effects of volatile organic compounds on ozone layer.

23.	Kiehl, J. T.; Trenberth, K. E., Earth's Annual Global Mean Energy Budget. *Bulletin of the American Meteorological Society* 1997, *78*, (2), 197-208.

24.	Atkinson, R.; Arey, J., Atmospheric Degradation of Volatile Organic Compounds. *Chemical Reviews* 2003, *103*, (12), 4605-4638.

25.	Calvert, J.; Mellouki, A.; Orlando, J.; Pilling, M.; Wallington, T., *Mechanisms of Atmospheric Oxidation of the Oxygenates*. Oxford University Press, USA: 2011.

26.	Suliga, G.; Idasiak, V.; Kratz, F., DispAtmo project: A framework for crisis management. In *Safety and Reliability of Complex Engineered Systems*, CRC Press: 2015; pp 265-270.

27.	IUPAC Task Group on Atmospheric Chemical Kinetic Data Evaluation. http://iupac.pole-ether.fr/

28.	M.Karaca, A. Z., Y. Fenard, A. Mellouki, P. Dagaut, I. Gokalp, Numerical simulation of hazardous material atmosheric disersion following an accidental release in an industrial site: The effects of atmospheric chemistry during dispersion. In *HARMO-15*, Madrid, Spain, 2013.

29.	INERIS - Portail Substances Chimiques, accueil. 2016.

30.	Calvert, J.; Mellouki, A.; Orlando, J.; Pilling, M.; Wallington, T., The oxygenates: Their Properties, Sources, and Use as Alternative Fuels. In *Mechanisms of Atmospheric Oxidation of the Oxygenates*, 2011; pp 3-111.

31.	Notario, A.; Le Bras, G.; Mellouki, A., Absolute Rate Constants for the Reactions of Cl Atoms with a Series of Esters. *J. Phys. Chem. A* 1998, *102*, (18), 3112-3117.

32.	Xing, J.-H.; Takahashi, K.; Hurley, M. D.; Wallington, T. J., Kinetics of the reactions of chlorine atoms with a series of acetates. *Chem. Phys. Lett.* 2009, *474*, 268-272.

33.	D. Hartmann, A. G., D. Rhasa, and R. Zellner *Rate constants for reactions of OH radicals with acetates and glycols in the gas phase*; Institut für Physikalische Chemie, Universität Göttingen 3400 Göttingen, FRG: D. REIDEL PUBLISHING COMPANY.

34.	Williams, D. C.; O'rji, L. N.; Stone, D. A., Kinetics of the reactions of OH radicals with selected acetates and other esters under simulated atmospheric conditions. *Int. J. Chem. Kinet.* 1993, *25*, 539-548.

35.	O'Donnel, S. M.; Sidebottom, H. W.; Wenger, J. C.; Mellouki, A.; Le Bras, G., Kinetic Studies on the Reactions of Hydroxyl Radicals with a Series of Alkoxy Esters. *J. Phys. Chem. A* 2004, *108*, (36), 7386-7392.

36.	Wells, J. R.; Wiseman, F. L.; Williams, D. C.; Baxley, J. S.; Smith, D. F., The Products of the Reaction of the Hydroxyl Radical with 2-Ethoxyethyl Acetate. *Int. J. Chem. Kinet.* 1996, *28*, (7), 475-480.

37.	Godavari-biorefineries 3-METHOXYBUTYL ACETATE. http://www.somaiya.com/3-methoxybutyl-acetate

38.	National Center for Biotechnology Information. PubChem Compound Database. CID=12348. https://pubchem.ncbi.nlm.nih.gov/compound/12348 (May 7, 2016),

39.	Hernandez, O. *SIDS Initial Assessment Report for Primary Amyl Acetate* U.S. Environmental Protection Agency: Oxo Process Panel, 2006.

40.	database, c. http://www.chemspider.com/.

41.	Lendar, M. Dégradation atmosphérique d'une série d'alcools, d'esters et de l'hexafluoroisobutène. University of Orleans, Orleans, 2012.

42.	Mu, Y. J.; Mellouki, A., The Near-UV Absorption Cross Sections for Several Ketones. *J. Photochem. Photobiol., A* 2000, *134*, (1-2), 31-36.

43.	Basting, D.; Marowsky, G., *Excimer Laser Technology*. Springer: 2005.

44.	Crosley, D. R., Rotational and translation effects in collisions of electronically excited diatomic hydrides. *The Journal of Physical Chemistry* 1989, *93*, (17), 6273-6282.

45.   Mellouki A., T. S., Laverdet G. , Quilgars A., Le Bras G. , Kinetic studies of OH reactions with H$_2$O, C$_3$H$_8$ and CH$_4$ using the pulsed laser photolysis - laser induced fluorescence method. *Journal de Chimie Physique* 1994, *91*, 473-487.

46.   Mellouki, A.; Téton, S.; Lebras, G., Kinetics of OH Radical Reactions with a Series of Ethers. *Int. J. Chem. Kinet.* 1995, *27*, (8), 791-805.

47.   Teton, S. Etudes cinétiques de réactions de dégradation atmosphérique par le radical OH de composés organiques volatils. University of Orleans, Orleans, 1995.

48.   Atkinson, R.; Baulch, D. L.; Cox, R. A.; Crowley, J. N.; Hampson, R. F.; Hynes, R. G.; Jenkin, M. E.; Rossi, M. J.; Troe, J., Evaluated kinetic and photochemical data for atmospheric chemistry: Volume I - gas phase reactions of Ox, HOx, NOx and SOx species. *Atmos. Chem. Phys.* 2004, *4*, (6), 1461-1738.

49.   Poulet, G.; Lancar, I. T.; Laverdet, G.; Le Bras, G., Kinetics and products of the bromine monoxide + chlorine monoxide reaction. *The Journal of Physical Chemistry* 1990, *94*, (1), 278-284.

50.   Bedjanian, Y.; Laverdet, G.; Le Bras, G., Low-pressure Study of the Reaction of Cl Atoms with Isoprene. *J. Phys. Chem. A* 1998, *102*, (6), 953-959.

51.   Su, M. C.; Kumaran, S. S.; Lim, K. P.; Michael, J. V.; Wagner, A. F.; Harding, L. B.; Fang, D. C., Rate Constants, 1100 ≤ T ≤ 2000 K, for H + NO2 → OH + NO Using Two Shock Tube Techniques: Comparison of Theory to Experiment. *J. Phys. Chem. A* 2002, *106*, (36), 8261-8270.

52.   Atkinson, R.; Baulch, D. L.; Cox, R. A.; Crowley, J. N.; Hampson, R. F.; Hynes, R. G.; Jenkin, M. E.; Rossi, M. J.; Troe, J., Evaluated Kinetic and Photochemical Data for Atmospheric Chemistry: Volume III - Gas Phase Reactions of Inorganic Halogens. *Atmos. Chem. Phys.* 2007, *7*, 981-1191.

53.   Kaufman, F., Kinetics of Elementary Radical Reactions in the Gas Phase. *J. Phys. Chem.* 1984, *88*, (21), 4909-4917.

54.   Bertram, A. K.; Ivanov, A. V.; Hunter, M.; Molina, L. T.; Molina, M. J., The Reaction Probability of OH on Organic Surfaces of Tropospheric Interest. *J. Phys. Chem. A* 2001, *105*, (41), 9415-9421.

55.   Ivanov, A. V.; Trakhtenberg, S.; Bertram, A. K.; Gershenzon, Y. M.; Molina, M. J., OH, HO2, and Ozone Gaseous Diffusion Coefficients. *J. Phys. Chem. A* 2007, *111*, (9), 1632-1637.

56.   Marrero, T. R.; Mason, E. A., Gaseous Diffusion Coefficients. *J. Phys. Chem. Ref. Data* 1972, *1*, (1), 3-118.

57.   Barnes, I.; Rudzinski, K. J., *Environmental Simulation Chambers: Application to Atmospheric Chemical Processes*. Springer Netherlands: 2006.

58.   Calvé, S. L. Cinétiques et mécanismes d'oxydation atmosphérique par le radical OH de composés organiques volatils oxygénés. University of Orleans, Orleans, 1998.

59.   Thévenet, R.; Mellouki, A.; Le Bras, G., Kinetics of OH and Cl reactions with a series of aldehydes. *International Journal of Chemical Kinetics* 2000, *32*, (11), 676-685.

60.   Faust, C. B., *Modern Chemical Techniques*. Royal Society of Chemistry: 1992.

61.   Kalsi, P. S., *Spectroscopy of Organic Compounds*. New Age International (P) Limited: 2007.

62.   Owen, T., *Fundamentals of Modern UV-visible Spectroscopy: Primer*. Agilent Technologies: 2000.

63.   Kumar, P. S. Spectroscopy of Organic Compounds, ORGANIC CHEMISTRY http://www.uobabylon.edu.iq/eprints/publication_11_8282_250.pdf

64.   Benayada, B.; Leila, D. O., UV absorption cross sections for acetates. *Desalination* 1999, *126*, (1–3), 83-86.

65.   Anderson, R. J.; Bendell, D. J.; Groundwater, P. W.; Chemistry, R. S. o., *Organic Spectroscopic Analysis*. Royal Society of Chemistry: 2004.

66.   Sivakumar, D. K. Unit: I I UV - VISIBLE SPECTROSCOPY Syllabus: Electronic transition Chromophores and Auxochromes. http://slideplayer.com/slide/1677031/ (25/11/2015),

67.   Atkinson, R.; Baulch, D. L.; Cox, R. A.; Crowley, J. N.; Hampson, R. F.; Hynes, R. G.; Jenkin, M. E.; Rossi, M. J.; Troe, J., Evaluated Kinetic and Photochemical Data for Atmospheric Chemistry: Volume II - Gas Phase Reactions of Organic Species. *Atmos. Chem. Phys.* 2006, *6*, 3625-4055.

68.   Le Calve, S.; Mellouki, A.; Le Bras, G., Kinetic Studies of OH Reactions with Propylal, Butylal and 1,3-Dioxolane. *Phys. Chem. Chem. Phys.* 2002, *4*, (22), 5622-5626.

69.   Wu, H.; Mu, Y.; Zhang, X.; Jiang, G., Relative Rate Constants for the Reactions of Hydroxyl Radicals and Chlorine Atoms with a Series of Aliphatic Alcohols. *Int. J. Chem. Kinet.* 2003, *35*, (2), 81-87.

70.   Lendar, M.; Aissat, A.; Cazaunau, M.; Daële, V.; Mellouki, A., Absolute and relative rate constants for the reactions of OH and Cl with pentanols. *Chemical Physics Letters* 2013, *582*, 38-43.

71.   Cavalli, F.; Barnes, I.; Becker, K. H., FT-IR Kinetic and Product Study of the OH Radical-Initiated Oxidation of 1-Pentanol. *Environmental Science & Technology* 2000, *34*, (19), 4111-4116.

72.   Dagaut, P.; Liu, R.; Wallington, T. J.; Kurylo, M. J., Flash photolysis resonance fluorescence investigation of the gas-phase reactions of hydroxyl radicals with cyclic ethers. *The Journal of Physical Chemistry* 1990, *94*, (5), 1881-1883.

73.   Moriarty, J.; Sidebottom, H.; Wenger, J.; Mellouki, A.; Le Bras, G., Kinetic Studies on the Reactions of Hydroxyl Radicals with Cyclic Ethers and Aliphatic Diethers. *J. Phys. Chem. A* 2003, *107*, (10), 1499-1505.

74.   Wallington, T. J.; Skewes, L. M.; Siegl, W. O.; Wu, C.-H.; Japar, S. M., Gas phase reaction of Cl atoms with a series of oxygenated organic species at 295 K. *International Journal of Chemical Kinetics* 1988, *20*, (11), 867-875.

75.   Atkinson, R.; Aschmann, S. M., Kinetics of the gas phase reaction of Cl atoms with a series of organics at 296 ± 2 K and atmospheric pressure. *International Journal of Chemical Kinetics* 1985, *17*, (1), 33-41.

76.   Hooshiyar, P. A.; Niki, H., Rate constants for the gas-phase reactions of Cl-atoms with C2⎯C8 alkanes at T = 296 ± 2 K. *International Journal of Chemical Kinetics* 1995, *27*, (12), 1197-1206.

77.   Yujing, M.; Mellouki, A., Temperature dependence for the rate constants of the reaction of OH radicals with selected alcohols. *Chemical Physics Letters* 2001, *333*, (1–2), 63-68.

78.   Wallington, T. J.; Dagaut, P.; Liu, R. H.; Kurylo, M. J., The Gas Phase Reactions of Hydroxy Radicals with a Series of Esters over the Temperature Range 240-440-K. *Int. J. Chem. Kinet.* 1988, *20*, (2), 177-186.

79.   Romanias, M. N.; Zogka, A. G.; Papadimitriou, V. C.; Papagiannakopoulos, P., Uptake Measurements of Acetic Acid on Ice and Nitric Acid-Doped Thin Ice Films over Upper Troposphere/Lower Stratosphere Temperatures. *J. Phys. Chem. A* 2012, *116*, (9), 2198-2208.

80.   Wallington, T. J.; Hurley, M. D.; Haryanto, A., Kinetics of the Gas Phase Reactions of Chlorine Atoms with a Series of Formates. *Chem. Phys. Lett.* 2006, *432*, (1-3), 57-61.

81.   Atkinson, R., Kinetics and Mechanisms of the Gas-phase Reactions of the Hydroxyl Radical with Organic Compounds under Atmospheric Conditions. *Chem. Rev.* 1986, *86*, (1), 69-201.

82.   Smith, I. W., Ravishankara, A. R., Role of Hydrogen-Bonded Intermediates in the Bimolecular Reactions of the Hydroxyl Radical. *J. Phys. Chem. A* 2002, *106*, (19), 4798-4807.

83.   Porter, E.; Wenger, J.; Treacy, J.; Sidebottom, H.; Mellouki, A.; Téton, S.; Le Bras, G., Kinetic Studies on the Reactions of Hydroxyl Radicals with Diethers and Hydroxyethers. *J. Phys. Chem. A* 1997, *101*, (32), 5770-5775.

84.   Meylan, W. M.; Howard, P. H., Computer Estimation of the Atmospheric Gas-Phase Reaction Rate of Organic Compounds with Hydroxyl Radicals and Ozone. *Chemosphere* 1993, *26*, (12), 2293-2299.

85.   El Boudali, A.; Le Calvé, S.; Le Bras, G.; Mellouki, A., Kinetic Studies of OH Reactions with a Series of Acetates. *The Journal of Physical Chemistry* 1996, *100*, (30), 12364-12368.

86.   Calvert, J. G., *Mechanisms of Atmospheric Oxidation of the Alkanes*. Oxford University Press: Oxford ; New York, 2008.

87.   Mellouki, A.; Wallington, T. J.; Chen, J., Atmospheric Chemistry of Oxygenated Volatile Organic Compounds: Impacts on Air Quality and Climate. *Chemical Reviews* 2015, *115*, (10), 3984-4014.

88.   Mellouki, A.; Le Bras, G.; Sidebottom, H., Kinetics and Mechanisms of the Oxidation of Oxygenated Organic Compounds in the Gas Phase. *Chemical Reviews* 2003, *103*, (12), 5077-5096.

89.   LeCalve, S.; LeBras, G.; Mellouki, A., Kinetic studies of OH Reactions with Iso-Propyl, Iso-Butyl, Sec-Butyl, and Tert-Butyl Acetate. *Int. J. Chem. Kinet.* 1997, *29*, (9), 683-688.

90.   Le Calvé, S.; Le Bras, G.; Mellouki, A., Temperature Dependence for the Rate Coefficients of the Reactions of the OH Radical with a Series of Formates. *The Journal of Physical Chemistry A* 1997, *101*, (30), 5489-5493.

91.   Jenkin, M. E. *Photochemical Ozone and PAN Creation Potentials: Rationalisation and Methods of Estimation, Report AEAT-4182/20150/003*; National Environmental Technology Center, AEA Technology plc: Oxfordshire, UK, 1998.

92.   Derwent, R. G.; Jenkin, M. E.; Saunders, S. M.; Pilling, M. J., Photochemical Ozone Creation Potentials for Organic Compounds in Northwest Europe Calculated with a Master Chemical Mechanism. *Atmos. Environ.* 1998, *32*, (14–15), 2429-2441.

Annexes

Annex I

TIFLEX composition

An Automated Thermal Desorption Gas Chromatography – Mass Spectrometer (GC-MS Clarus 600C coupled with ATD 150 from Perkin Elmer) was used for the qualitative analysis of Tiflex solvent. Chromatographic separation of the Tiflex constituents was achieved by using a 30m length Elite 5MS column (0.25µm film thickness) operated at 433 K, using helium as carrier gas. The chromatogram and the identification of its peaks are shown below.

Table 1: Qualitative analysis of TIFLEX solvent

| Molecular Formula	Name	Cas No
$C_4H_{10}O_2$	1-methoxy-2-propanol	107-98-2
$C_6H_{12}O_3$	1-methoxy-2-propyl acetate	108-65-6
C_9H_{12}	1,2,4-trimethylbenzene	95-63-6
	1,3,5-trimethylbenzene	108-67-8
	1,2,3-trimethylbenzene	526-73-8
	Isopropylbenzene (cumene)	98-82-8
	1-ethyl-4-methylbenzene	622-96-8
$C_{10}H_{14}$	n-Propylbenzene	103-65-1
	p-Cymene	99-87-6
	1-Ethyl-3-methylbenzene	620-14-4
	1-ethyl-2-methylbenzene	611-14-3
C_8H_{10}	o-Xylene	95-47-6
C_9H_{10}	Indane	496-11-7
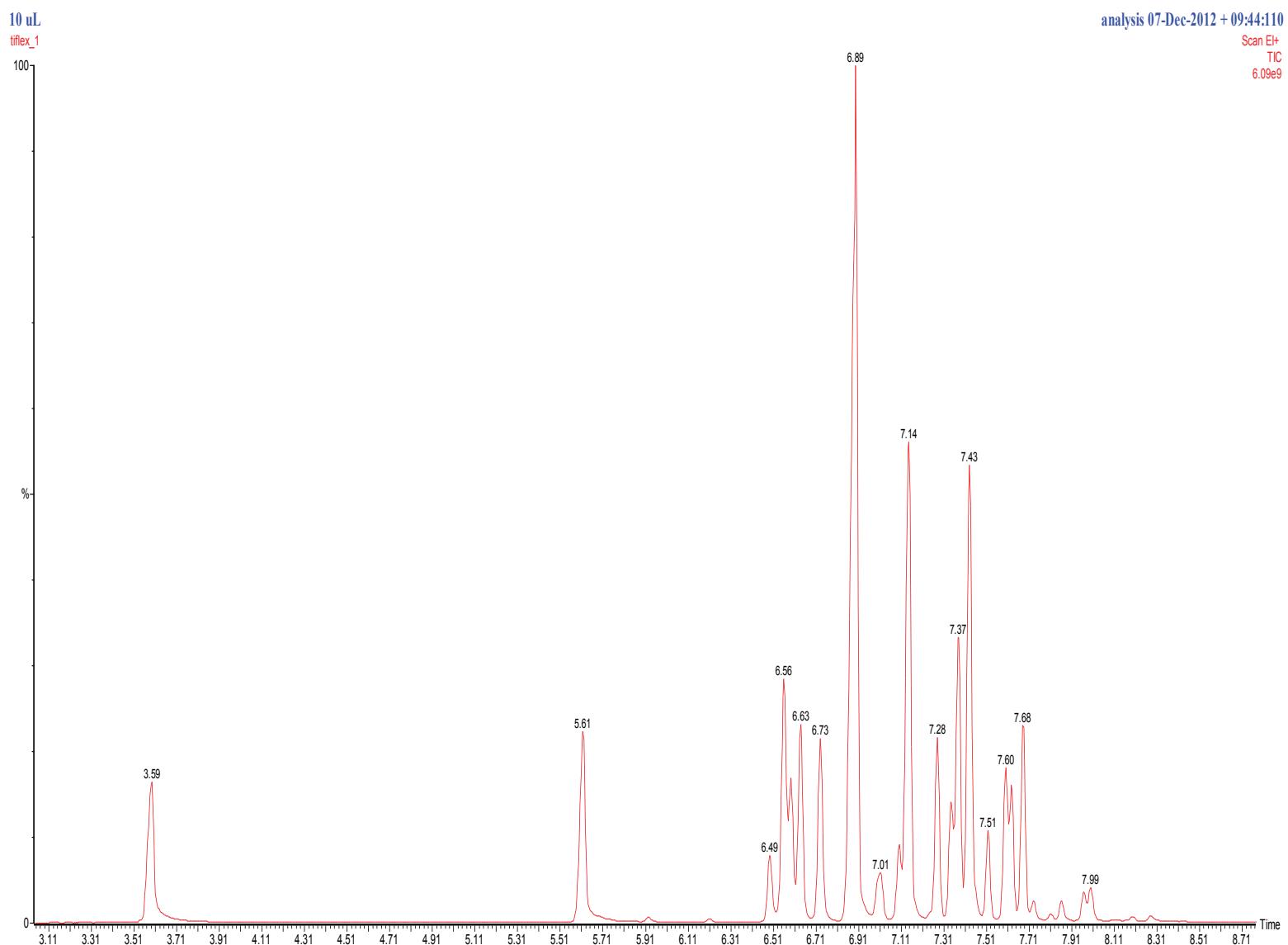
Figure 1: Chromatogram of Tiflex using the ATD-GC-MS.

In addition, another research group from ICARE (OH group, Ph Dagaut et al.) also involved in the Dispatmo project have analyzed the Tiflex sample and determined the chemical composition of Tiflex and the percentage of its constituents using gas chromatography (DB624 column and FID detector) coupled to a mass spectrometer. The identification and quantification of the major constituents is shown in table 2 and figure 2.

Table 2: Identification and quantification of the main Tiflex constituents (>2%) using GC-MS.[1]

Compound	%
1-methoxy-2-propanol	26,8
1,2,4-trimethylbenzene	19,1
1-methoxy-2-propyl acetate	18,8
1,2,3-trimethylbenzene	6,4
1,4-diethylbenzene	4,6
1-methyl-3-propylbenzene	4,5
1-ethyl-3-methylbenzene	3,3
1,3,5-trimethylbenzene	2,7
1-ethyl-2-methylbenzene	2,7
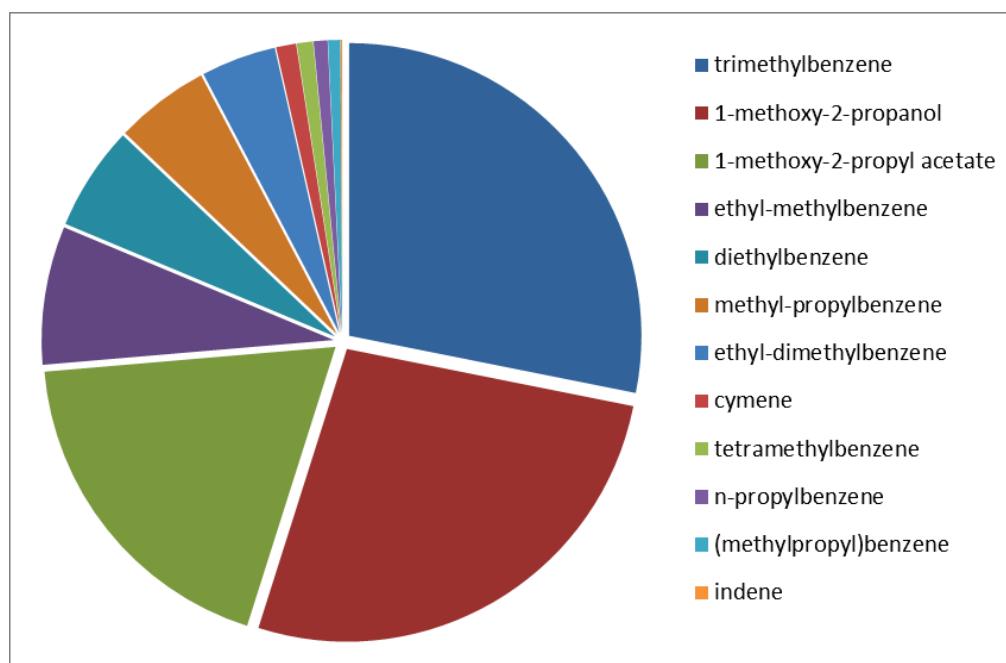
Figure 2: Identification and quantification of the Tiflex constituents after grouping the isomers.[1]

Annex II

Chemicals and materials

The chemicals used in the current study were commercially available with stated purities and are displayed in the following table.

Table 3: Materials used in this study, their stated purities and manufacturers.

Material	CAS	Purity (%)	Supplier
MPA	108-65-6	≥99.5	Sigma-Aldrich
2MBA	1173168-18-7	>97.0	TCI
3MBA	4435-53-4	>99.0	TCI
MEA	110-49-6	>98.0	TCI
EEA	111-15-9	>98.0	TCI
n-PA	628-63-7	≥99.0	Sigma-Aldrich
methyl formate	107-31-3	≥99.0	Fluka
acetic acid	64-19-7	≥99.7	Sigma-Aldrich
acetic anhydride	108-24-7	≥99.5	Fluka
1-pentanol	71-41-0	≥99.0	Fluka
n-heptane	142-82-5	≥99.5	Fluka
1-3 dioxane	505-22-6	>98.0	TCI
1-propanol	71-23-8	≥99.0	Fluka
1-butanol	71-36-3	≥99.8	Sigma-Aldrich
Cyclohexane	110-82-7	≥99.5	Sigma-Aldrich
n-pentane	109-66-0	≥99.5	Sigma-Aldrich
Br_2	7726-95-6	≥99.99	Sigma-Aldrich
1,3-dioxolane	646-06-0	≥99.0	Fluka
H_2O_2	7722-84-1	35 wt	Alfa Aesar
		60 wt	Elf Atochem
He	7440-59-7	>99.9995%	AlfaGaz
NO_2	10102-44-0	≥ 99%	AlfaGaz
Cl_2	7782-50-5	>99.5%	AlfaGaz
H_2	1333-74-0	>99.998%	AlfaGaz
NO	10102-43-9	0.997±0.02 mol-% in N_2	Air Liquide

Annex III
Emission lines of a Deuterium and a Zinc lamp

D_2 lamp emit an almost continuous spectrum of light ranging from the main UV wavelengths of 190 nm - 400 nm to the visible spectral range (800 nm) as shown in figure 3, while Zn lamp has major UV emission lines at 213.8 nm, 307.6 nm, 330.3 nm (figure 4).
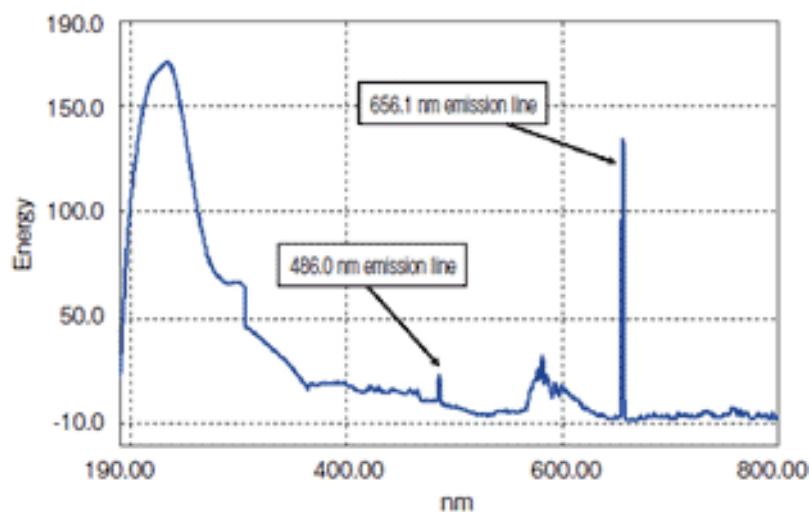

**Figure 3: Emission Lines of a Deuterium Lamp[2]**
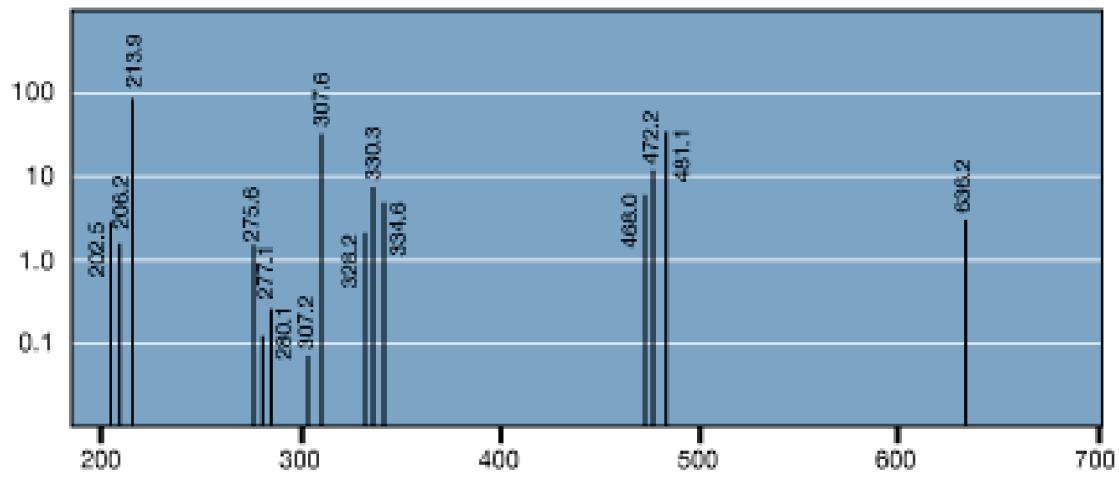
Figure 4: Emission Lines of a Zinc Lamp[3]

Annex IV

Mass Spectra of MPA, 2MBA and 3MBA

The mass spectra of MPA, 2MBA and 3MBA are displayed in figure 5. They were collected employing an Automated Thermal Desorption Gas Chromatography – Mass Spectrometer (GC-MS Clarus 600C coupled with ATD 150 from Perkin Elmer). The horizontal axis of each spectrum corresponds to the m/z ratio, while on the vertical axis the relative abundance of each ion detected is presented. On this scale, the most abundant ion, called the base peak, is set to 100%, and all other peaks are recorded relative to this value. For comparison purposes, in figure 6 the reference mass spectra of MPA and 3MBA listed in the NIST mass library are also given.[4, 5] Concerning 2MBA, there is no reference spectrum in the NIST library.
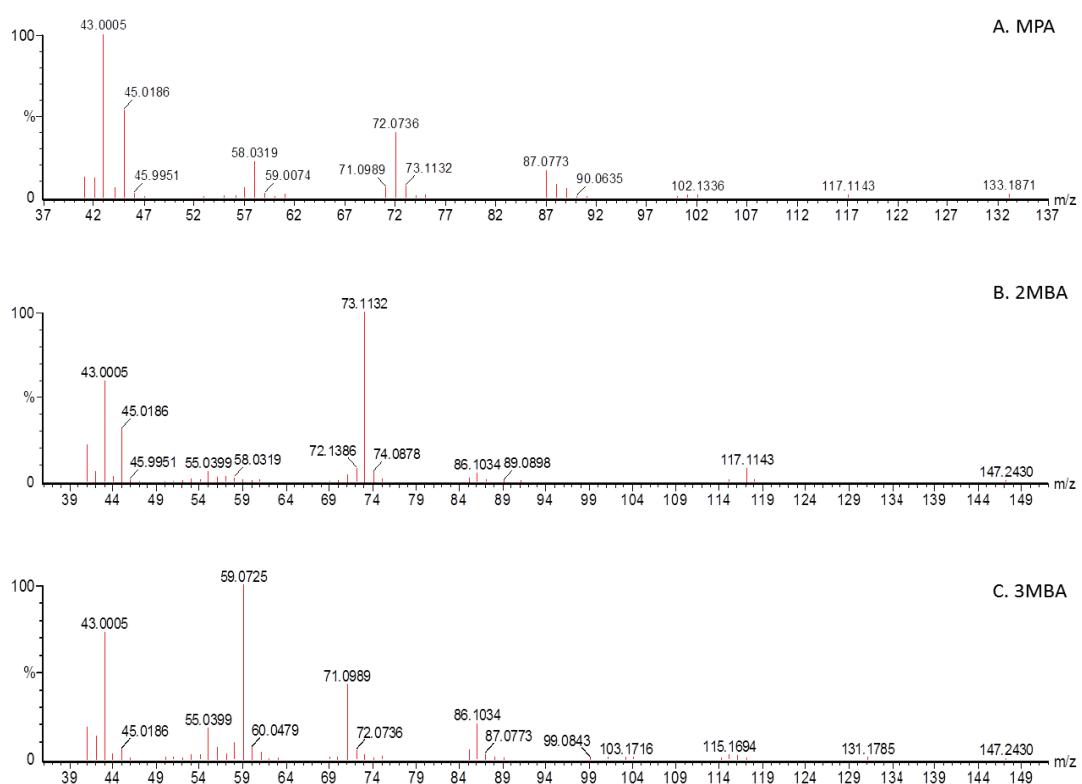
Figure 5: Mass spectra of A) MPA, B) 2MBA and C) 3MBA using the ATD-GC-MS.

182
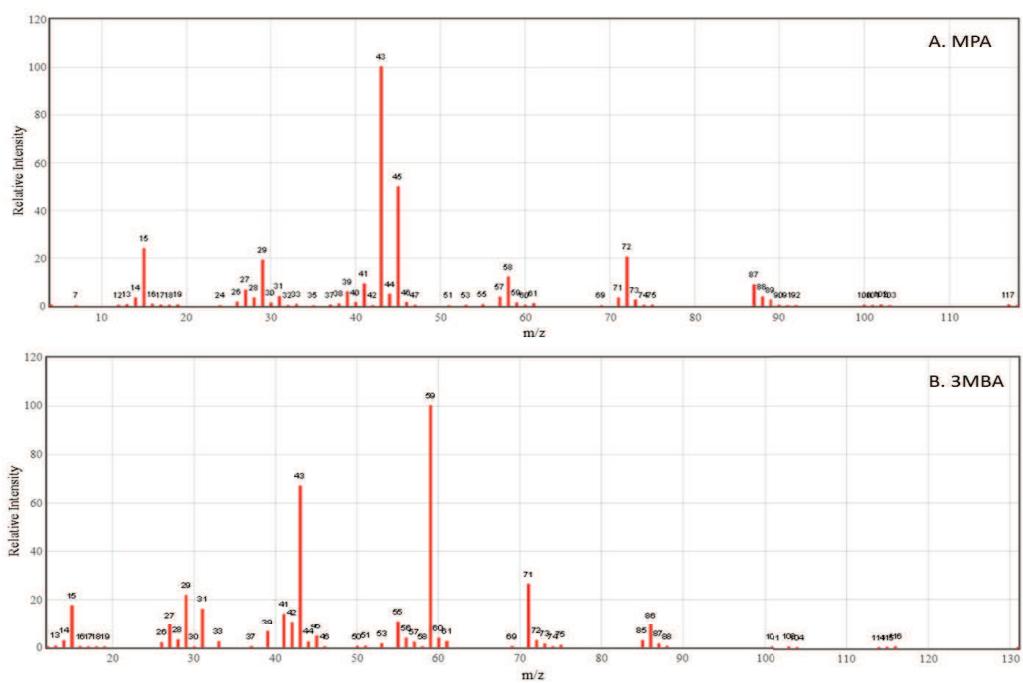
Figure 6: Mass spectrum of A) MPA, B) 3MBA given in the NIST mass spectra library.[4, 5]

Annex V

Estimation of OH reaction rate coefficients using Structure Activity Relationship (SAR)

Estimation method procedure in H-atom abstraction

The most common way to estimate rate coefficients for the gas-phase reaction of OH radical with organic compounds is through a structure activity relationship (SAR). This approach is described by Atkinson et al. (1982, 1984), it has been modified and up dated a number of times by Atkinson (1986 and 1987)[6,7], Kwok and Atkinson (1995)[8] and Bethel et al. (2001)[9]. This estimation method provides good agreement, generally to within a factor of 2, between experimentally measured and calculated rate constants.

As discussed by Atkinson[6], the calculation of H-atom abstraction rate constants from C-H and O-H bonds is based on the estimation of group rate constants for H-atom abstraction from $-CH_3$, $-CH_2-$, $>CH$ - and -OH groups. The rate constants for H-atom abstraction from $-CH_3$, - CH_2- and $>CH-$ groups depend on the identity of the substituents attached to these groups, with

$k(CH_3-X) = k_{prim} \times F(X)$

(1)

$k(X-CH_2-Y) = k_{sec} \times F(X) \times F(Y)$

(2)

$k(X-CH (Y)(Z)) = k_{tert} \times F(X) \times F(Y) \times F(Z)$

(3)

where k_{prim}, k_{sec}, and k_{tert} are the group rate coefficients for H-atom abstraction from $-CH_3$, $-CH_2-$ and $>CH-$ groups, respectively, for a "standard" substituent, and F(X), F(Y) and F(Z) are the substituent factors for the substituent groups X, Y and Z, respectively.

From a simultaneous fit of all the available data for the alkanes as a function of temperature, Kwok and Atkinson obtained the following group rate coefficients at 298 K, in units of 10^{-12} cm^3 molecule^{-1} s^{-1}.

k_{prim}=0.136 k_{sec} = 0.934 k_{tert} =1.94

The substituent factors F(X) obtained for the various substituent groups were also derived by simultaneously fitting a large number of rate coefficients and are given in table 4.

Table 4: *Example of substituent factors F(X) for OH abstraction reactions of alkanes and oxygenated compounds at 298 K.*[8]

Group	Factor
-CH$_3$	1.00
-CH$_2$-	1.23
-CH<	1.23
-OCH$_2$-R	8.4
-OCH$_3$	8.4
-OC(O)-R	1.6
-(O)CO-R	0.74

The total rate coefficient is calculated by the sum of the group rate coefficients of the molecule.

$$k_{tot}= \Sigma \ [k(CH_3\text{-}X) +k(X\text{-}CH_2\text{-}Y) + k(X\text{-}CH \ (Y)(Z))] \hspace{2cm} (4)$$

by using the equations 1,2 and 3, k_{tot} can be estimated by the following expression:

$$k_{tot} = \Sigma \ [k_{prim} \times F(X) + k_{sec} \times F(X) \times F(Y) + k_{tert}\times F(X) \times F(Y) \times F(Z)] \hspace{1cm} (5)$$

k_{OH} estimation by using SAR and possibility of the abstraction sites

a) 1-methoxy-2-propyl acetate (MPA):

CH$_3$ – O –**CH$_2$** – CH (CH$_3$) – O – C (O) – CH$_3$

Since there are five different positions of H-atom abstraction, k_{tot} consists of five rate coefficients.

k_{tot} = k(CH$_3$-X) + k((X-CH$_2$-Y) + k((X-CH(Y)(Z)) + k(CH$_3$-X) + k(CH$_3$-X)

k_{tot} = k_{prim} × F(-OCH$_2$-R) + k_{sec} × F(CH$_3$-O-) × F(-CH<) + k_{tert} × F(R-CH$_2$-) × F(-O-C(O)-R) × F(-CH$_3$) + k_{prim} × F(-CH<) + k_{prim} × F(R-OC(O)-)

k_{tot} = 1.36 × 10^{-13} × 8.4 + 9.34 × 10^{-13} × 8.4 × 1.23 + 1.94 × 10^{-12} × 1.23 × 1.6 × 1.00 + 1.36 × 10^{-13} × 1.23 + 1.36 × 10^{-13} × 0.74

k_{tot} = 11.424 × 10^{-13} + 96.501 × 10^{-13} + 3.818 × 10^{-13} + 1.673 × 10^{-13} + 1.006 × 10^{-13}

k_{tot} = 1.14 × 10^{-11} cm^3 molecule^{-1} s^{-1}

The estimation method can show the abstraction possibility for each C-H bond derived from the five rate coefficients.

k (H-abstraction from CH$_3$ − O −) = 11.424 × 10^{-13}, thus 9.99 % of the total rate coefficient

k (H-abstraction from O −CH$_2$ −) = 96.501 × 10^{-13}, thus 84.35 % of the total rate coefficient

k (H-abstraction from − CH −) = 3.818 × 10^{-13}, thus 3.34 % of the total rate coefficient

k (H-abstraction from − (CH$_3$)) = 1.673 × 10^{-13}, thus 1.46 % of the total rate coefficient

k (H-abstraction from − CH$_3$) = 1.006 × 10^{-13}, thus 0.88 % of the total rate coefficient

b) 2-methoxy-butyl acetate (2MBA):
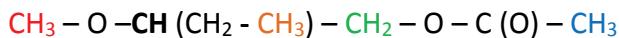
CH$_3$ − O −**CH** (CH$_2$ - CH$_3$) − CH$_2$ − O − C (O) − CH$_3$

Since there are six different positions of H-atom abstraction, k_{tot} consists of six rate coefficients.

k_{tot} = k(CH$_3$-X) + k((X-CH(Y)(Z)) + k((X-CH$_2$-Y) + k(CH$_3$-X) + k((X-CH$_2$-Y) + k(CH$_3$-X)

k_{tot} = k_{prim} × F(-OCH<) + k_{tert} × F(R-CH$_2$-) × F(-O-CH$_3$) × F(-CH$_2$-R) + k_{sec} × F(CH$_3$-) × F(-CH<) + k_{prim} × F(-CH$_2$-) + k_{sec} × F(-OC(O)-R) × F(-CH<) + k_{prim} × F(R-OC(O)-)

k_{tot} = 1.36 × 10^{-13} × 8.4 + 1.94 × 10^{-12} × 8.4 × 1.23 × 1.23 + 9.34 × 10^{-13} × 1.00 × 1.23 + 1.36 × 10^{-13} × 1.23 + 9.34 × 10^{-13} × 1.6 × 1.23 + 1.36 × 10^{-13} × 0.74

k_{tot} = 11.424 × 10^{-13} + 246.542 × 10^{-13} + 11.488 × 10^{-13} + 1.673 × 10^{-13} + 18.381 × 10^{-13} + 1.006 × 10^{-13}

k_{tot} = 2.90 × 10^{-11} cm^3 molecule^{-1} s^{-1}

The estimation method can show the abstraction possibility for each C-H bond derived from the six rate coefficients.

k (H-abstraction from CH$_3$ − O −) = 11.424 × 10^{-13}, thus 3.93 % of the total rate coefficient

k (H-abstraction from O −CH −) = 246.542 × 10⁻¹³, thus 84.87 % of the total rate coefficient

k (H-abstraction from − CH₂ −) = 11.488 × 10⁻¹³, thus 3.95 % of the total rate coefficient

k (H-abstraction from − (CH₃)) = 1.673 × 10⁻¹³, thus 0.58 % of the total rate coefficient

k (H-abstraction from − CH₂ −) = 18.381 × 10⁻¹³, thus 6.33 % of the total rate coefficient

k (H-abstraction from − CH₃) = 1.006 × 10⁻¹³, thus 0.35 % of the total rate coefficient

c) 3-methoxy-butyl acetate (3MBA):
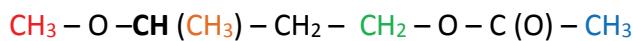
$CH_3 - O - \textbf{CH} (CH_3) - CH_2 - CH_2 - O - C (O) - CH_3$

Since there are six different positions of H-atom abstraction, k_{tot} consists of six rate coefficients.

k_{tot} = k(CH₃-X) + k((X-CH(Y)(Z)) + k(CH₃-X) + k((X-CH₂-Y) + k((X-CH₂-Y) + k(CH₃-X)

k_{tot} = k_{prim} × F(-OCH<) + k_{tert} × F(R-CH₂-) × F(-O-CH₃) × F(-CH₃) + k_{prim} × F(-CH<) + k_{sec} × F(-CH₂-) × F(-CH<) + k_{sec} × F(-OC(O)-R) × F(-CH₂-) + k_{prim} × F(R-OC(O)-)

k_{tot} = 1.36 × 10⁻¹³ × 8.4 + 1.94 × 10⁻¹² × 8.4 × 1.23 × 1.00 + 1.36 × 10⁻¹³ × 1.23 + 9.34 × 10⁻¹³ × 1.23 × 1.23 + 9.34 × 10⁻¹³ × 1.6 × 1.23 + 1.36 × 10⁻¹³ × 0.74

k_{tot} = 11.424 × 10⁻¹³ + 200.441 × 10⁻¹³ + 1.673 × 10⁻¹³ + 14.130 × 10⁻¹³ + 18.381 × 10⁻¹³ + 1.006 × 10⁻¹³

k_{tot} = 2.47 × 10⁻¹¹ cm³ molecule⁻¹ s⁻¹

The estimation method can show the abstraction possibility for each C-H bond derived from the six rate coefficients.

k (H-abstraction from CH₃ − O −) = 11.424 × 10⁻¹³, thus 4.62 % of the total rate coefficient

**k (H-abstraction from O −CH −) = 200.441 × 10⁻¹³, thus 81.13 % of the total rate coefficient**

k (H-abstraction from − CH₃) = 1.673 × 10⁻¹³, thus 0.68 % of the total rate coefficient

k (H-abstraction from − CH₂−) = 14.130 × 10⁻¹³, thus 5.72 % of the total rate coefficient

k (H-abstraction from − CH_2 −) = 18.381 × 10^{-13}, thus 7.44 % of the total rate coefficient

k (H-abstraction from − CH_3) = 1.006 × 10^{-13}, thus 0.41 % of the total rate coefficient

$CH_3 − O −\textbf{CH} (CH_3) − CH_2 − CH_2 − O − C (O) − CH_3$

d) methoxy-ethyl acetate (MEA):

$CH_3 - C(O) − O - CH_2 - CH_2 - O - CH_3$
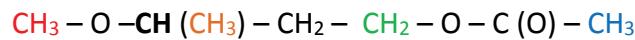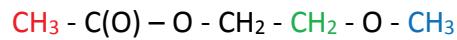
There are four different positions of H-atom abstraction; consequently k_{tot} consists of four rate coefficients.

k_{tot} = k(CH_3-X) + k((X-CH_2-Y) + k((X-CH_2-Y) + k(CH_3-X)

k_{tot} = k_{prim} × F(-C(O)-O-R) + k_{sec} × F(R-C(O)-O-) × F(-CH_2-) + k_{sec} × F(R-CH_2-) × F(-O-CH_2 -R) + k_{prim} × F(-O-R)

k_{tot} = 1.36 × 10^{-13} × 0.74 + 9.34 × 10^{-13} × 1.6 × 1.23 + 9.34 × 10^{-13} × 1.23 × 8.4 + 1.36 × 10^{-13} × 8.4

k_{tot} = 1.006 × 10^{-13} + 18.381 × 10^{-13} + 96.501 × 10^{-13} + 11.424 × 10^{-13}

k_{tot} = 1.27 × 10^{-11} cm^3 $molecule^{-1}$ s^{-1}

The estimation method can show the abstraction possibility for each C-H bond.

k (H-abstraction from CH_3 - C(O) − O -) = 1.006 × 10^{-13}, thus 0.79 % of the total rate coefficient

k (H-abstraction from - C(O) − O - CH_2 −) = 18.381 × 10^{-13}, thus 14.45 % of the total rate coefficient

k (H-abstraction from - CH_2 - O −) = 96.501 × 10^{-13}, thus 77.63 % of the total rate coefficient

k (H-abstraction from − CH_3) = 11.424 × 10^{-13}, thus 8.97 % of the total rate coefficient

e) 2-ethoxy-ethyl acetate (EEA):
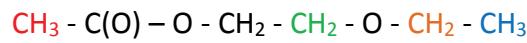
$CH_3 - C(O) − O - CH_2 - CH_2 - O - CH_2 - CH_3$

There are five different positions of H-atom abstraction; consequently k_{tot} consists of five rate coefficients.

k_{tot} = k(CH_3-X) + k((X-CH_2-Y) + k((X-CH_2-Y) + k(X-CH_2-Y) + k(CH_3-X)

k_{tot} = k_{prim} × F(-C(O)-O-R) + k_{sec} × F(R-C(O)-O-) × F(-CH$_2$-) + k_{sec} × F(R-CH$_2$-) × F(-O-CH$_2$ -R) + k_{sec} × F(R-CH$_2$-O-) × F(CH$_3$-) + k_{prim} × F(R-CH$_2$-)

k_{tot} = 1.36×10^{-13} × 0.74 + 9.34×10^{-13} × 1.6 × 1.23 + 9.34×10^{-12} × 1.23 × 8.4 + 9.34×10^{-13} × 8.4 × 1.00 + 1.36×10^{-13} × 1.23

k_{tot} = 1.006×10^{-13} + 18.381×10^{-13} + 96.501×10^{-13} + 78.456×10^{-13} + 1.673×10^{-13}

k_{tot} = 1.96×10^{-11} cm^3 molecule^{-1} s^{-1}

The estimation method can show the abstraction possibility for each C-H bond.

k (H-abstraction from CH$_3$ - C(O) – O -) = 1.006×10^{-13}, thus 0.51 % of the total rate coefficient

k (H-abstraction from - C(O) – O - CH$_2$ –) = 18.381×10^{-13}, thus 9.38 % of the total rate coefficient

k (H-abstraction from - CH$_2$ - O –) = 96.501×10^{-13}, thus 49.23 % of the total rate coefficient

k (H-abstraction from - O - CH$_2$ –) = 78.456×10^{-13}, thus 40.08 % of the total rate coefficient

k (H-abstraction from – CH$_3$) = 1.673×10^{-13}, thus 0.85 % of the total rate coefficient

f) n-pentyl acetate (n-PA):

CH$_3$ - C(O) – O - CH$_2$ - CH$_2$ - CH$_2$ - CH$_2$ - CH$_3$

There are six different positions of H-atom abstraction; consequently k_{tot} consists of six rate coefficients.

k_{tot} = k(CH$_3$-X) + k((X-CH$_2$-Y) + k((X-CH$_2$-Y) + k((X-CH$_2$-Y) + k(X-CH$_2$-Y) + k(CH$_3$-X)

k_{tot} = k_{prim} × F(-C(O)-O-R) + k_{sec} × F(R-C(O)-O-) × F(-CH$_2$-) + k_{sec} × F(R-CH$_2$-) × F(-CH$_2$ -R) + k_{sec} × F(R-CH$_2$-) × F(-CH$_2$ -R) + k_{sec} × F(R-CH$_2$-) × F(CH$_3$-) + k_{prim} × F(R-CH$_2$-)

k_{tot} = 1.36×10^{-13} × 0.74 + 9.34×10^{-13} × 1.6 × 1.23 + 9.34×10^{-12} × 1.23 × 1.23 + 9.34×10^{-12} × 1.23 × 1.23 + 9.34×10^{-13} × 1.23 × 1.00 + 1.36×10^{-13} × 1.23

k_{tot} = 1.006×10^{-13} + 18.381×10^{-13} + 14.130×10^{-13} + 14.130×10^{-13} + 11.488×10^{-13} + 1.673×10^{-13}

k_{tot} = 0.61×10^{-11} cm^3 molecule^{-1} s^{-1}

The estimation method can show the abstraction possibility for each C-H bond.

k (H-abstraction from CH_3 - C(O) – O -) = 1.006×10^{-13}, thus 1.65 % of the total rate coefficient

k (H-abstraction from - C(O) – O - CH_2 –) = 18.381×10^{-13}, thus 30.23 % of the total rate coefficient

k (H-abstraction from - CH_2 - O –) = 14.130×10^{-13}, thus 23.24 % of the total rate coefficient

k (H-abstraction from - C(O) – O - CH_2 –) = 14.130×10^{-13}, thus 23.24 % of the total rate coefficient

k (H-abstraction from - O - CH_2 –) = 11.488×10^{-13}, thus 18.89 % of the total rate coefficient

k (H-abstraction from – CH_3) = 1.673×10^{-13}, thus 2.75 % of the total rate coefficient

g) acetic anhydride

CH_3 – C (O) – O – C(O) – (CH_3)
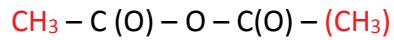
$k_{tot} = 2 \times k(CH_3\text{-X})$

$k_{tot} = 2 \times k_{prim} \times F(\text{-O-C(O)-R})$

$k_{tot} = 2.01 \times 10^{-13}$ cm^3 molecule^{-1} s^{-1}

Structures of the OVOCs

Density Functional Theory (DFT) calculations were conducted to specify the conformer structures. Geometry optimization calculations were performed at the B3LYP/6-31G(d) level of theory using Gaussian 09 program suite.

Table 5: 3D structures of the studied compounds.

Compound	Formula	3D structure
1-methoxy-2-propyl acetate (MPA)	$CH_3OCH_2CH(CH_3)OC(O)CH_3$	
2-methoxy butyl acetate (2MBA)	$CH_3OCH(CH_2CH_3)CH_2OC(O)CH_3$	
3-methoxy butyl acetate (3MBA)	$CH_3OCH(CH_3)CH_2CH_2OC(O)CH_3$	
2-Methoxy ethyl acetate (MEA)	$CH_3OCH_2CH_2OC(O)CH_3$	

2-Ethoxy ethyl acetate (EEA)	$CH_3CH_2OCH_2CH_2OC(O)CH_3$	
n-pentyl acetate (n-PA)	$CH_3CH_2CH_2CH_2CH_2OC(O)CH_3$	
methyl formate	$CH_3OC(O)H$	
Acetic acid (ethanoic acid)	$CH_3C(O)OH$	
Acetic anhydride	$CH_3C(O)O(O)CCH_3$	
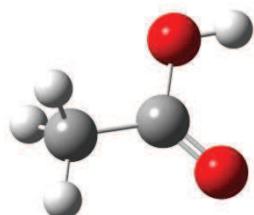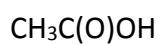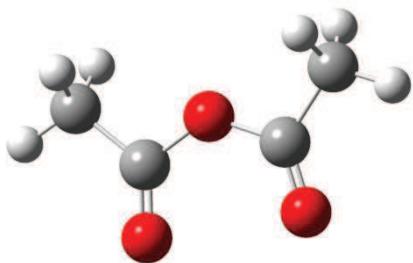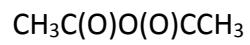
Annex VII

Uncertainty analysis

UV absorption measurements

The determination of the OVOC concentration represents the largest source of uncertainty in case of the UV absorption cross section measurements. In particular, the error on temperature (1%) and the OVOC pressure in the double wall optical cell (ca. 8%) were used to determine the overall uncertainty to OVOC concentration, estimated to be ca. 10%. The total uncertainty to σ values, including the standard deviation (1σ) of the beer-lambert linear fit, and the uncertainty of the intensity was ~11%.

PLP-LIF

The precision (2σ) and reproducibility in the PLP-LIF determinations of rate coefficient was high with typical ~5% fit precision uncertainties. The determination of the OVOC concentration in the LIF reactor and possible reactive sample impurities represent the largest potential sources of systematic error. The measurements of the flow, the mixture preparation, the pressure and the temperature were used to determine the concentration of the OVOC. The uncertainty in the mixture preparation was about 4-5%, in flow was about 2%, while in pressure and temperature measurements it made a minor contribution of 1 and 3%, respectively. Consequently, the uncertainty in the OVOC concentration was lower than 7% and a safe upper limit of 10% was considered. The set of the kinetic measurements were carried out using at least two different mixtures of the OVOC to eliminate systematic and random errors to the mixture preparation. Therefore, the overall uncertainty in k(T) determination including the 2σ precision of the measurements is given by the expression $(uncertainty)^2 = (2\sigma\ precision)^2 + (systematic\ errors)^2$ was always lower than ~15%.

ASC-FID

In case of the relative rate measurements in the ASC, the major source of absolute uncertainty in the k_{OVOC} determination was the uncertainty in the reference rate coefficient, k_{ref}, ranging between 10-12%. The precision (2σ) of the relative rate measurements, i.e. k_{OVOC}/k_{ref} ratio was better than 2%. The two reference compounds used for the RR measurements yield k_{OVOC} values with a typical uncertainty within ∼6%. Therefore, the absolute uncertainty in the relative rate determination of k_{OVOC} is estimated to be ∼15%.

FFT-QMS

The determination of the OVOC concentration in the flow tube represents the largest potential sources of systematic error in the FFT-QMS. The uncertainty to the concentration of the OVOC includes those of (i) the calibration factor (ca. 9%), (ii) the flow (ca. 3%), (iii) the pressure (2%) and (iv) temperature (2%). The quadrature sum of the above individual errors provides the total uncertainty to the OVOC concentration, being about 10%. Therefore, the overall uncertainty in k(T) determination including the 2σ precision of the measurements (ca. 10%) is given by the expression (uncertainty)^2 = (2σ precision)^2 + (systematic errors)^2 and was around 19 %. However, it should be noted that in a few kinetic runs due to experimental difficulties or possible random contributions the error of the precision of the fit was around 20% and the total uncertainty raised to approximately 22%.

In case of the relative rate measurements using FFT, the major source of absolute uncertainty in the k_{OVOC} determination was the uncertainty in the reference rate coefficient, k_{ref} (10-12%). The precision (2σ) of the relative rate measurements, i.e. k_{OVOC}/k_{ref} ratio was about 3%. Therefore, the absolute uncertainty in the relative rate measurement in FFT-QMS has a safe limit of ∼15%.

References

1.   FENARD, Y. Etude expérimentale et modélisation de l'oxydation de composés organiques à des fins de sécurité industrielle. Cinétique d'oxydation des butènes (1-, cis-2-, trans-2- et iso-). University of Orleans, Orleans, 2014.

2.   Corporation, S. Instrument Validation and Inspection Methods : SHIMADZU (Shimadzu Corporation). http://www.shimadzu.com/an/uv/support/fundamentals/validation.html

3.   Incorporated, B. BHK Incorporated. http://www.bhkinc.com/index.cfm?action=products

4.   NIST 1-Methoxy-2-propyl acetate. http://webbook.nist.gov/cgi/cbook.cgi?ID=108-65-6&Units=SI&cMS=on

5.   NIST 1-Butanol, 3-methoxy-, acetate. http://webbook.nist.gov/cgi/cbook.cgi?ID=4435-53-4&Units=SI&cMS=on

6.   Atkinson, R., Kinetics and mechanisms of the gas-phase reactions of the hydroxyl radical with organic compounds under atmospheric conditions. *Chemical Reviews* **1986,** *86*, (1), 69-201.

7.   Atkinson, R., A structure-activity relationship for the estimation of rate constants for the gas-phase reactions of OH radicals with organic compounds. *International Journal of Chemical Kinetics* **1987,** *19*, (9), 799-828.

8.   Kwok, E. S. C.; Atkinson, R., Estimation of hydroxyl radical reaction rate constants for gas-phase organic compounds using a structure-reactivity relationship: An update. *Atmospheric Environment* **1995,** *29*, (14), 1685-1695.

9.   Bethel, H. L.; Atkinson, R.; Arey, J., Kinetics and products of the reactions of selected diols with the OH radical. *International Journal of Chemical Kinetics* **2001,** *33*, (5), 310-316.

**Publication in "The Journal of Physical Chemistry"**

Atmospheric Chemistry of 1-Methoxy 2-Propyl Acetate: UV Absorption Cross Sections, Rate Coefficients, and Products of Its Reactions with OH Radicals and Cl Atoms

Antonia G. Zogka, Abdelwahid Mellouki,* Manolis N. Romanias, Yuri Bedjanian, Mahmoud Idir, Benoit Grosselin, and Véronique Daële

Institut de Combustion, Aérothermique, Réactivité et Environnement (ICARE), CNRS/OSUC, 45071 Orléans Cedex 2, France

ABSTRACT: The rate coefficients for the reactions of OH and Cl with 1-methoxy 2-propyl acetate (MPA) in the gas phase were measured using absolute and relative methods. The kinetic study on the OH reaction was conducted in the temperature (263−373) K and pressure (1−760) Torr ranges using the pulsed laser photolysis-laser-induced fluorescence technique, a low pressure fast flow tube reactor-quadrupole mass spectrometer, and an atmospheric simulation chamber/GC-FID. The derived Arrhenius expression is $k_{MPA+OH}(T) = (2.01 \pm 0.02) \times 10^{-12} \exp[(588 \pm 123/T)]$ cm^3 molecule^{-1} s^{-1}. The absolute and relative rate coefficients for the reaction of Cl with MPA were measured at room temperature in the flow reactor and the atmospheric simulation chamber, which led to $k_{(Cl+MPA)} = (1.98 \pm 0.31) \times 10^{-10}$ cm^3 molecule^{-1} s^{-1}. GC-FID, GC-MS, and FT-IR techniques were used to investigate the reaction mechanism in the presence of NO. The products formed from the reaction of MPA with OH and their yields were methyl formate (80 ± 7.3%), acetic acid (50 ± 4.8%), and acetic anhydride (22 ± 2.4%), while for Cl reaction, the obtained yields were 60 ± 5.4, 41 ± 3.8, and 11 ± 1.2%, respectively, for the same products. The UV absorption cross section spectrum of MPA was determined in the wavelength range 210−370 nm. The study has shown no photolysis of MPA under atmospheric conditions. The obtained results are used to derive the atmospheric implication.
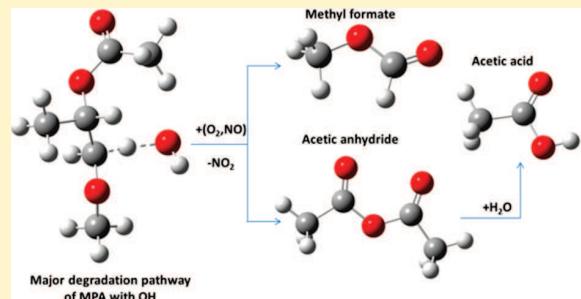
1. INTRODUCTION

Large quantities of oxygenated volatile organic compounds (OVOCs) are present in the atmosphere as a result of direct and indirect anthropogenic and biogenic emissions. These compounds are of environmental importance because they significantly influence the chemistry of the atmosphere, even when they are present at very low concentrations.[1] Photolysis and reactions with the oxidants, mainly with the reactive free hydroxyl radicals (OH), constitute the most dominant removal processes for the majority of OVOCs and determine their atmospheric lifetimes.[2,3] Nevertheless, the reaction of chlorine atoms with VOCs is considered of potential relevance in the marine troposphere, as well as in some industrial areas and in the continental regions where significant chlorine atom concentration may be present.[4,5]

The OVOC of interest in this work, 1-methoxy 2-propyl acetate (MPA, CH$_3$C(O)OCH(CH$_3$)CH$_2$OCH$_3$), is directly emitted into the atmosphere through numerous applications. It is widely used in coatings, industry of metals, plastics, and automotive, in printing, as a solvent for resins and dyes, and as a preservative in wood impregnation, varnishes, or stain removers.[5] MPA can be found in 366 chemical products on American market.[6] It is worth noting that MPA concentration in most paints reaches up to 5−20%.[6,7] Consequently, the production volume of MPA in a global scale is considerably high, estimated to be in the range 1−5 Mtons/year.[6,7] For

example, its emissions in the UK for the years 2000 and 2010 are estimated to be 3.01 and 1.71 Ktons/year, respectively.[7,8] In addition, significant concentrations of MPA are expected to be present in indoor environments. Indeed, Czajka and Pudliszak have reported that polyurethane lacquer coatings application to various wood species and to glass surfaces attribute high concentrations of MPA in the indoor air ranging approximately from 0.1 to 0.5 ppm after 48 h exposure.[8]

The current study aims at investigating the atmospheric degradation processes of MPA. The rate coefficient for the reaction of MPA with OH has been determined in the temperature range $T = 263−373$ K and three different pressures $P = 1$, 100, and 760 Torr using three complementary techniques, while that with Cl atoms has been measured at $T = 295 \pm 3$ K and $P = 1$ and 760 Torr employing two techniques. The OH and Cl initiated oxidation mechanisms are also studied, and the formation yields of the main products were measured. In addition, the UV absorption spectrum of MPA is reported in 200−370 nm range. To the best of our knowledge, this is the first experimental kinetic and mechanistic study aiming at understanding the atmospheric fate of MPA in the atmosphere.

2. EXPERIMENTAL SECTION

2.1. UV Absorption Cross Sections Set up. UV−visible absorption cross section measurements of MPA were performed at 300 and 335 K in a double-walled Pyrex temperature-controlled absorption cell (100 cm long and 2.5 cm internal diameter) equipped with quartz windows.[9] The measurements were performed in the wavelength region 200−370 nm using deuterium (D_2) and zinc (Zn) lamps as UV−vis light sources. The collimated output of the lamp passed through the absorption cell and was detected by a spectrophotometer (Princeton Instrument, Inc. ACTON SP2300i) equipped with a triple grating monochromator. The grating used was 1200 grooves/ mm with a focal length of 300 and 0.2 nm resolution. The spectrophotometer was coupled to a camera Charge Coupled Device ROPER (PIXIS 1024 × 256 pixels). The wavelength scale was calibrated using emission lines from Zn lamp (213.8 nm) and Hg pen ray lamp (253.65, 296.73, 313.15, and 365.02 nm) and was accurate to 0.1 nm.

2.2. PLP-LIF. The absolute rate coefficients for the OH reaction with MPA were measured by the pulsed-laser photolysis/laser-induced fluorescence (PLP-LIF) technique. The experiments were carried out in the temperature range 263−373 K and at total pressure of approximately 100 Torr of He, using a Pyrex double-walled reaction cell. The experimental setup and the methodology used have been extensively described in previous publication from the group;[10] hence, the description given is limited herein. OH radicals were generated via the photolysis of H_2O_2 at $\lambda = 248$ nm using a KrF excimer laser. Their concentration was monitored by pulsed laser-induced fluorescence at various reaction times. A Nd:YAG-pumped frequency-doubled dye laser was used to excite the OH radical at $\lambda = 282$ nm and its fluorescence was detected by a photomultiplier tube fitted with a 309 nm narrow-band-pass filter. Typically, the fluorescence signal resulting from 200 probe laser shots was measured for 8−20 different delay times and averaged to generate OH concentration−time profiles over at least six lifetimes. MPA was diluted in He in a 10 L glass bulb and total pressure of about 700 Torr. The experiments were conducted using two or three different mixtures at each temperature, varied from 0.3 to 0.6% MPA/He. The MPA gas mixture, OH radical precursor (H_2O_2), and bath gas were flowed through the cell with a linear velocity ranging from 5 to 20 cm s^{-1}. The concentration of MPA was calculated from its mass flow rate, the temperature, and the pressure in the reaction cell.

2.3. FFT-QMS. The discharge fast flow tube reactor combined with a modulated molecular beam quadrupole mass spectrometer (FFT-QMS) was used for the absolute and relative measurements of the rate coefficients of the OH and absolute measurements of the Cl reactions with MPA. The experimental technique and the methodology were discussed in detail in previous publications from the group.[11,12]

The walls of the reactor and the injector were coated with halocarbon wax in order to minimize the heterogeneous loss of OH radicals and Cl atoms. OH radicals were generated through the fast reaction of hydrogen atoms with NO_2:[13]

$$H + NO_2 \rightarrow OH + NO$$

$$k_{298} = 1.47 \times 10^{-10} \text{ cm}^3 \text{ molecule}^{-1} \text{ s}^{-1} \qquad \text{(R1)}$$
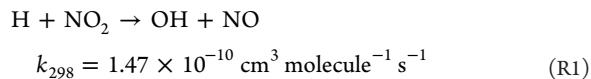
H atoms were produced in a microwave discharge of H_2/He mixtures. Reaction R1 was carried out in high excess of NO_2 ($[NO_2] = (0.7-1.0) \times 10^{14}$ molecules cm^{-3}) over H atoms in order to ensure their rapid and complete consumption.

Regarding Cl atoms, they were formed by the microwave discharge of a 5% Cl_2/He mixture.

As far as the absolute rate coefficient measurements were concerned, OH radicals and Cl atoms were detected by mass spectrometry as HOBr$^+$ ($m/z = 96/98$) and BrCl$^+$ at $m/z = 116$, respectively, after their rapid conversion by an excess of Br_2 ($[Br_2] = (3.5-5.1) \times 10^{13}$ molecules cm^{-3}), which was introduced at the end of the reaction zone, 5 cm upstream of the sampling cone of the mass spectrometer:[12,14]

$$OH + Br_2 \rightarrow HOBr + Br$$

$$k_{298} = 4.48 \times 10^{-11} \text{ cm}^3 \text{ molecule}^{-1} \text{ s}^{-1} \qquad \text{(R2)}$$

$$Cl + Br_2 \rightarrow BrCl + Br$$

$$k_{298} = 1.46 \times 10^{-10} \text{ cm}^3 \text{ molecule}^{-1} \text{ s}^{-1} \qquad \text{(R3)}$$
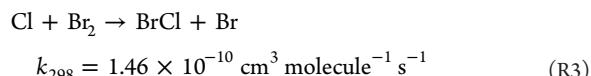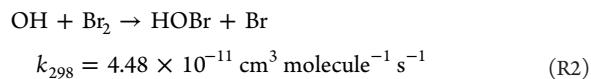
The chemical conversions of OH to HOBr and Cl to BrCl were also used for the measurement of the absolute concentrations of these species, considering that $[OH] = [HOBr] = \Delta[Br_2]$ and $[Cl] = [BrCl] = \Delta[Br_2]$. Thus, $[OH]$ and $[Cl]$ were determined from the consumed fraction of $[Br_2]$. In turn, the absolute concentrations of Br_2 were calculated from the measured flow rates of known Br_2/He mixtures. The possible influence of secondary chemistry on this method for HOBr and BrCl detection was discussed in detail in previous papers from this group.[12,15] MPA was detected by mass spectrometry using its fragment peaks at $m/z = 72$ ($CH_3OCH_2CHCH_3^+$) or $m/z = 45$ ($CH_3OCH_2^+$) since the sensitivity of the mass spectrometer to the parent peak ($m/z = 132$) was substantially lower ($I_{132} < 0.01 \times I_{72}$). It was verified that there were no reactant precursors or reaction product contributions at these peaks. All other species were detected at their parent peaks, $m/z = 160$ (Br_2^+), 98 (HOBr$^+$), 116 (BrCl$^+$), 46 (NO_2^+), 30 (NO$^+$). The absolute calibration of the mass spectrometer for MPA was performed by injecting known amounts of liquid MPA inside the flow tube with simultaneous recording of the mass peak intensity of MPA at $m/z = 72$. The integrated area of the mass spectrometric signals corresponding to a known total number of MPA molecules injected into the reactor allowed the determination of the calibration factor. Similar (within 10%) results were obtained when MPA was introduced into the reactor from a known MPA mixture with He, prepared in a calibrated volume, and its concentration was calculated from the measured flow rate.

2.4. Atmospheric Simulation Chamber. The conventional relative-rate method was used to measure the rate coefficients for the reactions of OH radicals and Cl atoms with MPA at 293 ± 2 K and atmospheric pressure ($P = 760$ Torr of purified air) in an atmospheric simulation chamber (ASC). The experimental setup for the kinetic and mechanistic study consisted of a 180 L atmospheric simulation chamber surrounded by six germicide lamps (Sylvania G30W) and six black lamps (Philips, TL 20W/05). They were all hosted in a wooden box with the internal faces covered with aluminum foil. The reactive OH and Cl species were produced via photolysis of H_2O_2 using 2−6 germicide lamps emitting at 254 nm and Cl_2 using the 2−4 black lamps with maximum irradiance at 365 nm. A gas chromatograph equipped with a DB-1 capillary column and a flame ionization detector (GC-FID, Star 3800 CX, Varian) was used for quantitative analysis of the reactants and products. The column was operated over the temperature range of 403−448 K, and helium was used as carrier gas. Gas samples were automatically collected from the chamber and introduced via a

heated sampling loop of 0.25 mL capacity to the gas chromatograph.

In order to perform a thorough mechanistic and product study, an automated thermal desorption gas chromatograph–mass spectrometer (GC-MS Clarus 600C coupled with ATD 150 from PerkinElmer) and a Fourier-transform infrared spectrometer (FT-IR, Nicolet Magna, IR 550) were additionally connected to the chamber for the detection of the chemical species involved. The mechanistic studies were performed in the presence of NO. Chromatographic separation was achieved by using a 30 m length Elite 5MS column (0.25 μm film thickness) operated at 433 K, using helium as carrier gas. The IR detector was a DTGS KBr and the infrared beam has an absorption path length of 10 m. The infrared spectra were collected within the range of 400–4000 cm^{-1} and correspond to the average of 100 scans recorded with resolution of 1 cm^{-1}.

2.5. Chemicals and Materials. The chemicals used in the current study were commercially available with stated purities: cyclohexane ($\geq$99.5%), MPA ($\geq$99.5%), pentane ($\geq$99%), acetic acid ($\geq$99.7%), and Br$_2$ ($\geq$99.99%), from Sigma-Aldrich, and 1,3-dioxolane ($\geq$99%), 1-pentanol ($\geq$99%), 1-propanol ($\geq$99%), acetic anhydride ($\geq$99.5%), and methyl formate ($\geq$99%), obtained from Fluka, were degassed by repeated freeze–pump–thaw cycles prior to their use. The 30% H$_2$O$_2$ solution in water for the relative rate measurements was supplied from Alfa Aesar, while for the absolute measurements in PLP-LIF system the 60% H$_2$O$_2$ solution was provided by Elf Atochem and concentrated by bubbling purified air through it for several days. He (>99.9995%), NO$_2$ ($\geq$99%), and Cl$_2$ (N25, H$_2$O < 40 ppm and HCl$_3$ < 20 ppm) from Air Liquide and NO from Air Liquide (0.997 $\pm$ 0.02 mol % in N$_2$) were used as supplied, while H$_2$ (>99.998%) from Air Liquide was diluted in He (10.85% in He).

3. RESULTS AND DISCUSSION

3.1. UV Absorption Cross Sections Measurements. The absorption cross sections of MPA were measured at T = 300 and 335 K using the Beer–Lambert's law, [eq 1]:

$$\sigma = -\frac{\ln(I(\lambda)/I_0(\lambda))}{LC} \tag{1}$$

where σ is the absorption cross section (cm^2 molecule^{-1}) at wavelength λ, L is the path length (cm), and C is the concentration (molecules cm^{-3}). I and I_0 are the measured light intensities at the exit of the absorption cell in the presence and absence of MPA, respectively. The measurements were conducted under static conditions in the wavelength region of 200–370 nm using a deuterium (D$_2$) lamp, while the transmitted light was detected by the spectrophotometer. Due to the low vapor pressure of MPA, the pressure range used was limited to 0.2–2.1 Torr, thus its concentration varied in the range (0.58–6.76) $\times$ 10^{16} molecules cm^{-3}. The obtained cross section spectrum for average concentrations of MPA at T = 300 K is displayed in Figure 1. Table 1 presents the cross section values averaged over 2 nm intervals. The estimated uncertainty of σ values was ca. 13% and includes the precision of the signal recorded, precision of the slope in a typical plot of $\ln(I_0/I)$ versus [MPA] as well as the uncertainty to the determination of MPA concentration. Furthermore, the inset in Figure 1 depicts the UV absorption cross section measurements at 216 nm for T = 300 and 335 K. The results showed that σ was temperature independent and that the values obtained were σ = (1.43 $\pm$ 0.17) $\times$ 10^{-19} and σ = (1.46 $\pm$ 0.18) $\times$ 10^{-19} cm^2 molecule^{-1} for

Figure 1. (A) UV absorption cross section spectrum of MPA ([MPA] = (2.5–6.8) $\times$ 10^{16} molecules cm^{-3}) between 200 and 300 nm at 300 K. (B) UV-absorption cross section of MPA at 216 nm was (1.43 $\pm$ 0.17) $\times$ 10^{-19} and (1.46 $\pm$ 0.18) $\times$ 10^{-19} cm^2 molecule^{-1} at 300 and 335 K, respectively.

Table 1. Absorption Cross Sections of MPA at the Wavelength Range 200–260 nm at 300 $\pm$ 2 K

| λ (nm)	σ (10^{-20} cm^2 molecule^{-1})
200	9.33
202	10.25
204	11.35
206	12.08
208	12.62
210	13.18
212	13.59
214	13.97
216	14.08
218	13.81
220	13.19
222	12.23
224	10.97
226	9.63
228	8.21
230	6.84
232	5.57
234	4.42
236	3.43
238	2.59
240	1.89
242	1.34
244	0.93
246	0.63
248	0.40
250	0.26
252	0.16
254	0.09
256	0.05
258	0.04
260	0.03

300 and 335 K, respectively. The errors bars in the inset of Figure 1 for MPA concentrations are 10%, considering the uncertainties in the temperature and pressure measurements, while the errors quoted on σ values include the standard deviation (1σ) of the slope and the estimated systematic uncertainties ([MPA], precision of the signal recorded).

In addition, a series of tests was performed to check the photolysis of MPA under our experimental conditions by irradiating known amount of MPA for about 1.5 h. No change was observed in the MPA concentration, which indicated that photolysis was negligible. A series of measurements at $\lambda = 216$ nm were conducted by adjusting a narrow band-pass filter using either D_2 or Zn lamps with the transmitted light detected by a photodiode or the spectrophotometer. The resulting cross section values under all these conditions were in fair agreement within the experimental uncertainties $\sigma = (1.6 \pm 0.2) \times 10^{-19}$ cm^2 molecule^{-1}. This maximum absorbance observed is due to the $n \rightarrow \pi^*$ transition of C=O of the ester functional group. The red shift from the base ester band, $\lambda_{max} = 207$ nm,[16] is attributed to the presence of an additional alkoxy functional group in the studied compound that acts as an auxochrome.

3.2. Kinetic Studies. *3.2.1. Reaction of OH with MPA. Absolute Methods. PLP-LIF.* The OH reaction was studied under pseudo-first-order conditions with the concentration of MPA in high excess, $(0.19-4.64) \times 10^{14}$ molecules cm^{-3}, over that of OH radicals $((4.3-59) \times 10^{10}$ molecules cm$^{-3})$. Under these conditions, the OH concentration−time profiles followed a simple exponential rate law according to eq 2:

$$[OH]_t = [OH]_0 \exp^{-k't} \text{ where } k' = k_{MPA} + k'_0 \quad (2)$$

in which k_{MPA} represents the rate coefficient for the reaction of OH radicals with MPA and k'_0 (s^{-1}) the first-order OH decay rate coefficient in the absence of the compound. k_{MPA} is then obtained by plotting the pseudo-first-order rate coefficient versus the MPA concentrations. The values of k_0' were typically in the range of 91−242 s^{-1}, while k' values were in the range of 301−8071 s^{-1}. Figure 2 shows an example of typical plots of k' versus
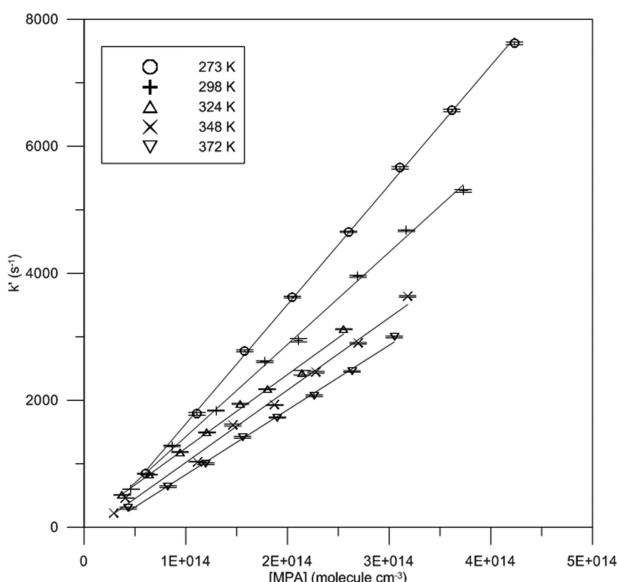
Figure 2. Absolute rate data for the reaction of OH radicals with MPA obtained in PLP-LIF at the temperature range of 273−372 K. One run is presented for each temperature.

MPA concentrations for different temperatures and from which the rate coefficients values were derived. The estimated error on the MPA concentration was ∼10%, considering the uncertainties in the flow of the reagents into the cell, in the MPA mixture preparation, and in the temperature and pressure measurements of the reactor. The errors quoted for k' values are the standard deviation (1σ) of the individual exponential and do not include systematic uncertainties.

The summary of the experimental conditions and the rate coefficients values obtained are given in Table 2.

Table 2. Reaction of OH with MPA: Summarized Experimental Conditions and Results Obtained from the Absolute Rate Measurements

T (K)	[MPA] $(10^{13}$ molecules cm$^{-3})$	$(k \pm 1\sigma)$ $(10^{-11}$ cm^3 molecule^{-1} s$^{-1})$
	AR, PLP-LIF[a]	
263	1.86−9.12	1.90[b] ± 0.14
273	6.28−46.39	1.84 ± 0.05
273	6.06−42.32	1.88 ± 0.02
298	4.62−37.28	1.45 ± 0.03
300	5.50−42.55	1.37 ± 0.03
300	4.46−37.28	1.58 ± 0.06
324	3.10−34.41	1.16 ± 0.04
323	3.75−25.54	1.17 ± 0.07
348	4.08−31.82	1.15 ± 0.04
348	2.93−32.82	0.97 ± 0.04
348	4.17−20.00	1.04 ± 0.03
372	4.34−30.50	1.02 ± 0.02
372	3.89−25.09	1.00 ± 0.02
372	3.01−29.53	1.05 ± 0.01
	AR, FFT-QMS[a]	
297	0.50−2.88	1.47 ± 0.13
303	0.16−1.99	1.47 ± 0.07
336	0.11−2.31	1.16 ± 0.03

[a]AR: absolute rate measurements. PLP-LIF: pulse laser photolysis-laser-induced fluorescence. FFT-QMS: fast flow tube-quadrupole mass spectrometer. [b]The average of three kinetic runs was used and is presented as unique value.

FFT-QMS. The absolute rate coefficient measurements of the reactions of OH with MPA were carried out under pseudo-first-order conditions in excess of MPA $(0.1-2.9) \times 10^{13}$ molecules cm^{-3} over OH radicals $(0.4-1.3) \times 10^{12}$ molecules cm^{-3}. The rate coefficients were derived from the time profiles of OH concentration according to eq 2. Experiments were carried out at a total pressure of 1 Torr of helium and at three temperatures $T = 297, 303,$ and 336 K. The linear velocity inside the reactor was in the range of 1231 to 1780 cm s^{-1}.

The concentration of MPA was also monitored as a function of the reaction time. Figure 3 shows the pseudo-first-order rate coefficients, $k' = k_{MPA} + k'_0$, as a function of the MPA concentration. k'_0 represents the rate of OH decay in the absence of MPA in the reactor and was measured before and after each experiment. It ranged from 10.3 to 22.5 s^{-1} and is in good agreement with the corresponding intercept in Figure 3. The errors shown for k' represent one standard deviation (1σ) of the individual exponential fits and do not include systematic uncertainties. The errors quoted for MPA concentrations are estimated to be nearly 10%.

All the measured values of k' were corrected for axial and radial diffusion of OH.[17] The diffusion coefficient of OH in He was calculated using the following expression: $D_0 = 640 \times (T/$
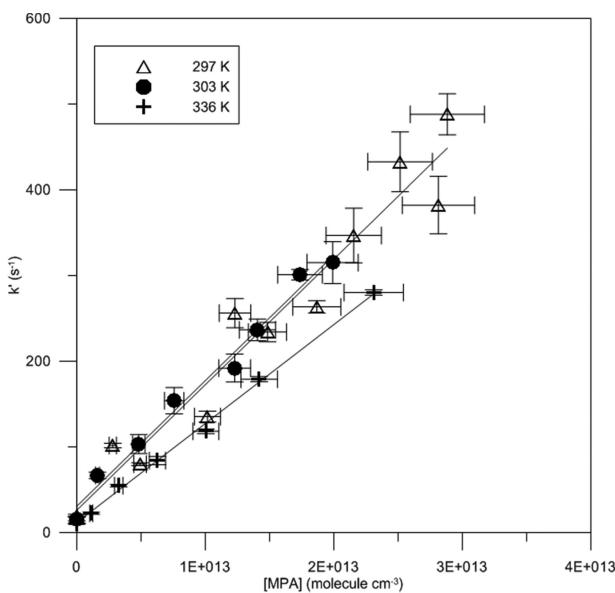
Figure 3. Absolute rate data for the reaction of OH radicals with MPA obtained in the FFT-QMS at 297, 303, and 336 K.

$298)^{1.85}$ Torr $cm^2 s^{-1}$ and ranged from 636 to 800 Torr $cm^2 s^{-1}$ at $P = 1$ Torr and $T = 297-336$ K.[18,19] The corrections on k' were generally less than 10%.

An abnormal increase of the OH rate coefficient was observed at low temperatures. This phenomenon was attributed to the heterogeneous interaction of OH with surface-adsorbed MPA since MPA is a sticky molecule.[20] For this reason, the absolute measurements of the rate coefficient were carried out at temperatures above 297 K. All the results obtained for the OH rate coefficients and a summary of the experimental conditions are presented in Table 2. As noted above, OH radicals were scavenged by Br_2 at the end of the reactor to be detected as HOBr molecules (reaction R2). This led to the simultaneous production of Br atoms, which could react with MPA. However, the important point is that the Br atom reactions could not affect the concentration of HOBr through its formation or consumption reactions, and therefore, they had no impact on the observed kinetics. In addition, it was verified that Br reaction with MPA had a negligible impact on [MPA] under the experimental conditions of the present study. In particular, in separate test experiments it was observed that MPA concentration did not change upon addition of 4×10^{12} Br-atoms cm^{-3} in the reactor. Secondary reactions of OH radicals with primary reaction products could also be considered as negligible, taking into account the sufficient excess of MPA over the radicals. This was confirmed by the observed independence of the reaction rate, k', of the initial concentrations of OH.

Relative Rate Measurements. Teflon Reaction Chamber. A Teflon reaction chamber was used to measure the relative rate coefficients of OH reaction with MPA. The principle of the relative rate method is to measure in the presence of OH radicals the decay rate of [MPA] relative to that of a reference compound for which the OH reaction rate coefficient is well-known. However, there are two presuppositions that need to be ensured: (a) both the reactant and reference compounds are removed solely via reaction with the oxidant in the gas phase; and (b) both the reactant and reference compound have the same exposure to the oxidant. The first requirement was achieved by minimizing

the heterogeneous losses and performing experiments in excess of O_2; note that synthetic air was used as bath gas in order to scavenge the R-radicals formed that would potentially lead to errors in k measurements. Moreover, the mixture of MPA and reference compound with and without H_2O_2 was stable in the dark when it was left in the chamber for about 1.5−2 h. In addition, photolysis of MPA or reference compounds was negligible when these compounds were irradiated at 254 nm for the same time scale. The second requirement was overtaken simply by leaving for sufficient time the reaction mixture to be homogeneously mixed within the reactor. Consequently, the relative rate coefficient can be obtained by the following relation [eq 3]:

$$\ln\left[\frac{[\text{MPA}]_0}{[\text{MPA}]_t}\right] = \frac{k_{\text{MPA}}}{k_{\text{ref}}} \times \ln\left[\frac{[\text{ref}]_0}{[\text{ref}]_t}\right] \tag{3}$$

where $[\text{MPA}]_0$, $[\text{ref}]_0$, $[\text{MPA}]_t$, and $[\text{ref}]_t$ are the concentrations of the MPA and reference compound at times $t = 0$ and t, respectively, and k_{MPA} and k_{ref} are the rate coefficients of MPA and reference reactions with the oxidant. Thus, the plot of $\ln([\text{MPA}]_0/[\text{MPA}]_t)$ versus $\ln([\text{reference}]_0/[\text{reference}]_t)$ exhibits linearity with a slope equal to $k_{\text{MPA}}/k_{\text{ref}}$.

The second order rate coefficient for OH reaction with MPA (cm^3 molecule^{-1} s^{-1}) was determined using 1,3-dioxolane and 1-pentanol as reference compounds with the corresponding rate coefficients: $k_{(\text{OH+1,3-dioxolane})} = (1.13 \pm 0.11) \times 10^{-11}$[21,22] and $k_{(\text{OH+1-pentanol})} = (1.11 \pm 0.10) \times 10^{-11}$[23−25] cm^3 molecule^{-1} s^{-1}. The initial concentrations of the precursor H_2O_2 into the Teflon reactor were in the range of 327−485 ppm. The concentrations of MPA and the reference compounds ranged between 15 and 50 ppm. The relative change in the concentrations of the alkoxy ester and reference compounds was derived from integration of the chromatogram peaks. For all the reference compounds three different runs were carried out. The plots of the experimental results according to eq 3, shown in Figure 4, have near-zero intercept, verifying the absence of secondary reactions. The experimental conditions and the obtained slopes and rate coefficients for OH reaction are summarized in Table 3. The errors quoted for $k_{\text{MPA}}/k_{\text{ref}}$ values in Table 3 are the standard deviation (1σ) of the slope and do not include systematic uncertainties. The errors quoted for k_{MPA} value in the individual experiments are the errors in $k_{\text{MPA}}/k_{\text{ref}}$ by taking into account the error of k_{ref}. Errors quoted to the average values of k for each reference compound is the standard deviation of the runs. Regarding the error quoted to the final average value for k relative, $k = (1.23 \pm 0.13) \times 10^{-11}$ cm^3 molecule^{-1} s^{-1}, it includes the standard deviation of the two individual k values and a conservative uncertainty of 10% corresponding to the k_{ref}.

FFT-QMS. Relative rate measurements of the OH reaction with MPA were also performed in FFT-QMS system, using two reference compounds, Br_2 and 1,3-dioxolane, at 313 and 297 K, respectively. The Arrhenius expressions used for the rate coefficients of the reference reactions were 2.0×10^{-11} $e^{2.00 \text{ [kJ/mol]}/RT}$[14] and 6.7×10^{-12} $e^{(1.28\pm0.30)\text{kJ/mol}/RT}$ cm^3 molecule^{-1} s^{-1},[22] respectively. Experiments were carried out at a total pressure of 1 Torr. The initial concentrations of MPA, Br_2, and 1,3-dioxolane were in the range of $(1.5-2.5) \times 10^{12}$, $(4.5-9.4) \times 10^{11}$, and $(1.9-2.1) \times 10^{12}$ molecules cm^{-3}, respectively, and those of NO_2 and OH radicals were $(7.5-8.6) \times 10^{13}$ and $(0.4-6.0) \times 10^{12}$ molecules cm^{-3}. The reference compounds were detected at their parent peaks: 160 (Br_2^+) and 73 ($C_3H_6O_2^+$) for 1,3-dioxolane. Reaction time was approximately 0.023 s.
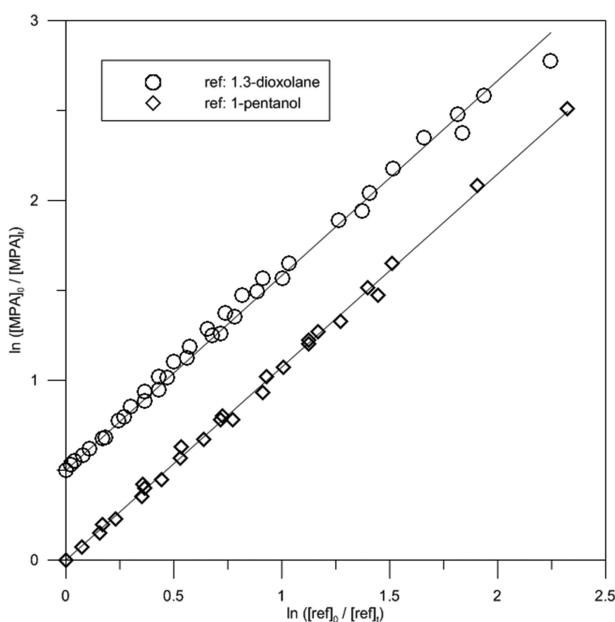
Figure 4. Relative rate data for the reaction of OH radicals with MPA obtained in the atmospheric simulation chamber using 1,3-dioxolane and 1-pentanol as reference compounds. The experimental measurements with 1,3-dioxolane are shifted up on the y axis by +0.5 $\ln([MPA]_0/[MPA]_t)$ units for clarity purposes.

Figure 5. Relative rate plots for the reaction of OH with MPA measured in the FFT-QMS system, using 1,3-dioxolane and Br_2 as reference compounds at 297 and 313 K, respectively.

The relative rate coefficients were obtained according to eq 3, as described previously. The experimental data are shown in Figure 5. The slopes of the straight lines correspond to k_{MPA}/k_{ref} ratio. A summary of the experimental conditions and the values obtained for the rate coefficients are presented in Table 4. The errors quoted for k_{MPA}/k_{ref} values in Table 4 correspond to one standard deviation (1σ) on the determination of the slopes of the straight lines in Figure 5 and do not include systematic uncertainties. The errors quoted for k_{MPA} values are the errors in k_{MPA}/k_{ref} by taking into account the errors of k_{ref}. As mentioned before, Br atoms formed could react with MPA. A series of experiments has shown that the concentration of MPA did not change in the presence of high concentration of Br atoms in the reactor, thus the Br reaction with MPA had a negligible impact on MPA concentrations.

Temperature and Pressure Dependence. The complementary use of PLP-LIF, FFT-QMS, and ASC techniques allowed us to determine the absolute and relative rate coefficient of MPA with OH radicals in the temperature range 263−373 K and the pressure range 1−760 Torr. The experimental conditions and

measured values of the rate coefficient are listed in Tables 2−4. The unweighted Arrhenius exponential fit to the k is presented in Figure 6 (solid line). The plot shows slight negative temperature dependence and provides the following Arrhenius expression:

$$k_{MPA+OH}(T) = (2.01 \pm 0.02) \times 10^{-12}$$
$$\exp[(588 \pm 123/T)] \; cm^3 \; molecule^{-1} \; s^{-1}$$

where the quoted uncertainties on the ratio E/R and on the preexponential factor (A) are the standard deviation (1σ) and $A\sigma_{\ln A}$, respectively. The room temperature rate coefficient is k_{298} = $(1.44 \pm 0.21) \times 10^{-11} \; cm^3 \; molecule^{-1} \; s^{-1}$. The error quoted includes the precision of the fit of $\ln(k)$ versus T and the estimated systematic uncertainties. The negative activation energy, $E = -4.89 \; kJ \; mol^{-1}$, indicates that the reaction follows probably a complicated, addition−elimination mechanism. The observation of the negative temperature dependence for MPA is consistent with the ones already reported for other acetates (see comparison section). It has been proposed in literature that for this class of compounds (alkoxy esters and ethers) the initial step for the reaction does not involve a direct H atom abstraction pathway but the formation of a complex in which a hydrogen

Table 3. Reaction of OH with MPA: Experimental Conditions and Results Obtained in the Atmospheric Simulation Chamber at 293 K and 760 Torr

reference compound	number of runs	[ref]$_0$ (ppm)	[MPA]$_0$ (ppm)	k_{MPA}/k_{ref} ($\pm 1\sigma$)	k_{MPA} (10^{-11} cm^3 molecule^{-1} s^{-1})
1,3-dioxolane	3	49.74	19.02	1.10 ± 0.004	1.24 ± 0.13
		39.86	21.58	1.19 ± 0.005	1.35 ± 0.14
		35.34	26.43	1.03 ± 0.007	1.16 ± 0.13
		average (1,3-dioxolane)			**1.25 ± 0.09**
1-pentanol	3	15.47	16.66	1.09 ± 0.002	1.21 ± 0.11
		15.68	24.29	1.04 ± 0.007	1.16 ± 0.11
		21.41	33.89	1.10 ± 0.010	1.22 ± 0.12
		average (1-pentanol)			**1.20 ± 0.04**
average					**1.23 ± 0.13**

Table 4. Reaction of OH with MPA: Experimental Conditions and Results Obtained Using FFT-QMS[a]

T (K)	reference compound	$[ref]_0$ (10^{12} molecules cm^{-3})	$[MPA]_0$ (10^{12} molecules cm^{-3})	k_{MPA}/k_{ref} ($\pm 1\sigma$)	k_{MPAb} (10^{-11} cm^3 molecule^{-1} s^{-1})
313	Br$_2$	0.5–1.0	2.3	0.32 ± 0.01	1.39 ± 0.16
297	1,3-dioxolane	1.9–2.0	1.5–2.5	1.47 ± 0.02	1.65 ± 0.19

[a]Br$_2$ and 1,3-dioxolane were used as reference compounds at 1 Torr and 297 and 313 K, respectively.
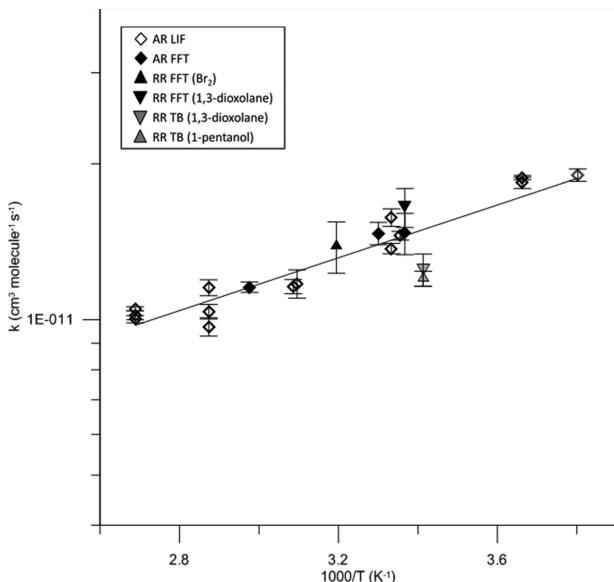
Figure 6. Arrhenius plot of the obtained relative and absolute OH rate coefficients using three complementary techniques, on a logarithmic scale, as a function of $1000/T$ (K^{-1}), over the temperature range 263–372 K.

bond exists between the H atom of the attacking OH radical and the O atom of the ether group.[21]

The dependence of the rate coefficient on pressure was investigated at $T = 297 \pm 4$ K within the pressure range of 1–760 Torr (Table 5). The change in the total pressure did not have any effect on the measured rate coefficients. In particular, the results showed no systematic increase of the rate coefficient with pressure; the observed discrepancies between the measurements could be attributed to experimental uncertainties from the

**Table 5. Reaction of OH with MPA at 297 ± 4 K: Pressure Dependence**

number of runs	P (Torr)	[MPA] (10^{13} molecules cm^{-3})	k (10^{-11} cm^3 molecule^{-1} s^{-1})	technique[a]
3	100	4.46–42.55	1.47 ± 0.18[b]	AR, PLP-LIF
1	1	0.50–2.88	1.47 ± 0.20[b]	AR, FFT-QMS
6	760	41.65–84.72	1.23 ± 0.13[c]	RR, ASC-GC/FID
1	1	0.15–0.25	1.65 ± 0.19[d]	RR, FFT-QMS

[a]AR: absolute rate measurements. RR: relative rate measurements. PLP-LIF: pulse laser photolysis-laser-induced fluorescence. FFT-QMS: fast flow tube-quadrupole mass spectrometer. ASC-GC/FID: atmospheric simulation chamber−gas chromatograph/flame ionization detector. [b]The error quoted includes the standard deviation (1σ) of the slope and the estimated systematic uncertainties. [c]The error quoted includes the standard deviation of the runs and the given uncertainty of the k_{ref}. [d]The error quoted includes the standard deviation (1σ) of the slope and the given uncertainty of the k_{ref}.

different experimental setups used and the different methods applied.

3.2.2. MPA+Cl. Absolute Rate Measurements. FFT-QMS. The absolute rate coefficient measurements of the reaction of Cl with MPA were carried out under pseudo-first-order conditions, as described previously, in excess of MPA $(0.6−3.9) \times 10^{12}$ molecules cm^{-3} over Cl atoms $(0.1−0.8) \times 10^{12}$ atoms cm^{-3}. The rate coefficients were derived from the time profiles of [Cl] according to eq 2. Experiments were carried out at a total pressure of 1 Torr of helium at 298 K. The linear velocity inside the reactor was in the range of (2395−3430) cm s^{-1}. The consumption of MPA was negligible as a result of its sufficient excess. However, in a few kinetic runs, a noticeable consumption of MPA was observed as a result of the use of insufficient excess of MPA over Cl atoms due to limited sensitivity of Cl detection and the high value of k_{MPA}. In these cases, the mean concentration of MPA along the reaction zone was used for the calculations of the rate coefficient.

Figure 7 shows the pseudo-first-order rate coefficients, $k' = k_{MPA} + k'_0$, as a function of the MPA concentration. The errors for
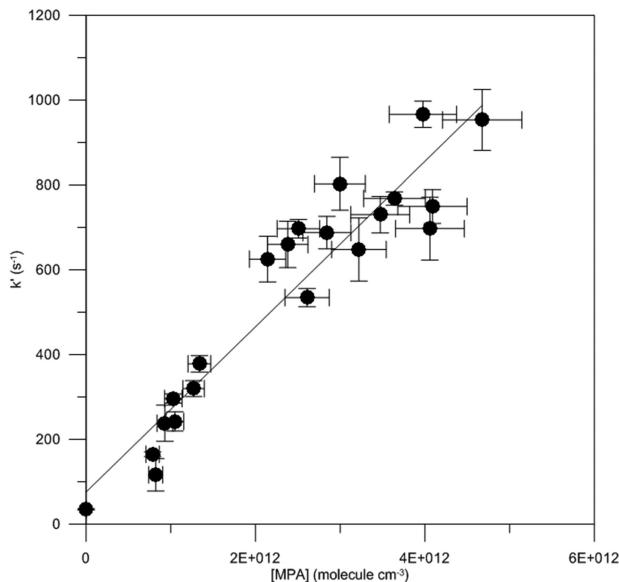
Figure 7. Absolute rate data for the reaction of Cl atoms with MPA obtained with the FFT-QMS setup at 298 K.

k' correspond to one standard deviation (1σ) of the individual exponential fits and do not include systematic uncertainties. The errors quoted for MPA concentrations are nearly 10%. k'_0 was measured before and after each experiment and ranged from 6 to 40 s^{-1}. These values are somewhat lower than the intercept in Figure 7, indicating the probable modification of the reactor surface in the presence of MPA. All the measured values of k' were corrected for axial and radial diffusion of Cl.[17] The diffusion coefficient of Cl in He, $D_{Cl−He}$, was calculated from $D_{Ar−He}$[26] and was 567 cm^2 s^{-1} at $P = 1$ Torr and $T = 298$ K. The corrections on k' were generally less than 10%.

The value of k_{MPA+Cl} measured at room temperature was $(1.95 \pm 0.28) \times 10^{-10}$ cm^3 molecule^{-1} s^{-1}, where the quoted error represents one standard deviation on the determination of the slope of the straight line in Figure 7 and the estimated systematic uncertainties.

Relative Rate Measurements. Teflon Reaction Chamber. The Teflon reaction chamber was used to measure the relative rate coefficient of Cl reaction with MPA at 293 K. The mixture of MPA and reference compound with and without Cl$_2$ was stable in the dark when it was left in the chamber for about 1.5−2 h. Furthermore, photolysis of MPA or reference compounds was negligible when these compounds were irradiated at 365 nm for the same time scale. Assuming that MPA and the reference compound are lost solely via reaction with the oxidant and that they are not reformed in any process, the relative rate coefficient was obtained from eq 3.

The rate coefficient for the reaction of Cl atoms with MPA was determined using cyclohexane $k_{(Cl+cyclohexane)} = (3.32 \pm 0.41) \times 10^{-10}$,[27,28] 1-propanol $k_{(Cl+1-propanol)} = (1.62 \pm 0.14) \times 10^{-10}$,[29] and pentane $k_{(Cl+pentane)} = (2.71 \pm 0.28) \times 10^{-10}$[27,28,30] in cm^3 molecule^{-1} s^{-1} as reference compounds. The initial concentrations of the precursor Cl$_2$ into the Teflon reactor were in the range of 58−83 ppm. The concentrations of MPA and the reference compounds ranged between 16 and 61 ppm. The relative change in concentration of the alkoxy ester and reference compounds was derived from integration of the chromatogram peaks. For pentane solely one run was conducted, while for all other reference compounds three different runs were carried out. The plots of the experimental results, according to eq 3, are shown in Figure 8. Three runs are presented in the case of 1-propanol and cyclohexane. The experimental conditions and the obtained slopes and rate coefficients for Cl reaction are summarized in Table 6. The uncertainties quoted for k_{MPA}/k_{ref} values in Table 6 are the standard deviation (1σ) of the slope and do not include systematic uncertainties. The errors quoted for k_{MPA} value in the individual experiments are the errors in $k_{MPA}/$

k_{ref} by taking into account the error of k_{ref}. Errors quoted to the average values of k for each reference compound is the standard deviation of the runs. Regarding the error quoted to the final average value for k relative, $k = (2.01 \pm 0.24) \times 10^{-10}$ cm^3 molecule^{-1} s^{-1}, it includes the standard deviation of the three individual k values and a conservative extreme uncertainty of 12% corresponding to the k_{ref}.

Pressure Dependence. The results obtained from the absolute and relative rate coefficient measurements of the Cl reaction with MPA at 295 ± 3 K and at 1 and 760 Torr are listed in Table 7. The results showed no pressure dependence since the measurements are in very good agreement. Note that the error quoted to the final average value of k, $k_{Cl+MPA} = (1.98 \pm 0.31) \times 10^{-10}$ cm^3 molecule^{-1} s^{-1}, includes the extreme overall uncertainty of the absolute and relative rate measurements (that have been listed in detail previously).

3.3. Mechanistic Studies: Proposed Mechanism. The mechanistic investigation and product analysis of the reaction of OH and Cl with MPA were performed using the Teflon reaction chamber. Methyl formate (HC(O)OCH$_3$), acetic acid (CH$_3$C(O)OH), acetic anhydride (CH$_3$C(O)OC(O)CH$_3$), carbon dioxide (CO$_2$), and carbon monoxide (CO) were identified as the major products of both OH and Cl reaction with MPA, by using GC-FID, FT-IR, and GC-MS as detection techniques. Figure 9 displays IR spectra obtained from the reaction of OH with MPA. The concentrations of MPA and H$_2$O$_2$ used for this set of experiment were 31 and 350 ppm, respectively. The consumption of MPA was approximately 94%. Panel (A) shows the IR spectrum of MPA and H$_2$O$_2$ before the reaction, while panel (B) is after 1 h and 30 min of reaction. The typical reference IR spectra of three identified products, methyl formate, acetic acid, and acetic anhydride, are presented in panels (C), (D), and (E) of Figure 9, respectively. Panel (F) is the IR spectrum after subtraction of reactants and the major identified products (methyl formate, acetic acid, and acetic anhydride), where mainly vibrations of CO$_2$, CO, and H$_2$O can be observed. Similarly, IR spectra of Cl with MPA are shown in Figure 10. MPA and Cl$_2$ concentrations were 35 and 74 ppm, respectively, while MPA consumption at the end of the experiment was ∼72%. The IR spectra of MPA and Cl$_2$ before (A) and after (B) 50 min of reaction, the typical reference IR spectra of methyl formate (C), acetic acid (D), and acetic anhydride (E), and the spectrum (F) after subtraction of reactants and products (methyl formate, acetic acid, and acetic anhydride) are presented in Figure 10.

The referred reaction products were calibrated using the integration of chromatogram peaks in GC-FID, and their yields, expressed as $\Delta[product]_t/\Delta[MPA]_t$, were measured. For the reaction of OH with MPA the product yields were 80 ± 7.3, 50 ± 4.8, and $22 \pm 2.4\%$ for (HC(O)OCH$_3$), (CH$_3$C(O)OH) and (CH$_3$C(O)OC(O)CH$_3$), respectively (Figure 11). For the reaction of Cl atoms with MPA, the recorded yields were slightly lower: 60 ± 5.4, 41 ± 3.8, and $11 \pm 1.2\%$ for (HC(O)OCH$_3$), (CH$_3$C(O)OH), and (CH$_3$C(O)OC(O)CH$_3$), respectively, as shown in Figure 12 where three runs are presented in all cases. The error quoted includes: the standard deviation (1σ) of the slope $\Delta[product]_t$ to $\Delta[MPA]$, the standard deviation (1σ) of the product and MPA calibration factors, and the systematic uncertainties. Note that the values given above correspond to molar yields, and they are not based on the carbon mass balance. Besides, the structure of the measured products indicates that they could be produced from the same MPA molecule. CO$_2$ and

Figure 8. Relative rate plots for the Cl reaction with MPA obtained using the atmospheric simulation chamber, using 1-propanol, cyclohexane, and pentane as reference compounds.

Table 6. Reaction of Cl with MPA: Experimental Conditions and Measured Rate Coefficients in the Atmospheric Simulation Chamber at 293 K and Atmospheric Pressure

reference compound	number of runs	$[\text{ref}]_0$ (ppm)	$[\text{MPA}]_0$ (ppm)	k_{MPA}/k_{ref} ($\pm 1\sigma$)	k_{MPA} (10^{-10} cm^3 molecule^{-1} s^1)
cyclohexane	3	21.14	17.83	0.63 ± 0.004	2.10 ± 0.27
		17.22	15.87	0.61 ± 0.006	2.01 ± 0.27
		23.59	16.93	0.61 ± 0.003	2.01 ± 0.26
		average (cyclohexane)			**2.04 ± 0.05**
1-propanol	3	30.02	27.46	1.30 ± 0.025	2.11 ± 0.22
		61.56	26.11	1.19 ± 0.012	1.93 ± 0.19
		44.10	25.03	1.27 ± 0.020	2.06 ± 0.21
		average (1-propanol)			**2.03 ± 0.09**
pentane	1	39.61	35.29	0.718 ± 0.006	1.94 ± 0.22
average					**2.01 ± 0.24**

Table 7. Reaction of Cl with MPA at 295 ± 3 K: Pressure Dependence

number of runs	P (Torr)	[MPA] (10^{12} molecules cm^{-3})	($k \pm 1\sigma$) (10^{-10} cm^3 molecule^{-1} s^{-1})	technique[a]
1	1	0.06−0.39	1.95 ± 0.28[b]	AR, FFT-QMS
7	760	39.68−88.22	2.01 ± 0.24[c]	RR, ASC-GC/FID
average			**1.98 ± 0.31[d]**	

[a]AR: absolute rate measurements. RR: relative rate measurements. FFT-QMS: fast flow tube-quadrupole mass spectrometer. ASC-GC/FID: atmospheric simulation chamber gas chromatograph-flame ionization detector. [b]The error quoted is the standard deviation (1σ) of the slope and the estimated systematic uncertainties. [c]The error quoted is the standard deviation of the k values measured using the three reference compounds and a conservative uncertainty of 12% (extreme error) to the values of k_{ref}. [d]The error quoted is the extreme overall uncertainty of the k values measured using the two techniques (including standard deviation, systematic uncertainties, and the error of k_{ref}).

CO were also produced and identified by FTIR but not quantified.

The slopes of the linear least-squares analysis with 97% confidence intervals indicate that products are not lost or produced by any other side/secondary reactions. This was also verified from the "relatively slow" rate coefficients of OH radicals with the products formed compared with that of OH with MPA. Particularly, the values of the rate coefficients reported in the literature are 6.90×10^{-13}[29] and 2.27×10^{-13}[31] cm^3 molecule^{-1} s^{-1} for $CH_3C(O)OH$ and $HC(O)OCH_3$ with OH and 2.62×10^{-14}[29,32] and 1.30×10^{-12} cm^3 molecule^{-1} s^{-1}[33] with Cl, respectively. Regarding acetic anhydride there are not experimental data. For these reasons, the yields quoted above were not corrected for secondary formation or loss.

MPA has five C−H sites available for attack from OH and Cl. Based on our experimental observations, reaction rates, and observed products, the oxidant abstracts one hydrogen atom principally from the methylene of the methoxy functional group; thus, the reaction scheme found in Figure 13 for the reaction of OH and Cl with MPA is proposed.

The presence of NO ensures rapid removal of HO$_2$ and RO$_2$ and simplifies the mechanistic interpretation of the product yields providing a more direct conversion of peroxy into alkoxy radicals, thus eliminating the reactions of HO$_2$ and RO$_2$ with RO$_2$. Subsequently, the most possible pathway for the alkoxy radical $CH_3-O-(CHO^\bullet)-CH(CH_3)-O-C(O)-CH_3$ formation is decomposition by breaking the C−C bond to form methyl formate and the $CH_3-(CH^\bullet)-O-C(O)-CH_3$ radical. Further

decomposition of this radical could follow a similar reaction sequence as shown in reactions:

$$CH_3-(CH^\bullet)-O-C(O)-CH_3 + O_2 + NO$$
$$\rightarrow CH_3-(CHO^\bullet)-O-C(O)-CH_3 + NO_2 \quad (R4)$$

$$CH_3-(CHO^\bullet)-O-C(O)-CH_3 + O_2$$
$$\rightarrow CH_3-C(O)-O-C(O)-CH_3 (\text{acetic anhydride})$$
$$+ HO_2 \quad (R5)$$
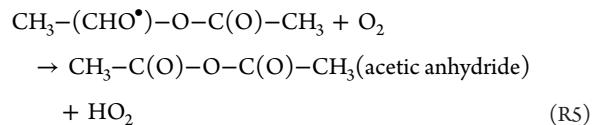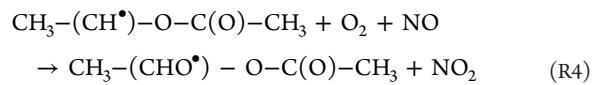
In the presence of water, acetic anhydride would decompose to acetic acid.

The estimation method SAR[34] shows that OH abstracts one hydrogen atom principally from the methylene and methane groups, which are bonded to the ether oxygen of the methoxy functional group. H-abstraction from the methylene group ($-O-CH_2-$) has a high percentage of 84%, which is in excellent agreement with the experimental determined yields in our work, 72−80%. However, the H-abstraction from methane group (CH_3-O-) has a possibility of 10%. This is consistent with the literature reports, which suggest that OH radical reacts predominantly with the alkoxy end of an ester rather than the acyl end[35] (and references therein). Several studies[36,37] have proposed that the initial step for the OH reaction with oxygenated organic compounds does not involve a direct H atom abstraction pathway, but the formation of a complex in which a hydrogen bond exists between the H atom of the attacking OH radical and the O atom of the ether group. A second hydrogen bond is then formed in the complex between the O atom of the OH radical and an H atom in the hydrocarbon chain, resulting in intramolecular hydrogen atom transfer via a cyclic transition state. This complex could be the explanation of the low negative activation energy for the reaction of OH with MPA.[36] In contrast, this transition state is not possible in Cl atom reactions.[38]

4. COMPARISON

To the best of our knowledge, this is the first kinetic and mechanistic study of MPA reaction with OH and Cl reported in the literature. There is only one theoretical determination for the reaction of the alkoxy ester with OH radicals from Meylan et al.,[39] and the calculated rate coefficient is 1.19×10^{-11} cm^3 molecule^{-1} s^{-1}. The estimated rate coefficient for the reaction of OH with MPA upon application of the SAR method is 1.14×10^{-11} cm^3 molecule^{-1} s^{-1} at 298 K; thus, it is in good agreement with the experimental value, $k_{298} = (1.44 \pm 0.21) \times 10^{-11}$ cm^3 molecule^{-1} s^{-1}, from the current study (within uncertainty, 21%).
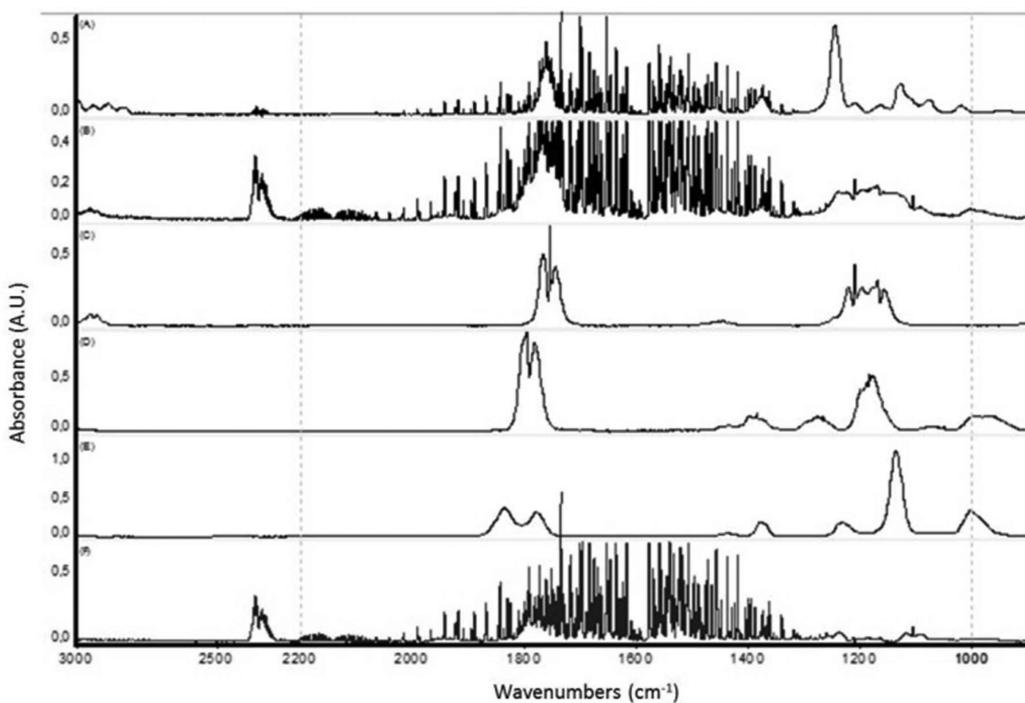
Figure 9. Reaction of MPA with OH. IR spectra obtained before (A) and after (B) a 1 h 30 min irradiation of a mixture of MPA and H_2O_2. Reference IR spectra of methyl formate (C), acetic acid (D), and acetic anhydride (E). (F) IR spectrum after subtraction of reactants and the identified products (methyl formate, acetic acid, and acetic anhydride).
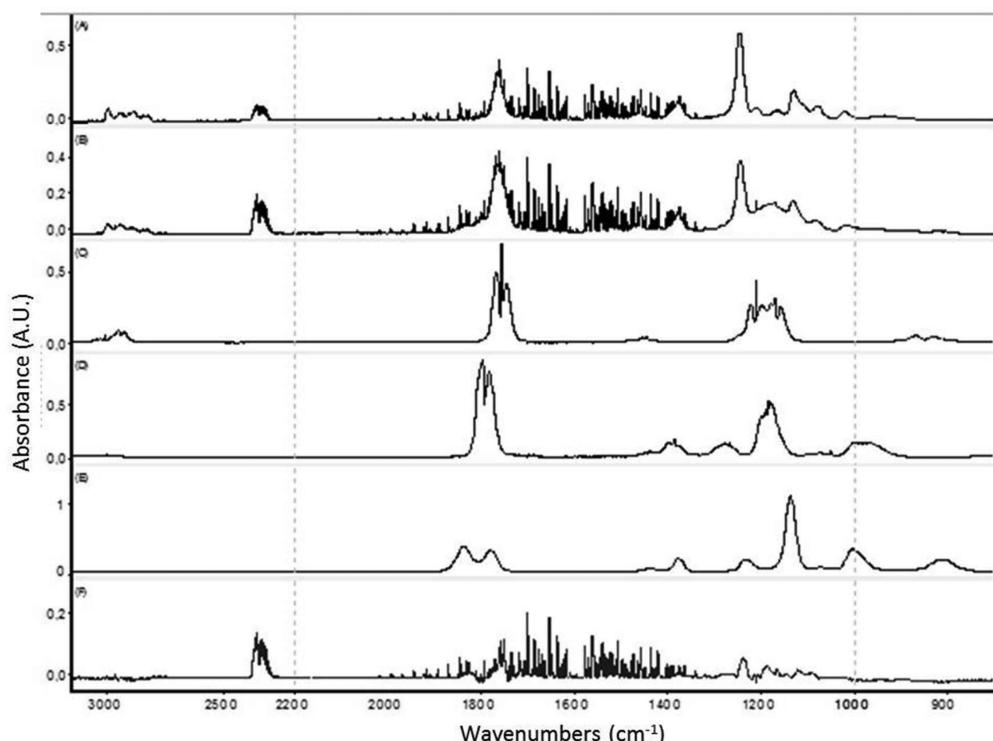
Figure 10. Reaction of MPA with Cl. IR spectra obtained before (A) and after (B) a 50 min irradiation of a mixture of MPA and Cl_2. Reference IR spectra of methyl formate (C), acetic acid (D), and acetic anhydride (E). (F) IR spectrum after subtraction of reactants and the identified products (methyl formate, acetic acid, and acetic anhydride).

Comparing our results with previous studies where the rate coefficients of molecules with similar structures were determined (Table 8), it is evident that the reactivity of the molecules is influenced by the presence of the ether group. Particularly, there
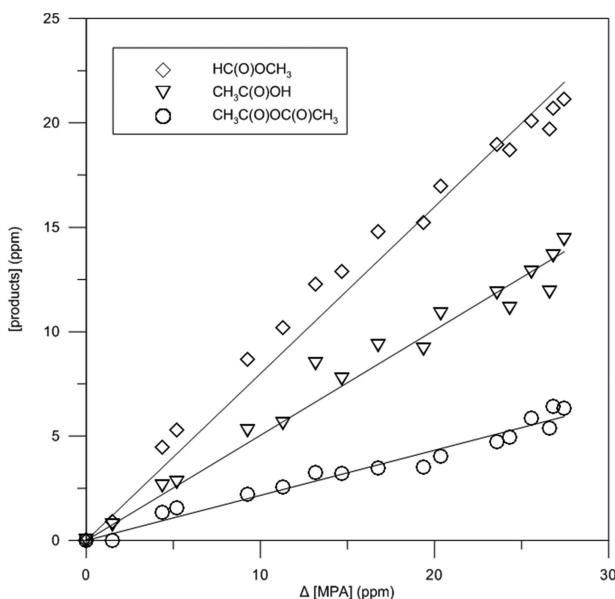
Figure 11. Time evolution of MPA and the identified products concentrations for the MPA + OH reaction in the presence of NO. The product yields are calculated from the slope of the fits: methyl formate, acetic acid, and acetic anhydride product yields were 80 ± 7.3, 50 ± 4.8, and $22 \pm 2.4\%$, respectively.
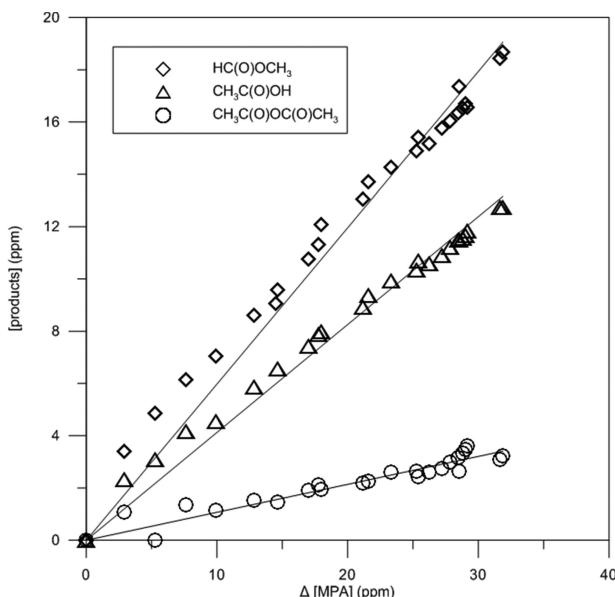
Figure 12. Time evolution of MPA and the identified product concentrations for the MPA + Cl reaction in the presence of NO. The product yields are calculated from the slope of the fit: methyl formate, acetic acid, and acetic anhydride product yields were 60 ± 5.4, 41 ± 3.8, and $11 \pm 1.2\%$, respectively.

is a difference by a factor of 2.5 between the OH rate coefficients for MPA and sec-butyl acetate (SBA), $k_{(CH3C(O)OCH(CH3)CH2CH3+Cl)} = 0.58 \times 10^{-11}$ cm^3 molecule^{-1} s^{-1} at 298 K.[40−42] In addition, attempting to compare the rate coefficients determined for MPA (CH$_3$ branching in β position of the ether group) and methoxy ethyl acetate (MEA) (unbranched), an increase ~58% to the k value was observed at 298 K. Nevertheless, this increase should not only be

attributed to the presence of the branching since the rate coefficient measured for MPA was found to be similar to that of its isomer, ethoxy ethyl acetate (EEA).[38,43] Therefore, the number of carbon atoms and the chain length possess the principal role affecting significantly the rate coefficient value. Finally, it should be noted that the measured temperature dependence of the rate coefficients for the reactions of OH with alkoxy esters[38] shows small negative activation energies. This fact was attributed to the formation of weakly bound complexes between the OH radical and the alkoxy esters, which either decompose back to reactant or eliminate H$_2$O.

In the case of Cl atoms, only the rate coefficients of SBA and MPA can be compared since there are no experimental data for the other compounds. The average value of the rate coefficient of Cl with SBA measured by Notario et al.[44] and Xing et al.[45] is $k_{(CH3C(O)OCH(CH3)CH2CH3+Cl)} = 8.67 \times 10^{-11}$ cm^3 molecule^{-1} s^{-1}, at 296 ± 2 K, thus by a factor of ~2.3 lower than the k_{MPA} measured herein. Therefore, it seems that the presence of the ether group increases the rate coefficient in a similar way as observed in the case of OH reaction.

5. CONCLUSIONS

Complementary experimental techniques were employed to determine the rate coefficients for MPA reactions with OH and Cl: $k_{MPA+OH}(T) = (2.01 \pm 0.02) \times 10^{-12} \exp[(588 \pm 123/T)]$ cm^3 molecule^{-1} s^{-1}, $k_{298} = (1.44 \pm 0.21) \times 10^{-11}$ cm^3 molecule^{-1} s^{-1}, and $k_{MPA+Cl} = (1.98 \pm 0.31) \times 10^{-10}$ cm^3 molecule^{-1} s^{-1} at 295 ± 3 K. In order to obtain more insights regarding the degradation mechanism, a detailed product study was conducted and the major degradation products were detected. The OH reaction formation yields were determined to be 80 ± 7.3, 50 ± 4.8, and $22 \pm 2.4\%$ for methyl formate (HC(O)OCH$_3$), acetic acid (CH$_3$C(O)OH), and acetic anhydride (CH$_3$C(O)OC(O)-CH$_3$), while for Cl reaction 60 ± 5.4, 41 ± 3.8, and $11 \pm 1.2\%$, respectively. The H atom abstraction is predominantly conducted from the methylene group (~80% for OH and 60% for Cl) bonded to the ether oxygen of the methoxy functional group (−O−CH$_2$−). In addition, the MPA UV absorption cross section study has shown no photolysis under atmospheric conditions. The resulting cross section value was $\sigma = (1.6 \pm 0.2) \times 10^{-19}$ cm^2 molecule^{-1}.

Assuming that MPA is mainly removed from the atmosphere through the gas phase reactions with OH radicals and Cl atoms, reactions with O$_3$ and NO$_3$ are expected to be negligible, the atmospheric lifetime, τ_x, where x is the corresponding oxidant, can be estimated from the following equation:

$$\tau_{OH} = 1/(k_{OH} \times [OH]) \text{ and } \tau_{Cl} = 1/(k_{Cl} \times [Cl]) \quad (4)$$

where k_{OH} and k_{Cl} are the bimolecular rate coefficients for the corresponding reactions of MPA with OH radicals and Cl atoms, and [OH] and [Cl] are the average tropospheric gas phase concentration of OH (2×10^6 radical cm^{-3}) and Cl (10^4 atom cm^{-3}), respectively.[46] The obtained results show relatively short lifetime for OH, $\tau_{OH} \approx 10$ h, and substantially longer for Cl, $\tau_{Cl} \approx 6$ days. Hence, the long-range transportation of MPA will be of little importance since it will be degraded close to its emission source.

It is well established that ozone is generated in situ from the sunlight-initiated oxidation of VOCs, in the presence of nitrogen oxides. The photochemical ozone creation potential (POCP) presents a value that can classify VOCs by their ability to form ozone in the tropospheric boundary layer through Europe during 5 days along a given trajectory.[47] POCP is derived from
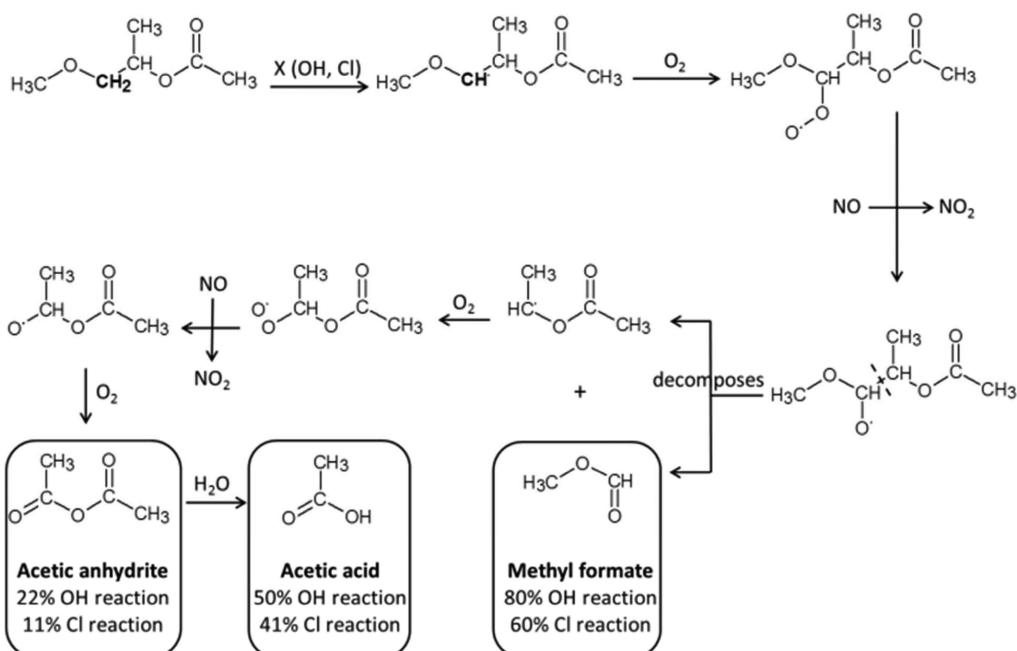
Figure 13. Reaction of MPA with oxidant in the presence of NO. Proposed mechanism scheme for H abstraction from methylene of the methoxy functional group.

Table 8. Comparison of the Rate Coefficients for the Reactions of OH Radicals with MPA, *sec*-Butyl Acetate, Methoxy Ethyl Acetate, and Ethoxy Ethyl Acetate at 300 ± 5 K[a]

molecule	k_{OH} (10^{-11} cm^3 molecule^{-1} s^{-1})	A (10^{-12} cm^3 molecule^{-1} s^{-1})	$(E/R)^d$ (K)	T range (K)	technique	ref	SAR[b]
CH$_3$C(O)OCH(CH$_3$) CH$_2$OCH$_3$, MPA	1.44	2.01 ± 0.02	-(588 ± 123)	263−372	PLP-LIF FFT-QMS ASC	this work	1.14
CH$_3$C(O)OCH(CH$_3$) CH$_2$CH$_3$, SBA	0.58[c,d,e]	0.73 ± 0.08	-(640 ± 62)	263−372	PLP-LIF	Le Calvé et al.[c]	0.54
CH$_3$C(O)OCH$_2$CH$_2$OCH$_3$, MEA	0.83[f]	2.90 ± 1.50	-(309 ± 162)	273−372	PLP-LIF	O'Donnel et al.[d]	1.30
CH$_3$C(O)OCH$_2$CH$_2$O CH$_2$CH$_3$, EEA	1.24[f,g]	1.40 ± 0.60	-(642 ± 148)	273−368	PLP-LIF	O'Donnel et al.[f]	2.00

[a]The rate coefficient values given at 300 K for SBA and EEA correspond to the average of different studies. [b]$k_{OH} \times 10^{-11}$. [c]Ref 41. [d]Ref 42. [e]Ref 43. [f]Ref 39. [g]Ref 44.

chemistry-transport models, while a method was developed by Derwent et al.[48] to estimate POCPs of VOCs in terms of their structures, their OH reactivities, and their product yields and reactivities. For this end, considering the OH gas-phase loss of MPA as its main degradation pathway, the impact of MPA oxidation on the ozone formation in the troposphere can be estimated by calculating its POCP using the $k_{OH} = (1.44 \pm 0.21) \times 10^{-11}$ cm^3 molecule^{-1} s^{-1} at 298 K measured in this work. The estimated POCP of MPA is 36.1 (ethylene is by definition the reference compound with an estimated POCP of 100), while methyl formate, the main OH reaction product (80%), is 2.7.[49] The obtained value for acetic acid (50%), by estimation and modeling, respectively, is approximately 11.8[47] and 15.6.[50] These low values are partially due to the low OH reactivity of methyl formate and acetic acid.

■ AUTHOR INFORMATION

Corresponding Author
*Tel: +33 238257612. E-mail: mellouki@cnrs-orleans.fr.

Notes
The authors declare no competing financial interest.

■ REFERENCES

(1) Mellouki, A.; Wallington, T. J.; Chen, J. Atmospheric Chemistry of Oxygenated Volatile Organic Compounds: Impacts on Air Quality and Climate. *Chem. Rev.* **2015**, *115*, 3984−4014.

(2) Derwent, R. G. Sources, Distributions, and Fates of VOCs in the Atmosphere. In *Volatile Organic Compounds in the Atmosphere*; Hester, R. E., Harrison, R. M., Eds.; The Royal Society of Chemistry, 1995; Vol. 4; pp 1−16.

(3) Calvert, J.; Mellouki, A.; Orlando, J.; Pilling, M.; Wallington, T. *Mechanisms of Atmospheric Oxidation of the Oxygenates*; Oxford University Press, 2011.

(4) Ezell, M. J.; Wang, W. H.; Ezell, A. A.; Soskin, G.; Finlayson-Pitts, B. J. Kinetics of Reactions of Chlorine Atoms with a Series of Alkenes at 1 atm and 298 K: Structure and Reactivity. *Phys. Chem. Chem. Phys.* **2002**, *4*, 5813−5820.

(5) Galán, E.; González, I.; Fabbri, B. Estimation of Fluorine and Chlorine Emissions from Spanish Structural Ceramic Industries. The Case Study of the Bailén Area, Southern Spain. *Atmos. Environ.* **2002**, *36*, 5289–5298.

(6) CEFIC. Consolidated Glycol Ether Production and Supply Information (v2 Amended 31/3/04) CEFIC. Brussels, 2004.

(7) European-Commission. European Union Risk Assessment Report 2-Methoxy-1-Methylethyl Acetate (PGMA)– Part I – Environment, 2006.

(8) Czajka, M.; Pudliszak, D. Emission of Volatile Organic Compounds (VOC) from Lacquered Surfaces. In *Management of Indoor Air Quality*; Dudzinska, M. R., Ed.; CRC Press, 2011; pp 45–55.

(9) Yujing, M.; Mellouki, A. The Near-UV Absorption Cross Sections for Several Ketones. *J. Photochem. Photobiol., A* **2000**, *134*, 31–36.

(10) Mellouki, A.; Téton, S.; Lebras, G. Kinetics of OH Radical Reactions with a Series of Ethers. *Int. J. Chem. Kinet.* **1995**, *27*, 791–805.

(11) Braure, T.; Bedjanian, Y.; Romanias, M. N.; Morin, J.; Riffault, V.; Tomas, A.; Coddeville, P. Experimental Study of the Reactions of Limonene with OH and OD Radicals: Kinetics and Products. *J. Phys. Chem. A* **2014**, *118*, 9482–9490.

(12) Bedjanian, Y.; Laverdet, G.; Le Bras, G. Low-pressure Study of the Reaction of Cl Atoms with Isoprene. *J. Phys. Chem. A* **1998**, *102*, 953–959.

(13) Su, M. C.; Kumaran, S. S.; Lim, K. P.; Michael, J. V.; Wagner, A. F.; Harding, L. B.; Fang, D. C. Rate Constants, $1100 \leq T \leq 2000$ K, for H + NO2 → OH + NO Using Two Shock Tube Techniques: Comparison of Theory to Experiment. *J. Phys. Chem. A* **2002**, *106*, 8261–8270.

(14) Atkinson, R.; Baulch, D. L.; Cox, R. A.; Crowley, J. N.; Hampson, R. F.; Hynes, R. G.; Jenkin, M. E.; Rossi, M. J.; Troe, J. Evaluated Kinetic and Photochemical Data for Atmospheric Chemistry: Volume III - Gas Phase Reactions of Inorganic Halogens. *Atmos. Chem. Phys.* **2007**, *7* (7), 981–1191.

(15) Bedjanian, Y.; Le Bras, G.; Poulet, G. Kinetic Study of OH + OH and OD + OD Reactions. *J. Phys. Chem. A* **1999**, *103*, 7017–7025.

(16) Anderson, R. J.; Bendell, D. J.; Groundwater, P. W.; Chemistry, R. S. o. *Organic Spectroscopic Analysis*; Royal Society of Chemistry, 2004.

(17) Kaufman, F. Kinetics of Elementary Radical Reactions in the Gas Phase. *J. Phys. Chem.* **1984**, *88*, 4909–4917.

(18) Bertram, A. K.; Ivanov, A. V.; Hunter, M.; Molina, L. T.; Molina, M. J. The Reaction Probability of OH on Organic Surfaces of Tropospheric Interest. *J. Phys. Chem. A* **2001**, *105*, 9415–9421.

(19) Ivanov, A. V.; Trakhtenberg, S.; Bertram, A. K.; Gershenzon, Y. M.; Molina, M. J. OH HO2, and Ozone Gaseous Diffusion Coefficients. *J. Phys. Chem. A* **2007**, *111*, 1632–1637.

(20) Bedjanian, Y.; Morin, J.; Romanias, M. N. Gas-Phase Reaction of Hydroxyl Radical with p-Cymene over an Extended Temperature Range. *J. Phys. Chem. A* **2015**, *119*, 11076–11083.

(21) Moriarty, J.; Sidebottom, H.; Wenger, J.; Mellouki, A.; Le Bras, G. Kinetic Studies on the Reactions of Hydroxyl Radicals with Cyclic Ethers and Aliphatic Diethers. *J. Phys. Chem. A* **2003**, *107*, 1499–1505.

(22) Le Calve, S.; Mellouki, A.; Le Bras, G. Kinetic Studies of OH Reactions with Propylal, Butylal and 1,3-Dioxolane. *Phys. Chem. Chem. Phys.* **2002**, *4*, 5622–5626.

(23) Lendar, M.; Aissat, A.; Cazaunau, M.; Daële, V.; Mellouki, A. Absolute and relative rate constants for the reactions of OH and Cl with pentanols. *Chem. Phys. Lett.* **2013**, *582*, 38–43.

(24) Wu, H.; Mu, Y.; Zhang, X.; Jiang, G. Relative Rate Constants for the Reactions of Hydroxyl Radicals and Chlorine Atoms with a Series of Aliphatic Alcohols. *Int. J. Chem. Kinet.* **2003**, *35*, 81–87.

(25) Cavalli, F.; Barnes, I.; Becker, K. H. FT-IR Kinetic and Product Study of the OH Radical-Initiated Oxidation of 1-Pentanol. *Environ. Sci. Technol.* **2000**, *34*, 4111–4116.

(26) Marrero, T. R.; Mason, E. A. Gaseous Diffusion Coefficients. *J. Phys. Chem. Ref. Data* **1972**, *1*, 3–118.

(27) Wallington, T. J.; Skewes, L. M.; Siegl, W. O.; Wu, C.-H.; Japar, S. M. Gas phase reaction of Cl atoms with a series of oxygenated organic species at 295 K. *Int. J. Chem. Kinet.* **1988**, *20*, 867–875.

(28) Atkinson, R.; Aschmann, S. M. Kinetics of the gas phase reaction of Cl atoms with a series of organics at 296 ± 2 K and atmospheric pressure. *Int. J. Chem. Kinet.* **1985**, *17*, 33–41.

(29) Atkinson, R.; Baulch, D. L.; Cox, R. A.; Crowley, J. N.; Hampson, R. F.; Hynes, R. G.; Jenkin, M. E.; Rossi, M. J.; Troe, J. Evaluated Kinetic and Photochemical Data for Atmospheric Chemistry: Volume II - Gas Phase Reactions of Organic Species. *Atmos. Chem. Phys.* **2006**, *6* (6), 3625–4055.

(30) Hooshiyar, P. A.; Niki, H. Rate constants for the gas-phase reactions of Cl-atoms with C2–C8 alkanes at T = 296 ± 2 K. *Int. J. Chem. Kinet.* **1995**, *27*, 1197–1206.

(31) Wallington, T. J.; Dagaut, P.; Liu, R. H.; Kurylo, M. J. The Gas Phase Reactions of Hydroxy Radicals with a Series of Esters over the Temperature Range 240–440-K. *Int. J. Chem. Kinet.* **1988**, *20*, 177–186.

(32) Romanias, M. N.; Zogka, A. G.; Papadimitriou, V. C.; Papagiannakopoulos, P. Uptake Measurements of Acetic Acid on Ice and Nitric Acid-Doped Thin Ice Films over Upper Troposphere/Lower Stratosphere Temperatures. *J. Phys. Chem. A* **2012**, *116*, 2198–2208.

(33) Wallington, T. J.; Hurley, M. D.; Haryanto, A. Kinetics of the Gas Phase Reactions of Chlorine Atoms with a Series of Formates. *Chem. Phys. Lett.* **2006**, *432*, 57–61.

(34) Atkinson, R. Kinetics and Mechanisms of the Gas-phase Reactions of the Hydroxyl Radical with Organic Compounds under Atmospheric Conditions. *Chem. Rev.* **1986**, *86*, 69–201.

(35) Wells, J. R.; Wiseman, F. L.; Williams, D. C.; Baxley, J. S.; Smith, D. F. The Products of the Reaction of the Hydroxyl Radical with 2-Ethoxyethyl Acetate. *Int. J. Chem. Kinet.* **1996**, *28*, 475–480.

(36) Smith, I. W.; Ravishankara, A. R. Role of Hydrogen-Bonded Intermediates in the Bimolecular Reactions of the Hydroxyl Radical. *J. Phys. Chem. A* **2002**, *106*, 4798–4807.

(37) Porter, E.; Wenger, J.; Treacy, J.; Sidebottom, H.; Mellouki, A.; Téton, S.; Le Bras, G. Kinetic Studies on the Reactions of Hydroxyl Radicals with Diethers and Hydroxyethers. *J. Phys. Chem. A* **1997**, *101*, 5770–5775.

(38) O'Donnel, S. M.; Sidebottom, H. W.; Wenger, J. C.; Mellouki, A.; Le Bras, G. Kinetic Studies on the Reactions of Hydroxyl Radicals with a Series of Alkoxy Esters. *J. Phys. Chem. A* **2004**, *108*, 7386–7392.

(39) Meylan, W. M.; Howard, P. H. Computer Estimation of the Atmospheric Gas-Phase Reaction Rate of Organic Compounds with Hydroxyl Radicals and Ozone. *Chemosphere* **1993**, *26*, 2293–2299.

(40) LeCalve, S.; LeBras, G.; Mellouki, A. Kinetic studies of OH Reactions with Iso-Propyl, Iso-Butyl, Sec-Butyl, and Tert-Butyl Acetate. *Int. J. Chem. Kinet.* **1997**, *29*, 683–688.

(41) Wallington, T. J.; Dagaut, P.; Liu, R.; Kurylo, M. J. The gas phase reactions of hydroxyl radicals with a series of esters over the temperature range 240–440. *Int. J. Chem. Kinet.* **1988**, *20*, 177–186.

(42) Winer, A.; Lloyd, A. C.; Darnall, K. R.; Atkinson, R.; Pitts, J. N., Jr Rate constants for the reactions of OH radicals with n-propyl acetate, sec-butyl acetate, tetrahydrofuran and peroxyacetyl nitrate. *Chem. Phys. Lett.* **1977**, *51*, 221–226.

(43) Williams, D. C.; O'rji, L. N.; Stone, D. A. Kinetics of the reactions of OH radicals with selected acetates and other esters under simulated atmospheric conditions. *Int. J. Chem. Kinet.* **1993**, *25*, 539–548.

(44) Notario, A.; Le Bras, G.; Mellouki, A. Absolute Rate Constants for the Reactions of Cl Atoms with a Series of Esters. *J. Phys. Chem. A* **1998**, *102*, 3112–3117.

(45) Xing, J.-H.; Takahashi, K.; Hurley, M. D.; Wallington, T. J. Kinetics of the reactions of chlorine atoms with a series of acetates. *Chem. Phys. Lett.* **2009**, *474*, 268–272.

(46) Hein, R.; Crutzen, P. J.; Heimann, M. An Inverse Modeling Approach to Investigate the Global Atmospheric Methane Cycle. *Global Biogeochem. Cycles* **1997**, *11*, 43–76.

(47) Jenkin, M. E. Photochemical Ozone and PAN Creation Potentials: Rationalisation and Methods of Estimation, Report AEAT-4182/20150/003, *National Environmental Technology Center, AEA Technology plc*, **1998**.

(48) Derwent, R. G.; Jenkin, M. E.; Saunders, S. M.; Pilling, M. J. Photochemical Ozone Creation Potentials for Organic Compounds in

Northwest Europe Calculated with a Master Chemical Mechanism. *Atmos. Environ.* **1998**, *32*, 2429−2441.

(49) Jenkin, M. E.; Hayman, G. D. Photochemical Ozone Creation Potentials for Oxygenated Volatile Organic Compounds: Sensitivity to Variations in Kinetic and Mechanistic Parameters. *Atmos. Environ.* **1999**, *33*, 1275−1293.

(50) Derwent, R. G.; Jenkin, M. E.; Saunders, S. M. Photochemical ozone creation potentials for a large number of reactive hydrocarbons under European conditions. *Atmos. Environ.* **1996**, *30*, 181−199.

Antonia ZOGKA

Dégradation atmosphérique d'une série d'acétates de méthoxy et éthoxy ainsi que d'acétate de n-pentyle

Dans le cadre du projet DISPATMO (étude de prévision des risques de pollution liés à la dispersion atmosphérique de produits chimiques), des études de risques liés aux incendies et explosions dus aux produits chimiques ont été menées. L'objectif de cette thèse était de réaliser une étude cinétique et mécanistique approfondie afin de déterminer la dégradation en phase gazeuse de l'un des principaux constituants du solvant Tiflex, acétate de 1-méthoxy-2-propyle (MPA), par les radicaux OH et les atomes de Cl. En outre, les constantes de vitesse de réaction de OH et Cl avec une série d' acétates d'alcoxyle largement utilisés dans l'industrie du revêtement et la peinture, l'acétate de méthoxy-2-butyle (2MBA), l'acétate de méthoxy-3-butyle (3MBA), l'acétate de méthoxy-éthyle (MEA), l'acétate d'éthoxy-éthyle (EEE) et l'acétate de n-pentyle (n-PA), ont été déterminées. Les expériences ont été conduites en utilisant la technique de photolyse laser pulsée couplée à la fluorescence induite par laser, un réacteur à écoulement à basse pression couplé à un spectromètre de masse et une chambre de simulation atmosphérique couplé à GC-FID, FTIR et GC-MS en utilisant les méthodes absolue et relative. Les données cinétiques ont été utilisées pour déterminer les expressions Arrhenius pour évaluer le devenir environnemental des composés étudiés tels que leur durée de vie et le potentiel de formation d'ozone. D'autre part, le mécanisme réactionnel a été étudié et les principaux produits de dégradation et leurs rendements ont été déterminés en présence de NO. Les spectres d'absorption UV-Vis de MPA, 2MBA et 3MBA ont également été déterminés afin d'évaluer le potentiel de photolyse de ces composés dans l'atmosphère. Les paramètres cinétiques et mécanistiques ainsi que les durées de vie troposphérique déterminés sont utilisés comme données d'entrée dans les modèles de simulation atmosphériques photochimiques et dans les modèles de dispersion atmosphérique de produits chimiques pour évaluer leur impact atmosphérique.

Mots clés : Chimie atmosphérique, Acétates d'alkoxy, Radical OH, Atome Cl, Constante de vitesse, Mécanisme, durée de vie.

Atmospheric degradation of a series of methoxy and ethoxy acetates and n-pentyl acetate

In the context of DISPATMO project (forecast study of pollution risks related to the atmospheric dispersal of chemicals), risk studies linked to the fires and the explosions due to chemical storage were conducted. The purpose of this thesis was to perform a thorough kinetic and mechanistic study to determine the gas phase degradation of one of the main component of Tiflex solvent, the 1-methoxy 2-propyl acetate (MPA). Furthermore, the rate coefficients of OH and Cl with a series of alkoxy acetates widely used in painting and coating industries, 2-methoxy-butyl acetate (2MBA), 3-methoxy-butyl acetate (3MBA), methoxy ethyl acetate (MEA), ethoxy ethyl acetate (EEA) and n-pentyl acetate (n-PA), were determined. The experiments were performed employing the pulsed laser photolysis-laser induced fluorescence technique, a low pressure flow tube reactor coupled with a quadrupole mass spectrometer and an atmospheric simulation chamber coupled with a GC-FID, a FTIR and a GC-MS using complementary absolute and relative rate methods. The kinetic data were used to derive the Arrhenius expressions as well as to evaluate the environmental fate of the studied compounds such as their lifetimes and the Photochemical Ozone Creation Potential. Besides, the reaction mechanism was investigated, while the major degradation products and their yields were determined in presence of NO. In addition, the UV-Vis absorption cross sections of MPA, 2MBA and 3MBA were measured in order to evaluate their potential photolysis in the atmosphere. The investigation of the chemical processes and the tropospheric lifetimes of the compounds are used as input data in photochemical atmospheric simulation models and in chemical agent atmospheric dispersion models to evaluate their atmospheric impact.

Keywords : Atmospheric chemistry, Alkoxy acetates, OH radical, Cl atom, rate coefficient, mechanism, lifetime.